A New Gallium-68 Labelled Imaging Agent for Prostate Cancer

Nawaz, Saima

Awarding institution:
King's College London

A New Gallium-68 Labelled Imaging Agent for Prostate Cancer

Saima Nawaz

A dissertation submitted in partial fulfilment of the requirements for the degree of

Doctor of Philosophy

of

King's College London

September 2013

ABSTRACT:

The prostate is an exocrine gland of the male reproductive system. There is a wide array of techniques available for imaging prostate cancer (PCa). However, there is a need to develop a new PET radiotracer to image PCa as the most commonly used PET tracer ^{18}F-FDG is not very successful in imaging of PCa. The aim of this project is to evaluate the chelator CP256 and its bifunctional modificaton (YM103), together with a new molecular targeting vehicle J591-scFv which shows specificity for an extracellular epitope of prostate specific membrane antigen (PSMA), an extensively studied antigen for imaging PCa. The radionuclide used is gallium-68 (^{68}Ga), which is a generator based metallic radionuclide with a half-life of 68 min.

A comparative study of CP256 with other gallium chelators such as NOTA, DOTA and HBED showed that CP256 gave a higher radiolabelling yield and greater serum stability. It also gave good radiolabelling yields with other radionuclides such as ^{111}In, ^{90}Y, ^{99m}Tc and ^{89}Zr. It was demonstrated that CP256 could chelate ^{68}Ga *in vivo*, allowing a pre-targeting approach in which an antibody conjugated with CP256 could be administered to a patient, followed hours to days later by ^{68}Ga-acetate or citrate. This technique could be quite useful with ^{68}Ga because of its short half-life. CP256 is a unique and promising chelator as compared to the NOTA and HBED, which are unable to bind with ^{68}Ga which was previously bound to serum protein.

The antibody fragment J591-scFv incorporating a His-tag for labelling with ^{99m}Tc tricarbonyl was produced and its binding evaluated using human PCa cell lines PC3LN3 (PSMA negative) and a variant engineered to express PSMA (PC3LN3-PSMA). It was observed that J591(scFv) can be radiolabelled with $^{99m}Tc(CO)_3^+$ conveniently and efficiently. The labelled product was stable in serum. It showed selective binding to PSMA positive cells compared to PSMA negative cells.

A cysteine residue was incorporated into the J591c(scFv) sequence along with a His-tag to facilitate radiolabelling with ^{68}Ga through YM103, a bifunctional chelator which contains a maleimide group to attach with cysteine of J591c(scFv). Conjugated J591c(scFv) gave good (95%) radiolabelling yields with ^{68}Ga within 5 minutes. The radiolabelled conjugated J591c(scFv) showed selective binding with PSMA positive cells (Du145-PSMA) compared to PSMA negative cells (Du145) *in vitro*.

For *in vivo* evaluation of ^{68}Ga labelled J591c(scFv), one group of male SCID beige mice was injected with Du145-PSMA cells and another group with Du145 cells for tumour growth over the period of a few weeks. For imaging and biodistribution studies mice were injected with 7 MBq/10 µg of radiolabelled conjugated J591c(scFv). The PSMA positive tumour showed clear uptake of the radiotracer compared to the PSMA negative tumour with a specific vs nonspecific uptake ratio of 9.1.

Conclusion:

CP256 is a unique and versatile chelator for ^{68}Ga. Its radiolabelling yield and reaction conditions are better than available gallium chelators such as DOTA. Its bifunctional version (YM103) conjugated with J591c(scFv) showed quantitative radiolabelling (depending upon concentration) within 5 minutes with ^{68}Ga and showed specific binding to a PSMA positive cell line (Du145-PSMA) and high uptake in PSMA positive tumours as opposed to PSMA negative tumours.

Acknowledgements

I would like to thank first and foremost to my first supervisor Dr. James Ballinger. It is with immense and deepest gratitude that I acknowledge all the support and guidance he provided me throughout my PhD and MSc at King's College London. I would also like to thank my second supervisor Prof. Philip Blower for his encouragement, help and patience in my PhD. This thesis would have remained a dream without the support of Prof. Philip Blower. I consider it an honour to work with him and his team.

I would also like to thank Dr. Gregory Mullen and Dr. Florian Kampmeier for introducing me to the subject of molecular biology. I am grateful for their valuable advice and input in my PhD and also for their in-depth knowledge on single chain fragments and prostate cancer. Many thanks to Dr. Maggie Cooper and Dr. Dave Berry for all the guidance and support they have provided me regarding radiochemistry and inorganic chemistry. Many thanks to all the members of the Imaging Sciences group, especially Dr. Michelle Ma for her help in mass-spectroscopy, and Dr. Ehsan Sharif, Krisanat Chaumsaamarkkee, Zaitul Safee and Dr. Kavitha Sunassee for their help in *in vivo*, biodistribution and image analysis work.

A big thank you to my funding provider, IEL (Imaging Equipment Ltd), and graduate school funding from King's College London for giving me the opportunity to do this work.

Finally, I would like to say thank you to my family, particularly to my husband Wasim for being my best friend and for keeping me sane for the past few months. To my baby Eishaal as now I have all the time to play with her. To my parents for always trusting and believing in me and for all their love, support and inspiration which they provided throughout my life and especially during my PhD, I would like to dedicate all my work to them.

Table of Contents

Title page 1
Abstract 2
Acknowledgements 4
Table of Contents 5
List of Figures 10
List of Tables 14
Abbreviations 15

Chapter 1: Introduction

1.1-Radiopharmacological Strategy 17
1.2-Structure and Function of Prostate Gland 18
1.3-Prostate Cancer 19
1.4-Effect of Hormones and Growth Factors on Normal Prostate Gland and Prostate Cancer 20
1.4.1-Effect of Androgen and Androgen Receptors 20
1.4.2-Vitamin D Pathway 20
1.4.3-Growth Factors 21
1.5-Screening of Prostate Cancer 21
1.5.1-DRE, PSA and Needle Biopsy 21
1.5.2-Gleason Score 22
1.6-Current Methods for Imaging Prostate Cancer 22
1.7-PSMA and PCa 24
1.8-Small Molecules and PCa 27
1.9-Antibodies and PCa 32
1.10-^{68}Ga 37
1.11-^{68}Ge/^{68}Ga Generator System 38
1.11.1-Concentration and purification methods of the ^{68}Ga eluate 40
1.12-Ligands for Gallium 42
1.13-The Pre-targeting Approach for CP256: 49
1.14-Aims and Objectives: 50

Chapter 2: Characterisation and Evaluation of CP256

2.0-Introduction 51
2.1- Method 52

2.1.1-Elution of $^{68}Ge/^{68}Ga$ Generator 52
2.1.2-General Radiolabelling Methods 52
2.1.3-Thin Layer Chromatography (TLC) 52
2.1.3a-Method-1 53
2.1.3b-Method-2 53
2.1.3c-Method-3 53
2.1.3d-Method 4 53
2.1.3e-Method 5 54
2.1.4-Size Exclusion Column Chromatography 55
2.1.5-Effect of concentration and time on formation of ^{68}Ga-CP256 complex 55
2.1.6-Changes in radiolabelling yield (%) of CP256 with 1st and 2nd elution over time……..55
2.1.7-Comparison of CP256 with NOTA, HBED and DOTA for ^{68}Ga radiolabelling……...56
2.1.8-Stability in Human Blood Serum……...56
2.1.9-Radiolabelling of CP256 and NOTA with eluates from different generators……...57
2.1.10-Radiolabelling of C2A protein with ^{68}Ga……....57
2.1.11- CP256 and binding with different radionuclides……57
2.1.11a-Radiolabelling with ^{111}In-Acetate ..... ……..57
2.1.11b-Radiolabelling with ^{90}Y 58
2.1.11c-Radiolabelling with ^{99m}Tc tricarbonyl 58
2.1.11d-Radiolabelling with ^{89}Zr (Zirconium) 58
2.1.12-Formation of ^{68}Ga-CP256 complex in serum……..58
2.2-Results 59
2.2.1-Effect of concentration and time on formation of ^{68}Ga-CP256 complex 59
2.2.2-Changes in radiolabelling yield of CP256 with 1st and 2nd generator elutions over time60
2.2.3-Comparison of CP256 with NOTA, HBED and DOTA for ^{68}Ga radiolabelling 61
2.2.4-Stability in Human Blood Serum 63
2.2.5-Radiolabelling of CP256 and NOTA with eluates from different generators 67
2.2.6-Radiolabelling of C2A protein with ^{68}Ga 68
2.2.7- Evaluation of CP256 binding with other radionuclides 69
2.2.7a-Radiolabelling with ^{111}In-Acetate 70
2.2.7b-Radiolabelling with ^{90}Y 71
2.2.7c-Radiolabelling with ^{99m}Tc-tricarbonyl 73
2.2.7d-Radiolabelling with ^{89}Zr (Zirconium) 75
2.2.8-Formation of ^{68}Ga-CP256 complex in serum……76

2.4- Summary 88

Chapter 3: Production of J591(scFv) and J591c(scFv)

3.0-Introduction 89

3.1-Methods 91

3.1.1-Preparation of Chemically Competent BL21 Cells 91

3.1.2-Transformation of E-Coli with Plasmid DNA 92

3.2-Expression in BL21 (DE3)-T1R Competent Cells 92

3.2.1-Peri-plasmic protein extraction 93

3.3-Production of J591(scFv)& J591c(scFv) from Mammalian 293-T cells 93

3.3.1-Purification through Ni-NTA column using AKTA 94

3.3.2-Size-exclusion chromatography 94

3.3.3-SDS-PAGE and Western Blotting 94

3.4-Effect of temperature and glycerol on dimer formation 95

3.5-Results 96

3.5.1-Production of J591(scFv) and J591c(scFv) 96

3.5.2-Purification through Ni-NTA column using AKTA 96

3.5.3-Size-exclusion step 98

3.5.4-Effect of storage temperature and glycerol on dimer formation 102

3.6: Discussion 104

3.7- Summary 106

Chapter4: Radiolabelling of J591(scFv) with Technetium-99m Tricarbonyl

4.0-Introduction 107

4.1-Method 108

4.1.1-Preparation of Tricarbonyl kit 108

4.1.2-Splitting of Tricarbonyl kit and radiolabelling 108

4.1.3-Radiolabelling of Full Kit 108

4.2-General method of Radiolabelling of J591(scFv) and effect of time on radiolabelling yield 109

4.2.1-Mini-trap purification step 109

4.3-Radiolabelling of different concentrations of J591(scFv) 109

4.4-Difference between 140 mM and 500 mM salt concentration 110

4.5-Serum stability 110

4.6-FACS analysis 111

4.7-Cell-binding experiments with labelled antibodies 112

4.8-Mass spectrometry 113

4.9- Results 114

4.9.1-Preparation of ^{99m}Tc Tricarbonyl 114
4.9.2-Time course of Radiolabelling of J591(scFv) 114
4.9.3-Mini-trap purification step 115
4.9.4-Radiolabelling of different concentrations of J591(scFv) 118
4.9.5 -Difference between 140 mM and 500 mM salt concentration 122
4.9.6 -Serum stability 123
4.9.7 -FACS 125
4.9.8 -Cell-binding experiment 128
4.9.9 -Electrospray Mass-Spectroscopy: 130
4.10-Discussion 130
4.11-Summary 133

Chapter 5: Radiolabelling of J591c(scFv) with Gallium-68

5.0-Introduction 134
5.1-Methods 134
5.1.1- Reduction of J591c(scFv) with TCEP 134
5.1.2- Conjugation of J591c(scFv) with Fluorescein-5-maleimide (F-5-M) and YM103 135
5.2- ^{68}Ga generator elution protocol and radiolabelling of J591c(scFv)-YM103 with ^{68}Ga. 135
5.3- Effect of time and temperature on radiolabelling of different concentrations of J591c(scFv)-YM103 with ^{68}Ga 136
5.4- Mass spectroscopy 136
5.5- Serum stability 136
5.6- FACS analysis 137
5.7- Cell binding 138
5.8- In vivo experiment 139
5.9-Results: 140
5.9.1- Reduction of J591c with TCEP 140
5.9.2- Conjugation of J591c(scFv) with F-5-M and YM103……...142
5.9.3- ^{68}Ga generator elution protocol and radiolabelling of J591c(scFv)-YM103 with ^{68}Ga 143
5.9.4- Effect of time and temperature on radiolabelling of different concentrations of J591c(scFv)-YM103 with ^{68}Ga 144
5.9.5- Mass spectroscopy 148
5.9.6- Serum stability 150
5.9.7- FACS analysis 151
5.9.8-Cell binding 152

5.9.9- In vivo experiment..... 153
5.10-Discussion..... 163
5.10.1-In vivo work..... 164
5.11-Summary..... 166
Chapter 6: Discussion
6.1-Aims of the project 167
6.2-Thesis Discussion 167
6.3-Summary..... 174
6.4-Future work..... 175
Chapter 7: References
7.0- References: 176

List of Figures:

Figure 1.1: Main components of radiopharmacological strategy 17
Figure 1.2: Normal prostate gland along with surrounding tissues and organs. 18
Figure 1.3: Prostate cancer originating from different zones of prostate gland. 19
Figure 1.4: Structure of ^{18}F-FDHT (fluoro-5α dihydrotestrone), a steroidal AR ligand. 23
Figure 1.5: Non-steriodal AR ligand (R)-[^{11}C]-dimethylaminehydroxy-flutamide 24
Figure 1.6: Schematic diagram of the globular nature of Prostate-Specific Membrane Antigen (PSMA). 24
Figure- 1.7: Mechanistic scheme of PSMA function..... 25
Figure- 1.8: PSMA surface rendering 26
Figure- 1.9:Modular Lab by Eckert&Zeigler for the production of ^{68}Ga-DOTATOC. 39
Figure- 1.10: ^{68}Ge/^{68}Ga-Generator IGG100 and ^{68}Ge/^{68}Ga-Generator (Obninsk) 39
Figure-1.11:Structures of Acyclic Bifunctional Chelators. 44
Figure-1.12: Structures of Macrocyclic Chelators. 46
Figure 1.13: TRAP(1,4,7-triazacyclononane-1,4,7-tris[methyl(2-carboxyethyl)phosphinic acid) 47
Figure 1.14: TRAP(1,4,7-triazacyclononane-1,4,7-tris[methyl(2-carboxyethyl)phosphinic acid) conjugated with RGD peptide. 47
Figure 1.15: Tripodal Hexadentate Chelator (CP256) 48
Figure 1.16: YM103, bifunctional version of CP256 49
Figure 2.0:New itlc Method for CP256 54

Figure-2.1: Changes in radiolabelling yield of 11µM of NOTA at different time periods. 63
Figure-2.2a: Changes in radiolabelling yield of HBED at different time period. 64
Figure-2.2b: Radiolabelling of Apo-Transferrin with ^{67}Ga-Citrate at different time points 64
Figure-2.3: Comparative study of $^{68}GaCl_3$, ^{68}Ga-CP256 and ^{68}Ga-human serum protein with ^{68}Ga-CP256 in human serum protein 65
Figure -2.4: Comparative study of ^{68}Ga acetate, ^{68}Ga-HBED and ^{68}Ga-human serum protein with ^{68}Ga-HBED in human serum protein 66
Figure -2.5: Comparative study of ^{68}Gaacetate, ^{68}Ga-NOTA and ^{68}Ga-human serum protein with ^{68}Ga-NOTA in Human serum protein 66
Figure-2.6: Changes in radiolabelling yield of CP256 (11.8 µM) with ^{68}Ga eluted from Obninsk and IGG 100 generators 67
Figure-2.7: Changes in radiolabelling yield of NOTA (11 µM) with ^{68}Ga eluted from Obninsk and IGG 100 generators. 68
Figure-2.8: Reference-^{68}Ga-Citrate (A) . ^{68}Ga-Conjugated C2A protein (B). ^{68}Ga-Conjugated C2A protein after 5 minutes. 69
Figure-2.9: ^{111}In-Acetate 70
Figure-2.10: ^{111}In-CP256 70
Figure -2.11: Comparative study of ^{111}In-acetate, ^{111}In-CP256, Serum protein with ^{111}In-CP256 complex in serum protein at three different time-points i.e.5-min ,60-min and 2hrs. 71
Figure-2.12: ^{90}Y-acetate 72

Figure-2.13: ^{90}Y-CP256 72
Figure-2.14: Comparative Study of ^{90}Y-Acetate and ^{90}Y-CP256, ^{90}Y human serum protein, ^{90}Y+CP256 incubated in human serum protein and samples are taken out at 10 min, 60 min,120min and 4 h 73
Figure -2.15: QC for tricarbonyl. 74
Figure-2.16: Tricarbony,.Free pertechnetate. 74
Figure-2.17: CP256-tricarbonyl complex 74
Figure-2.18: Graphical representation of radiolabelling yield at different time-points 75
Figure-2.19: ^{89}Zr citrate and ^{89}Zr-CP256. 75
Figure-2.20: Comparative study of ^{89}Zr-Acetate and ^{89}Zr-CP256, ^{89}Zr human serum protein, ^{89}Zr+CP256 incubated in human serum protein 76
Figure-2.21: Elution profile of ^{68}Ga-Acetate (A), ^{68}Ga-NOTA (B), ^{68}Ga-HBED (C), ^{68}Ga-CP256 (D) and human serum protein (E) 77
Figure-2.22: Elution profile of ^{68}Ga-\cp256 (A) at 60 min in pretargetting manner in a sequence (CP256+human serum protein+^{68}Ga). Elution profile (B) of pretargetting in a sequence (^{68}Ga+serum protein+CP256) 77
Figure-2.23: Comparative study of ^{68}Ga-CP256 with two different concentrations of CP256 in human serum protein and ^{68}Ga in a pretargetting approach..... 78
Figure-2.24: Comparative study of ^{68}Ga-CP256 with two different concentrations of CP256 in human serum protein and ^{68}Ga. 78
Figure-2.25: Comparative study of ^{68}Ga-CP256 with Pre (^{68}Ga+human serum protein) and Post (^{68}Ga+human serum protein+CP256) samples. 79
Figure-2.26: Elution profile of ^{68}Ga-NOTA in human serum protein. Pretargetting with NOTA in a sequence (NOTA+Serum+^{68}Ga). Pretargetting with NOTA in a sequence (^{68}Ga+serum protein+ NOTA).80
Figure-2.27:Elution Profile of ^{68}Ga-HBED in human serum protein.Elution Profile of Pretargetting in a sequence(^{68}Ga+serum protein+HBED). Elution Profile of Pretargetting in a sequence (HBED+serum protein+^{68}Ga)..... 81
Figure-2.28: Comparative study of ^{68}Ga-acetate, ^{68}Ga-NOTA and ^{68}Ga-human serum protein with two different techniques of pretargetting with NOTA using PD-10 column. Both the techniques of pretargetting have proved that ^{68}Ga prefers to bind with human serum protein instead of NOTA. 82
Figure-2.29: Comparative study of ^{68}Ga-acetate, ^{68}Ga-HBED and ^{68}Ga-human serum protein with two different techniques of pretargetting with HBED..... 83
Figure-2.30: $^{68}GaCl_3$ (A). ^{68}Ga-CP256 (B). Supernatant sample (1 mg/ml) (C).Supernatant sample (0.1 mg/ml) (D). 83
Figure 3.0 : A full length antibody and single chain fragment..... 90
Figure-3.1: Chromatogram showing different fraction eluted from Ni-NTA column using FPLC..... 97
Figure-3.2: SDS-PAGE gel of J591 after Ni-NTA step. 97
Figure-3.3: Chromatogram showing different fractions eluted from Ni-NTA column using FPLC.. 98
Figure-3.4: SDS-PAGE gel of J591c after Ni-NTA 98
Figure-3.5: Chromatogram showing monomer and dimer fractions of J591c as eluted from size-exclusion column using FPLC..... 99

Figure-3.6: SDS-PAGE gel of J591 after buffer adjustment using Superdex 75 10/300GL column. 99
Figure-3.7: Chromatogram showing monomer and dimer fractions of J591c as eluted from size-exclusion column using FPLC..... 100
Figure-3.8: SDS-PAGE gel of J591c after buffer adjustment using Superdex 75 10/300GL column.. ... 100
Figure-3.9:J591 Mixture of monomer (9 min) and dimers (8 min) in SEC-2000 column (A) using PBS as running buffer. Monomer fraction of J591 at 9 min (B). 101
Figure-3.10: J591c predominantly monomer (9 min) and small amount of dimers (8 min) in SEC-2000 column (A). Mixture of monomer (9 min) and dimers (8 min) (B)..... 101
Figure-3.11: Western blot with DAB (3, 3-Daminobenzidine Peroxidase). 102
Figure-3.12: J591 & J591c dimerization 103
Figure-3.13: SDS-PAGE gel mammalian 293T cells vs bacterial BL21 cells 104
Figure-4.1: QC for tricarbonyl. 114
Figure-4.2:J591 % radiolabelling yield against time. 115
Figure-4.3: Elution profiles of J591, tricarbonyl and free pertechnetate from mini-trap column based on their sizes..... 116
Figure-4.4: HPLC of free pertechnetate (A), Tricarbonyl (B), radiolabelled J591 before mini-trap (C) and after mini-trap (D) 116
Figure-4.5: iTLC(sa) is used as a stationary phase and 0.1 M citrate buffer as a running buffer. iTLC of free pertechnetate (A), Tricarbonyl (B), radiolabelled J591 before mini-trap (C), radiolabelled J591 after mini-trap (D). 117
Figure-4.6: Different concentrations of protein are radiolabelled J591 at 30 min and 60 min..... 119
Figure-4.7: 72.2 µM of protein radiolabelled with tricarbonyl.. 119
Figure-4.8: 36.1 µM of protein radiolabelled with tricarbonyl. 120
Figure-4.9: 18.2 µM of protein radiolabelled with tricarbonyl. Radiolabelled J591 eluted around 9 min in sec-2000 column in HPLC. 120
Figure-4.10: 7.22 µM of protein radiolabelled with tricarbonyl 121
Figure-4.11: 3.61 µM of protein radiolabelled with tricarbonyl.. 121
Figure-4.12: J591 1 mg/ml radiolabelling yield with 500 mM salt conc is better than 140 mM. 122
Figure-4.13: J591 0.5 mg/ml radiolabelling yield with 500 mM salt conc is better than 140 mM. 123
Figure-4.14: SDS-PAGE gel for serum stability for J591. 124
Figure-4.15: Radiochromatogram showing the result of strong binding of J591-scFv with tricarbonyl in the presence of human serum protein at different time points..... 125
Figure-4.16:Cell binding experiment PC3LN3 127
Figure-4.17: Cell binding experimentPC3LN3(PSMA)..... 128
Figure-4.18: Non-specific binding with negative cell lines (PC3LN3) vs total binding with PSMA positive cell lines (PSMA-PC3LN3). 129
Figure-4.19: Mass-spec of J591 130
Figure-5.1:Effect of different molar concentrations of TCEP on dimerization in J591c (scFv). 141
Figure-5.2: J591c(ScFv) conjugated with fluorecein-5-maleimide (F-5-M)..... 142
Figure-5.3: Sephadex GL column to remove excess of YM103 via FPLC 143

Figure-5.4:^{68}Ga acetate in size-exclusion .column. 144
Figure-5.5:^{68}Ga J591c(scFv) in size-exclusion column. 144
Figure-5.6: SDS-PAGE 12% gel of conjugated J591c(scFv). 145
Figure-5.7: Effect of temperature on the radiolabelling yield of conjugated J591c(scFv)-YM103. 147
Figure -5.8: Changes in radiolabelling yield with time at different concentrations of J591(scFv)-YM103. 147
Figure-5.9:^{68}Ga acetate (A). Unconjugated J591c(scFv)(B) ^{68}Ga-CP256(C) Conjugated J591c(scFv) radiolabelled with ^{68}Ga(D) 148
Figure-5.10: Chromatograms obtained after the mass-spectrometry of conjugated and unconjugated J591c(scFv). 150
Figure-5.11: SDS-PAGE gel for serum stability of ^{68}Ga-J591c(scFv)-YM103 151
Figure-5.12: Comparative study of PSMA positive(Du145-PSMA) and negative cell lines(Du-145) 152
Figure-5.13: Graph shows the competitive binding of conjugated J591c with PSMA positive cell line .Du-145 (PSMA negative) shows non-specific cell binding. 153
Figure-5.14: PET/CT Imaging data for ^{68}Ga acetate and ^{68}Ga CP256.&0-10 min time-course for ^{68}GaCP256. 154
Figure- 5.15: Biodistribution data for ^{68}Ga acetate after 4hrs. 155
Figure- 5.16: Biodistribution data of ^{68}Ga CP256 after 4hrs. 156
Figure-5. 17: PET/CT imaging data of the mouse containing tumour produced from Du145 (PSMA negative) cells. 157
Figure-5.18: Transverse view of PSMA negative tumour at different time points. A: 0-30 min, B: 60-90 min, C: 180-210 min. 157
Figure-5.19: Graph shows the biodistribution data for PSMA negative tumour based on four mice 158
Figure-5.20: Graph shows the biodistribution data (with out kidneys) for PSMA negative tumour based on four mice 158
Figure-5.21: Dynamic scan of the mouse with PSMA positive tumour (left flank). 159
Figure-5.22: Transverse view of PSMA positive tumour. Accumulation of activity at different time points. A: 0-30 min, B: 60-90 min, C: 180-210 min. 159
Figure-5.23: Biodistribution data based on four mice for in PSMA positive tumour 160
Figure-5.24: Biodistribution data based on four mice for in PSMA positive tumour(without kidney) 161
Figure -5.25: Specific vs non-specific uptake in PSMA positive and PSMA negative tumours 162
Figure -5.26: Comparison of uptake in PSMA positive and negative tumour based on imaging data over the period of 4 h. 162

List of Tables:

Table 1:

Radioactive isotopes of gallium.....38

Table 2:

Concentration and moles of CP256.....59

Table 3:

%age radiolabelling yield of CP256 at different concentration.....60

Table 4:

Comparative study of 1st and 2nd elution.....61

Table 5:

Comparative study of different chelatotors of gallium.....62

Table 6:

Buffers used in the preparation and purification of scFv.....91

Abbreviations:

AR	Androgen receptors
BFC	Bifunctional Chelator
CT	Computed tomography
DFO	Desferrioxamine
DMSO	Dimethylsulfoxide
DOTA	1,4,7,10-tetraazacyclododecane-1,4,7,10-tetraacetic acid
DTPA	Diethylenetriaminepentaacetic acid
DOTATOC	$DOTA^{0}$-$_{D}$ -Phe^{1}-Tyr^{3}-octreotide
DHT	Dihydrotestostrone
DRE	Digital rectal examination
GRPR	Gastrin releasing peptide receptors
EGF	Epidermal growth factor
FPLC	Fast protein liquid chromatography
HBED	*N*,*N*'-bis(2-hydroxybenzyl)ethylenedinitrilo-*N*,*N*'-diacetic acid
HPLC	High Performance Liquid Chromatography
HSA	Human serum albumin
MRI	Magnetic resonance maging
ITLC-SA	Instant Thin Layer Chromatography-Silicic Acid
ITLC-SG	Instant Thin Layer Chromatography-Silica Gel
IGF-I	Insulin like growth factor I
NOTA	1,4,7-triazacyclononane-1,4,7-triacetic acid
PBS	Phosphate Buffered Saline
PET	Positron emission tomography
PCa	Prostate Cancer
PSA	Prostate specific antigen
PAP	Prostatic acid phosphatise
PDGF	Platelet derived growth factor
PSMA	Prostate specific membrane antigen

QC	Quality Control
VDR	Vitamin D receptor
VEGF	Vascular endothelial growth factor
RCY	Radiochemical yield
R_f	Retention Factor
SAX	Strong anion exchange
scFv	Single chain Fv variable fragment
SPECT	Single photon emission computed tomography
TACN	1,4,7-triazacyclononane
TLC	Thin layer Chromatography
TRIS-HCl	Tris(hydroxymethyl)aminomethane-Hydrochloride
UV	Ultraviolet

Chapter 1: Introduction

For most of the metallic radionuclides the radiopharmacological strategy involved has the following components.

1.1-Radiopharmacological Strategy

Metal radiopharmaceuticals are those which incorporate a diagnostic or therapeutic metallic radionuclide. Radiometals can provide useful pharmacological properties in their ionic form or can be used for labelling of various biomolecular (target specific) vectors. A target specific radiopharmaceutical can be divided in to four parts as shown in Fig-1.1.

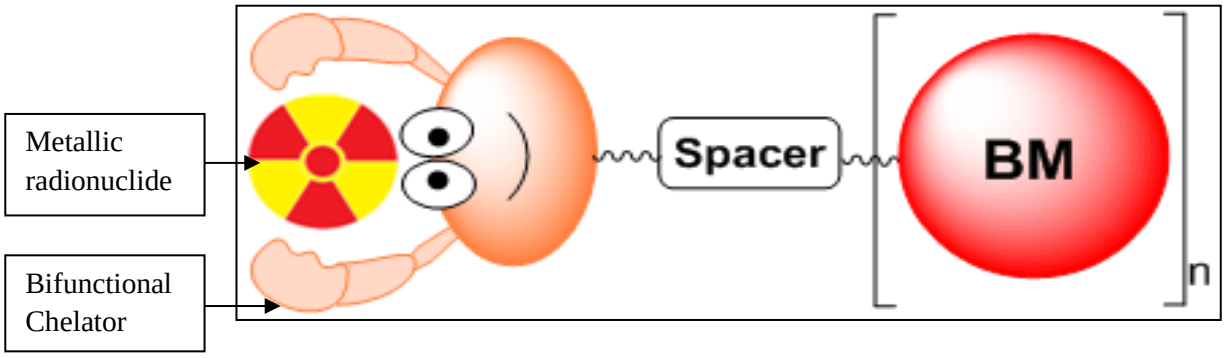

Figure 1.1: Main components of radiopharmacological strategy

1: a targeting biomolecule (BM), which acts as a target specific vector

2: a linker/spacer, which can be used to control pharmacokinetics (PKM, pharmaco-kinetics modifying).

3: a bifunctional chelator (BFC)

4: a metallic radionuclide.

Each of these components must be optimised to obtain a radiopharmaceutical with the best properties [1].

1.2-Structure and Function of Prostate Gland

The prostate is an exocrine gland of the male reproductive system in most mammals. It is a donut shaped gland and its size is about that of a walnut. It is located under the bladder in front of the rectum and it wraps around the urethra (a tube which carries urine from bladder to penis) (Fig-1.2). It is made up of 70% glandular and 30% muscular tissue. The prostate gland makes 30% of the fluid part of the semen. The remaining amount of fluid is secreted by the testes, seminal vesicles, bulbourethral and urethral glands. It needs male sex hormone to grow and function [2].

The prostatic epithelium is composed of two layers: basal layer and luminal layer. In these two layers three types of cell are present: basal, neuroendocrine and secretory. Basal cells rest on the basement membrane. They are undifferentiated and non-secretory cells and are not dependent on androgen for survival. Neuroendocrine cells are spread throughout the basal and luminal layers. They lack androgen receptors (AR). However, they do express serotonin and chromogranin A and play an important role in growth and differentiation. Secretory cells are present in the luminal layer and they form the exocrine region and are well differentiated. They secrete prostate specific antigen (PSA) and prostatic acid phosphatase (PAP) into the glandular lumina. They express high levels of AR and are dependent on androgen for survival [3].

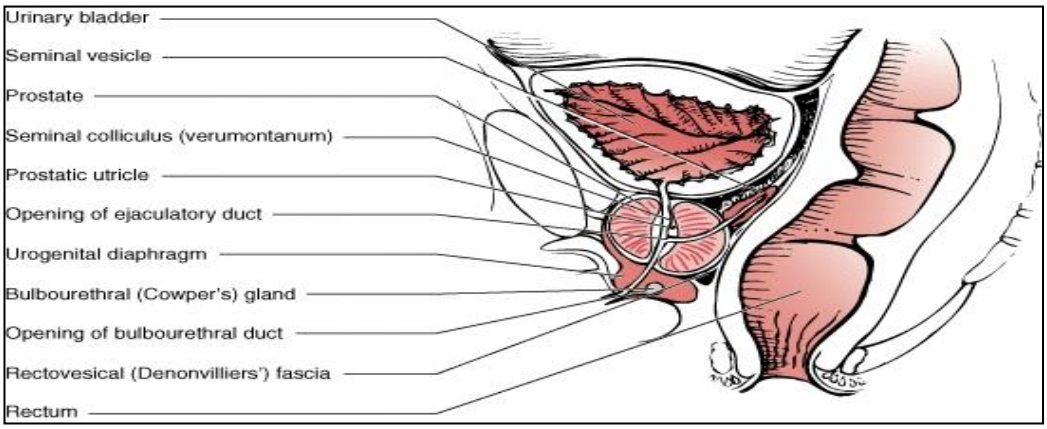

Figure 1.2: Normal prostate gland along with surrounding tissues and organs [8]

1.3-Prostate Cancer

Prostate cancer (PCa) was first described in 1853 by a surgeon at the London Hospital, J Adams, by histological examination [4]. In his report, he noted that the condition was "a very rare disease". Remarkably, 150 years later, PCa has become a significant health problem and disease. PCa is commonly found in elderly men and is the second leading cause of death among men in the USA [5]. In the UK, after skin cancer PCa is one of the four most common cancers along with breast, lung and colorectal cancers [6]. In the latest international data which covered five continents from 1988-1992, it was observed that occurrence of this disease is highest in North America, intermediate in Australia and low in Asia [7]. There are many risk factors, which include family history and genetics, hormone and other growth factors, diet and nutrition, and other lifestyle factors.

In one study it was observed that approximately 60-70% of PCa occurs in the peripheral zone of the prostate gland (the largest zone, located near the rectum), and 10-20% in the transition zone (surrounding the proximal urethra), with only 5-10% originating from the central zone (involved in the connection of the seminal vesicles to the prostate) [8].

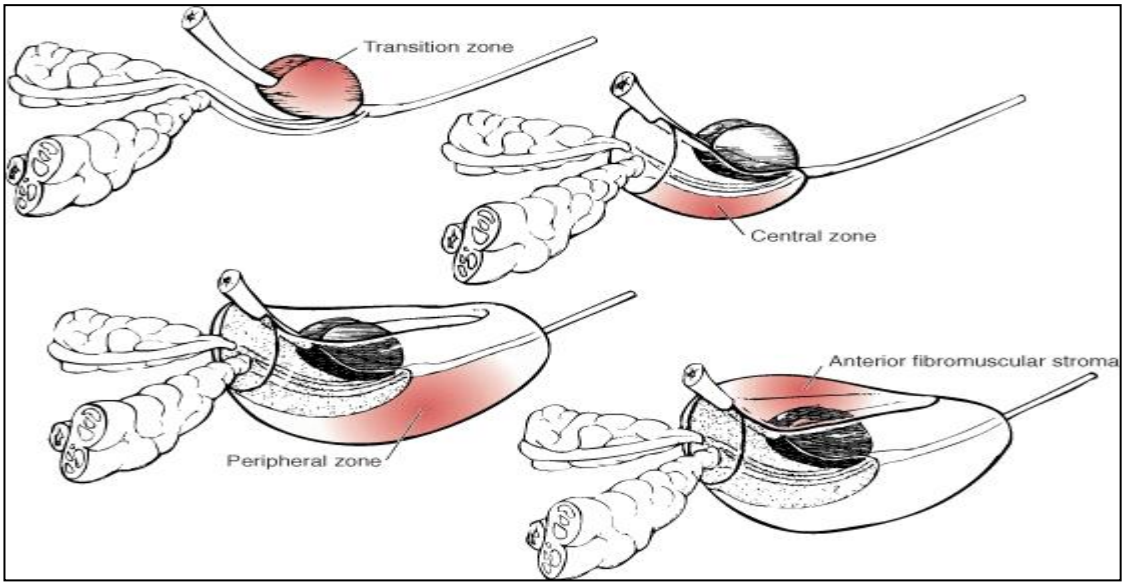

Figure 1.3: Prostate cancer originating from different zones of prostate gland [8]

1.4-Effect of Hormones and Growth Factors on Normal Prostate Gland and Prostate Cancer

Androgen, Vitamin D and insulin like growth factor I (IGF-I) play an important role in the growth of the normal prostate gland. Androgen and Vitamin D act in an opposing way. Androgen stimulates cell proliferation and Vitamin D inhibits cell proliferation. Both interact at various levels, with one end-point of both being the IGF-1 axis [7]. In most of cases, any abnormality in the pathways of these hormones may result in abnormal hyperplastic growth or may be associated with the presence of PCa.

1.4.1-Effect of Androgen and Androgen Receptors

Testosterone controls cell division in the prostate gland. After diffusing into the cell it is converted irreversibly into 5α-dihydrotestostrone (DHT) by the catalytic activity of enzyme 5α-reductase type 2. Both testosterone and DHT can bind to the AR, although DHT has 2- to 10-fold greater affinity for the AR and produces conformational changes in the receptors, dimerisation and transcriptional activity. In the early stage, 80-90% of PCa are dependent upon AR activity. However, androgen ablation therapy ultimately fails, as prostate cancer progresses to a hormone refractory state. AR is expressed throughout PCa progression and persists in the majority of patients with hormone refractory disease. The main cause of failure of androgen ablation is the alteration in the expression of AR co-regulators and mutation of the AR [7, 9].

1.4.2-Vitamin D Pathway

Vitamin D is responsible for maintaining normal concentrations of calcium and phosphorus in blood plasma. It is formed in the skin by sunlight-stimulated conversion of 7-dehydrocholesterol. The vitamin D receptor (VDR) regulates the transcription of VDR-responsive genes by binding with 1α,25-hydroxyvitamin D3 (1,25D3) after relocating into the nucleus. In one study, various PCa cell lines were treated with 1,25D3 and it was observed that it crippled the growth of the cells via multiple mechanisms, which include cell cycle arrest, the induction of apoptosis, and regulation of growth factor signalling. It was also observed in a separate study that high levels of 1,25D3 resulted in lower level of PCa risk especially in older males [7,10].

1.4.3-Growth Factors

Abnormalities in certain growth factors result in the occurrence of PCa. These include insulin-like growth factors I and II (IGF-I and -II), epidermal growth factor (EGF), vascular endothelial growth factor (VEGF), platelet-derived growth factor (PDGF), and transforming growth factor (TGF)-β. IGF is thought to play an important role in the development of the prostate and it regulates cell growth by interacting with IGF-IR (IGF-I receptor). AR and VDR produce some of their effects through IGF-I [7,8]. It is found that many prostate xenograft models express both IGF-I and -II as well as receptors for each. PC-3, an androgen-independent PCa cell line, secretes IGF-II. In addition, experiments indicate that IGF-II levels are increased in adenocarcinoma cells, suggesting a role in prostate carcinogenesis. Chan and colleagues observed that high levels of plasma IGF-I are observed in PCa. Further, there is an association between the circulating IGF levels and prostate cancer risk and it increased the detection rate of prostate cancer over PSA alone [7,8].

1.5-Screening of Prostate Cancer

There are various techniques available for the diagnosis and monitoring of PCa. The commonly used methods to identify and diagnose PCa include DRE (digital rectal examination), PSA (prostate specific antigen) levels, needle biopsy and Gleason score. Along with these traditional methods for the diagnosis of PCa there are various modern imaging modalities, which are gaining popularity because of their accuracy. These include CT (computed tomography) [11], MRI (magnetic resonance imaging) [12], SPECT (single photon emission computed tomography) and PET (positron emission tomography) [13,14]. Among the molecular imaging techniques, PET is the most sensitive and has been applied in the diagnosis of PCa [15]. PET is a non-invasive imaging technique. It involves injection of a radiopharmaceutical followed by imaging. The imaging protocol depends upon the radionuclide, its physical half-life, decay mode, chemistry for tracer preparation, *in vivo* kinetics and availability/cost.

1.5.1-DRE, PSA and Needle Biopsy

Normally these three screening tests are carried out together. In DRE the doctor or nurse feels the prostate gland to assess any irregularity in its size and shape [5]. In one study DRE and PSA were compared and it was observed that DRE has poor performance if

PSA blood levels are low [16]. Usually biopsy is done after the blood test to check the PSA level, since if it is done before then it might raise the PSA levels in the blood. In needle biopsy, a thin needle is inserted through rectum and urethra to collect samples from the prostate gland and these are then further analysed to assess the Gleason score [5].

1.5.2-Gleason Score

The Gleason score was developed by Donald Gleason in 1974 when very little was known about the disease and it is still used to identify PCa. The Gleason score is a system to grade the aggressiveness of the tumour. The Gleason grade has values from 1-5, and these values are assigned to the different biopsy samples. In the end the Gleason grades given to the different biopsy samples are added up to give the Gleason score and its value ranges from 2-10. The higher the value the more aggressive is the cancer and it helps in staging of the cancer and ultimately management by providing proper treatment to the patient. Conservative management is a reasonable option for Gleason score 2 to 4 cancer and for some patients with Gleason score 5 to 6 cancer depending upon the disease progression [17]. Prostatectomy or radiation therapy (RT) is recommended for Gleason score 7 to 10 cancer [5, 18].

1.6-Current Methods for Imaging Prostate Cancer

The diagnostic imaging methods available include CT [11], MRI [12], SPECT and PET [13,14]. Among all molecular imaging techniques, PET is the most sensitive and has been applied in the diagnosis of PCa [15]. The two critical needs for PET imaging of PCa are early detection of primary lesions and accurate localisation of PCa bone metastasis. However, the most commonly used PET tracer ^{18}F-FDG (fluorodeoxyglucose) is not very successful in imaging PCa. The main reason for this is that the glucose utilisation in well-differentiated PCa is often low because expression of GLUT-1 transporters is lower than in other tumour types, which leads to the low uptake of ^{18}F-FDG and poor image contrast [19]. Additionally, the intense accumulation of ^{18}F-FDG in the urinary bladder, which is in close proximity to the prostate, often overshadows the tumour uptake and no correlation was observed between tumour grade/stage and ^{18}F-FDG uptake in PCa [20]. Zaheer *et al.* in their review of new agents and techniques for imaging PCa have shown that although there are no definitive markers that can predict tumour progression for PCa, more careful study and validation

of markers such as PSMA and AR may provide a clue in approaching this pressing clinical issue [21].

Generally speaking, AR radiolabelled ligands can be divided into two main structural classes, steroidal (such as ^{18}F-FDHT) and nonsteroidal (such as flutamide and bicalutamide, labelled with ^{11}C), or into two different functional classes, androgenic and anti-androgenic [22,23]. ^{18}F-FDHT (fluoro-5α-dihydrotestrone) (Fig-1.4) was developed as a useful PET tracer for androgen dependent PCa [24,25].

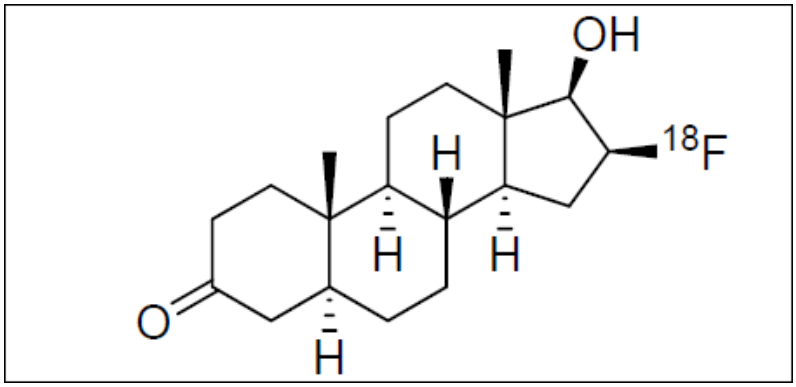

Figure 1.4: Structure of 18F-FDHT (fluoro-5α dihydrotestrone), a steroidal AR ligand.

FDHT is a structural analogue of 5R-dihydrotestosterone, a principal intraprostatic form of androgen. In the relevant study of fluorinated androgen analogues in baboon, performed by the Welch group, the uptake of FDHT in the prostate was blocked by co-administration of cold testosterone (reduced about 10-fold) [26]. To date, FDHT appears to bind specifically to androgen receptors *in vivo* and showed the most favourable targeting properties for non-invasive imaging among all receptor-binding radiotracers studied previously. In other research, ^{18}F-FDHT presents some advantages such as fast tumour uptake and prolonged retention of radioactivity observed in human studies. However, limitations such as rapid metabolic rate of this labelled compound have been observed [24-27].

Nonsteroidal AR radioligands, (R)-[^{11}C]-dimethylaminehydroxy-flutamide derivative (Fig-1.5), were designed, synthesised and radiosynthesised by Jacobson *et al.* in 2006 [28]. These compounds have an electron-rich group (dimethylamine) located on the methyl moiety, which may confer a better stability to the molecule. Additionally, they

serve as an anchor for carbon-11 labelling in a more straightforward approach than labelling with fluorine-18 or bromine-76.

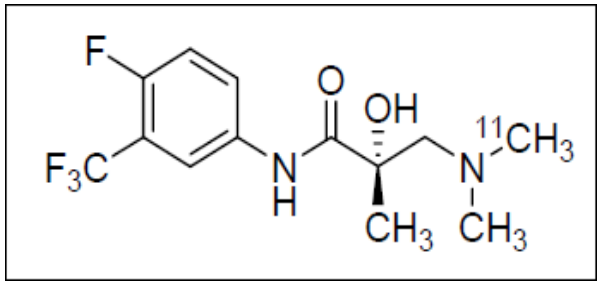

Figure 1.5: Non-steriodal AR ligand (R)-[^{11}C]-dimethylaminehydroxy-flutamide

1.7-PSMA and PCa

The most extensively studied antigen in PCa for antibody-based imaging is PSMA (prostate specific membrane antigen) [29]. It is expressed in virtually all PCa. Recent studies have suggested that PSMA is also expressed in tumour associated neovasculature [30,31]. Its molecular weight is 100 kDa [32]. It contains an intracellular domain of 1-18 amino acids. Although it is quite small in size, the cytoplasmic domain interacts with a number of proteins and has a major impact on the localisation and molecular properties of PSMA. It has a transmembrane domain of 19-43 amino acids and an extracellular domain of 44-750 (Fig-1.6) amino acids [32].

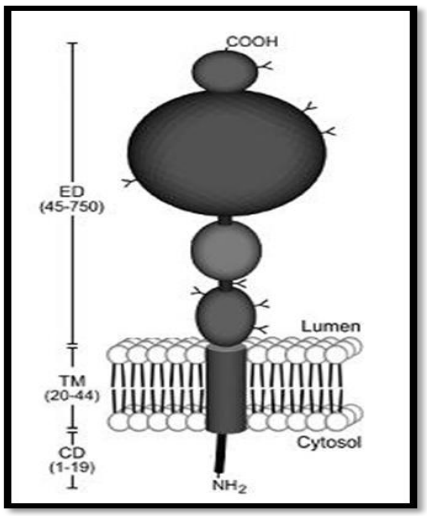

Figure 1.6: Schematic diagram of the globular nature of Prostate-Specific Membrane Antigen (PSMA). It has a small cytoplasmic domain (CD) which anchors it to the cell, a hydrophobic transmembrane domain (TM), and a large extracellular domain (ED) [32].

One of the many functions of PSMA is to hydrolyse peptide bonds between *N*-acetylaspartate and glutamate in the abundant neuropeptide *N*-acetylaspartyl glutamate (NAAG) and the glutamyl linkages in pteroylpolyglutamate, respectively, as it contains *N*-acetylated linked acidic dipeptidase (NAALADase) and folate hydrolase (FOLH). Thus this enzyme has been referred to alternatively as glutamate carboxypeptidase II (GCP-II) and folate hydrolase 1 (FOLH1) [32].

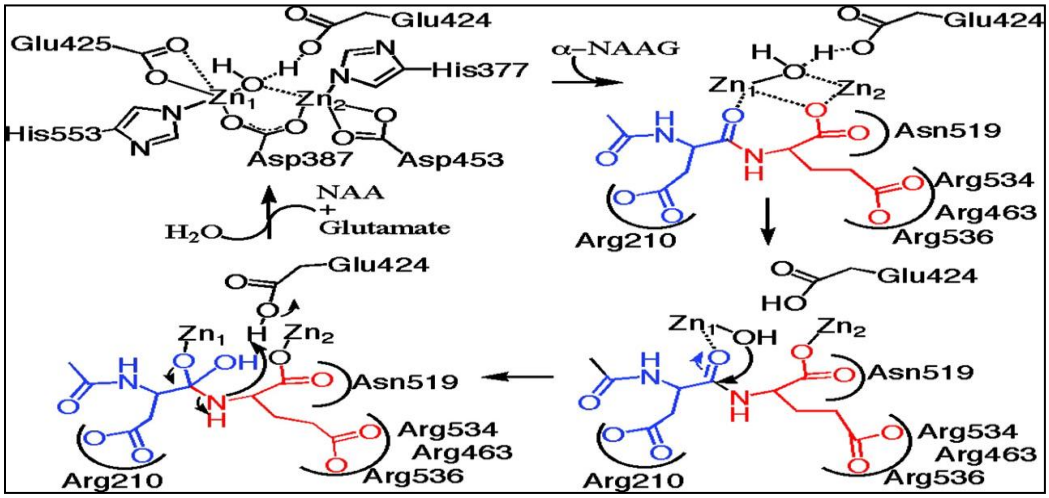

Figure 1.7: A mechanistic scheme for α-NAAG (glutamate is red, and NAA is blue) binding and cleavage by PSMA (black). The zinc-binding PSMA residues are assumed to remain bound during the reaction mechanism. The C-terminal carboxyl group binds the zinc ions in a bridging fashion, and there are electrostatic interactions between the glutamate side chain and the arginine patch and the aspartate side chain and Arg-210. The zinc-bound water molecule is poised to attack the peptide bond of the bound substrate, leading to a tetrahedral intermediate, bond cleavage, and product dissociation. An analogous mechanism would be expected for the cleavage of α-NAAG by NLD2 [33].

The crystal structure of PSMA clarifies the epitopes recognised by monoclonal antibodies being studied for applications in cancer imaging and therapy. The epitope for the J591 antibody that is in clinical trials has been mapped by using truncated PSMA constructs to residues 153–347 [33]. The structure reveals that this region corresponds to the majority of the apical domain, which is distant from the membrane surface and hence generally exposed and accessible. The PSMA structure shows that Asn-476 is distant from the apical domain and is instead located in the membrane-proximal region of the molecule, where it is less accessible to antibodies [34]. The apical domain of PSMA (also called the protease-associated domain) consists of two β-sheets, three α-helices, and one helical turn. It forms one side of the substrate-binding cavity (residues 687-704). Another important function of the helical domain is in forming the dimer interface, which involves three helices. PSMA can convert between a dimeric and

monomeric form *in vitro* by addition of metal chelators or changes in salt concentration; only the dimeric form of PSMA has folate hydrolase and naaladase activity and is expressed on the surface of prostate cells. By removing the 15 C-terminal (721-747) residues in PSMA hinders the enzymatic activity. The crystal structure reveals two zinc atoms which are coordinated by three endogenous ligands: a histidine (His-553 or -377), a terminal aspartate (Asp-453) or glutamate (Glu-425), and a bridging aspartate (Asp-387). Along with this, a water ligand asymmetrically bridges the zinc ions. Another residue that could potentially act as an active site base is Tyr-552 [33].

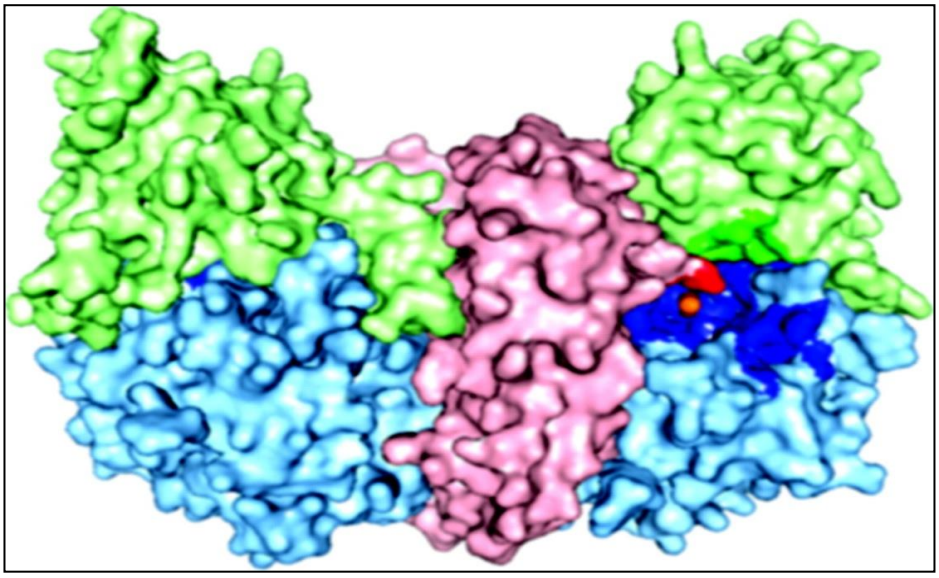

Figure 1.8: PSMA surface rendering in which the helical domain is light red, the apical domain is light green, the protease domain is light blue, and zinc ions are orange. The residues lining the substrate-binding cavity are highlighted in a darker version of the color corresponding to the domain from which the residue originates [33].

In one of the studies PSMA is reported as a noncovalently associated homodimer. It was observed that the extracellular domain is sufficient for dimerization and that dimerization is required for enzymatic activity. It was also observed that PSMA dimers displayed a native conformation and possessed high-level carboxypeptidase activity and monomers did not display this behavour. The stability of the dimer is dependent upon the presence of metal ions, such as Zn^{2+} in the active site of PSMA. However, other metal ions (e.g., Ca^{2+}) stabilize the dimer. It was also observed that regardless of the initial oligomeric state of the protein, high salt concentrations promote dimerization, whereas metal-chelating agents dissociate dimers into monomers [35].

1.8-Small Molecules and PCa

In the case of radiolabelled peptides for PCa imaging, bombesin (BBN) peptides and their derivatives, which can bind to the GRPR (gastrin releasing peptide receptor), are the most popular choice [36]. The full length version (^{64}Cu-DOTA-[Lys3]BBN) or C-terminal truncated form of BBN (^{64}Cu-DOTA-Aca-BBN) can be used for GRPR targeting *in vivo* [37]. One study investigated the importance of various aliphatic linkers between the BBN analogue and the DOTA chelator to the imaging characteristics of the tracer. It was concluded that the use of amino acid linkers (combination of glycine, serine and/or glutamic acid) between the DOTA, NOTA and CB-TE2A chelator and the BBN analogue could reduce non-specific tissue uptake, while maintaining good PCa uptake of the tracer [38,39,40]. However in a more recent study it was observed that negatively charged linkers may minimize non-specific binding and decrease overall background. These negatively charged linkers have been used to connect urea inhibitors and bulky radionuclide chelates for *in vivo* imaging and biodistribution studies with the radiolabeled tracers [41]. In one study of five ^{64}Cu-labeled inhibitors of PSMA based on the lysine–glutamate urea scaffold used a variety of macrocyclic chelators, namely NOTA, PCTA, Oxo-DO3A, CB-TE2A, and DOTA, to determine which provides the most suitable pharmacokinetics for *in vivo* PET imaging. The favorable kinetics and high image contrast provided by CB-TE2A chelated ^{64}Cu suggest it as the most promising among the candidates tested. That could be due to the higher stability of ^{64}Cu-CB-TE2A as compared with ^{64}Cu-NOTA, ^{64}Cu-PCTA, ^{64}Cu-Oxo-DO3A, and ^{64}Cu-DOTA chelates *in vivo* [42].

Multi-presentation of a targeting molecule on a single entity has been recognized as a practical way for imaging signal amplification. In one study image signal amplification was achieved by using a bivalent imaging probe design built upon a bifunctional chelator scaffold using a small molecular PSMA inhibitor (GPI: 2[(3-amino-3-carboxypropyl)(hydroxy)(phosphinyl)-methyl]pentane-1,5-dioic acid) for specific PSMA detection and imaging quantification. For study purposes both monovalent (H_2CBT1G) and bivalent (H_2CBT2G) conjugates were prepared and labelled with ^{64}Cu for evaluation. PET imaging studies were conducted on mouse xenograft models established with a $PSMA^+$ cell line, LNCaP, and $PSMA^-$ PC3 and H2009 cell lines. It was observed that bivalent H_2CBT2G gave 4-fold enhancement of PSMA binding affinity compared to monovalent H_2CBT1G [43].

Furthermore, in another study it was demonstrated that the ^{86}Y-labelled peptide (MP2346 (DOTA-(Pro(1),Tyr(4))-bombesin(1-14)) exhibited better PET image quality in all PCa models for delineation of GRPR (gastrin-releasing peptide receptor)-positive tumour as compared to ^{64}Cu-MP2346 due to lower uptake in clearance organs and lower background activity [44]. ^{68}Ga was also used to label the dual-receptor targeting heterodimer, BBN-RGD [45]. In one investigation it was observed that the ^{99m}Tc-labelled PSMA-targeted small molecule ^{99m}Tc-MAS_3-NHS (^{99m}Tc-S-acetyl-mercaptoacetyltriserine-N-hydroxysuccinimide ester) demonstrated gamma imaging of living human PCa cells. The ^{99m}Tc labelled complex takes only 25 min to prepare and gives greater than 99% radiochemical purity [46].

In one comparison study, 15 patients were imaged within 7 days and the rate of detection of recurrent PCa was measured by PET/CT using anti-3-^{18}F-FACBC (anti-1-amino-3-^{18}F-fluorocyclobutane-1-carboxylic acid), a new synthetic amino acid in comparison with ^{11}C-choline, an established tracer used for detection of PCa relapse [47]. ^{11}C-choline is considered sufficient for restaging patients with rising PSA levels. Anti-3-^{18}F-FACBC uptake was found to correlate with the expression level of the amino acid system ASC (alanine, serine, cysteine) on the PCa cells, along with the expression of LAT1 (sodium-independent "L" large neutral amino acid transport system).

Physiological uptake of anti-3-^{18}F-FACBC is different from ^{11}C-choline. Anti-3-^{18}F-FACBC showed uptake in the pancreas and liver, and mild and diffuse uptake in the bone marrow. On the other hand ^{11}C-choline showed uptake in spleen and kidneys along with liver, pancreas and bone marrow. The detection rates using the two compounds were determined and the target–to-background ratio (TBR) of each lesion was measured. No adverse reactions were observed. The detection rate with ^{11}C-choline PET/CT was 20% and anti-3-^{18}F-FACBC PET/CT 40%. The TBR of anti-3-^{18}F-FACBC was greater than that of ^{11}C-choline, as were image quality and contrast. These results indicate that anti-3-^{18}F-FACBC may be superior to ^{11}C-choline for the identification of disease recurrence in the setting of biochemical failure. Further studies are required to assess efficacy of anti-3-^{18}F-FACBC in a larger series of prostate cancer patients [47].

It was also observed that ^{11}C-choline (a quaternary ammonium salt containing the *N*,*N*,*N*-trimethylethanolammonium cation) as well as ^{11}C-acetate have insufficient diagnostic accuracy for the staging of the primary tumour and are unable to differentiate

PCa from benign prostate hyperplasia, chronic prostatitis and high-grade intraepithelial neoplasia [48]. Regarding lymph node staging, choline tracers have demonstrated a high specificity. Unfortunately, the sensitivity is only moderate. For staging recurrent disease, sensitivity depends on the level of serum PSA (PSA should be >2 ng/ml). This applies to both choline and acetate. However, despite these limitations, a significant number of patients with recurrent disease can benefit from PET imaging by a change in treatment planning [48]. ^{11}C-methionine is one of the earliest amino acid based PET tracers studied for imaging of androgen independent PCa. For PSMA targeting (^{11}C-DCMC and ^{18}F-DCFBC) have been developed [49,50].

In one study ^{18}F-Choline was used to image 46 consecutive patients with PCa previously treated by definitive radiotherapy and with suspicion of relapse with negative or inconclusive conventional imaging. Twelve out of 46 were treated with brachytherapy and 34 with external beam radiation therapy. Twenty-three patients were under androgen depriviation therapy at the time of the examination. PSA was measured within 1 month before the treatment. Patients were subdivided into four groups according to their PSA level: $1.0 < PSA \leq 2.0$ ng/ml (11 patients), $2.0 < PSA \leq 4.0$ ng/ml (16 patients), $4.0 < PSA \leq 6.0$ ng/ml (9 patients) and $PSA > 6.0$ ng/ml (10 patients). Correlation between androgen depriviation therapy and positive detection rate was investigated as well as between PSA and distribution of metastatic spread. The overall positive detection rate of ^{18}F-Choline was 80.4 %. Positive detection rate of ^{18}F-Choline was not influenced by androgen depriviation therapy (82.6 %). The majority of the patients (59 %, 22/37 patients) showed local relapse only, confined to the prostatic bed; 22 % of the PET/CT-positive patients (8/37 patients) showed distant relapse only (bone localizations in all of them), while the remaining 19 % (7/37 patients) showed both local and distant (lymph node and bone) spread. ^{18}F-Choline is proposed as a first-line imaging procedure in restaging prostate cancer patients primarily treated with radiotherapy [51].

Recently, synthesis, *in vitro* binding, biodistribution and imaging of two new ^{68}Ga-labelled, conjugated PSMA inhibitors were reported. These compounds demonstrated PSMA-specific tumour imaging *in vivo* [52]. A small-molecule based approach using radiolabelled urea-based PSMA inhibitors as imaging agents has shown promise for PCa imaging. ^{18}F labelled phosphoramidate is a representative of a new class of PSMA

targeting peptidomimetic molecules that shows great promise as imaging agents for detecting PSMA+ prostate tumours [53]. The design strategy of this class of compounds is largely based on the binding features of PSMA endogenous substrates and potent inhibitors. Phosphoramidate scaffold is used as a targeting element for prostate cancer imaging. N-succinimidyl-4-^{18}F-fluorobenzoate (^{18}F-SFB) was conjugated to S-2-((2-(S-4-amino-4-carboxybutanamido)-S-2-carboxyethoxy)-hydroxyphosphorylamino)-pentanedioic acid (phosphoramidate-PSMA inhibitor), yielding S- 2-((2-(S-4-(4-^{18}F-fluorobenzamido)-4-carboxy-butanamido)-S-2 carboxyethoxy)hydroxyphosphoryl-amino)-pentanedioic acid, which has 20-fold more inhibiting capacity. In another clinical study direct comparison of ^{68}Ga-labelled small molecule targeting PSMA was done with ^{18}F-choline and it was observed that ^{68}Ga-Glu-NH-CO-NH-Lys(Ahx)-HBED-CC showed better detection of small lesions compared to ^{18}F-choline in patients with low PSA values. The main reason for this better detection is high intensification of radiopharmaceutical in small metastasis and quick clearance from background. Considering the growing accessibility of ^{68}Ga from a generator and the ease of labelling, ^{68}Ga PSMA-targeted imaging has high potential to become a valuable diagnostic agent in recurrent PCa and therapy monitoring [54,55,56].

In more recent research, a novel ^{18}F-labelled small molecule inhibitor of PSMA enzymatic activity (BAY 1075553), a 9:1 mixture of (2*S*,4*S*)- and (2*R*,4*S*)-2-[^{18}F]fluoro-4-phosphonomethyl-pentanedioic acid), was synthesized from pure precursors dimethyl-2-{[bis(benzyloxy)phosphoryl]methyl}-4-(tosyloxy)pentanedioate. *In vivo* imaging and biodistribution studies were conducted in mice bearing LNCaP, 22Rv1 and PC-3 tumours. The radiotracer showed high tumour accumulation specific to PSMA-positive tumour-bearing mice. Fast clearance resulted in overall low background signals in other organs except for high uptake in kidney and bladder due to renal elimination of the compound. A modest uptake into bone was observed which decreased over time, indicating organ-specific uptake. Pharmacokinetic, toxicology and safety pharmacology studies support the application of BAY 1075553 in a first-in-man microdose study with single i.v. administration [57].

For treatment of PCa it was observed that PSMA-VRP (vaccine replicon particles) increased the expression of cell surface PSMA *in vitro*. Anti-PSMA responses were produced after a single injection of PSMA-VRP, and these responses were boosted on repeated dosing. The cellular immune responses in BALB/c and C57BL/6 mice were

determined to be directed toward different defined peptide sequences within PSMA. Anti-PSMA immunity was elicited with a favourable safety profile both in mice and in a rabbit toxicology study and it represents a promising approach for immunotherapy of prostate cancer [58]. Another study which involving Phase I/II clinical trials for the treatment of prostate cancer showed 50% reduction in PSA using dendritic cells and PSMA peptide HLA-A0201 [59].

Molecular Insight has developed a number of radiopharmaceuticals both for diagnostic and therapeutic purposes. One of these is Trofex, which is radiolabelled with ^{123}I. It is a small molecule inhibitor of PSMA which binds to PCa cells. It could play an important role in diagnosis and monitoring of PCa and potentially therapy with ^{131}I-Trofex [60]. A Phase II study is ongoing in metastatic PCa. In parallel studies using the same targeting principle, ^{99m}Tc-MIP-1340 and MIP-1404 (Trofolastat) are being evaluated. MIP-1404 was evaluated in two Phase I studies to differentiate clinically significant PCa from silent or indolent**.** ^{99m}Tc-MIP-1404 cleared rapidly from the circulation, showed minimal urinary activity, but moderate (15-20%) liver and kidney uptake. In men with metastatic PCa, ^{99m}Tc-MIP-1404 rapidly accumulated in lesions in lymph nodes and bone as early as 1 h post injection. In this study it was also observed that SPECT/CT images demonstrated excellent lesion contrast. This result led to a multi-centre, international Phase II study with ^{99m}Tc-MIP-1404 in patients scheduled for prostatectomy which is in progress [61]. ^{131}I-MIP-1095 administered intravenously circulates throughout the body, binds to the extracellular domain of PSMA and is subsequently internalised by PCa cells. In pre-clinical tumour models, ^{131}I-MIP-1095 was retained within the prostate cancer cell, allowing beta particles from ^{131}I to cause targeted cell death of PCa. One of the experiments employed spheroids derived from LNCaP prostate carcinoma cells to determine the radiosensitizing potential of various chemotherapeutic drugs in combination with ^{131}I-MIP-1095. It was also used in studies to detect and treat metastatic castration resistant prostate cancer (mCRPC). To estimate radiation dosimetry, tissue kinetics has been studied for the potential therapeutic use of ^{131}I-MIP-1095 in men with mCRPC. In a study 28 consecutive patients were treated with a single cycle of ^{131}I-MIP-1095. Sixteen patients with known prostate cancer underwent PET/CT imaging 1, 4, 24, 48 and 72 h post injection of ^{124}IMIP-1095. The images showed excellent tumour uptake and moderate uptake in liver, proximal intestine and within a few hours post-injection also in the kidneys. High uptake values

were observed only in salivary and lacrimal glands. Dosimetry estimates for ^{131}I-MIP-1095 revealed that the highest absorbed doses were delivered to the salivary glands (3.8 mSv/MBq), liver (1.7 mSv/MBq) and kidneys (1.4 mSv/MBq). The absorbed dose calculated for the red marrow was 0.37 mSv/MBq. PSA values decreased by >50% in 60.7% of the men treated. Of men with bone pain, 84.6% showed complete or moderate reduction in pain. No adverse effects on renal function were observed. Targeted tumour therapy was able to deliver unprecedented doses to tumour lesions. Lymph node and bone metastases were exposed to estimated absorbed doses of 300 Gy [62].

Various chemotherapeutic drugs were investigated for synergistic interaction: olaparib (PARP-1 inhibitor), topotecan (topoisomerase I inhibitor), docetaxel (mitotic spindle-targeting agent), nutlin-3 (inhibitor of the P53-MDM2 interaction) and DSF:Cu (the copper-chelated form of disulfiram). It was observed that DSF:Cu enhanced the efficacy not only of external beam radiation but also of targeted radionuclide therapy [63]. MIP-1500 and -2100 are second generation analogues of 1095 and are under further investigation [60,64]. In one study with MIP-1466, considerable reduction (50%) in the blood PSA level was observed in the patients with late metastatic PCa [60].

In another study, four PSMA inhibitors MIP-1427, MIP-1404, MIP-1428, and MIP-1405 derived from the glutamate-urea-glutamate or glutamate-urea-lysine pharmacophores conjugated to CIM or TIM chelators were radiolabeled with ^{99m}Tc and evaluated *in vitro* and *in vivo*. It was observed that ^{99m}Tc-MIP-1404 showed the best combination of high tumour uptake and rapid clearance from kidney and non-target tissues. ^{99m}Tc-MIP-1404 specifically bound to PSMA *in vivo* [65].

1.9-Antibodies and PCa

Radiolabelled antibodies against PSMA have been used in the clinic for diagnosis of PCa and the ^{111}In-labelled monoclonal antibody (7E11), capromab pendetide (Prostascint), has been extensively evaluated for SPECT imaging applications. The PSMA epitope recognised by monoclonal antibody (mAb) 7E11 is located in the cytoplasmic (i.e. intracellular) domain. In theory, antibody imaging with ^{111}In-capromab allows for a specific molecular diagnosis of primary and secondary PCa lesions. A limitation of ^{111}In-capromab imaging is that it is suboptimal for the detection of bone metastases, and is significantly less sensitive than bone scans in this regard. Furthermore, ^{111}In-capromab is not currently considered a promising agent for lesion

detection within the prostate gland or for determining extracapsular extension, primarily because the internal target of ^{111}In-capromab requires that cell membranes be damaged before the antibody can bind. Excess unbound antibody leads to high background signal and poor spatial resolution [66]. Recently, an *in vivo* method to quantify antibody uptake by using ^{111}In-capromab SPECT combined with CT was developed [67].

The immunohistochemical characteristics of the antibodies 7E11, J591, J415, PEQ226.5 and PM2J004.5 have been studied. Each of these antibodies binds to a distinct epitope of PSMA. Their characteristics were evaluated using the steptavidin-biotin method [31]. It was also observed that 7E11 is not available for binding in viable PCa cell lines because it recognises an intracellular epitope [33]. However, J591, J533, J415 and E99 showed binding with viable PCa cell lines, as they recognise extracellular epitopes [33]. It was also found that PSMA has two distinct extracellular epitopes, PSMAext1 and PSMAext2 [68]. Laser scanning confocal microscopy was used to demonstrate that J591 accumulates in endosomes after internalisation [68]. Another antibody (MU J591) that recognises the extracellular domain of PSMA has been designed and investigated for localisation and staging of PCa [69]. In one approach, docetaxel encapsulated targeted nanoparticles developed using PLA and PLGA polymer systems were conjugated with the A10 2′-fluoropyrimidine RNA aptamers. These nanoparticles target PSMA on the surface of PCa cells (LnCaP) and are engulfed by these cells specifically and efficiently, *in vitro* and *in vivo* resulting in significantly enhanced *in vitro* cellular toxicity as compared with nontargeted nanoparticles that lack the PSMA aptamer [70,71,72]. More recently, J591-targeted controlled release nanoparticles have been developed for effective gene delivery to prostate cancer cells [73,74]. An anti-PSMA antibody was also conjugated with QDs (quantum dots, tiny particles of a semiconductor material such as CdSe or ZnS, ranging from 2 to 10 nanometers in diameter) that emit light in the near-infrared (NIR) 800 nm range (QD800). QD800 is superior and more sensitive than QD655 for detecting human C4-2 and C4-2B prostate tumours in mouse tibia and is not compromised by autofluorescence interference. QD800 accumulated maximally in intratibial sites within 30 min after tail vein administration. The QD800 images could be detected <1 h after tail vein administration. This represents an approximately 1000-fold better sensitivity than other currently available technologies [75].

In one of the experiments superparamagnetic iron oxide nanoparticles (SPIONs) were attached to an antibody (J591) that binds to the extracellular domain of PSMA, to specifically enhance the contrast of PSMA-expressing prostate cancer cells. Conjugation of mAb J591 to commercial SPIONs was achieved using a heterobifunctional linker, sulfo-SMCC. Two types of prostate cancer cell lines LNCaP (PSMA+) and DU145 (PSMA−) were used in the experiments. MRI and cell uptake experiments demonstrated the high potential of the synthesized nanoprobe as a specific MRI contrast agent for detection of PSMA-expressing prostate cancer cells [76].

In recent years there has been massive development in antibody design. Full length mAb are broken down into various fragments. The smaller size and target affinity of the fragments affects the penetration properties into tissues which are inaccessible to full-size mAbs, clears rapidly from blood circulation and this also matches with the short half-life of some of the radionuclides [77]. The engineering of single chain variable region fragments (scFv) of mAb is another route to improve their kinetics for imaging. Full length mAb have long serum half life, but due to the short half-life of ^{68}Ga blood clearance needs to be rapid [78]. The scFv can be produced in large quantitites and is cost effective as compared to the full length mAb [79]. Lack of the Fc region in single chain fragments results in low immunogenicity and makes them better therapeutic agents. Rapid clearance also minimises the damage to the healthy tissue compared to the full length mAb except for the kidneys [79].

A chimeric mAb that binds phosphatidylserine was labelled with ^{74}As for PET imaging of PCa in a rat model [80]. ^{124}I-labelled IG8 mAb against PSCA (prostate stem cell antigen) was more PCa specific [81]. A hu1G8-based minibody was engineered for PET imaging of PCa in xenograft models upon ^{124}I-labelling [82]. PET imaging results with the diabody, engineered from the same parent mAb, were also encouraging [83]. In one of the recent studies the scFv was engineered starting from the variable heavy and light domains of the murine anti-PSMA mAb D2B, a small protein that can better penetrate tissue. It was then analysed *in vitro* for activity, stability, internalisation ability and *in vivo* for targeting specificity. Maintenance of function and immunoreactivity as well as extremely high radiolabelling efficiency and radiochemical purity were demonstrated by *in vitro* assays and under different experimental conditions. Despite its monovalent binding, D2B-scFv retained a good strength of binding and was able to internalise

around 40% of bound antigen. *In vivo* it specifically target only PSMA expressing PCa xenografts. Due to these advantageous properties, D2B-scFv has the potential to become a good theranostic reagent for early detection and therapy of PCa [84]. Another prostate tumour-targeting scFv, UA20, along with a nonbinding control scFv, N3M2, gave promising results when labelled with ^{99m}Tc and evaluated for binding and rapid internalization into human PCa cells *in vitro* and *in vivo* using xenograft models. The tumour-to-blood and tumour-to-muscle ratios were 12:1 and 70:1, respectively. In contrast, the control antibody exhibited a tumour uptake of only 0.26 %ID/g, similar to that of muscle and fat. Kidney uptake was nonspecific, consistent with the route of excretion by scFvs [85].

One of the radionuclides which is used to radiolabel these mAb fragments is ^{99m}Tc, which is the most commonly used radioisotope in nuclear pharmacy. Radiolabelling of scFv with ^{99m}Tc tricarbonyl is achieved via a His-tag. The basis of ^{99m}Tc tricarbonyl kit formulation is disodium boron carbonate, which serves as CO source and reducing agent [86]. The group at the Paul Scherrer Institute and Pluckthun *et al.* have successfully developed a direct labelling protocol for scFv and minibodies carrying and N or C terminal His-tag with ^{99m}Tc tricarbonyl [87].

PSMA was also suggested as a marker for angiogenesis and could represent a target for deliverable agents recognising the prostatic tumour and serve as unique target for treatment of patients in their development of prostatic metastasis [88]. The J591 monoclonal antibody has been shown to deliver an alpha–emitting radionuclide (actinium-225) to PCa both *in vitro* and *in vivo*. *In vivo* studies conducted in male severe combined immune deficient (SCID) mice bearing PSMA-positive, subcutaneous LNCaP tumour demonstrated that tumour-specific uptake of ^{89}Zr-DFO-J591 could be visualised by both immuno-PET and CLI (Cerenkov luminescence imaging). Biodistribution studies were found to correlate well with both modalities [89]. The ^{64}Cu-labelled mAb 3/A12 showed high and specific uptake in PSMA-positive tumours and is an excellent candidate for prostate cancer imaging [90].

^{177}Lu-J591 was administered to thirty-five patients with progressing androgen-independent PCa. All patients underwent ^{177}Lu-J591 imaging, therapy and biodistribution determinations. The maximum tolerated dose (MTD) of ^{177}Lu-J591 was 70 mCi/m^2 and multiple doses of 30 mCi/m^2 were well tolerated. Acceptable toxicity,

excellent targeting of known sites of PCa metastases, and biologic activity in patients with androgen-independent PCa warrant further investigation [91]. At Johns-Hopkins University, Sedelear and colleagues designed two imaging and therapeutic drugs which are PSMA and PSA activated pro-drugs. They retooled chemotherapy agents for drug delivery, accurate treatment, monitoring and follow-up imaging drugs with a core of thapsigargin, a nonspecific highly cytotoxic agent. These therapeutic agents were modified by adding a tyrosine ring for imaging. The prodrugs are bound by a specific amino acid sequence, which causes them to be inactive until the sequence is clipped off by either PSMA or PSA proteases [5]. Provenge is another drug, created by Dendreon Ltd., which is reported to increase the survival rate for patients with PCa [92]. Progenics Ltd, which has now bought Molecular Insight, is currently working on development of two drugs for prostate cancer, both of which are PSMA based. Another novel antibody-drug conjugate (ADC) was generated for treatment purposes by linking a fully human PSMA mAb to chemotherapeutic monomethylauristatin E (MMAE), a potent inhibitor of tubulin polymerisation. The PSMA ADC was evaluated for antitumour activity *in vitro* and in a mouse xenograft model of androgen-independent PCa. The PSMA ADC eliminated PSMA-expressing cells with picomolar potency and >700-fold selectivity in culture. When used to treat mice with established human C4-2 tumours, the PSMA ADC significantly improved median survival 9-fold relative to vehicle or isotype-matched ADC without toxicity. Treatment effects were also manifest as a significant reduction in serum levels of PSA. Importantly, 40% of treated animals had no detectable tumour or measurable PSA at day 500 and could be considered cured. The findings support development of PSMA antibody-auristatin conjugates for therapy of PCa. The second drug is in Phase I clinical trials and involves a therapeutic recombinant protein vaccine, a genetically engineered form of PSMA protein combined with potent immunological stimulant, which is designed to stimulate patients' immune system to recognise and destroy PCa cells [58]. In a more recent article Lourdes Castaneda et al presented a novel acid-cleavable linker strategy for antibody-drug conjugation. Functional disulfide bridging of the single interchain disulfide bond of a trastuzumab Fab fragment yields a homogeneous antibody-drug conjugate bearing a thiomaleamic acid linker. This linker is stable at physiological pH and temperature, but quantitatively cleaves at lysosomal pH to release the drug payload [93].

In one investigation liposomes were loaded with ^{225}Ac which emits alpha particles and coupled with antihuman PSMA J591 antibody or with the A10 PSMA aptamer. The targeting selectivity, extent of internalization, and killing efficacy of liposomes were tested on monolayers of prostate cancer cells expressing PSMA and HUVEC induced to express PSMA. J591-coupled liposomes displayed higher levels of total specific binding to all cell lines than A10 aptamer-labeled liposomes. Cytotoxicity studies demonstrated that radiolabelled J591-labelled liposomes were most cytotoxic in killing PSMA-expressing cells including endothelial cells induced to express PSMA [94].

1.10-^{68}Ga

This project exploits gallium-68 (^{68}Ga), a generator produced positron emitting radionuclide with a half-life of 68 minutes. The most commonly used and successful PET tracer ^{18}F-FDG is not very useful in imaging some tumour types including PCa. The main reasons for this are low uptake of ^{18}F-FDG, poor image contrast, and intense accumulation of ^{18}F-FDG in the urinary bladder, which is in close proximity to the prostate, overshadowing tumour uptake. No correlation was observed between tumour grade/stage and ^{18}F-FDG uptake in PCa [19,20]. Recently, the application of ^{68}Ga-labelled peptides has attracted considerable interest for cancer imaging because of the physical characteristics of ^{68}Ga. Gallium, an element in group 13 of the periodic table, has two stable isotopes (^{69}Ga, ^{71}Ga) and 10 radioactive isotopes as shown in Table 1.

^{68}Ga is a positron emitter whose 68 minute physical half-life is compatible with the pharmacokinetics of many radiopharmaceuticals of low molecular weight such as antibody fragments, peptides, aptamers, and oligonucleotides. ^{68}Ga decays 89% by positron emission and 11% via electron capture and the average energy per disintegration is 740 keV [95]. The maximum positron energy of ^{68}Ga is 1.92 MeV, which is higher than ^{18}F (max=0.63 MeV) and thus would be expected to result in somewhat poorer spatial resolution. However, in one study of spatial resolution, which was done using Monte Carlo analysis, it was observed that there was no detectable difference between ^{18}F and ^{68}Ga in soft tissues in humans. ^{68}Ga can be introduced into biomolecules through chelators, which allows possible kit formulation and wide availability of the corresponding imaging agents [52]. This has stimulated interest in the development of ^{68}Ga-labelled compounds for medical imaging.

TABLE 1

Radioactive isotopes	Half-Life	Decay Mode	Type of Emission
^{64}Ga	2.63 min	EC to ^{64}Zn	β+
^{65}Ga	15.2 min	EC to ^{65}Zn	β+
^{66}Ga	9.5 h	EC to ^{66}Zn	β+
^{67}Ga	3.2 days	EC to ^{67}Zn	gamma
^{68}Ga	68 min	EC to ^{68}Zn	β+
^{70}Ga	21.1 min	EC to ^{70}Zn ,β- to ^{70}Zn	β- to gamma
^{72}Ga	14.1 h	β- to ^{72}Ge	β- to gamma
^{73}Ga	74.87 h	β- to ^{73}Ge	β-
^{74}Ga	8.1 min	β- to ^{74}Ge	β-
^{75}Ga	2.1 min	β- to ^{75}Ge	β-

Table 1- Radioactive isotopes of gallium, along with their half-life, decay mode and type of emission.

1.11-^{68}Ge/^{68}Ga Generator System

One of the benefits of ^{68}Ga is that it is easily available, as it is obtained from a ^{68}Ge/^{68}Ga generator system. The generator system is quite easy to handle, cost-effective and comparable to the ^{99}Mo/^{99m}Tc generator system in traditional nuclear medicine. ^{68}Ga can form complexes with chelators, either free or conjugated with biomolecules. These characteristics make ^{68}Ga an alternative to ^{18}F as a PET radionuclide for centres without a cyclotron and straightforward preparation of a tracer using radiometal chelation with a generator produced radionuclide, resulting in a kit type production of PET radiopharmaceuticals. That is the goal, once various technical and regulatory challenges have been overcome.

The daughter isotope ^{68}Ga has a half-life of 68 min and the parent isotope ^{68}Ge has a very long half-life of 271 days that allows routine manufacture, shipment, and use of the generator for up to 1 year while the chemical properties of ^{68}Ge and ^{68}Ga are sufficiently different to allow several different methods of efficient separation. The use of a generator allows the development, at least in principle, of a range of cold, freeze-dried kits, which can be reconstituted and labelled when required. There is a well

established coordination chemistry of Ga^{3+} which allows development of agents resistant to *in vivo* transchelation of $^{68}Ga^{3+}$. The preferred production route of ^{68}Ge is via the (p, 2n) reaction on a gallium target [95].

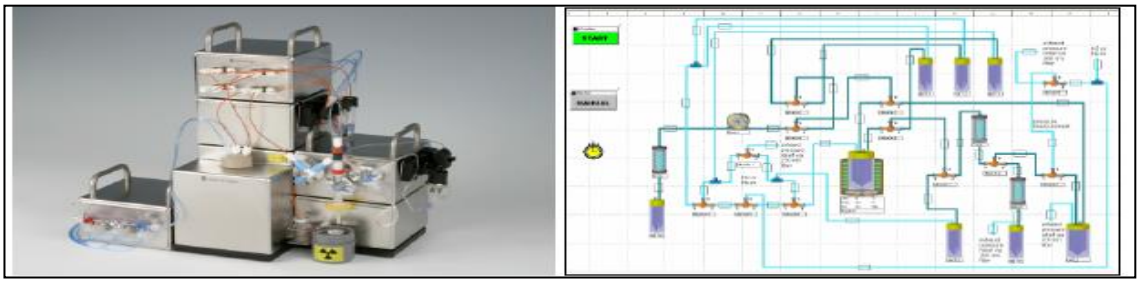

Figure- 1.9: Modular Lab by Eckert&Zeigler for the production of ^{68}Ga-DOTATOC.

Figure- 1.10: ^{68}Ge/^{68}Ga-Generator IGG100 **^{68}Ge/^{68}Ga-Generator (Obninsk)**

Usually the column in the generator is made up of solid oxides which can be organic or inorganic in nature and used to achieve the efficient separation of the daughter from parent radionuclide by elution with dilute HCl. The radioactivity in aliquots of the generator elute are measured using an ionisation chamber and a NaI(Tl) scintillation detector immediately after and 24-48 h later in order to determine the ^{68}Ge breakthrough in the eluate [96]. The generator eluates have been analysed for the content of trace metals by inductively coupled plasma atomic emission spectrometry (ICP-AES). In general, the second elution is used for labelling purposes instead of first because of its low metal content and low ^{68}Ge breakthrough [96]. There are at least four ^{68}Ga generators available in the market but this project is based on the Eckert & Ziegler TiO_2

based generator (IGG100) (Fig-1.10). One part of the experimental section in this work also includes the comparison of IGG100 with the Obninsk generator (Fig-1.10) from the same company. The column material in both generators is titanium dioxide. ^{68}Ge breakthrough in the case of Obninsk is 0.01% and IGG100 is 0.001%. Total impurities (Pb, Zn, Al, Ni, Cu) in case of IGG100 is <2 ppm (total) whereas in Obninsk it ranges from 5-150 ppm (total). Guaranteed useful life in both the cases is 1 y or 300 elutions. Both generators provide $^{68}Ga^{3+}$ in 0.1 M HCl [97].

1.11.1-Concentration and purification methods of the ^{68}Ga eluate

Different methods have evolved to purify and concentrate the ^{68}Ga generator eluate. It can involve a cation or anion exchange column or fractional elution. In the case of ModularLab, a microchromatography column carrying a strongly basic cation-exchange resin is used to concentrate the eluate and to reduce the acidity [97] (Fig-1.9). Zhernosekov *et al.* also used a cation exchange column, further improving the Rosch et al. technique [98]. They developed an efficient route for the processing of ^{68}Ga eluates, including the labelling and purification of biomolecules. They performed the preconcentration and purification of the generator eluate by using a miniaturised column with organic cation exchanger resin and hydrochloric acid/acetone as eluant. The purified fraction was used for the labelling of nanomolar amounts of octreotide derivatives either in pure aqueous form or in buffers. Greater than 97% of the initially eluted ^{68}Ga activity was obtained within 4 min as a 0.4 ml volume of HCl/acetone. The amount of ^{68}Ge was decreased by 10^4, whereas Zn(II), Ti(IV) and Fe(III) were reduced by 10^5, 10^2 and 10, respectively, after the processing of generator eluate. The processed ^{68}Ga fraction was directly transferred to a solution containing labelling precursor, DOTATOC. Greater than 95% radiochemical yield was obtained within 10 min by using manual labelling approach [99]. Ocak *et al.* described a fully automated approach for the synthesis of ^{68}Ga-labelled DOTA-peptides based on preconcentration and purification of the generator eluate by using both resin based and a disposable cation exchange cartridge [100].

Alternatively, in the case of a strong anion-exchange column, the column adsorbs ^{68}Ga in the form of ^{68}Ga anionic tetrachloro complex $[^{68}GaCl_4]^-$ present in 4 M HCl. This method removes any cationic impurities and concentrates the generator eluate. This strategy separates ^{68}Ge, but does not allow direct loading of ^{68}Ga onto the anion

exchange resin from 0.1 N HCl eluate. In this method the $^{68}Ge/^{68}Ga$-generator was eluted with 6 ml 0.1 N HCl, to which was added 30% HCl, making final HCl concentration of 4.0 M. The resulting solution was then passed through an anion-exchange column, trapping the ^{68}Ga. The ^{68}Ga was then eluted with small fractions of deionised water (50-200 µl). Finally, the pH was adjusted by adding sodium acetate [101]. Similarly, in Mueller *et al* method an anion exchange column was used to purify the generator eluate by conversion into the gallate anion $[^{68}GaCl_4]^-$ via the addition of concentrated HCl (5 M). It is trapped on the anion exchange cartridge and then subsequently eluted with a small volume of water directly into the buffer 4-(2-hydroxyethyl)-1-piperazineethanesulfonic acid (HEPES) for the labelling step. After labelling, further purification steps were necessary in order to remove HEPES. In addition, ^{68}Ge that might still be present was removed by solid-phase extraction, while the final product was eluted with ethanol [102]. Another method which involves both anion exchange and cation exchange columns was developed, taking advantage of the occurrence of different Ga species, both cationic and anionic, depending on varying pH and chloride concentrations. In this procedure, ^{68}Ga was trapped on a strong cation exchange cartridge (SCX) and then converted to $[^{68}GaCl_4]^-$ and eluted with a small volume of 5.5 M HCl. In step two, the $[^{68}GaCl_4]^-$ was adsorbed on a strong anion exchange cartridge (SAX) and $^{68}Ga^{3+}$ was subsequently eluted with water [102].

Another approach to overcome these problems is to fractionate the initial generator eluate as described by Breeman *et al.* [103]. The rationale resides in the fact that, although the total eluate volume is 5-6 ml, about two-thirds of the ^{68}Ga activity elutes within a 1–2 ml activity peak. However, ^{68}Ge and metallic impurities are only minimised, because of the lower eluate volume, rather than being chemically removed [103]. Another method was developed for the removal of chemical impurities with simultaneous preconcentration of the radionuclide by ion-exchange chromatography [104]. An automated computer controlled ^{68}Ga milking and concentration system was developed based on the Scintomics modular system [105]. Another new and simple method reported by Mueller *et al.* involved a sodium chloride based ^{68}Ga eluate concentration and labelling technique, which enables rapid and very efficient labelling of DOTA-conjugated peptides in high radiochemical purity (97 ± 2%). The SCX cartridge used in this method was from Varian, Bond Elut-SCX, 100 mg, 1 ml. The column was preconditioned with 1 ml 5.5 M HCl and 10 ml water prior to the elution

step. The ^{68}Ga generator was eluted with 10 ml of 0.1 M HCl. On a SCX cartridge, 99.9% of ^{68}Ga in the generator eluate was collected and subsequently eluted with minimal loss using a mixture of 12.5 µl of 5.5 M HCl and 500 µl of 5 M NaCl. The pH was neutralised by adding it into 200-400 µl of ammonium acetate buffer (1 M) [102].

1.12-Ligands for Gallium

The Ga^{3+} ion is classified as a hard Lewis acid, forming thermodynamically stable complexes with ligands that are hard Lewis bases [106]. Gallium (III) is suitable for complexation with polydentate ligands, both cyclic and open chain structures. The majority of the ligands designed for Ga^{3+} have denticity 6 or higher than 6, although several chelates have been reported which are stable *in vivo* and have denticity of four and five [95]. The extent of complexation increases with pH, owing to the release of protons but there may also be competition by hydroxide ions. Electron-withdrawing substituents such as halogens, nitriles, carbonyls and nitro group decrease the stability of the complex [106]. The pM value takes into account the ligand basicity, metal-ion hydrolysis, metal-ligand stoichiometry, dilution effects and other conditions. The larger the pM value (pM = -log[$Ga(H_2O)_6$]), (pM values evaluate how effective a ligand is at binding a specific metal ion in solution by measuring the concentration of the free metal ion under a predetermined set of conditions like pH) the better is the ligand for Ga^{+3}. This value provides a direct head-to-head comparison among the various chelating agents under physiological conditions. Under these conditions transferrin (TFK_1-pM = 21.3; TFK_2-pM = 20.3), the iron–binding protein in the blood, has a stability constant and pM comparable to DTPA (pM = 22.8) and EDTA (pM = 21.7). The OH^- (pM = 19.1) has also high value, only one order of magnitude lower than one of the TF binding sites, which suggests that if blood levels of TF were reduced by an order of magnitude $[Ga(OH)_4]^-$ would be thermodynamically favoured. A reduction in the concentration of available TF sites increases the gallate concentration. This would increase gallate kidney excretion and could dramatically alter the biodistribution. The speed with which Ga transfer occurs is also equally important with pM values [106]. A bifunctional chelator should meet the following criteria: (1) when linked the macromolecule it should chelate the radiometal rapidly and efficiently; (2) the obtained chelate should be kinetically stable to demetallation over a pH range of 4-8 and in the presence of other serum cations (Ca^{2+}, Zn^{2+}, Mg^{2+}) [81]. Along with this it has to be resistant to competing endogenous chelators.

For radiolabelling of macromolecules using the ^{68}Ga generator eluate, both direct and indirect methods can be used. In the direct method, the chelating ability of a macromolecule itself is used, e.g. lactoferrin [107]. However, if the macromolecule lacks the ability to form a complex with the radiometal and requires site-specific labelling then it can be conjugated with a bifunctional chelator before radiolabelling. Various chelators are available and they can be broadly classified in to acyclic chelators (HBED, DTPA) and cyclic chelators (NOTA, DOTA). However, we have used an in-house produced tripodal hexadentate hydropyridinone chelator (CP256) and its bifunctional version (YM103) [108]. CP256 has three bidentate 3-hydroxy-4-pyridinone groups attached to a tripodal network as shown in Fig-1.15. Initial work with this chelator showed its Ga complex to be quite stable in serum and radiolabelling is possible at room temperature within a few minutes. In its bifunctional version (YM103), a maleimide group in the side chain is used to attach this group to a free thiol on the biomolecule as in Fig-1.16.

1.12.1-Acyclic bifunctional chelators

Acyclic chelators such as DTPA (diethylenetriamine pentaacetic acid), DFO (Desferrioxamine-B), HBED (N,N′-bis (2-hydroxybenzyl) ethylenediamine-N,N′-diacetic acid) (Fig-1.11) can be labelled with gallium. DFO complexes Ga^{3+} rapidly with high affinity and radiochemical yield. It has three hydroxamate groups as metal coordinating sites [109]. Our in-house produced gallium chelator CP256 gives more than 80% radiolabelling yield at 1 µM chelator concentration. Cutler *et al.* have shown the Ga^{3+} complex of the tetradentate tripodal ligand NS3 is neutral and lipophilic. It retains its tetrahedral geometry and its conjugation with phenylalanine will result in stable $^{67/68}$Ga–labelled peptides. However, it requires a long reaction time and has to be purified by liquid chromatography before it can be used *in vivo* [110].

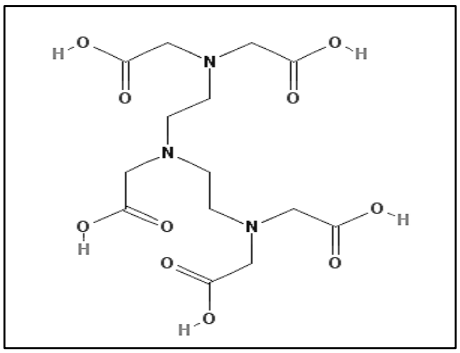

DTPA

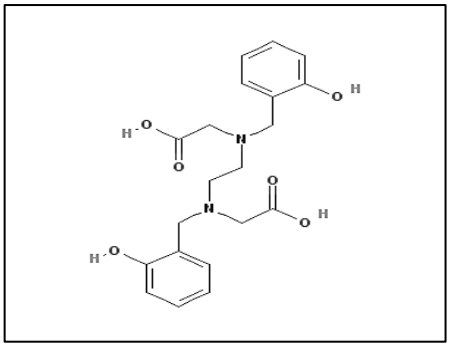

HBED

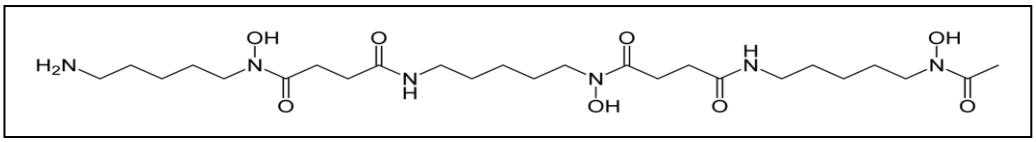

DFO-B

Figure-1.11: Structures of acyclic bifunctional chelators.

1.12.2-Macrocyclic chelators

Macrocyclic chelators provide more thermodynamic and kinetic stability but many of these require heat during the labelling step. Triaza ligands display conformational and size selectivity towards metal ions. The thermodynamic stability of the Ga^{3+} chelates of triazamacrocyclic ligands is due to good fit of the relatively small cation in the cyclic cavity [1] (Fig-1.12). This category of chelators can encapsulate a metal ion with high efficiency, keeping it away from competitor species such as blood transferrin. TACN-TM, a triaza ligand with three mercaptoethyl pendent arms; NOTA, a triazatricarboxylic ligand; NOTP and NOTPME, two phosphonate–bearing triaza ligands, are appropriate hexadentate chelators for Ga. This is illustrated by the neutral Ga(NOTA), which only undergoes acid–catalysed dissociation at non-physiological low pH values. NODASA is a very stable Ga chelator that additionally has potential for biomolecule coupling using the pre labelling approach (i.e. the radiometal-chelate complex is formed prior to conjugation with the target molecule). It has a free carboxylate group available for coupling to biomolecules whereas the other three carboxylates are protected by the metal ion. This chelate has been rapidly coupled to D-phenylalanine amide as a model peptide which renders the coupling of ^{68}Ga(NODASA) to peptides. The same type of chelator has been derivatised (NODAGATOC) in order to make it available for the post–labelling approach (i.e. the chelator is conjugated with the target molecule before radiolabelling with the radiometal) [1]. The thermodynamic stability constant of the Ga^{3+} complex of the tetraaza tetra acetic acid chelator DOTA is much lower than that of Ga(NOTA) due to the larger dimensions of its cavity. Despite the lower value of its stability constant, Ga(DOTA) is sufficiently stable to be used in clinical practice. DOTATOC, a somatostatin receptor targeting peptide, showed very promising *in vivo*

and *in vitro* properties when labelled with ^{67}Ga [11]. As an alternative to thermal heating, we can use microwave activation, which serves as an attractive tool for accelerating the labelling process. The chemical reaction time is shortened by this method and the reaction is completed within 2 min instead of 10 min. Microwave heating will lead to fewer side reactions and high chemical yield due to increased rate of reaction, as shown by Velikyan *et al.* They have used microwave technique to accelerate the rate of reaction between the purified ^{68}Ga eluate and DOTATOC. The reaction is completed within 10 min [96,111].

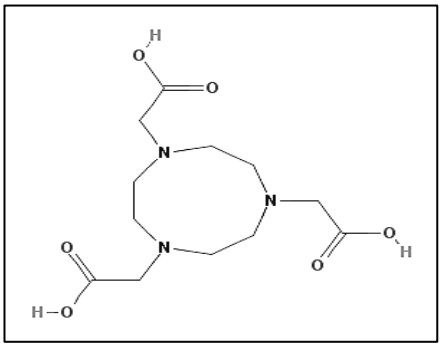

NOTA

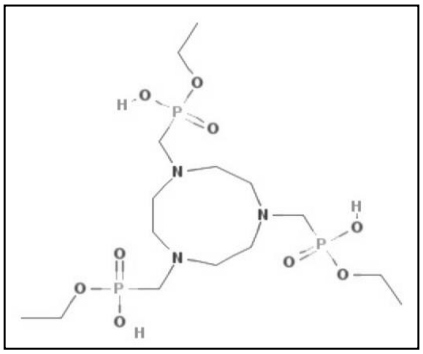

NOTPM

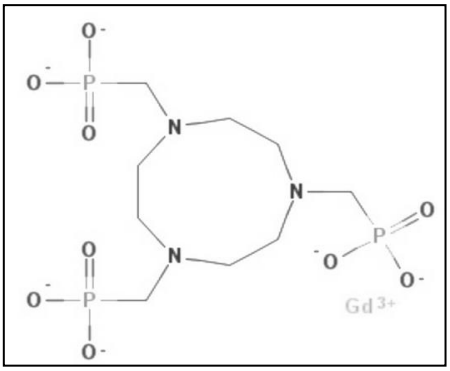

NOTP

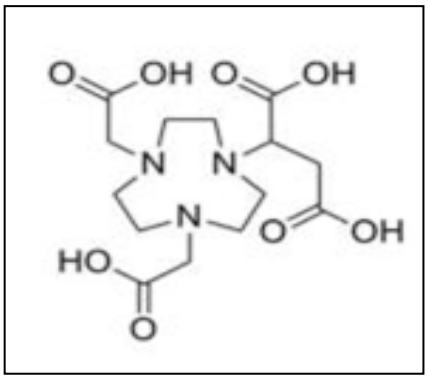

NODASA

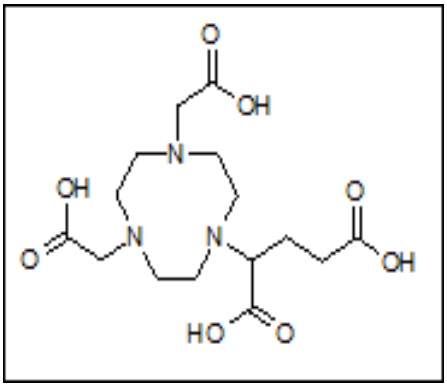

NODAGA

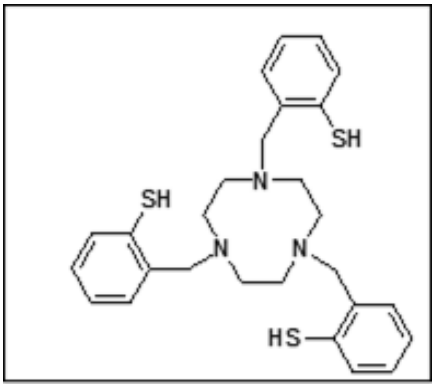

TACN-TM

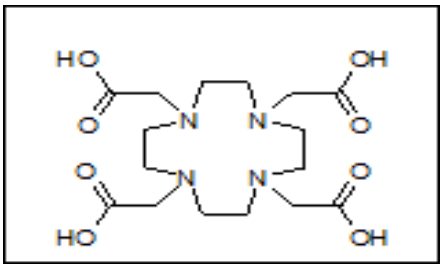

DOTA

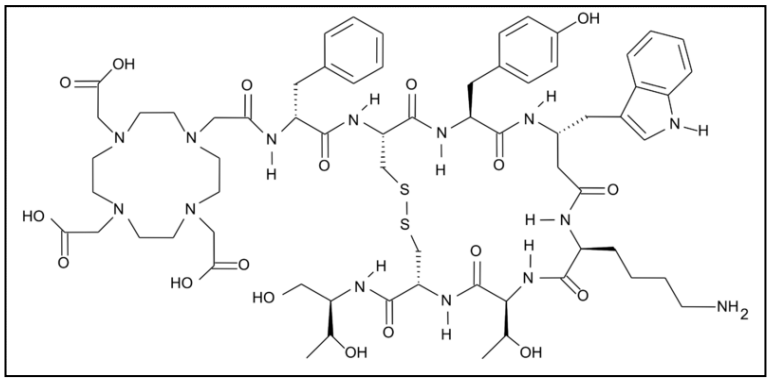

DOTATOC

Figure-1.12: Structures of Macrocyclic Chelators.

1.12.3-New generation of gallium chelators:

A new generation of Ga chelators includes TRAP (1,4,7-triazacyclononane-1,4,7-tris[methyl(2-carboxyethyl)phosphinic acid]). Its properties include substantially improved selectivity for Ga^{3+}, allowing more robust and reliable ^{68}Ga labelling procedures compared to DOTA and NOTA [112].

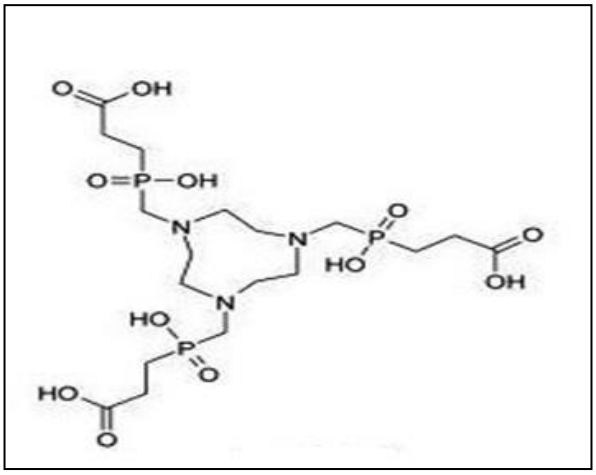

Figure 1.13: TRAP(1,4,7-triazacyclononane-1,4,7-tris[methyl(2-carboxyethyl)phosphinic acid]).

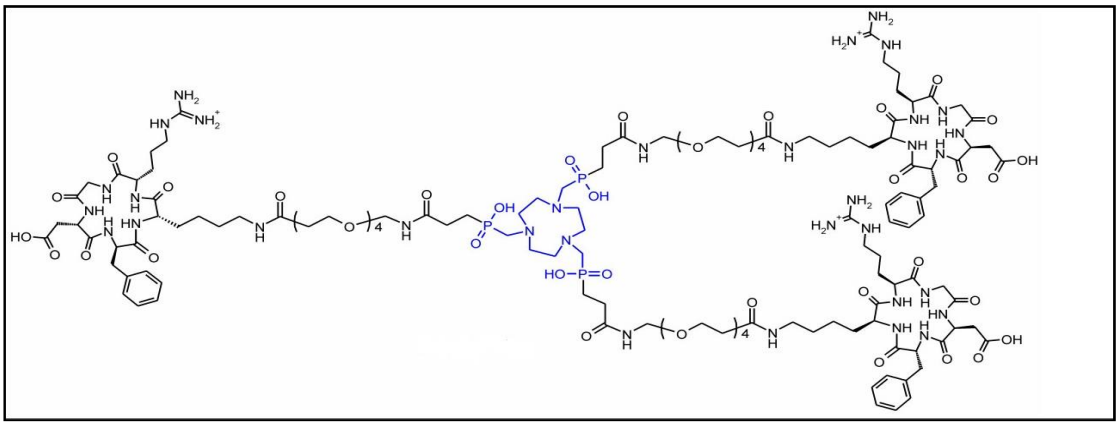

Figure 1.14: TRAP (1,4,7-triazacyclononane-1,4,7-tris[methyl(2-carboxyethyl)phosphinic acid]) conjugated with RGD peptide.

Compared to NOTA- and DOTA-peptides, achievable specific activity (AS) for TRAP-peptide is approximately 10 and 20 times higher, respectively. The TRAP-peptide could be ^{68}Ga-labelled with excellent reproducibility and >95% radiochemical yield for precursor amounts as low as 1 nmol at the elevated temperature of 95^{o}C for 5 min. The other advantage of TRAP is that it can also be labelled over a wide pH range and thus does not require buffering before the labelling reaction [112]. High ^{68}Ga labelling efficiency of TRAP-peptides could facilitate realisation of kit labelling procedures.

Hexadentate Hydroxypyridinones

The main aim in synthesing this chelator was to develop a gallium chelator which can bind with the biomolecules at room temperature efficiently and quickly, thus reducing the need for heating as in the case of DOTA. The synthesis of hexadentate HP (hydroxypyridinones) involves the attachment of three bidentate 3-hydroxy-4-pyridinone synthons to a tripodal framework. The acidic oxygen of the hydroxypyridinone synthons is protected by a benzyl ester to prevent binding of trace iron and other metal contaminants during synthesis. These protecting groups are then removed in the final step of the synthesis [108]. CP256 was synthesised in 13 steps and characterised by NMR and mass spectrometry. Radiolabelling studies with ^{67}Ga-citrate showed that radiolabelling took less than 5 min at room temperature and neutral pH. *In vitro* stability studies in transferrin solution showed the ^{67}Ga-complex to be 100% stable for at least 4 hours at pH 7 and chelator concentration of 227 nM. A further 130-fold excess of apotransferrin was used to check the stability of the CP256 complex in apotransferrin (a 260-fold excess in terms of Ga-binding capacity since there are two metal binding sites per transferrin molecule) at 37^{o}C. ^{67}Ga-CP256 shows stability when incubated with human serum, using ^{67}Ga-citrate as a control. It remained stable even after 24 h compared to ^{67}Ga-citrate [108]. The chelator is effective and worthy of further studies and development. This is a class of ligand that could be very suitable for imaging with the Ga radioisotopes. A bifunctional chelator (YM103) which has two active sites and can bind with the radiometal and biomolecule simultaneously has also been synthesised in order to produce bioconjugates.

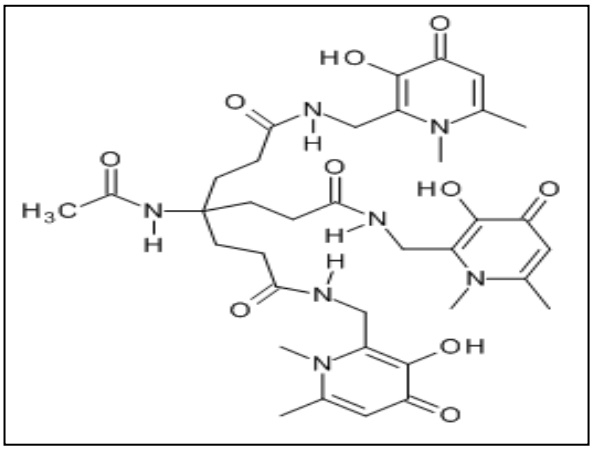

Figure 1.15: Tripodal Hexadentate Chelator (CP256) [108,113]

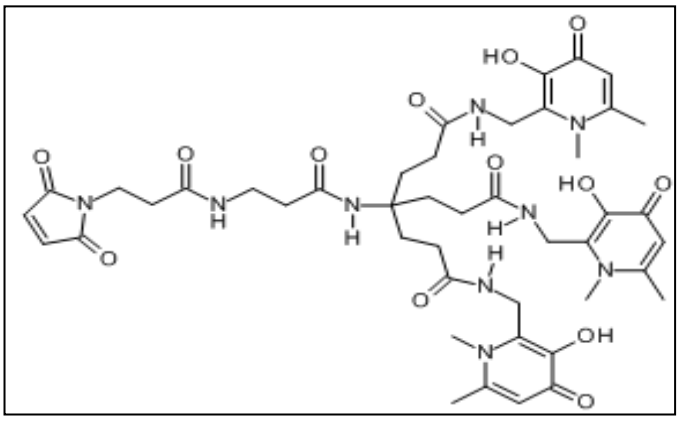

Figure 1.16: YM103, bifunctional version of CP256 containing maleimide group.

1.13-The Pre-targeting Approach for CP256:

Traditionally radioimmunotherapy (RIT) involves the radiolabelling of an antibody with a radionuclide to deliver cytotoxic radiation to the tumour. It is quite good in the treatment of hematologic malignancies such as non-Hodgkin lymphoma. However, for solid malignancies it was not proved to be very effective due to lower radiosensitivity, difficult penetration of the antibody into the tumour, and potential excessive radiation to normal tissues. To overcome these shortcomings of traditional RIT, pretargeted radioimmunotherapy (pRIT) was developed [71]. The concept of pre-targeting was introduced in late 1980s and can improve the target to non-target ratio as compared to traditional RIT and the delivery of a higher therapeutic dose. The essence of pre-targeting involves the use of a macromolecule that is capable of binding with a high affinity to a radioactive agent of low molecular weight and can also selectively target a tumour antigen. The macromolecule is injected first, followed by the radioactive agent (effector) given at later time, ideally when the concentration of the macromolecule in the tumour is greater than in other tissues, particularly the blood pool. This sequence of events is normally referred to as the Two Step Protocol. An alternative is the Three Step Protocol which involves injecting a chaser (a specific scavenger molecule to remove residual macromolecule) before the effector (radioactive agent) to clear any residual macromolecule from the bloodstream to further enhance the tumour to blood ratios [11].

Promising results have been reported using streptavidin-antibody constructs with biotin-radionuclide conjugates in the treatment of patients with malignant gliomas, and of bispecific antibodies with hapten-radionuclides in the therapy of tumors expressing carcinoembryonic antigen, such as medullary thyroid and small-cell lung cancers [115].

1.14-Aims and Objectives:

1. Evaluate the full potential of the CP256 chelator for Ga in comparison with its competitors.

2. Test a bifunctional derivative of CP256 suitable for linkage to a cysteine residue in a biomolecule.

3. Produce an anti-PSMA scFv with a modification for site specific incorporation of radiolabel.

4. Evaluate the targeting ability of these ^{68}Ga labelled bioconjugates in cultured cell lines relevant to prostate cancer, and select the tracers that show promise *in vitro* and evaluate them in animal xenograft models of PCa using PET imaging and biodistribution studies.

Chapter 2: Characterisation and Evaluation of CP256

2.0-Introduction

CP256 and ^{68}Ga are two important components of this project. The bifunctional chelator (YM103) for ^{68}Ga is derived from CP256. The main aim of this chapter is therefore to characterise CP256 and ^{68}Ga and evaluate the efficacy of the chelator for ^{68}Ga. To achieve this objective we have compared CP256 with other chelators available commercially for gallium, including DOTA, NOTA and HBED to demonstrate that CP256 is better than the other chelators. This involved studies of the effect of time and concentration on the formation of the ^{68}Ga complex, a comparative study of the stability of different ^{68}Ga complexes in human serum and the discovery of a novel potential pretargeting approach employing the unique features of CP256. Radiochemical binding of CP256 not only with ^{68}Ga but also with other radionuclides was studied. ^{111}In is a cyclotron produced radionuclide with a half-life of 67 h which emits gamma photons of 173 keV and 247 keV. It is widely used in gamma scintigraphy. Majority of the ^{111}In radiopharmaceuticals are biomolecules such as peptides and proteins. In aqueous solution it is stable in the +3 oxidation state. ^{99m}Tc has a half-life of 6 h and is widely used as a diagnostic imaging radionuclide. Its coordination chemistry is diverse because of the available oxidation states (-1 to +7), a wide number of coordination geometries and its ability to bind with large range of donor ligands to fulfill its coordination requirements. ^{90}Y is a beta emitter with a half-life of 64 h and it has utility in therapy applications. Its maximum β^- energy is 2.27 MeV and maximum particle range is 11 mm in tissue. ^{89}Zr has a half-life of 78 hours. It is produced by proton irradiation of natural ^{89}Y. ^{89}Zr disintegrates through positron decay (22.7%) and electron capture (73.3%). The maximum positron energy is 897 keV. Its most prominent gamma photon has an energy of 909 keV. ^{89}Zr is employed in specialised diagnostic applications requiring a long half-life PET radionuclide.

The second important factor in this project is the generator produced ^{68}Ga radionuclide, so one part of this chapter involved comparison of eluates from the different generators available in the market (effect on radiochemical yield with chelators) and the effect of first and second elution on the radiochemical yield.

2.1- Methods

2.1.1-Elution of $^{68}Ge/^{68}Ga$ Generator

The $^{68}Ge/^{68}Ga$ generator (IGG100) from Eckert & Ziegler of 1.1 GBq nominal activity was eluted with 0.1 N HCl of high purity and low in trivalent metals, using a syringe without a metal needle. This syringe was attached to the inlet valve and an empty vial in a lead pot was connected to the outlet valve. A volume of 5 ml 0.1 N HCl was pushed through by a syringe slowly over 2 min. The activity in the eluate was measured in a dose calibrator (Capintec CRC-15R).

Another method of eluting the generator to get concentrated activity is by fractional elution. In this case 5 ml of 0.1 N HCl was used and it was collected in 1-2-2 ml fractions, with >90% of activity concentrated in middle 2 ml fraction.

2.1.2-General Radiolabelling Methods

A 200 µl aliquot of generator eluate was mixed with 600 µl of buffer (sodium citrate or sodium acetate ~pH 6) and allowed to incubate at room temperature. Stock solutions of chelator were prepared in PBS by dissolving 1 mg of chelator in 1 ml of PBS (0.1 M). The remaining concentrations were prepared by serial dilutions of 100 µl of chelator solution with 900 µl of PBS. For each labelling reaction 800 µl of chelator solution was mixed with 200 µl (~100 MBq) of radionuclide solution in buffer.

2.1.3-Thin Layer Chromatography (TLC)

Five different TLC methods were developed and used in this project. Details of these TLC systems are in the following along with there results. Method 1 was used to analyse the CP256, Method 2 was used for the quality control of ^{99m}Tc tricarbonyl. Methods 3 and 4 were developed for CP256 complexes, as these chelates are quite hydrophobic and stay at the base-line in most of the TLC techniques including Method 1, so these two methods were developed to have a TLC system in which CP256 complexes can move to the solvent front. Method 5 was for NOTA, HBED and DOTA complex analysis.

2.1.3a-Method-1

Strips of ITLC-SG (Pall Gelman, later Agilent), 10 x 80 mm, were marked with the origin at 10 mm from the bottom. Chromatograms were spotted with the reaction mixture at different times ranging from 0 min to 10 min. The drop was allowed to dry and the ITLC strip was placed in the mobile phase of 0.1 M trisodium citrate. When the solvent reached the solvent front, the strip was removed, dried for few minutes, and analysed with a radio-TLC scanner (Raytest Mini Gita with Gina Star software).

2.1.3b-Method-2

For quality control purposes to check the formation of ^{99m}Tc-tricarbonyl, glass-back TLC(sg) plates were developed in the mobile phase of 1% HCl in 99% methanol. Any colloid will stay at the baseline, free pertechnetate moves to the solvent front and tricarbonyl will be at centre (Rf 0.4) (Fig-3.18) [116].

2.1.3c-Method 3

Since ^{68}Ga-CP256 did not migrate in any of the standard chromatography systems, an alternative system was developed which used ITLC-SG strips presaturated with human (or bovine) serum albumin. Strips were immersed in HSA or BSA solution (5 mg/ml) for 30 min, then washed with distilled water for 5 sec, dried and stored in a fridge. The mobile phase was a freshly prepared mixture of water, ethanol and ammonium hydroxide (14 M) in the ratio of 5:2:1 [117].

The strips with origin marked at 10 mm were spotted with a 1-5 μl drop from the reaction mixture. The drop was allowed to dry and the ITLC strip was placed in the mobile phase. When the solvent reached the solvent front, the strip was removed, dried for a few minutes, and analysed with the radio-TLC scanner.

2.1.3d-Method 4

In this method, although we have used two different mobile phases with stationary phase of ITLC-SG we are presenting them together as they were developed side by side as a new TLC method development for ^{68}Ga- CP256 in which CP256 moves with the solvent front and ^{68}Ga acetate stays at the origin (Figure-2.0). The results were also attached with this section as this method was not further used. The main reason to develop this method is to have some easy and straightforward TLC technique for ^{68}Ga-

CP256 as it does not require preparation of the ITLC strips impregnated with HSA or BSA.

Mobile Phase 1 was composed of ammonia (14 M), acetone, and water in a ratio of 5:3:2, while Mobile Phase 2 contained acetone, water, and ammonia (14 M) in a ratio of 5:4:1 respectively.

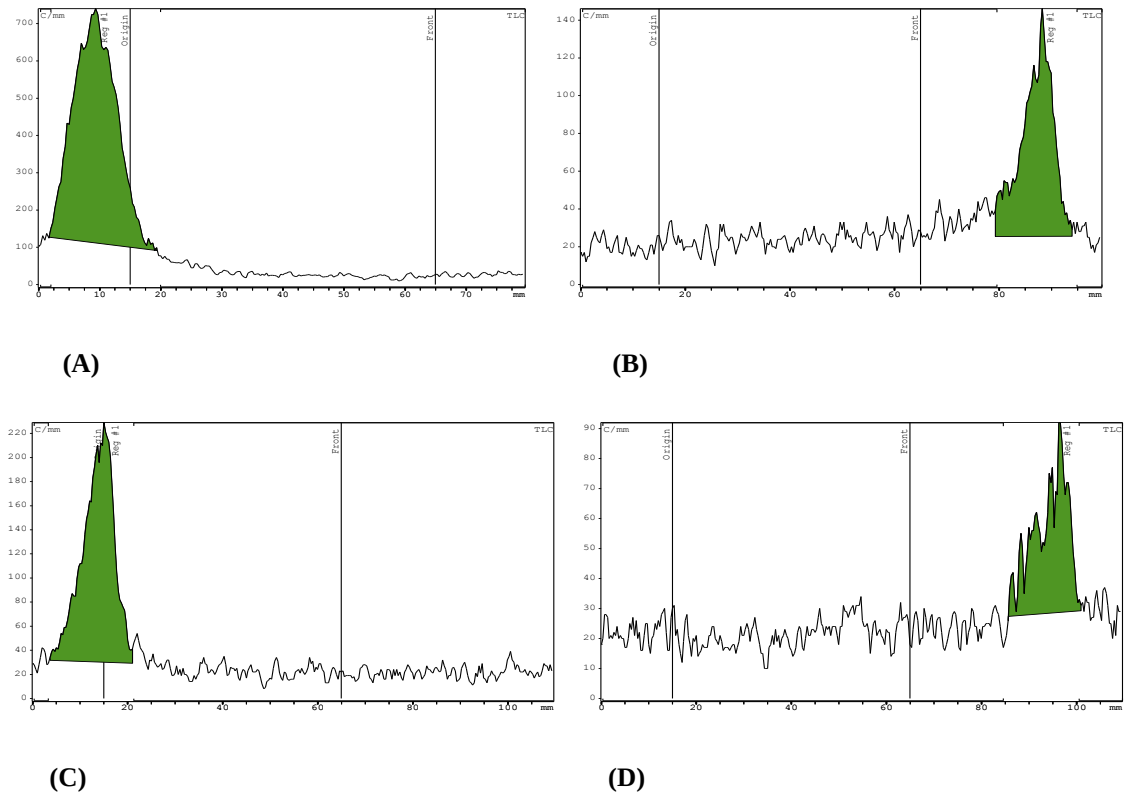

Figure-2.0: Mobile phase 1 and stationary phase of ITLC-SG, ^{68}Ga stays at origin with Rf value of 0 (A). ^{68}Ga –CP256 moves with the solvent front with Rf value of 1 (B). Mobile phase 2 and stationary phase of ITLC-SG, ^{68}Ga stays at origin with Rf value of 0 (C) and ^{68}Ga-CP256 moves with the solvent front with Rf value of 1 (D).

2.1.3e-Method 5

In another TLC system the mobile phase was composed of NaH_2PO_4 (0.4 M, pH 4-4.5, 0.552 g/10 ml) and stationary phase was composed of ITLC-SG [118]. ITLC-SG strips were cut in the dimensions of 10 x 80 mm and marked with the origin at 10 mm. The strips were finally analysed with the radio-TLC scanner. This method is used to analyse HBED, NOTA and DOTA labelling. In this case ^{68}Ga acetate stays at the origin with Rf value of 0 and the radiolabelled complex of chelator moves toward the solvent front

with an Rf value of 0.7 for NOTA, 0.9 for HBED and 1 for DOTA. Results for HBED, NOTA and DOTA analysed by this method are shown in Fig 3.3.

2.1.4-Size exclusion column chromatography

PD-10 columns containing Sephadex G25 (Pharmacia) were equilibrated with 25 ml of PBS before 50 µl (~200 kBq) of the reaction mixture was applied. Twenty fractions of 0.5 ml were collected with PBS as eluent in numbered tubes and counted in a gamma counter with a window set to include the 511 keV annihilation gamma photons (Perkin Elmer 1480 automatic gamma counter Wizard 3, 10 seconds per sample). The results were plotted as histograms.

2.1.5-Effect of concentration and time on formation of ^{68}Ga-CP256 complex

Five different concentrations of CP-256 from 1.0 mg/ml to 0.0001 mg/ml were prepared in PBS (1.186 mM, 118 µM, 11.8 µM, 1.18 µM, 118 nM). The number of moles used in each labeling was 1.18 µmol, 118 nmol, 11.8 nmol, 1.18nmol and 118.06 pmol. ^{68}Ge/^{68}Ga Generator was eluted according to the method described above. A 200 µl aliquot of generator eluate was mixed with 600 µl of buffer (sodium citrate or sodium acetate ~pH 6) and allowed to incubate at room temperature. For each labelling reaction 800 µl of chelator solution was mixed with 200 µl (~100 MBq) of radionuclide solution in buffer. The samples were analysed by using TLC Method 1. In this method radiolabelled ^{68}Ga-CP256 stays at the origin and free ^{68}Ga moves with the solvent front.

2.1.6-Changes in radiolabelling yield of CP256 with 1st and 2nd elution over time

Radiolabelling was done with the 1st and 2nd elutions of the day to see any difference in binding of ^{68}Ga with CP256 at a concentration of 11 µM. The time difference between the two elutions was 2 h. The generator was eluted by fractional elution. This CP256 concentration (11 µM) was selected based on the above experiment because it was likely to be most sensitive to effects of eluate composition. A 200 µl aliquot of generator eluate was mixed with 600 µl of buffer (sodium acetate ~pH 6). For the labelling reaction 800 µl of chelator solution was mixed with 200 µl (~100 MBq) of ^{68}Ga acetate and incubated at room temperature. TLC analysis was performed using Method 1.

2.1.7-Comparison of CP256 with NOTA, HBED and DOTA for ^{68}Ga radiolabelling

^{68}Ga-acetate was prepared by adding 20 µL (1 – 5 MBq) of $^{68}GaCl_3$ (obtained by fractional elution) to 60 µL of 1 M ammonium acetate solution. To obtain pH 4.5 for NOTA labelling, 1-2 µL of 1 N HCl and for pH 7 for HBED, 1-2 µL of 10 mg/ml sodium carbonate solution was added to the chelator solutions. For radiolabelling reactions, 20 µl of ^{68}Ga-acetate was added to 80 µl of NOTA solution and incubated for 7 min (time is based on the increase in radiolabelling yield with time experiment) at room temperature before analysis. The stock solution of NOTA (p-SCN-Bn-NOTA, Macrocyclics, MW = 559.9) was prepared by dissolving 1 mg in 1 ml of PBS (1.78 mM). Five different concentrations were prepared by diluting this stock solution with PBS, i.e.1 mM, 100 µM, 10 µM, 1 µM, and 100 nM. The 1 mM solution was prepared by diluting 56 µl of stock solution with 34 µl of PBS. The remaining concentrations were prepared by serial dilutions of 10 µl with 90 µl of PBS. The same radiolabelling and dilution method was used for HBED (MW = 424.89). The stock solution was prepared by dissolving 1 mg in 1 ml of PBS (2.35 mM). A 1 mM solution was prepared by taking 42 µl from the stock solution and diluting it by adding 58 µl of PBS. The remaining concentrations were prepared by serial dilutions. Similarly, for DOTA (MW = 404.42), the stock solution was prepared by dissolving 1 mg in 1 ml of PBS (2.4 mM). A 1 mM solution was prepared by taking 41.6 µl from stock solution and diluting it by adding 58.4 µl of PBS. The remaining concentrations were prepared by serial dilutions of 10 µl with 90 µl of PBS.

In the case of NOTA and HBED radiolabelling reactions were performed at room temperature. On the other hand, for DOTA different concentrations of chelator were incubated with ^{68}Ga for 30 min at 100^{o}C. Finally, the samples were analysed by TLC Method 5, in which ^{68}Ga acetate stays at the origin with Rf value of 0 and the complex moves toward the solvent front with an Rf value of 0.7 for NOTA, 0.9 for HBED and 1 for DOTA.

2.1.8-Stability in human blood serum

Stability in human blood serum was analysed using PD-10 columns containing Sephadex G25. For CP256, NOTA and HBED the stability of a sample (^{68}Ga + CP256 or HBED) in serum was measured at two time points, 5 min and 60 min. There were

three reference standards: one was human blood serum preincubated with ^{68}Ga acetate, the second was ^{68}Ga buffered with either citrate or acetate and the last reference was the chelator (CP256 or HBED) radiolabelled with ^{68}Ga. The chelator was radiolabelled with ^{68}Ga and once the complex was formed it was incubated in human serum at 37^{o}C. The first reading was taken after 5 min of incubation and the second after 60 min. To further analyse the stability of the ^{68}Ga-CP256 complex in human serum, TLC Method 3 was used [117].

2.1.9-Radiolabelling of CP256 and NOTA with eluates from different generators

A 20 µl (5 MBq) aliquot of a fresh second elution from the generator (Eckert & Ziegler IGG100) was added to 80 µl of a decayed previous elution from the same generator, 1st and 3rd decayed eluate from an Obninsk generator (courtesy of the Royal Marsden Hospital and Barts Health) and 0.1 N HCl and buffered with citrate (60 µL, 0.1 M, pH 6). These elutions were then used to radiolabel CP256 and NOTA by taking 20 µl from each solution and adding it to 80 µl of CP256 (11.8 µM) and NOTA (11 µM). After 5-7 min a 1 µl drop was spotted on ITLC-SG strips and analysed by Method 1.

2.1.10-Radiolabelling of C2A protein with ^{68}Ga

The conjugated protein was obtained from the group of Dr Greg Mullen, Imaging Sciences, King's College London [108,116]. A 30 µl (20 µg) aliquot of conjugated C2A protein was mixed with 20 µl (20MBq) ^{68}Ga-citrate and analysed after 0, 5 and 10 min using TLC Method 1.

2.1.11- CP256 and binding with different radionuclides

2.1.11a-Radiolabelling with ^{111}In-acetate

A 50 µl aliquot of acetate buffer (pH 6) was added to vial containing $^{111}InCl_3$ (Covidien Healthcare) (7 MBq) in HCl (50 µl). A 589 µM solution of CP256 was prepared by dissolving 0.5 mg of CP256 in 1 ml of PBS. A 100 µl aliquot of CP256 was mixed with 50 µl of ^{111}In-acetate and analysed using TLC Method 3. Along with binding of ^{111}In with CP256, its stability in human blood serum was also tested at different time intervals using PD-10 column chromatography. Radiolabelled CP256 (100 µl) was incubated in human serum protein (300 µl) and samples (50 µl) were taken out at three

time–points: 5 min, 60 min and 120 min and applied to the PD-10 column as described above.

2.1.11b-Radiolabelling with ^{90}Y

$^{90}YCl_3$ (~20 µl) (Yttriga, Eckert & Ziegler) was neutralised by adding 60 µl of acetate buffer (pH 6) and 20 µl of this solution was then added to the 80 µl of CP256 (1 mM). Both TLC Method 3 and the PD-10 column method were used to check the radiolabelling of CP256 with ^{90}Y.

2.1.11c-Radiolabelling with ^{99m}Tc tricarbonyl

^{99m}Tc tricarbonyl was prepared by using the ISOLINK tricarbonyl kit (Covidien). Up to 1000 MBq of ^{99m}Tc pertechnetate can be used to prepare the kit. The pH of the kit contents was adjusted to 7 by adding 1 M HCl (~120 µl). To check the formation of ^{99m}Tc-tricarbonyl, TLC Method 2 was used. ^{99m}Tc tricarbonyl was then incubated with CP256 and the radiolabelled complex was analysed by TLC Method 1.

2.1.11d-Radiolabelling with ^{89}Zr (Zirconium)

^{89}Zr (IDB, Amsterdam) comes in the oxalate form. It is converted in to citrate form by adding citrate buffer (60 µl, pH 6) [119]. Following incubation with CP256, the formation of radiolabelled complex was analysed by TLC Method 1. ^{89}Zr-CP256 (100 µl) was incubated with human serum (300 µl) and samples were taken at different time points (1, 2, 3, 5, and 24 h) and analysed by the PD-10 column method.

2.1.12-Formation of ^{68}Ga-CP256 complex in serum

Hexadentate chelator (CP256) stock solutions were prepared by adding the required amount of CP256 to 1 ml of PBS and adjusting the pH to 7-7.5. Different concentrations of the chelator from 2 mg/ml to 0.01 mg/ml (2.35 mM, 1.17 mM, 589 µM, 117 µM, 23 µM and 11.7 µM) were assessed. Two different radiolabelling techniques were used. In the first, 100 µl of CP256 (all concentrations mentioned above) was added to 300 µl of human serum. After 10-15 minutes 20 µl of ^{68}Ga-citrate was added and binding was assessed after 15-20 minutes. For time studies human serum was incubated at 37^{o}C in a plastic tube. In the second method, 20 µl of $^{68}GaCl_3$ was added to 300 µl of human serum. After 15-20 minutes 100 µl of chelator was added.

Three reference standards were prepared. The first consisted of 300 µl of chelator solution in PBS without any serum mixed with 20 µl of ^{68}Ga-citrate. The second reference was composed of 300 µl of human serum incubated at 37^{o}C and radiolabelled with 20 µl of ^{68}Ga-citrate. The third reference was composed of simply $^{68}GaCl_3$ with no chelator or serum buffered with 60 µl citrate.This approach was also assessed with NOTA and HBED (1 mg/ml) using the same protocol as CP256 and size exclusion chromatography.

2.2-Results

2.2.1-Effect of concentration and time on formation of ^{68}Ga-CP256 complex

Five different concentrations of CP256 used were shown in Table 2. The samples were analysed by using method 1 of the TLC. In this method radiolabelled Ga-CP256 stays at the origin and free ^{68}Ga moves with the solvent front. The results are presented in Table 3.

Table 2

Concentration (CP256)	No of Moles (CP256)
1.186 mM	1.18 µmol
118 µM	118 nmol
11.8 µM	11.8 nmol
1.186 µM	1.18 nmol
118 nM	118 pmol

Table 2-Five different concentrations and no of moles of CP256, to analyse the effect of time and concentration on radiolabelling yield.

Table 3

Radiolabelling Yield					
Time (min)	**1.186 mM**	**118 µM**	**11.8 µM**	**1.186 µM**	**118 nM**
0	89%	49%	11%	0%	0%
1	95%	98%	63%	8%	8%
2	100%	98%	64%	11%	9%
3	100%	100%	73%	13%	8%
4	100%	100%	79%	14%	8%
5	100%	100%	87%	15%	8%
6	100%	100%	91%	16%	10%
8	100%	100%	94%	22%	11%
10	100%	100%	97%	25%	11%

Table 3-% radiolabelling yield obtained with five different concentrations of CP256 at different time points.

CP256 by increasing time from 0 min to 10 min at very high concentration and low concentration. At concentrations of 118 µM and higher, quantitative labelling was achieved within 1 min. However, time is the critical factor in case of intermediate concentration (11.8 µM). Radiolabelling increased from ~60% at 2 min to 100% at 10 min. Most probably, the low yield at low concentration is limited by time (slow rate).

2.2.2-Changes in radiolabelling yield of CP256 with 1st and 2nd generator elutions over time

The changes observed in the radiolabelling yield of CP256 (11 µM) with 1st and 2nd generator elution with time are summarized in Table 4. There was 5% radiolabelling yield difference between 1st and 2nd elution of the generator. The first elution gave 95% radiolabelling yield in 10 min and 2nd elution gave 100% radiolabelling yield in same time period. The 1st elution was done to remove any build-up of trace metals and to increase radiolabelling yield in the second elution. However, this result indicates that there is small difference in 1st and 2nd elution and extent of radiolabelling yield; we can use the first elution directly instead of doing the first elution and then waiting for 2 hours for the 2nd unless special circumstances demand it. However, it is better to do a 2nd elution to remove any build-up of metallic impurities in the eluant and the 2nd elution might make a difference in the case of very small amounts of chelator.

Table 4

Time (min)	Radiolabelling (%)with 1st Elution	Radiolabelling (%)with 2nd Elution
0	3	5
1	21	29
2	37	43
3	49	54
4	61	65
5	70	79
6	79	87
8	88	95
10	95	100

Table 4-Difference in radiolabelling yield (%) of CP256 with 1st and 2nd elutions of ^{68}Ga generator (IGG100).

2.2.3-Comparison of CP256 with NOTA, HBED and DOTA for ^{68}Ga radiolabelling

The reaction conditions and radiolabelling yield obtained at different concentrations are summarised in Table 5. Each sample was analysed three times using TLC Method 5, in which ^{68}Ga acetate stays at the origin and the complex moves toward the solvent front with an Rf value of 0.7 for NOTA, 0.9 for HBED and 1 for DOTA. NOTA showed quantitative labelling with ^{68}Ga at concentrations ≥100 µM, with reduced yields at lower concentrations and no binding at 100 nM. NOTA showed slightly different behaviour at two different pH values and a lower concentration of 1 µM. NOTA with pH=7 still showed 40% binding, whereas at pH=4.5 the radiolabelling yield was almost zero after the incubation time of 7 min. In the case of HBED there was 100% binding till 100 µM and almost 90% binding at 10 µM. It sharply decreased to 70% at 1 µM and almost negligible binding at 100 nM after incubation of 10 min.

Table 5

Ligand conc	NOTA (pH-7) 7 min at room temp	NOTA (pH-4.5) 7 min at room temp	CP256 3 min at room temp	DOTA 30 min at 100^0C	HBED 10 min at room temp
100 nM	0%	0%	0%	0%	0%
1 µM	41%	2%	84%	0%	70%
10 µM	64%	57%	100%	35%	93%
100 µM	97%	97%	100%	100%	100%
1 mM	100%	100%	100%	100%	100%

Table 5- Comparative study of the radiolabelling yield of different concentrations of the various chelators, when radiolabelled with ^{68}Ga.

The comparison of the radiolabelling yield of CP256, NOTA, HBED and DOTA shows that CP256 and HBED gave best binding with ^{68}Ga (i.e high yield persisted at lowest ligand concentration). Results with NOTA were intermediate between DOTA and CP256. All four chelators showed 100% binding at the two higher concentrations, i.e. 1 mM and 100 µM. However, the behaviour of the chelators differed at lower concentrations. At 10 µM CP256 and HBED still showed maximum binding around 100% and 90% respectively but the radiolabelling yield of DOTA reduced to almost 40% and in case of NOTA at both pH values was ~60%. Further below at 1 µM CP256 still showed a radiolabelling yield of more than 80% and HBED gave a radiolabelling yield of 70%. NOTA at pH 7 was ~40%. With both DOTA and NOTA (pH 4.5) there was almost no binding. At the concentration of 100 nM all the chelators showed 0% binding with ^{68}Ga. Another ligand, Desferrioxamine-B (DFO), is reported to complex Ga^{3+} rapidly with high affinity and radiochemical yield [70]. In summary, CP256 (incubation time 3 min) and HBED (incubation time 10 min) gave a better radiolabelling yield even at lower concentrations and at higher concentration showed 100% binding and stability (Table 5) at neutral pH.

The effect of time on the critical concentrations of both NOTA (10 µM) and HBED (10 µM) was studied. It was observed that for both NOTA and HBED radiolabelling yield increased from 40% at 2 min to 85% at 10 min (Fig-2.1).

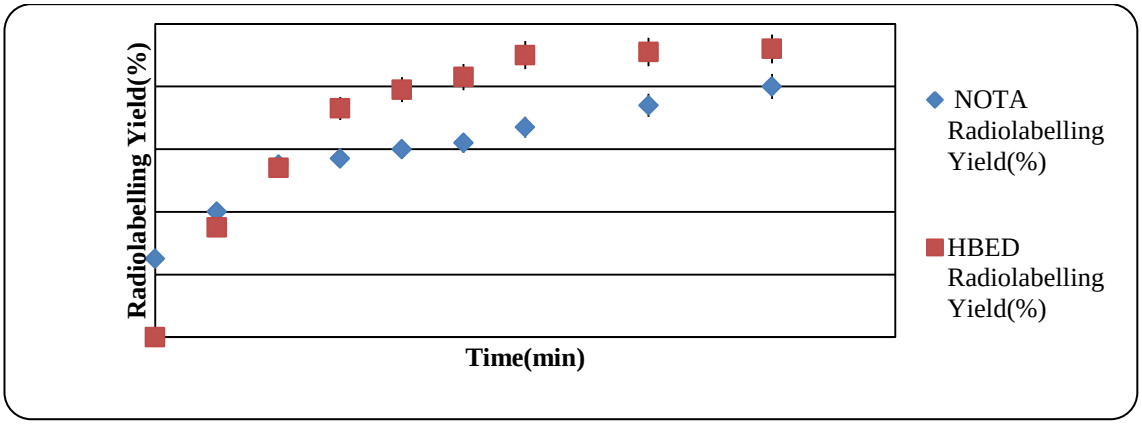

Figure-2.1: Changes in radiolabelling yield of 10 µM HBED and NOTA after different time periods. For HBED, maximum radiolabelling yield of 90% was achieved in 7 min. For HBED maximum radiolabelling yield of 80% was obtained in 9 min.

2.2.4-Stability in Human Blood Serum

Direct comparison of the three reference standards and the sample at two different time–points, i.e. 0 min and 60 min showed that CP256 and HBED have higher affinities for ^{68}Ga than do the metal binding components of human serum. The complexes were stable even after 60 min in serum (Fig-2.2, 2.4, 2.5). These two time points give an ample window to ascertain any dissociation of the complex in human serum with time. On the basis of size, human serum elutes from the PD-10 column first, followed by the radiolabelled chelator complex. Radiolabelled human serum elutes around 3-3.5 ml. $^{68}GaCl_3$ and ^{68}Ga acetate elute in the form of broad peak in the last fractions from 7-10.5 ml. In the case of ^{68}Ga-CP256, it elutes in the middle fractions from 5-7 ml. Radiolabelled CP256 in the presence of human serum also elutes in the same fractions, which indicates that the radiolabelled complex is quite stable even in the excess of serum (Fig-2.2a). Similarly, radiolabelled HBED and NOTA eluted at 6.5-10 ml, which is similar to ^{68}Ga acetate. However, when the radiolabelled complexes of both these chelators were incubated with human serum, the samples eluted in the same fractions as ^{68}Ga-HBED, ^{68}Ga-NOTA and ^{68}Ga acetate, which showed that these radiolabelled complexes were quite stable, otherwise free ^{68}Ga would attach to the serum and elute around 3-3.5 ml. In Fig-2.2a, where human serum was incubated with ^{68}Ga, the first peak is most probably ^{68}Ga-transferrin. This is assumed on the basis of MSc thesis research work, reproduced as Fig-2.2b [140], and the second peak eluted between ^{68}Ga-

acetate and ^{68}Ga-human serum. Most probably, this peak indicates the loosely held serum with ^{68}Ga-acetate or ^{68}Ga-acetate leaching out of serum gallium complex (Fig-2.4, 2.5).

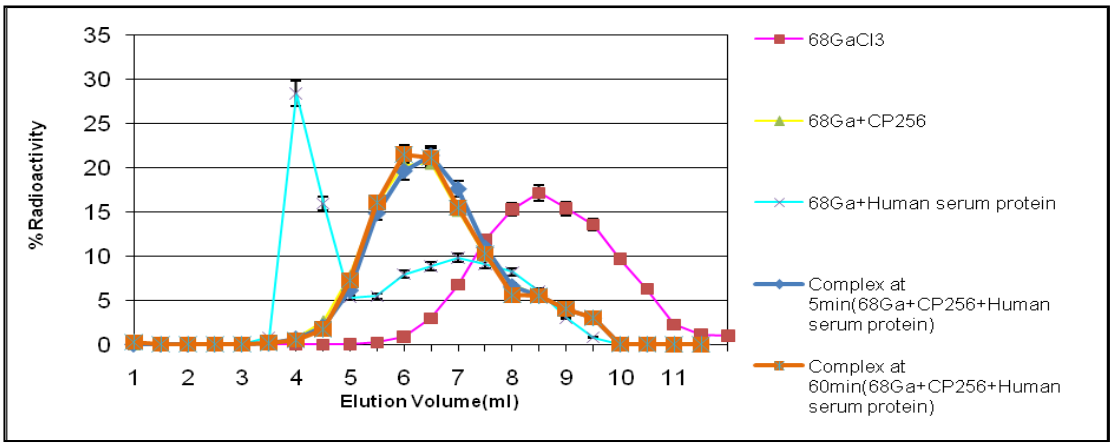

Figure-2.2a: Comparative study of $^{68}GaCl_3$, ^{68}Ga-CP256 and ^{68}Ga-human serum with ^{68}Ga-CP256 in human serum protein by using PD-10 column method at two different time points i.e.5-min and 60-min. It was observed that even after 60-min ^{68}Ga-CP256 stayed stable in human serum.

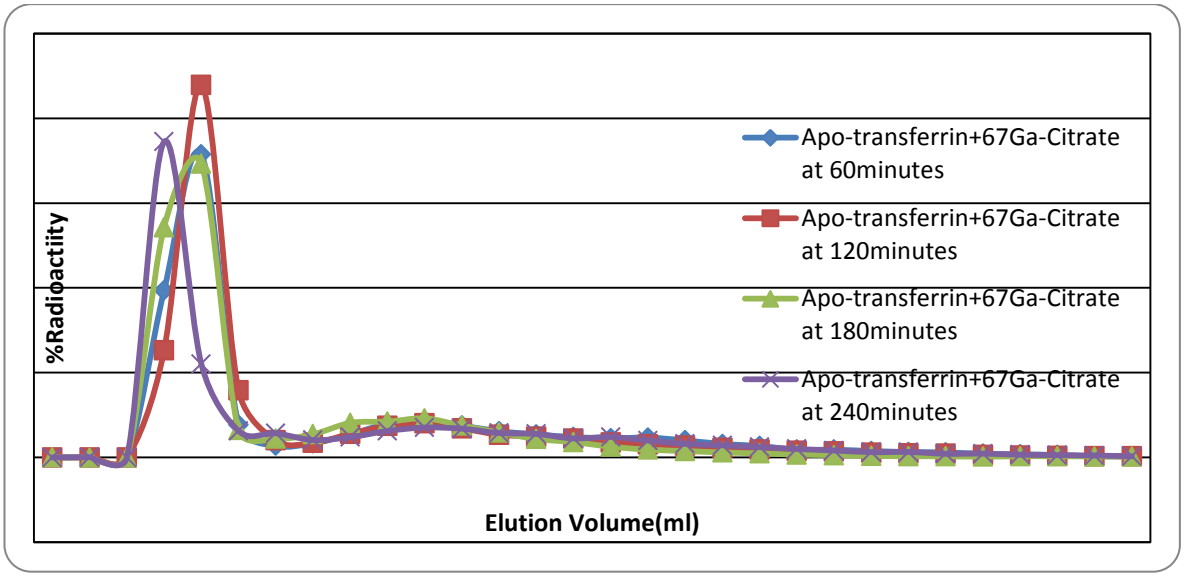

Figure-2.2b: Apo-transferrin was incubated with ^{67}Ga-Citrate. Samples wre taken out at different time-points and analysed by PD-10 column. 30-fractions were collected at each time point [140].

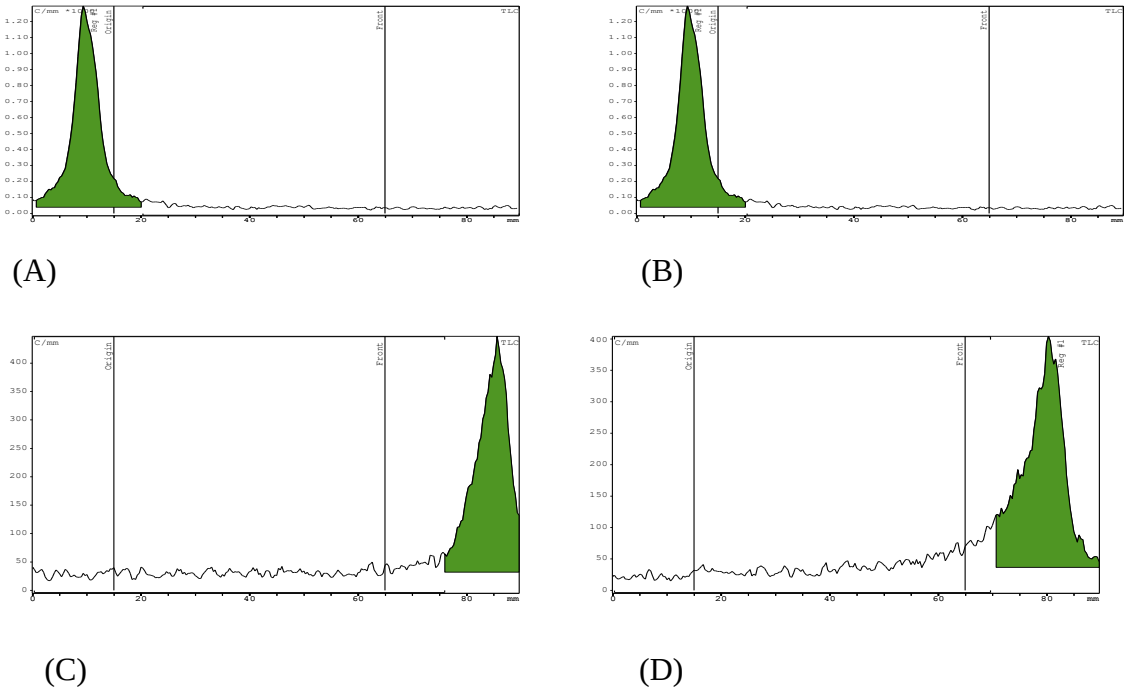

Figure-2.3: HSA-ITLC(sg) chromatography results. ^{68}Ga-human blood serum stays at origin (A). ^{68}Ga-citrate stays at origin because of its hydrophilic nature (B). ^{68}Ga-CP256 moves with the solvent front because of its hydrophobic nature (C). ^{68}Ga-CP256 in serum moves with the solvent front (D).

Figure 2.3 presents results obtained with TLC Method 3, which uses HSA-saturated ITLC-SG strips. Fig-2.3-A,B show that ^{68}Ga-citrate and labelled human serum stayed at the origin. Fig-2.3-C shows that ^{68}Ga-CP256 moved with the solvent front. ^{68}Ga preferred to bind with the chelator even in the presence of human serum (Fig-2.3-D). CP256 is quite hydrophobic in nature and sticks to the origin in hydrophilic systems. This is the first TLC method in which it migrates with the solvent front, probably because of the hydrophobic nature of the stationary phase and the presence of ammonia in the mobile phase (Fig-2.3-C,D). On the other hand ^{68}Ga-citrate stayed at the origin because of its hydrophilic nature (Fig-2.3-A). Human serum also stayed at the origin because of its high molecular weight (Fig-2.3-B).

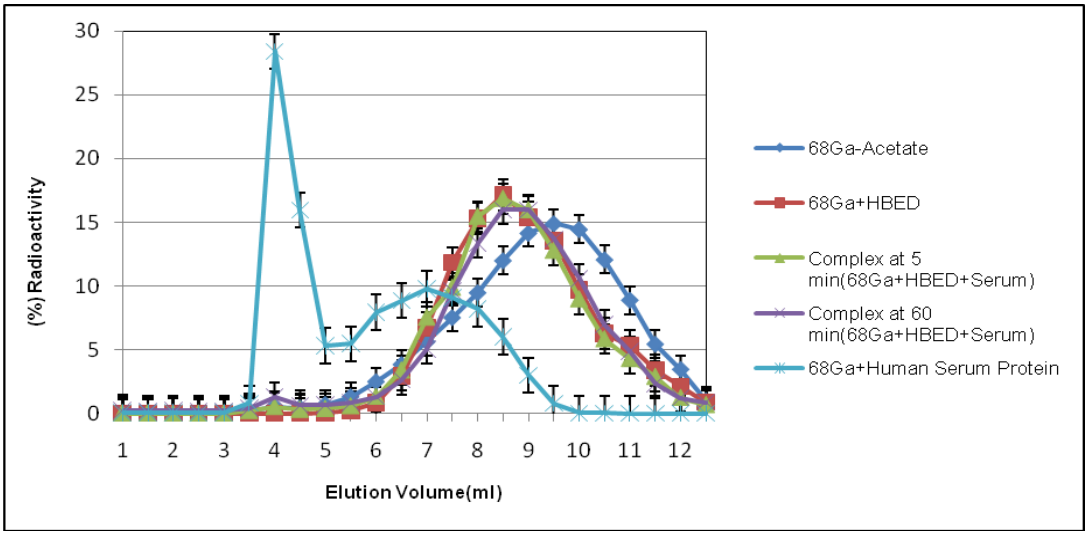

Figure -2.4: Comparative study of ^{68}Ga acetate, ^{68}Ga-HBED and ^{68}Ga-human serum with ^{68}Ga-HBED in human serum by using the PD-10 column method at two different time points i.e. 5-min and 60-min. Even after 60-min ^{68}Ga-HBED stayed stable in human serum.

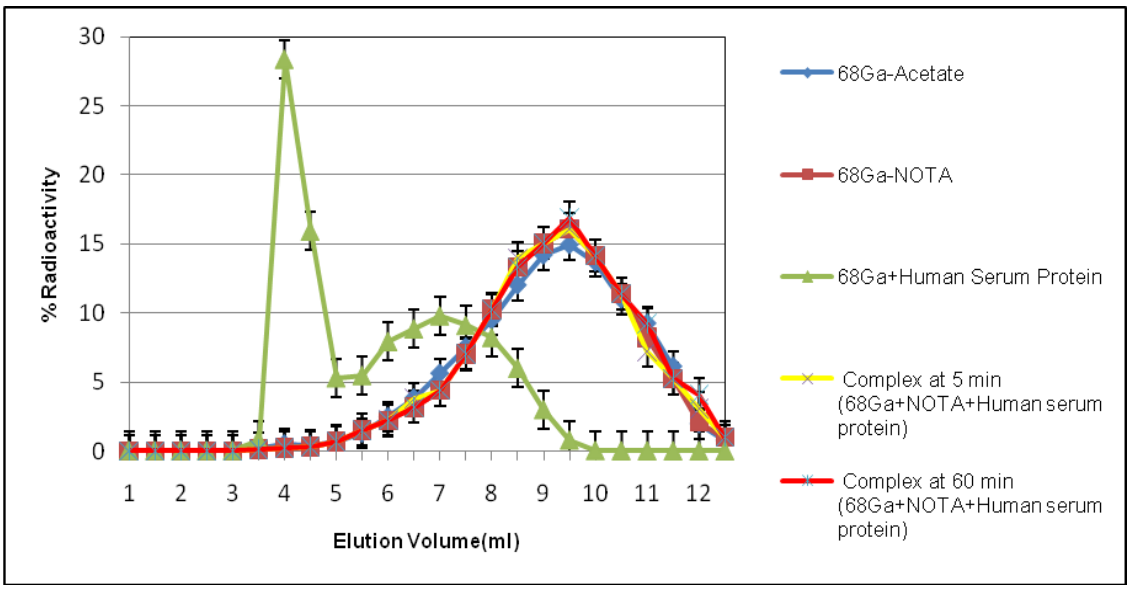

Figure -2.5: Comparative study of ^{68}Ga-acetate, ^{68}Ga-NOTA and ^{68}Ga-human serum with ^{68}Ga-NOTA in human serum by using the PD-10 column method at two different time points i.e. 5-min and 60-min. Even after 60 min ^{68}Ga-NOTA stayed stable in human serum.

2.2.5-Radiolabelling of CP256 and NOTA with eluates from different generators

The main purpose of this experiment was to compare the elutions from two different generators and to check the difference in extent of binding with two chelators under the same conditions. It was observed in case of CP256 that binding in the presence of the 1st elution from the Obninsk generator showed only 40% radiolabelling yield and the 3rd elution, which is done 2 hrs after the 2nd elution gave 65-70% binding. In contrast, a previous elution from the IGG100 generator and a reference which contained 0.1 N HCl showed 100% radiolabelling yield (Fig-2.6). This suggests that even a 2nd or 3rd eluate of the Obninsk generator contains metal contaminants which interfere with labelling. This does not appear to be a problem with the IGG100 generator.

The same experiment was repeated using NOTA and it was observed that the IGG100 generator gave 85%-100% binding whereas the 1st elution from the Obninsk generator gave 30% binding and the 3rd elution showed 60% binding (Fig-2.7).

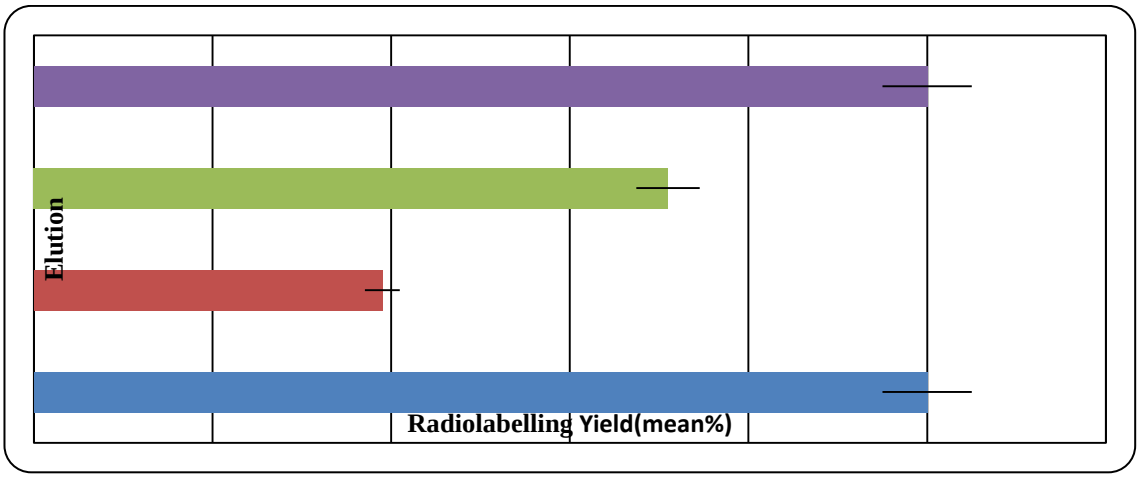

Figure-2.6: Changes in radiolabelling yield of CP256 (11.8 µM) with ^{68}Ga eluted from Obninsk and IGG 100 generators and spiked with fresh elution from IGG 100 (20 µL, ~5 MBq). Each value is mean and standard deviation for three experiments.

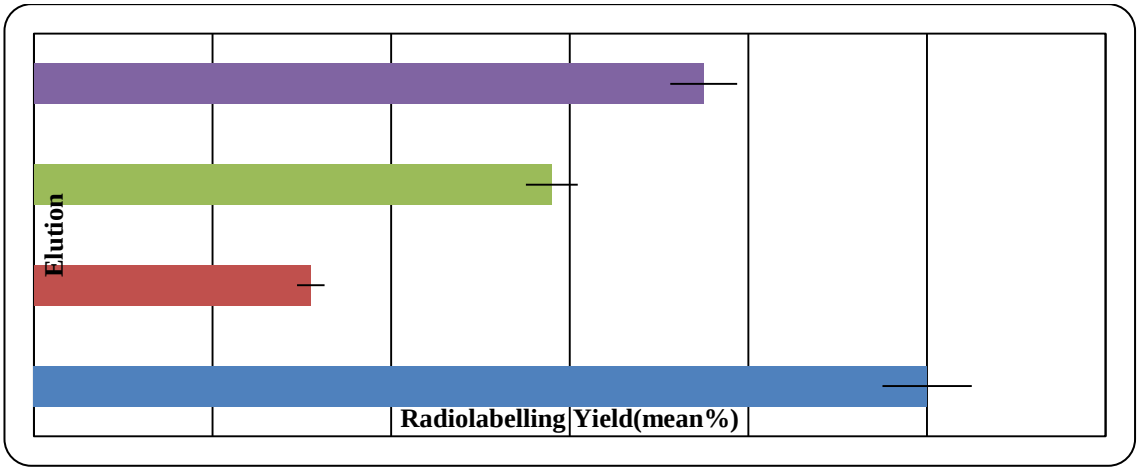

Figure-2.7: Changes in radiolabelling yield of NOTA (11 µM) with ^{68}Ga eluted from Obninsk and IGG100 generators spiked with fresh elution from IGG 100 (20 µL, ~5 MBq). Each value is mean and standard deviation for three experiments.

2.2.6-Radiolabelling of C2A protein with ^{68}Ga

The C2A protein (Complement C2) is a protein that in humans is encoded by the C2 gene and is part of the classical pathway of complement system. Activated C1 cleaves C2 into C2a and C2b. C2A leads to activation of C3. Deficiency of C2 has been reported to be associated with certain autoimmune diseases. It binds to phosphatidylserine and has potential use as imaging agent for apoptosis/cell death [75]. This protein is used as a model protein here, to see how ^{68}Ga binds with the protein. The protein contains a cysteine, which was used to conjugate with YM103, a maleimide derivatised form of CP256.

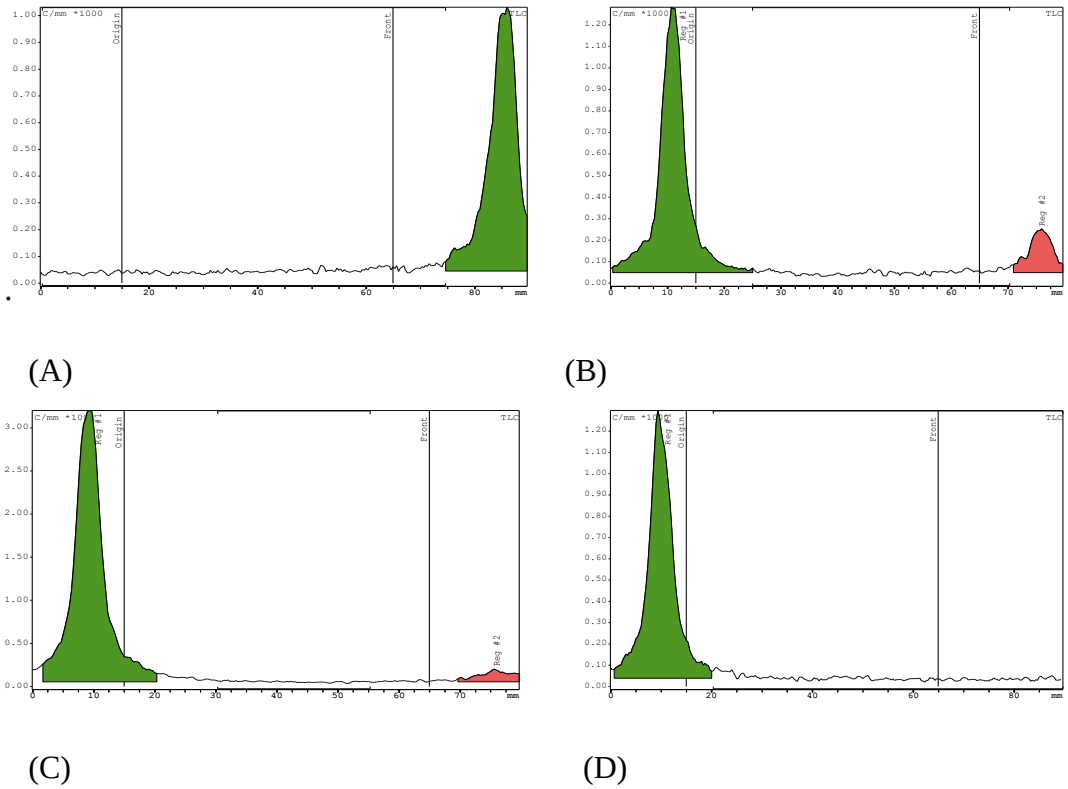

Figure-2.8: Reference-^{68}Ga-Citrate (A) moved with the solvent front. ^{68}Ga-Conjugated C2A protein remained at the origin after 1-2 min, with some unbound ^{68}Ga-citrate at the solvent front (B). ^{68}Ga-Conjugated C2A protein at the origin after 5 min. The amount of unbound ^{68}Ga-citrate reduced at the solvent front (C). ^{68}Ga-Conjugated C2A protein at the origin with no unbound ^{68}Ga-citrate at solvent front after 10 min (D).

Fig-2.8-A shows that reference ^{68}Ga-Citrate moved with the solvent front. Conjugated C2A protein showed 87% radiolabelling yield within 1-2 min (Fig-2.8-B). After 5 min binding increased to 97% (Fig-2.8-C) and within 10 min it gave 100% radiolabelling yield at room temperature and pH of 7 (Fig-2.8-D).

2.2.7- Evaluation of CP256 binding with other radionuclides

Although ^{68}Ga is the main radioisotope used in this project, to further ascertain the importance and versatility of this novel chelator (CP256), it was radiolabelled with some other imaging and therapeutic radioisotopes including ^{111}In, ^{99m}Tc, ^{90}Y, and ^{89}Zr.

Simple radiolabelling of the above mentioned radioisotopes was carried out and analysed by TLC, followed by stability in human serum, analysed by the PD-10 column method.

2.2.7a-Radiolabelling with ^{111}In-Acetate

Radiolabelling of CP256 with ^{111}In was analysed with TLC Method 3. In this method ^{111}In-acetate stays at the origin in ITLC-SG (HSA) (Fig-2.9), whereas ^{111}In-CP256 moves with solvent front (Fig-2.10). This behaviour is similar to ^{68}Ga-CP256.

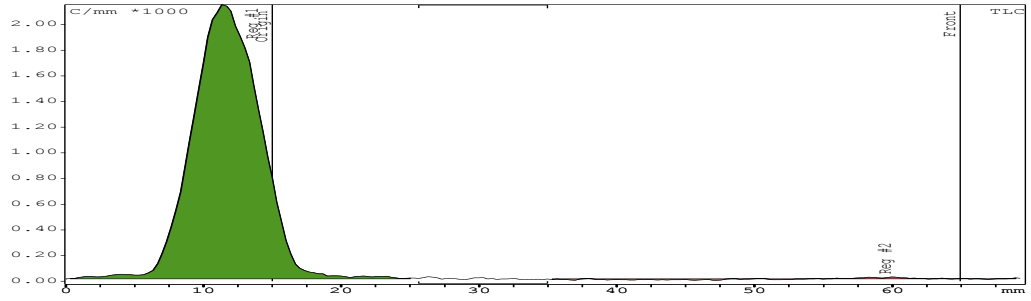

Figure-2.9: HSA-ITLC-SG+Reference ^{111}In-acetate stayed at the origin with Rf value of 0.

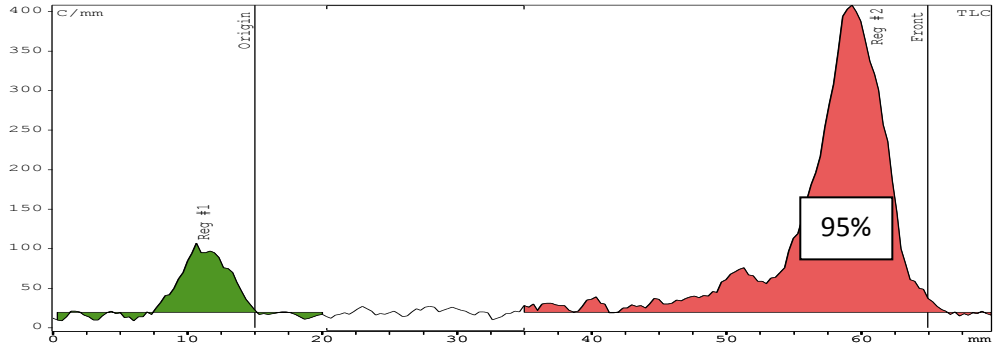

Figure-2.10: HSA-ITLC-SG+^{111}In-CP256 Complex moved with solvent front because of its hydrophobic nature and small amount of ^{111}In-acetate remained at the origin.

.

^{111}In formed a complex with CP256 in appreciable quantities although it is not 100% binding as there is still some unbound ^{111}In after the incubation of 20 min. The radiolabelling yield obtained was around 95% (Fig-2.10).

Along with radiolabelling, binding of ^{111}In with CP256 and its stability in human blood serum was also tested at different time intervals. In PD-10 column chromatography, human serum eluted in fractions 3-3.5 ml followed by ^{111}In acetate from 4.5-6.5 ml and CP256 radiolabelled with ^{111}In eluted from 5.5-8.5 ml. Radiolabelled CP256 was incubated in human serum and samples were taken out at three time-points: 5 min, 60 min and 120 min. It was observed that the complex remained stable in human blood

serum even after 2 h and ^{111}In has higher affinity for CP256 even in serum and there was no dissociation of radiolabelled complex and association with serum (Fig-2.11). Both In and Ga belong to the same group in periodic table (III A). Both elements have oxidation state of +3 [106]. In is a larger ion with a higher expected coordination number, so we expect some differences in their behaviour. Radiolabelling of CP256 with ^{68}Ga was 100% within a few minutes, however with ^{111}In we achieved 95% radiolabelling yield after 20 min of incubation. CP256 forms quite a stable complex with ^{68}Ga in human serum so we expect similar behaviour with ^{111}In.

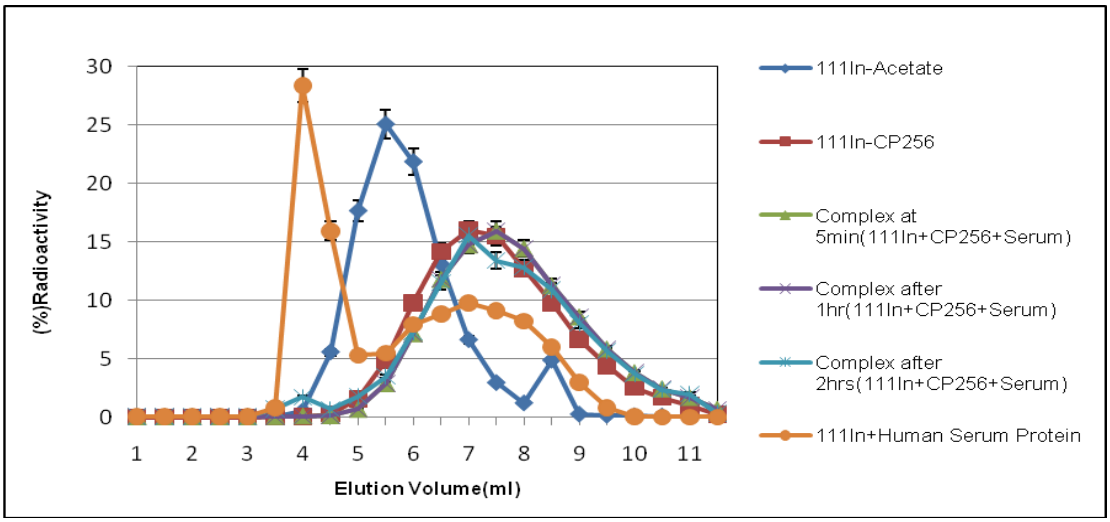

Figure -2.11: Comparative study of ^{111}In-acetate, ^{111}In-CP256, and serum with ^{111}In-CP256 complex in serum at 3 different time-points, i.e. 5-min, 60-min and 2 h, to evaluate the stability of ^{111}In-CP256 in serum. ^{111}In-CP256 stayed stable in serum even after 2 h.

2.2.7b-Radiolabelling with ^{90}Y

To analyse the radiolabelling of CP256 with ^{90}Y, TLC Method 3 was used. In Fig-2.12, ^{90}Y-acetate stayed at the origin and ^{90}Y-CP256 moved with the solvent front (Fig-2.13). The yield of ^{90}Y-CP256 appeared to be quantitative within 10 min at room temperature.

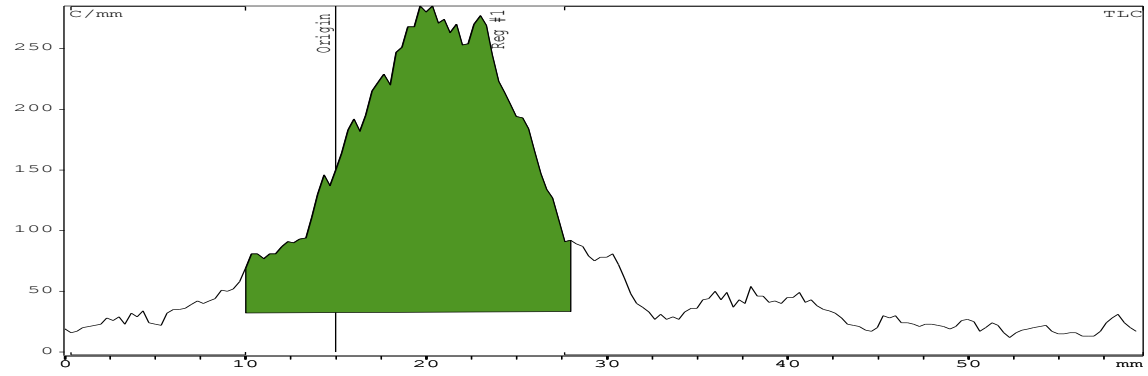

Figure-2.12: HSA-ITLC-SG, ^{90}Y-acetate stays at the origin with Rf value of 0.

.

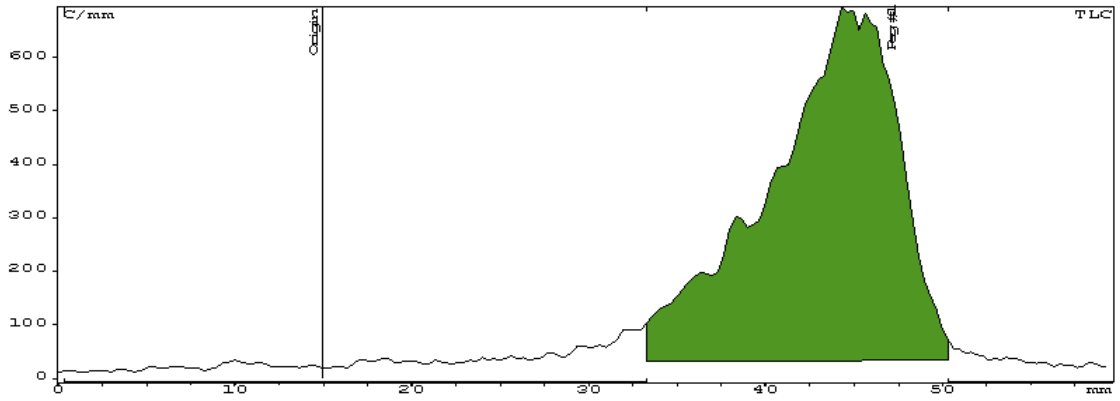

Figure-2.13: HSA-ITLC-SG, ^{90}Y-CP256 moves with the solvent front with Rf value of 1.

.

Stability of ^{90}Y-CP256 in human serum was tested by the PD-10 column method. The ^{90}Y-CP256 complex (100 µl) was incubated with human serum (300 µl) and samples were taken at 10 min, 60 min and 4 h and applied to a PD-10 column. However, it was evident that ^{90}Y-CP256 was not very stable in human serum, as most of the ^{90}Y became attached to components of serum and eluted with the serum fractions (Fig-2.14). Although the oxidation state of Y is also +3 and it belongs to the III-B group, there are many differences in the chemical behaviour of Y with respect to Ga and In [106,120].

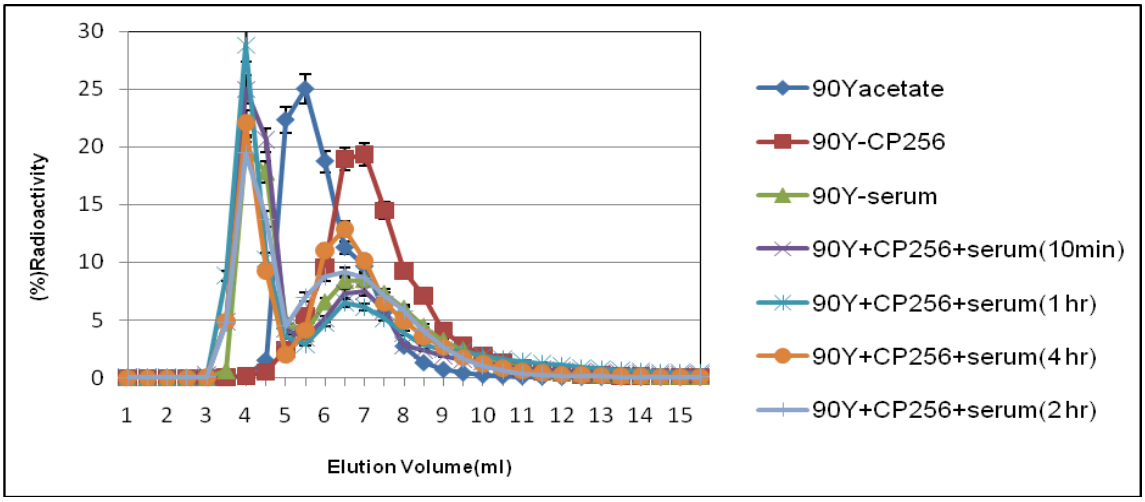

Figure-2.14: Comparative Study of ^{90}Y-acetate and ^{90}Y-CP256, ^{90}Y human serum, ^{90}Y+CP256 incubated in human serum and samples were taken at 10 min, 1 h, 2 h and 4 h for PD-10 column analysis.

2.2.7c-Radiolabelling with ^{99m}Tc-tricarbonyl

The $[Tc(OH_2)_3(CO)_3]^+$ complex can also be described as a semi aqua ion. One half of the coordination sphere is shielded, whereas the other half is prone to substitution with classical or nonclassical ligands. Three carbonyl ligands of small size and low molecular weight are tightly bound, while three water ligands can be exchange by incoming chelators.

For quality control purposes to check the formation of ^{99m}Tc-tricarbonyl, glass-backed TLC-SG plates were developed with 1% HCl in methanol. Any colloid will stay at the baseline, free pertechnetate moves to the solvent front and tricarbonyl will be at centre (Rf=0.4) (Fig-2.15) [116]. ^{99m}Tc tricarbonyl was incubated with CP256 and the radiolabelled complex was analysed using TLC Method 1. A radiolabelling yield of 60% was obtained within 5 min (Fig-2.17, 2.18) and it increased to 90% within 30 min at room temperature (Fig-2.18). The complex was quite stable even after 4 h and there was no evidence of dissociation between tricarbonyl and CP256 (Fig-2.16, 2.17, 2.18).

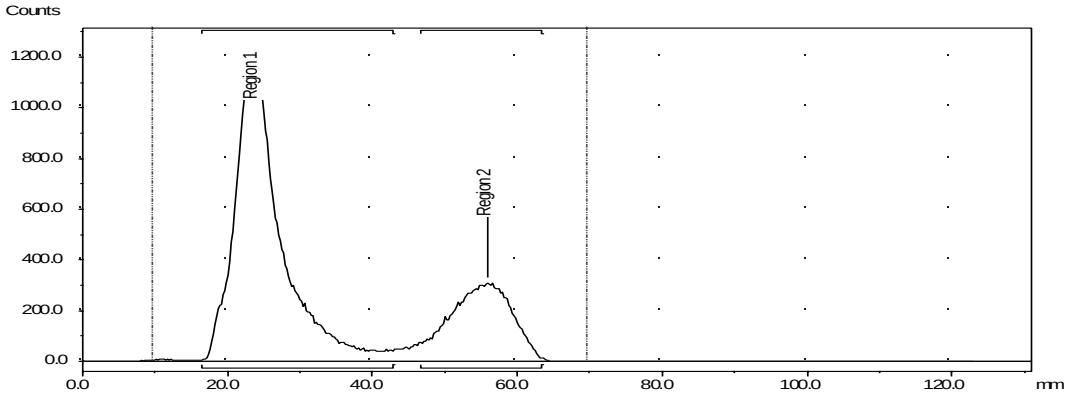

Figure -2.15: QC for ^{99m}Tc tricarbonyl showed that 80% of ^{99m}Tc tricarbonyl was formed (region 1) and the remaining 20% was in the form of free pertechnetate (region 2).using TLC Method 2.

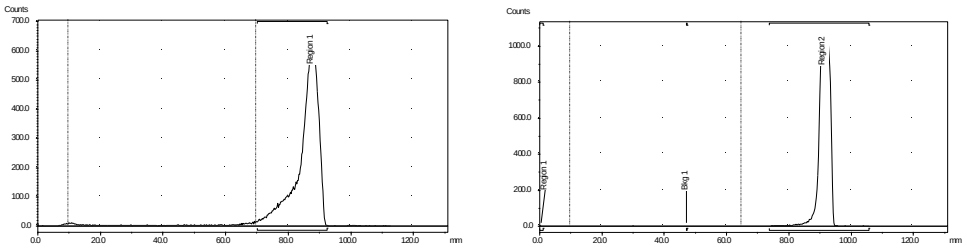

(A) **(B)**

Figure-2.16: TLC Method 1 was used for analysis. ^{99m}Tc tricarbonyl moved with the solvent front (A) because of its hydrophilic nature. Free pertechnetate (hydrophilic) also moved with solvent front (B) and thus Method 1 was unable to distinguish the two species.

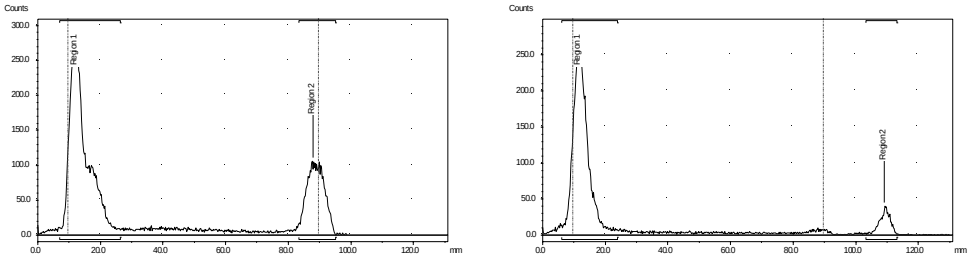

(C)

(D)

Figure-2.17: TLC Method 1 was used for analysis. Unreated ^{99m}Tc tricarbonyl and/or free pertechnetate moved with the solvent front and the CP256-tricarbonyl complex stayed at the origin. At 10 min 80% radiolabelling yield was obtained (C) and at 60 min 100% radiolabelling yield is obtained (D). We have to keep in mind that we started with 80% of tricarbonyl.

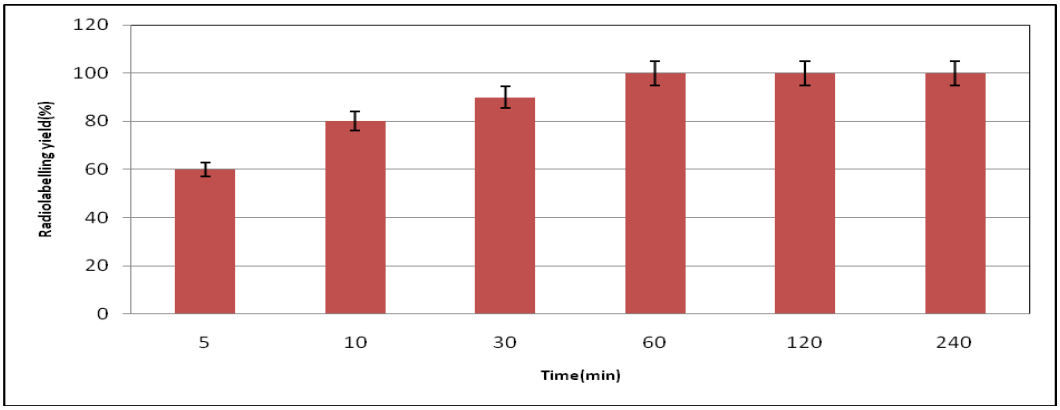

Figure-2.18: Graphical representation of radiolabelling yield obtained at different time points, when CP256 was incubated with ^{99m}Tc tricarbonyl and samples were taken out at different time points to be analysed by the TLC Method 1.

2.2.7d-Radiolabelling with ^{89}Zr (Zirconium)

^{89}Zr (IDB, Amsterdam) comes in the oxalate form (C_4O_8Zr). It was converted to the citrate form by adding citrate buffer (60 µl, pH 6) [119]. It was observed that ^{89}Zr bound with CP256 within 20 min of incubation at room temperature. ^{89}Zr-citrate moved with the solvent front and ^{89}Zr-CP256 stayed at the origin because of its hydrophobic nature in TLC Method 1 as shown in Fig-2.19. When ^{89}Zr-CP256 was incubated with human serum and samples were taken at different time points and analysed by the PD-10 column method, it was evident that the Zr complex of CP256 was quite stable in human serum (Fig-2.20). Zr belongs to group IVB of the periodic table, forms an extremely hard acidic 4+ cation and because of its coordination number requirements it forms stable complexs with octadentate lanthanide chelators (DOTA-L39) [120].

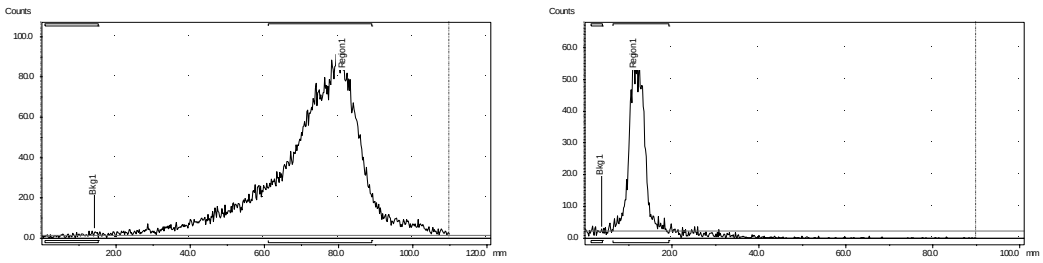

(A) **(B)**

Figure-2.19: TLC Method 1 was used for analysis. ^{89}Zr citrate moved with the solvent front (A). However in the same system ^{89}Zr-CP256 stayed at the origin (B).

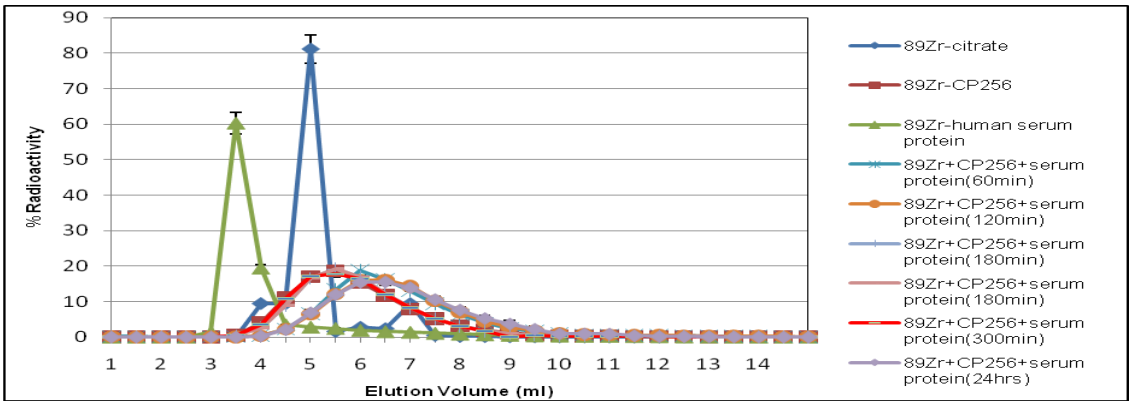

Figure-2.20: Comparative study of ^{89}Zr-acetate and ^{89}Zr-CP256, ^{89}Zr human serum, ^{89}Zr+CP256 incubated in human serum with samples are taken up to 24 h.

2.2.8-Formation of ^{68}Ga-CP256 complex in serum

The extremely high affinity and rapid chelation of CP256 for Ga prompted us to test the hypothesis that CP256 could chelate ^{68}Ga *in vivo*, allowing a pre-targeting approach in which an antibody conjugated with CP256 could be administered to a patient, followed hours to days later by ^{68}Ga-acetate or citrate. The elution profile of human serum radiolabelled with ^{68}Ga with incubation time of 30 min (Reference 2) showed that most of the ^{68}Ga eluted in 4-4.5 ml (Figure 2.21-E) showing that it became bound to serum.

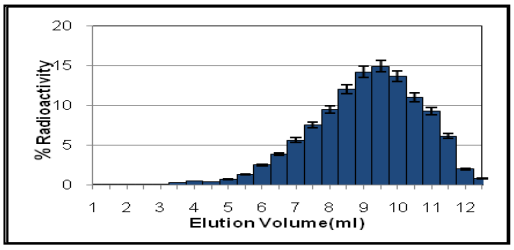

(A)

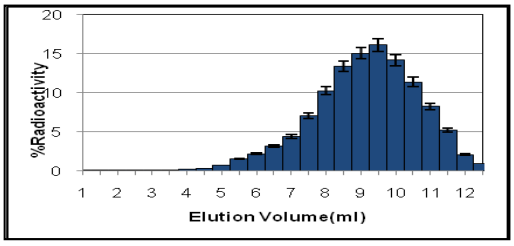

(B)

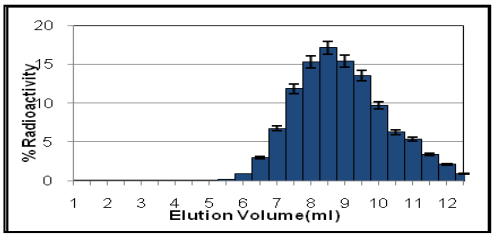

(C)

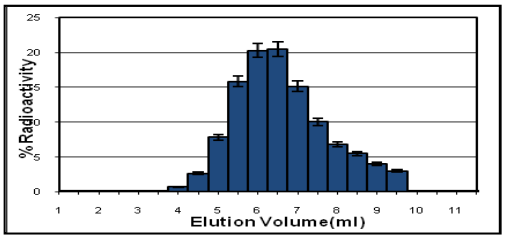

(D)

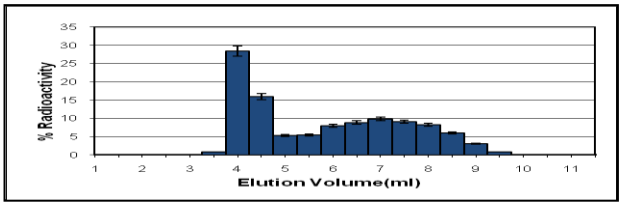

(E)

Figure-2.21: Elution profile of ^{68}Ga-Acetate (A), ^{68}Ga-NOTA (B), ^{68}Ga-HBED (C), ^{68}Ga-CP256 (D) and ^{68}Ga-human serum (E) using PD-10 column.

In contrast, ^{68}Ga-CP256 (Reference 1) eluted at 5.5-6 ml (Figure 2.21-D) and simple ^{68}Ga-acetate or citrate (Reference 3) eluted in 8.5-10 ml as a broad peak (Figure 2.21-A). ^{68}Ga-NOTA eluted in 9-10 ml and ^{68}Ga- HBED eluted in 8-9 ml.

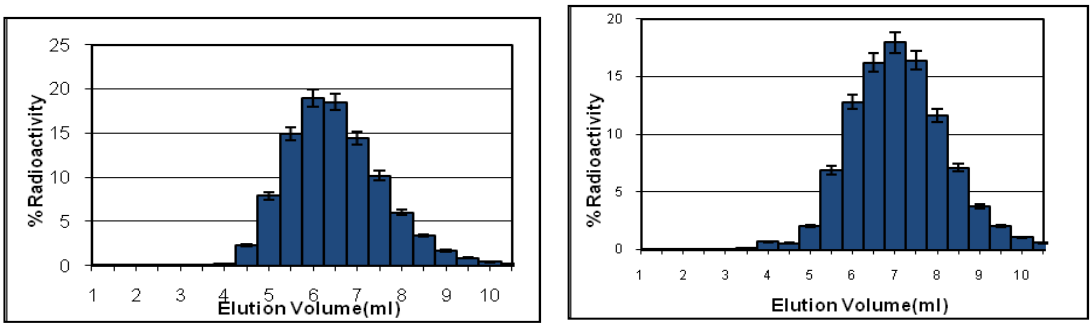

(A) **(B)**

Figure-2.22: Elution profile of ^{68}Ga-CP256 (A) at 60 min using PD-10 column in the sequence (CP256+human serum+^{68}Ga). ^{68}Ga preferred to bind with CP256 in serum after 60 min and eluted in the 5.5-6 ml fraction. Elution profile (B) is in the sequence (^{68}Ga+serum+CP256). ^{68}Ga again preferred to bind with CP256 instead of serum and also removed most of the ^{68}Ga which had been attached to serum.

The elution profile of the sample (CP256+human serum+$^{68}GaCl_3$) shows that there was binding between CP256 and ^{68}Ga, as the radioactivity eluted in the middle fractions (Figure 2.22) i.e. 5.5-6 ml, like Reference 1 ^{68}Ga-CP256. The complex between the chelator and ^{68}Ga formed in the presence of human serum even at a low chelator concentration of 23 µM or 0.02 mg/ml (Figure-2.23, 2.24). However, when the concentration of the chelator was as low as 0.01 mg/ml, ^{68}Ga started binding with the human serum (Figure 2.24).

In the second study which used a different sequence of addition (i.e. human serum+ $^{68}GaCl_3$+CP256), comparison of Reference 1 (^{68}Ga-CP256) with pre-sample (human serum+^{68}Ga; before addition of CP256) and post-sample (human serum+^{68}Ga+CP256) showed that ^{68}Ga in the pre-sample combined with human serum or eluted as free ^{68}Ga. However, in the post-sample when the chelator was added to the pre-sample, not only the free ^{68}Ga bound with the chelator but the ^{68}Ga which was previously bound to serum prefered to detach from serum and bind with CP256 (Figure 2.25).

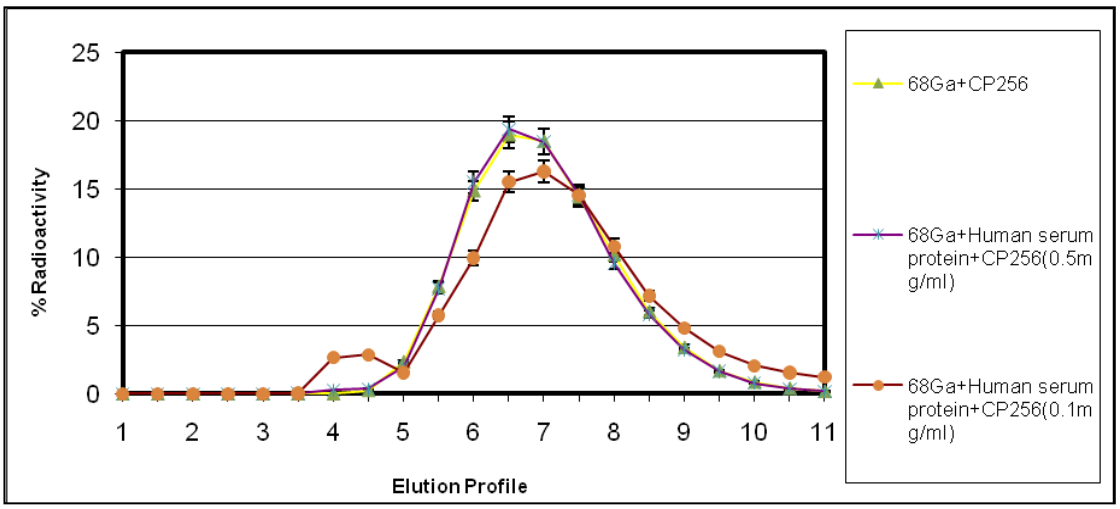

Figure-2.23: Comparative study of ^{68}Ga-CP256 with two different concentrations of CP256 in human serum and ^{68}Ga . ^{68}Ga preferred binding with CP256 instead of human serum.

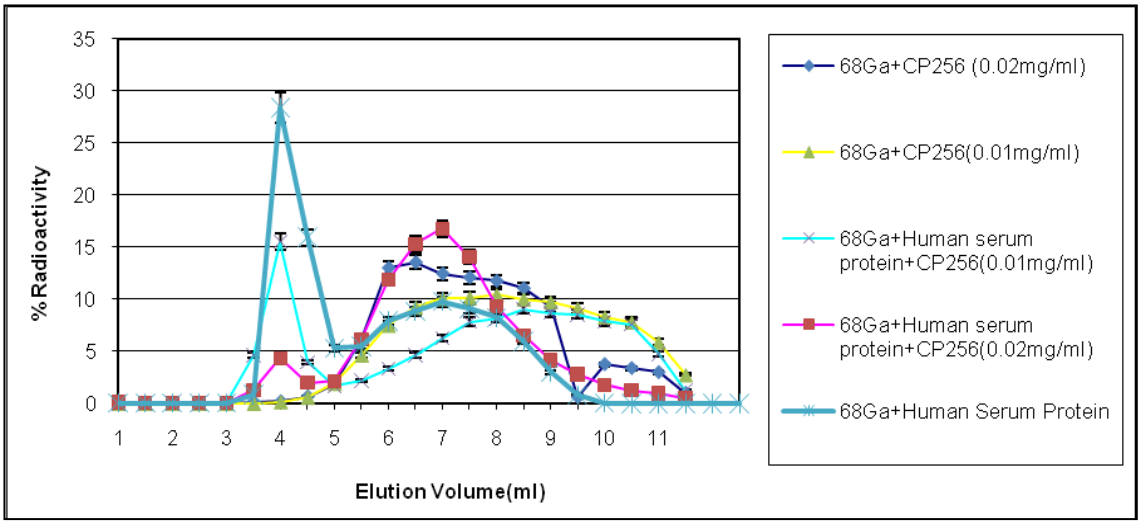

Figure-2.24: Formation of ^{68}Ga-CP256 with two different concentrations of CP256 in human serum and ^{68}Ga analysed using PD-10 column method. ^{68}Ga CP256 complex formed in serum at a concentration of 0.02 mg/ml. At the concentration of 0.01 mg/ml of CP256 ^{68}Ga starts dissociating from CP256 and binding with serum.

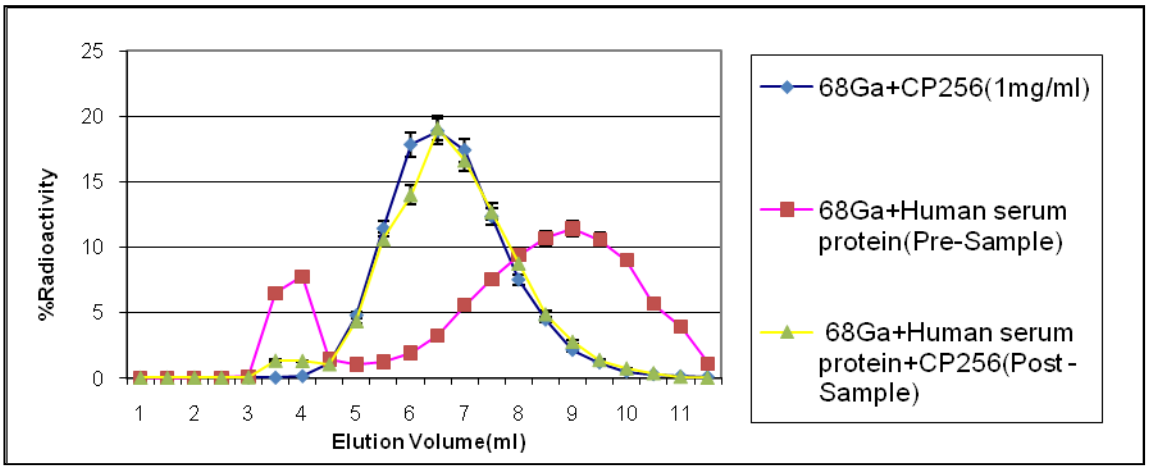

Figure-2.25: In this study we have radiolabelled human serum with ^{68}Ga-and this sample is called Pre-Sample (^{68}Ga+serum). Then CP256 was added to this Pre-sample and now this sample is called Post –Sample (^{68}Ga+serum+CP256). It is evident that ^{68}Ga attached to serum in Pre-sample became detached from it and preferred to bind with CP256 in the Post–sample, which indicates that pretargetting is possible with CP256. These results indicate that ^{68}Ga-CP256 is not only stable in serum, but it can also snatch ^{68}Ga which is already attached to serum.

For further evaluation of the pretargeting approach, size exclusion chromatography was supplemented by studies in which the protein was precipitated with absolute ethanol, the activities in the supernatant and pellet were measured, and the supernatant was analysed by TLC Method 1. In the first sample CP256 was added to human serum which already contained ^{68}Ga and in the second sample CP256 was added to serum followed by the addition of ^{68}Ga. Both samples were incubated for 60 min, then diluted with an equal volume of absolute ethanol to precipitate serum proteins. Tubes were centrifuged for 2 min at 12000*g*. The supernatant was transferred to separate tubes and the activity of both supernatant and pellets (serum protein) was measured in the dose calibrator. It was observed that the entire radioactivity stayed with the supernatant and there was no activity in the pellet.

Further, supernatant samples were analysed using TLC Method 1, in which $^{68}GaCl_3$ moves with the solvent front (Fig-2.26-A) and ^{68}Ga-CP256 stays at the origin (Fig-2.26-B). The TLC of supernatant samples showed that the activity stayed at the origin, indicating formation of ^{68}Ga-CP256 (Fig-2.26-C,D). There was zero activity in the pellets, showing that there is no binding of ^{68}Ga to serum.

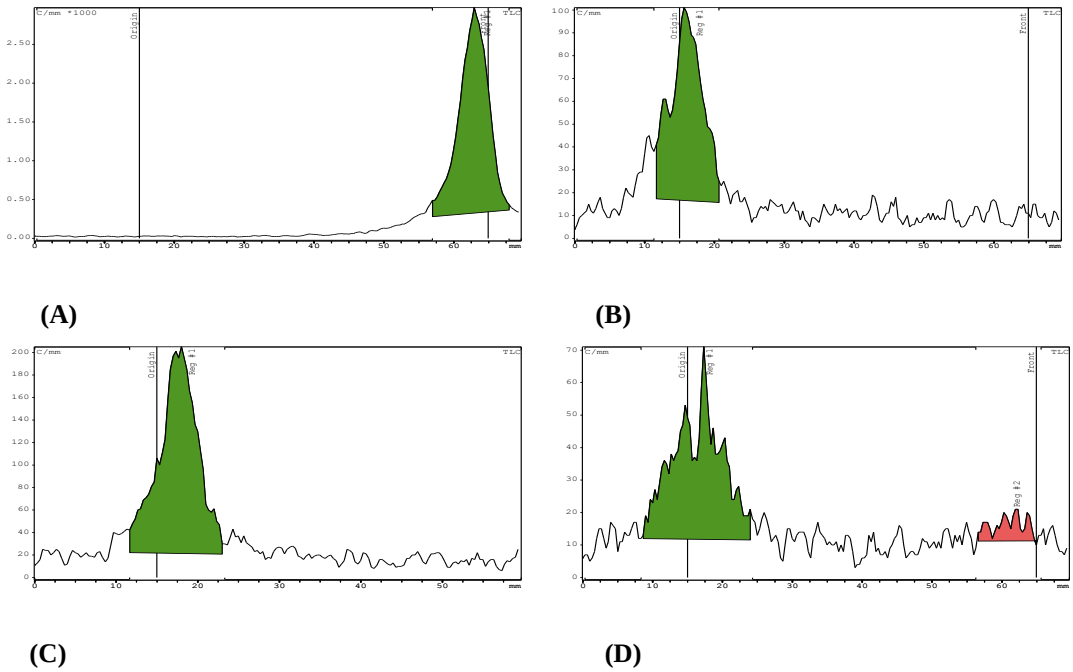

Figure-2.26: $^{68}GaCl_3$ moved with the solvent front (A). ^{68}Ga-CP256 stayed at the origin because of its hydrophobic nature (B). Supernatant sample (1 mg/ml) stayed at the origin, suggesting it contained ^{68}Ga-CP256 (C). Supernatant sample (0.1 mg/ml) also stayed mainly at the origin with a small amount of free $^{68}GaCl_3$ moves with the solvent front (D).

For comparison with the results obtained with CP256, similar experiments were performed with NOTA and HBED.

In evaluation of pretargeting approaches with NOTA, the elution patterns of the reference mixtures from PD-10 columns were studied. Most of the ^{68}Ga-acetate and ^{68}Ga-NOTA eluted in the last fractions from 8.5-9.5 ml (Figure 2.21). However, ^{68}Ga-binding components of human serum eluted in 4.0-4.5 ml (Figure 2.21). In both the addition sequences evaluated for pretargetting it was observed that most of the activity eluted in 3.5-4 ml, which shows that ^{68}Ga is bound to the serum, instead of chelator, NOTA (Figure 2.27, 2.29). This behaviour of NOTA is quite opposite of CP256 and thus NOTA does not appear to be suitable for a pretargeting approach.

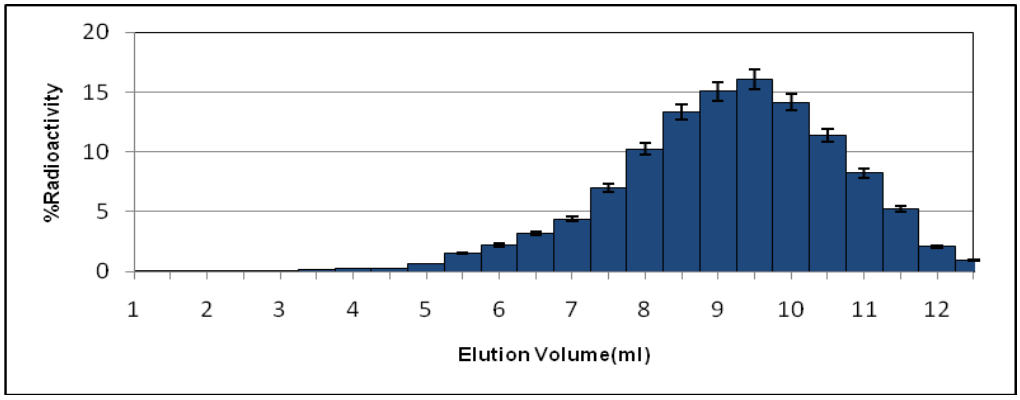

(A)

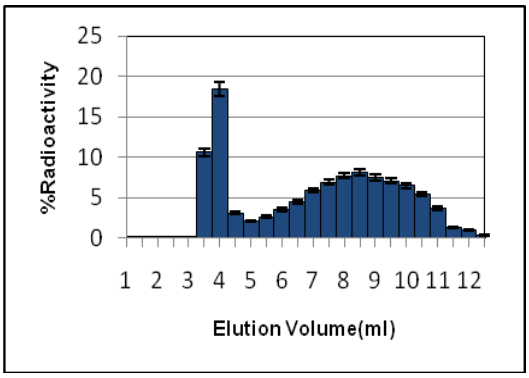

(B)

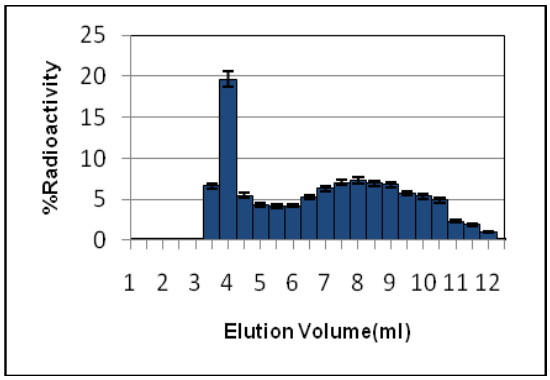

(C)

Figure-2.27: Elution profile of ^{68}Ga-NOTA in human serum using a PD-10 column. ^{68}Ga-NOTA was quite stable when incubated in serum (A). However, NOTA did not show any binding with ^{68}Ga. When ^{68}Ga was added to the solution containing serum and NOTA in a sequence (NOTA+serum+^{68}Ga) it preferred binding with serum and eluted in 4 ml (B). Similarly, when NOTA was added to serum which was already radiolabelled with ^{68}Ga in a sequence (^{68}Ga+serum+ NOTA) ^{68}Ga remained attached to serum and eluted in 3.5-4 ml fraction (C).

Similar experiments were conducted with HBED. Most of the ^{68}Ga-HBED eluted from 7.5-8.5 ml (Figure 2.28). Serum stability studies indicated that the complex eluted in the same volume, 7.5-8.5 ml (Figure 2.28-A).

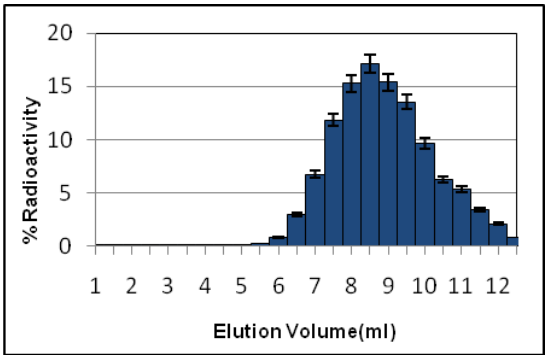

(A)

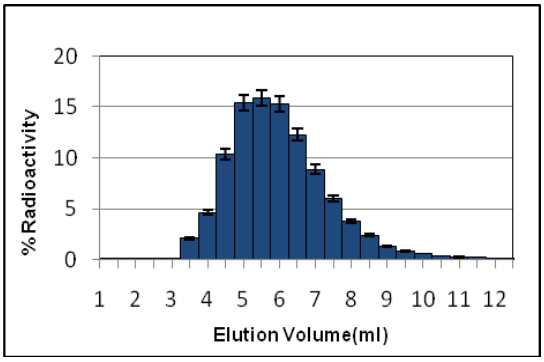

(B)

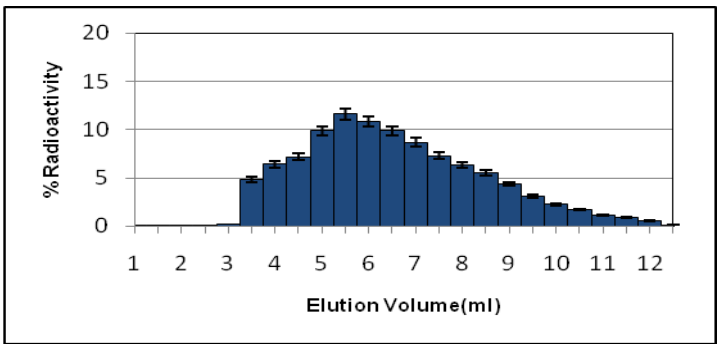

(C)

Figure-2.28: Elution profile of ^{68}Ga-HBED in serum using PD-10 column. ^{68}Ga-HBED was quite stable when incubated in serum (A). However, the behaviour of HBED was quite complex compared to CP256 and NOTA. When ^{68}Ga was added to a solution containing serum and HBED in a sequence (HBED+serum+^{68}Ga) (B) and when HBED was added to serum which was already radiolabelled with ^{68}Ga in the sequence (^{68}Ga+serum+HBED) (C) it eluted in a broad peak at 4.5-7.5 ml. In comparison, serum eluted at 4-4.5 ml and radiolabelled HBED eluted at 7.5-8.5 ml. This showed that the behaviour of HBED was intermediate between NOTA and CP256.

However, when the pretargeting approach (both addition sequences) was evaluated with HBED its behaviour was different from CP256 and NOTA. Labelled serum eluted in fraction 4-4.5 ml as shown earlier. ^{68}Ga-HBED eluted in a broad peak from 7.5-8.5 ml and in pretargetting using both sequences it eluted in a broad 4.5-7.5 ml fraction (Figure 2.28, 2.30), showing no clear evidence of either serum or HBED binding. These results were quite different from CP256, which showed very prominent binding to ^{68}Ga in the presence of serum, even extracting ^{68}Ga that was already bound to serum (Figure 2.22-2.25). At the same time the behaviour of HBED was not as poor as NOTA in pretargetting. The behaviour of HBED was more complex and intermediate between the

CP256 and NOTA. The (^{68}Ga+serum+HBED) peak (4.5-7.5 ml) was different and overlapping with both ^{68}Ga-serum (4-4.5 ml) and ^{68}Ga-HBED peak (7.5-8.5 ml) (Figure 2.30).

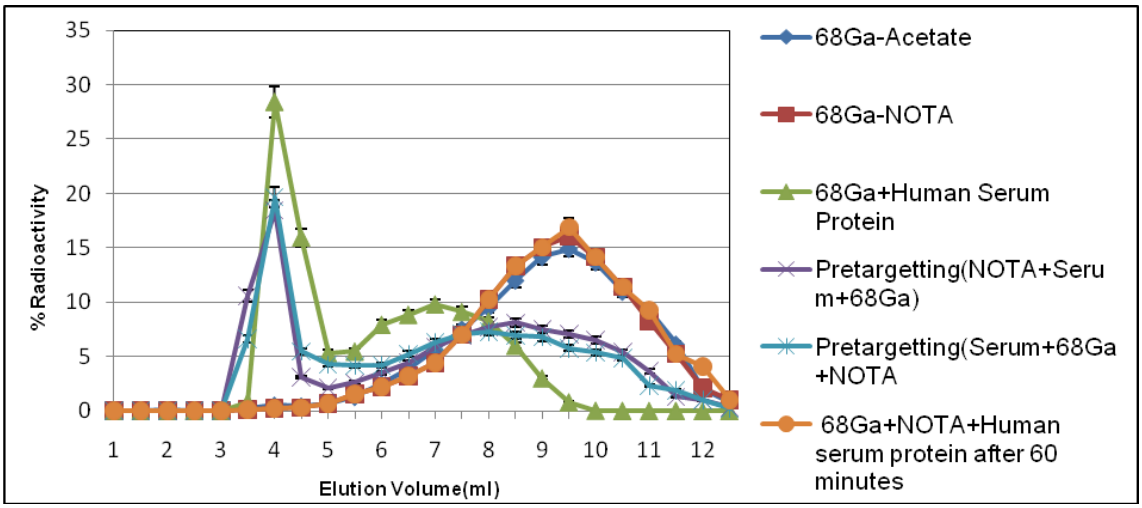

Figure-2.29: Comparative study of ^{68}Ga-acetate, ^{68}Ga-NOTA and ^{68}Ga-serum with two different sequences of pretargetting with NOTA using PD-10 column. Both the sequences of pretargetting showed that ^{68}Ga preferred to bind with serum instead of NOTA.

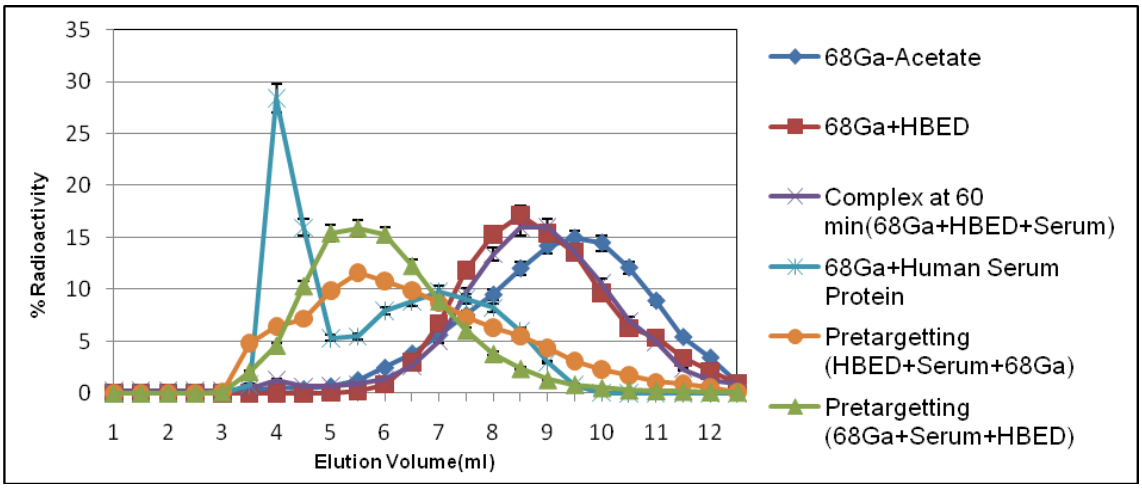

Figure-2.30: Comparative study of ^{68}Ga-acetate, ^{68}Ga-HBED and ^{68}Ga-serum with two different sequences of pretargetting with HBED using PD-10 column. Both the sequences of pretargetting showed intermediate results.

2.3-Discussion

The Obninsk generator was the first which provided cationic ^{68}Ga. Both the IGG100 and Obninsk generators are based on a closed system composed of borosilicate glass containing titanium dioxide in which ^{68}Ge is embedded and then the decay product ^{68}Ga is eluted with 0.1 M HCl. The result of the experiments using the 1st and 2nd elutions from the IGG100 generator showed that there was little difference in radiolabelling yield or kinetics between the 1st and 2nd elution and therefore the 2 h waiting time between the elutions can be omitted, although by doing the pre-elution we can minimise the extent of metallic contamination in the eluant. When 11.8 µM CP256 was radiolabelled with ^{68}Ga from the 1st elution it gave a radiolabelling yield of 95%. The same concentration of CP256 gave 100% radiolabelling yield with the 2nd elution of the day (Table 4).

The eluate of the IGG100 generator gave a better radiolabelling yield compared to the Obninsk generator when eluant from these generators was used to radiolabel CP256 and NOTA. It was also observed that there was a difference in radiolabelling yield of the 1st and 2nd elutions of both generators, though the difference was minimal in the case of IGG100. On the other hand, the 1st elution from the Obninsk generator gave only 40% radiolabelling yield with CP256 and 30% with NOTA, increasing to 70% in 3rd the elution with CP256 and 59% with NOTA. It appears that metal contaminants from the Obninsk generator interfere with the radiolabelling of chelator with ^{68}Ga.

The effect of chelator concentration and time on the radiolabelling yield of CP256 was also analysed. At very high concentrations of CP256 (1 mM) 100% radiolabelling yield was achieved within 2-3 min and at low concentrations (118 nM) it gave only 11% radiolabelled complex even after 10 min. However, for intermediate concentrations of chelator (11.8 µM) time of incubation was quite critical as radiolabelling yield increased from 11% at 2 min to 97% at 10 min (Table 3).

The utility of the CP256 chelator may not be limited to ^{68}Ga. CP256 in a series of experiments was radiolabelled with other radionuclides (^{111}In, ^{90}Y, ^{89}Zr, ^{99m}Tc). The main purpose of these experiments was to fully assess the ability of CP256 for radiolabelling with some other imaging and therapeutic radiostopes. CP256 showed an appreciable amount of binding with ^{111}In and ^{90}Y, ^{99m}Tc and ^{89}Zr, which makes it potentially quite a versatile and unique chelator (Figures 2.9, 2.10, 2.13, 2.19, 2.16). Its

stability was further analysed in human serum, with the exception of ^{99m}Tc. It was observed that the CP256 complex with ^{90}Y (group III) was not very stable in serum (Fig-2.14) while the ^{111}In-CP256 and ^{89}Zr-CP256 complexes seemed to be fairly stable in serum (Fig-2.11 and 2.20).

In order to fully evaluate the potential of CP256, we have also done a comparative study with the other chelators available in the market for ^{68}Ga including DOTA, NOTA and HBED. Although, DOTA is considered to be the "gold standard" but it is not fair to make the comparison of CP256 with DOTA and other chelators because of the differences in the conditions for radiolabelling; e.g. DOTA requires 30 min heating at 100^{o}C for complete radiolabelling, NOTA and HBED require 7 and 10 min incubation at room temperature, whereas for CP256 only 3-5 min of incubation with ^{68}Ga at room temperature and neutral pH is enough to obtain 100% radiolabelling yield depending upon the concentration of ligand (Table 5). At nanomolar levels all the chelators behaved similarly, zero (0%) radiolabelling yield. At 1 µM concentration NOTA (pH 7) gave 41% radiolabelling yield, NOTA (pH 4.5) gave 2% radiolabelling yield, DOTA gave 0%, HBED gave 70%, while for CP256 84% radiolabelling yield was obtained (Table 5). Thus, DOTA was the worst performing chelator in this case, as it required high temperature and longer incubation time, which is not compatible with the short half life of ^{68}Ga, followed by NOTA and HBED. CP256 gave good radiolabelling yield (84%) at low concentration (1 µM) with minimum time for incubation (3 min) at room temperature and pH 7, which is a great advantage for CP256 compared to the other available chelators.

The human serum stability of radiolabelled complexes of these chelators was also analysed. The biological environment *in vivo* is quite different from the *in vitro* environment because of the presence of the various types of protein such as albumin and transferrin. Human blood serum proteins show affinity for metals such as Fe and Ga. So, *in vivo* if the complex between the radiometal and chelator dissociates then radiometal will bind to blood serum proteins, which are quite abundant in the biological environment and they compete with the chelator, which is in most cases in pM concentration. The only thing which we can do under these conditions is to delay the process of dissociation between the radiometal and chelator to enable the complex to reach its target. That is, to make it kinetically stable. In one of the experiments the radiolabelled complex of NOTA (Fig-2.5), HBED (Fig-2.4) and CP256 (Fig-2.2, 2.3)

was incubated with human serum and samples were taken out at two different time points, 5 min and 60 min, to analyse the stability of these radiolabelled complexes in human serum via PD-10 column. It was observed that the radiolabelled complexes with all these chelators were quite stable in human serum at both time points and no binding of ^{68}Ga with the serum was observed for any of the chelators.

The high affinity of CP256 for ^{68}Ga and the speed with which the complex forms under mild conditions prompted us to evaluate the potential for the use of CP256 in a pretargeting approach. An antibody derivatised with YM103 would be administered to the patient, allowed to distribute for several days, then a simple ^{68}Ga chelate such as citrate or acetate would be given. In theory the ^{68}Ga would rapidly distribute and find the derivatised antibody in the tumour, bind to it and allow imaging within the half life of ^{68}Ga. This has never been done before using chelate chemistry. An *in vitro* model was used to check the binding and stability of ^{68}Ga with CP256 in human blood serum in a pretargeting approach, with analysis by a PD-10 column, which is a type of size-exclusion column and it allows the large molecules or proteins to leave the column first followed by smaller molecules in order of their size. This is the reason that we have human blood serum proteins in seventh and eighth fractions (4 ml) of the elution profile (Fig-2.21-E). In the first set of experiments, human serum was exposed to chelator first and then radiolabelled with free ^{68}Ga instead of the usual method of radiolabelling the chelator first and then exposing it to serum. It was observed that ^{68}Ga showed higher affinity for the chelator even in the presence of the human serum transferrin. Furthermore, even after 60 min and at chelator concentrations as low as 0.02 mg/ml ^{68}Ga showed higher affinity for the chelator than for components of serum (Fig-2.22, 2.27).

In the second set of experiments, ^{68}Ga was first added to the human serum followed by the chelator and it was observed that not only the free ^{68}Ga in the pre-sample bound to the chelator, almost all of the ^{68}Ga which bound with the serum in the pre-sample (^{68}Ga+serum) detached from it and exhibited high affinity for CP256 instead of serum in the post-sample (^{68}Ga+serum+CP256) (Fig-2.25).

The same pretargeting model was evaluated with HBED and NOTA, two other chelators which bind ^{68}Ga at room temperature. However, NOTA showed no promise for pretargetting using the same techniques with ^{68}Ga and CP256. On the other hand the

behaviour of HBED was quite complex and intermediate between the CP256 and NOTA. HBED, when incubated with serum according to the above mentioned techniques, eluted around 4.5-7.5 ml. This fraction overlapped with radiolabelled serum (4-4.5 ml) and with radiolabelled HBED (7.5-8.5 ml), suggesting that some of the activity bound to serum and HBED was also able to hold to some ^{68}Ga (Fig-2.26, 2.30). We cannot say with certainty with respect to the behaviour of HBED related to pretargetting but it was not as good as CP256 and not as bad as NOTA.

Different TLC methods were developed which are quite simple and able to differentiate between the reference standard and the radioactive complex formed. TLC is the most common method used to check radiochemical purity (RCP) around the world in the radiopharmacies. It gives easy, quick and quite reliable results within a short period of time. The solvent systems used in TLC methods were 0.1 M sodium citrate (Method 1), in Method 3 water: ethanol: ammonia (5:2:1) and in Method 5 NaH_2PO_4 (0.4 M, pH 4-4.5). The hexadentate chelator CP256 stayed at the origin in the case of 0.1 M sodium citrate and ITLC-SG as a stationary phase, which reflects that the complex is quite hydrophobic in nature as the mobile phase is polar and hydrophilic in nature (Fig-2.26). The reference standard (free ^{68}Ga) moved with the solvent front (Fig-2.26). ITLC further confirmed the results of the PD-10 column. As human serum was separated from the sample with denaturation with ethanol and centrifugation, measuring the radioactivity in the supernatant and protein pellet it was observed that all the activity remained in the supernatant. A drop of supernatant was then applied to ITLC strip and developed in the mobile phase and it was observed that the activity stayed at the origin, indicating the presence of ^{68}Ga-CP256 (Fig-2.26). However, in the other system in which water, ethanol and ammonia (5:2:1) was employed as a mobile phase and HSA-ITLC-(SG) as a stationary phase, ^{68}Ga-CP256 moved with the solvent front and free ^{68}Ga stayed at the origin (Fig-2.3). For NOTA and HBED, ITLC-SG was used as a stationary phase and NaH_2PO_4 as a mobile phase. In both the cases free ^{68}Ga stayed at the origin and the chelator complex moved with the solvent front.

Another new method (Method 4) for ITLC was developed in which CP256 moved with the solvent front and free ^{68}Ga stayed at the origin; this is quite simple and easy (Fig-2.0) compared to the HSA or BSA saturated ITLC-SG strips (Method 3), avoiding the need to pretreat the strips. Two mobile phases were used. The mobile phase 1 was composed of ammonia, acetone, and water in a ratio of 5:3:2, while mobile phase 2

contained acetone, water, and ammonia in a ratio of 5:4:1 respectively. This method is quite useful for the routine purposes in radiopharmacy as it is quick and easy.

2.4-Summary

We have seen that CP256 forms a stable complex with ^{68}Ga at lower concentrations, room temperature, neutral pH and with very short time of incubation compared to other ^{68}Ga chelators available in the market, which makes it a unique chelator. CP256 may be a useful chelator for other radiometals such as ^{111}In and ^{89}Zr, and there is possibility of exploring its usage as a chelator for therapeutic radionuclides. CP256 shows promise for a novel pretargeting approach since it can also bind with ^{68}Ga which is first bound to the transferrin in human serum by snatching it from transferrin. It is quite stable in human serum, at least for the time scale which is required for PET imaging with ^{68}Ga. It opens the door to true kit based ^{68}Ga protein labelling as shown by the labelling of conjugated C2A protein with ^{68}Ga very efficiently within 5 min. The simplicity of labelling at very high specific activity is a huge step forward for the routine, low cost availability of PET molecular imaging agents in centres without a cyclotron or extensive radiochemistry expertise.

Chapter 3: Production of J591(scFv) and J591c(scFv)

3.0-Introduction

Several PSMA mAb have been developed, including ^{111}In-labelled mAb 7E11, capromab-pendetide (Prostascint). It has been extensively evaluated for SPECT imaging applications. However, Prostascint requires a long period of time between injection and imaging. Furthermore, ^{111}In-capromab is not currently considered a promising agent for lesion detection within the prostate gland or for determining extracapsular extension, primarily because the internal target of ^{111}In-capromab requires that cell membranes be damaged before the antibody can bind. Excess unbound antibody leads to high background signal and poor spatial resolution [66]. In contrast, another full-length mAb that targets PSMA, J591, recognises and binds an extracellular epitope on PSMA.

In recent years there have been massive advances in antibody design. Full length antibodies are broken down into various fragments. The smaller size of the fragments improves the penetration properties into tissues which are inaccessible to full-size mAbs and this also matches the short half-life of some of the radionuclides for imaging [77]. The engineering of single chain variable region fragments (scFv) of mAb is another route to improve their kinetics for imaging. The J591(scFv) not only binds specifically to PSMA but also competes for the same extracellular epitope of PSMA as the J591 mAb [121].

Construction of the J591(scFv) genes encoding the VH and VL chains of the J591 mAb was carried out by IDT (Integrated DNA Technologies, Inc., Coralville, IA, USA). A 17-amino acid linker sequence fused the VH and VL chains to generate a single 0.7 kb peptide. The PCR amplified J591(scFv) fragment was sub-cloned with the pCR2.1 (Life Technologies, Carlsbad, CA, USA) [121]. The scFv can be used to make fusion proteins such as for treatment and detection of cancer growth and metastasis. The targeting biomolecule which we have developed is a single chain fragment (scFv) of J591 instead of full length antibody (Fig-3.0).

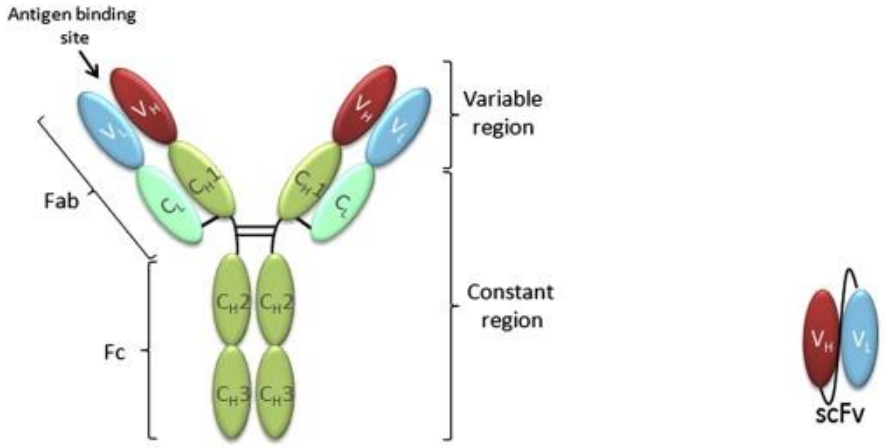

Figure 3.0: A full length antibody and single chain fragment [139]

We used J591(scFv) plasmid (PET26bJ591) which was kindly provided by Dr. John Maher, King's College London [79]. The C-terminal cysteine was introduced in house by Dr. Florian Kampmeier (PET26bJ591c). Both VH and VL sequences of J591(scFv) are available and can be found at http://www.ncbi.nlm.nih.gov/protein/J591.

DAAQPAMAEVQLQQSGPELVKPGTSVRISCKTSGYTFTEYTIHWVKQSHGKSLEWIGNI
NPNNGGTTYNQKFEDKATLTVDKSSSTAYMELRSLTSEDSAVYYCAAGWNFDYWGQ
GTTVTVSSGGGGSGGGGSGGGGSDIVMTQSHKFMSTSVGDRVSIICKASQDVGTAVD
WYQQKPGQSPKLLIYWASTRHTGVPDRFTGSGSGTDFTLTITNVQSEDLADYFCQQYN
SYPLTFGAGTMLDLKRAAALEHHHHHH(C).

The main reason to select the scFv is that its pharmacokinetic characteristics matched perfectly with the short half-life of ^{68}Ga (68 min). This scFv has a His-tag attached to it, which can be used for radiolabelling with ^{99m}Tc tricarbonyl. Near this His-tag a cysteine is attached in case of J591c(scFv), which can be further used for conjugation with thiol-reactive bifunctional chelators, such as (YM103) for radiolabelling with ^{68}Ga.

The main aim of Chapter 3 is to deal with the production of J591(scFv) and J591c(scFv) on small and large scale purification and storage. Initially bacterial BL21 cells were used to produce the scFv via peri-plasmic extraction followed by Ni-NTA purification. However, later mammalian 293T cells were used to produce the scFv, as the yield was much better compared to the bacterial BL21 cells. Different techniques were employed to get purified scFv involving AKTA and analysis by HPLC. For storage of scFv,

different temperatures were evaluated by HPLC to find optimum conditions for storage which prevents formation of dimers in scFv.

3.1-Methods

Some of the buffers used in the preparation and purification of the scFv are listed in the Table 6:

Table 6

Buffer	Composition	Concentration
4x binding buffer (Ni-NTA purification, pH 8)	Na_2HPO_4 NaCl Imidazole	200 mM 1.2 M 40 mM
Wash buffer (Ni-NTA purification, pH 8)	Na_2HPO_4 NaCl Imidazole	50 mM 300 mM 40 mM
Elution buffer (Ni-NTA purification, pH 8)	Na_2HPO_4 NaCl Imidazole	50 mM 300 mM 500 mM
LB (pH 7)	NaCl Peptone Yeast extract	1%(w/v) 1%(w/v) 0.5%(w/v)
SOC	Peptone Yeast extract NaCl KCl $MgCl_2$ $MgSO_4$ glucose	2% (w/v) 0.5% (w/v) 10 mM 25 mM 10 mM 10 mM 20 mM

Table 6: Buffers and media used in the preparation and purification of scFv

3.1.1-Preparation of Chemically Competent BL21 Cells

BL21 strains are descended from the E. coli B strain and have been specifically constructed for high-level expression of recombinant proteins. For the preparation of BL21 cells, 5 ml of overnight culture of BL21 cells was grown in LB media. This culture was diluted by adding 40 ml of fresh LB media and the flask was put in an

incubator at 37^{o}C until an optical density at 600 nm of 0.2-0.5 was obtained, measured by spectrophotometer. The flask was centrifuged for 10 min to get a hard pellet at 875*g* at 4^{o}C after cooling it down on ice for few minutes. The pellet was resuspended in 4 ml of chilled TSS buffer by vortexing. Aliquots of 100 µl were transferred to chilled microcentrifuge tubes and stored at -80^{o}C.

3.1.2-Transformation of E-Coli with Plasmid DNA

LB agar plates were prepared with kanamycin (50 µg/ml) and warmed to 37^{o}C. The BL21 cells were removed from the freezer, thawed on ice, and the cells were resuspended by vortexing. The purified plasmid DNA (1 µl of pET26b J591-Clone 1 or pET26b J591c-Clone 3) obtained from Dr. John Maher, King's College London (cysteine added in-house by Dr. Florian Kampmeier) was added to BL21 cells and mixed gently. The cells were incubated on ice for 30 min followed by heat shock treatment of the cells by incubating them at 37^{o}C for 45 sec and then returning them to ice immediately for 2 min. After addition of 450 µl of SOC medium at room temperature, the cells were transferred to a 15 ml polypropylene tube with a loose cap for air exchange for full recovery. The cells were incubated at 37^{o}C with shaking at 225-250 rpm for 1 h. Aliquots of 5-10 µl of SOC media were pipetted onto an LB agar plate containing antibiotics and 20 µl of transformed cells were transferred to this SOC media and spread evenly by using a sterile spreader. The plates were sealed and stored at 4^{o}C.

3.2-Expression in BL21 (DE3)-T1R Competent Cells

For production of BL21 cells 5-6 well-isolated colonies were selected from each transformation reaction and cultured in 20 ml LB broth containing antibiotics (kanamycin, 20 µl) at 37^{o}C overnight with constant shaking. An aliquot of 8000 µl of overnight culture was diluted by adding 400 ml of fresh LB media containing 400 µl of kanamycin in pre-weighed flasks. This culture was then incubated at 30^{o}C with constant shaking until the OD600 was roughly 0.6. An aliquot of 1 ml of this culture was taken out as a pre-induction control. Expression in the cells was induced with 1 mM IPTG. The induced culture was then kept for 3-4 h at 30^{o}C, after which a 1 ml sample was removed for SDS-PAGE and the rest was centrifuged at 10,000*g* for 10 min at 4^{o}C to obtain a pellet. The bottle was weighed again to find out the increase in the weight of the bottle and hence the weight of the pellet.

3.2.1-Peri-plasmic protein extraction

The pellet was resuspended in 20% sucrose buffer followed by the addition of 1 mmol/L EDTA, and the mixture was cooled down by incubating on ice for 10 min. A hard pellet was obtained after centrifugation at 10,000*g* for 20 min. The pellet was resuspended in 150 ml of $MgSO_4$ (5 mM) and incubated on ice for 10 min with occasional vortexing, and again centrifuged at 10,000*g* for 20 min. The supernatant was further analysed by SDS-PAGE and Western blot. Peri-plasmic extract was filtered through a 0.22 µm filter, and concentrated using a cross-flow membrane. The concentrated peri-plasmic extract was further purified using a Ni-NTA column (Qiagen -Amersham, 1 ml His trap fast flow column) using AKTA (FPLC) at a maximum pressure of 0.5 MPa and flow rate of 1 ml/min. After the sample was loaded onto the column, it was washed with binding buffer (10 mM imidazole) followed by wash 2 with wash buffer (20 mM imidazole) and finally the protein was eluted using elution buffer (250 mM imidazole). The protein buffer was adjusted to PBS (pH 7) by dialysis overnight (spectra/pro dialysis membrane MWCO 3500) in 4 L of PBS.

3.3-Production of J591(scFv) and J591c(scFv) from Mammalian 293-T cells

For production of J591(scFv) and J591c(scFv) from mammalian HEK 293-T cells (human embryonic kidney 293 T cells), the growth medium used was RPMI 1640 with 10% FBS, 1 µl of penicillin/streptomycin: 100 µl of growth medium antibiotic pen-strep (penicillin + streptomycin) and Zeocin (1 µl of zeocin:1000 µl of growth medium) in a T-75cm^3 (20 ml) bottle. Cells were cultured in 5% CO_2 at 37^oC. When the medium was acidified it changes its colour to yellow from phenol red because of the decrease in pH indicating that growth medium needs to be changed. For large scale production, cells were scraped from T-75cm^3 flasks and transferred to a triple flask bottle. The triple flask was then filled with 150 ml of growth medium and kept at 37^oC. The media were collected every three days and replaced with fresh media. The supernatant was stored at 4^oC. When a sufficient amount of supernatant had been collected (1600 ml), it was filtered through 0.22 µm filters and 400 ml of 4x binding buffer was added.

3.3.1-Purification through Ni-NTA column using AKTA

Purification of the filtered supernatant was performed using a 5 ml Ni-NTA column (Qiagen) using AKTA (FPLC) at a maximum pressure of 0.5 MPa and flow rate of 1 ml/min. The sample was loaded onto the column overnight, then the column was washed with binding buffer (10 mM imidazole) followed by wash 2 with wash buffer (20 mM imidazole) and finally the protein was eluted with elution buffer (250 mM imidazole). The elution fractions were concentrated by using centrifugal concentrators (Vivaspin 6 PES, MWCO 5000, Fisher-Sartorius). Proteins were further purified by a size exclusion chromatography step.

3.3.2-Size-exclusion chromatography

The buffer in the J591(scFv) and J591c(scFv) solutions was adjusted with AKTA and a size exclusion column (Superdex 75 10/300 GL from GE) at a flow rate of 0.5 ml/min and maximum pressure of 1.8MPa. The main purpose of this step is further purification. The column was equilibrated with water followed by PBS of pH 7. J591(scFv) or J591c(scFv) (500 µl) was injected from the injection loop. All the fractions were collected automatically. The fractions containing protein were separated from the rest of the fractions as they were eluted in the form of peak and at the same time UV detector of AKTA gave an enhanced signal (Fig-3.5, 3.7).

3.3.3-SDS-PAGE and Western Blotting

After the size–exclusion step the protein was analysed by SDS-PAGE using pre-cast polyacrylamide gels (Nupage 12% with MES buffer, Life Technologies) and Western blotting. For the preparation of samples 10 µl aliquots of scFv (J591 or J591c) were placed in microcentrifuge tubes and 5 µl of LDS loading buffer (4x) was added. For reduced samples, the reducing agent (Nupage reducing agent of strength 10x, 2 µl) was added along with LDS buffer of 4x concentration (5 µl). All the samples were placed on a heating block for 5 min at 95^{o}C and afterward put on ice for 1 min. The Nupage chambers were filled with the MES buffer (50 ml of 20x MES buffer + 950 ml of deionised water). The samples were loaded on the gel with a pipette (10 µl). The gels were 12% Nupage Novex Bis-Tris mini gels. The Novex sharp pre-stained protein standard was loaded in one of the wells. The voltage used was 200 V with constant

current (125 mA) and the gel was run for 40 min, after which the gel was removed and developed with simple blue safe stain for 1-2 h, then destained with water overnight.

In the case of Western blotting, the 12% gel was prepared in the same way as in SDS-PAGE but instead of developing it in simple blue safe stain the gel was loaded on nitrocellulose plates (transfer membrane) and then developed in non-reduced transfer buffer (Nupage transfer buffer (20x) 50 ml + methanol (100 ml) + deionised water (850 ml)). The gel was developed for 1 h at 30 V constant and current of 170-130 mA. After 1 h the transfer membrane was removed and placed in a blocking agent (4% milk in 50 ml of PBS with 0.05% Tween 20) for at least 90 min. The transfer membrane was washed briefly with PBS to remove any traces of milk, then placed in a solution containing antibody against His-tag (6.3 µl of antibody diluted (1:4000 dilution) by adding 25 ml of PBS with 0.5% BSA, which is almost 0.125 g/25ml of BSA) overnight at 4^{o}C with shaking. The transfer membrane was washed four times with 10 ml of PBST (1 L of phosphate buffered saline with 0.05% Tween 20) before incubating with secondary antibody (goat anti-mouse HRP, horseradish peroxidase) for 60 min (1:5000 dilution, approximately 4 µl of HRP in 20,000 µl of PBS). The transfer membrane was washed with PBST at least four times before immersing it in the solution of substrate. DAB [(3,3-Diaminobenzidine) Peroxidase Substrate Tablet Set from Sigma Aldrich] was used as a substrate to detect HRP (one DAB tablet and one Urea Hydrogen Peroxide tablet dissolved in 15 ml of ultrapure water). DAB produces an intense brown-black stain. The transfer membrane was developed in the dark until the brown–black precipitation was visible.

3.4-Effect of temperature and glycerol on dimer formation

Twenty four samples of J591(scFv) and J591c(scFv) each of equal concentration (0.5 µg/µl) were placed in microcentrifuge tubes. The volume of each sample was 20 µl. Eight samples were kept at each temperature: -80^{o}C, -20^{o}C and 4^{o}C. Five percent glycerol was added into half of the samples (4) at each time point. Samples were removed from all the temperature points every week of both with glycerol and without over the period of 3 weeks to analyse the formation of dimers in each sample. Samples were analysed with HPLC using PBS as a running buffer and a size-exclusion column (SEC-2000, Phenomenex).

3.5-Results

3.5.1-Production of J591(scFv) and J591c(scFv)

Initially, J591(scFv) and J591c(scFv) were produced using bacterial BL21 (DE3)-T1R cells. The yields of J591(scFv) and J591c(scFv) obtained using this method were not very high (6 mg/L for J591(scFv) and 2 mg/L for J591c(scFv)). In order to achieve higher expression yields the production system was switched from bacterial cells to mammalian HEK293T cells. In expression system HEK293T cells are transfected with expression vector and the recombinant targeted protein is secreted into the culture media supernatant. The yield of J591(scFv) using mammalian 293T cells was better than bacterial cells, reaching 10-12 mg/L for J591(scFv) and 4-6 mg/L for J591c(scFv).

3.5.2-Purification through Ni-NTA column using AKTA

Most of the J591(scFv) was eluted in the elution fractions 2, 3, 4 with a small amount in 5 (1.5 ml each) from the Ni-NTA column in the form of single peak (Fig-3.1). The total amount of protein obtained in these fractions was roughly 12.0 mg in 6 ml according to the measurement using a NanoDrop device (Thermo-Scientific). One of the common problems observed with the scFv is the formation of dimeric aggregates; however, it was observed that monomeric form is purified during the size-exclusion step. There were no dimers (non-covalent or covalent association between the molecules) in these fractions with the exception of 1 as analysed by SDS-PAGE. Strong bands of protein were obtained roughly at 30 kDa for fractions 2, 3 and 4 (Fig-3.2). In the case of J591c(scFv) most of the protein was collected as a single peak in fraction 2 (Fig-3.3). Dimers were present in all the fractions which can be reduced using a reducing agent (DTT) as seen in SDS-PAGE (Fig-3.4). The total amount of protein obtained in these fractions was roughly 4-6 mg/L.

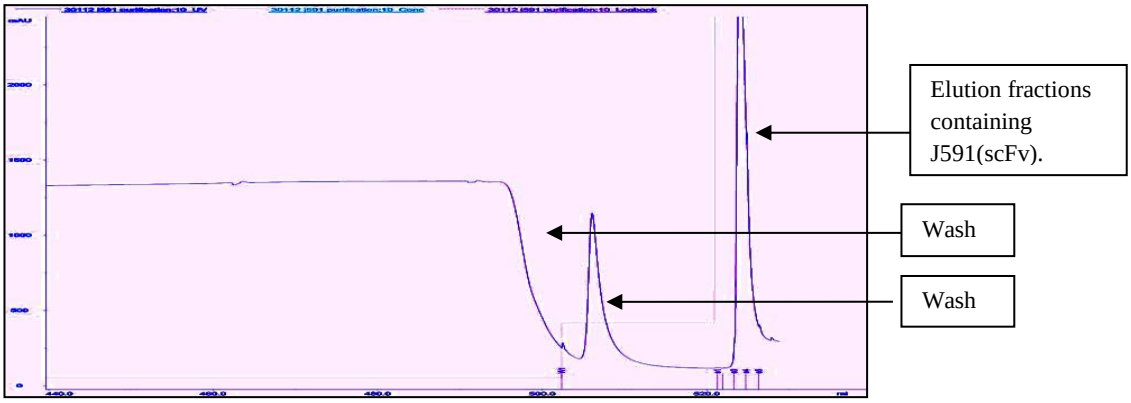

Figure-3.1: UV Chromatogram showing different fraction of J591(scFv) eluted from Ni-NTA column using FPLC. Wash 1 (10 mM imidiazole), Wash 2 (20 mM imidiazole) and elution fractions (250 mM imidiazole).

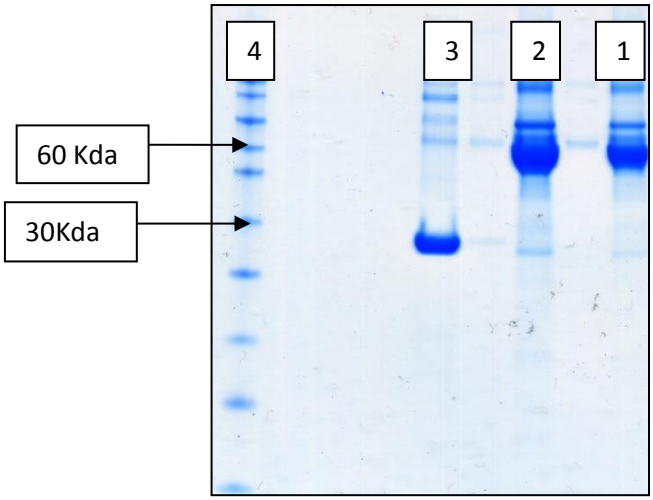

Figure-3.2: SDS-PAGE gel of J591(scFv) after Ni-NTA step. 1: Wash 1. 2: Wash 2. 3: Elution fraction. 4: Marker

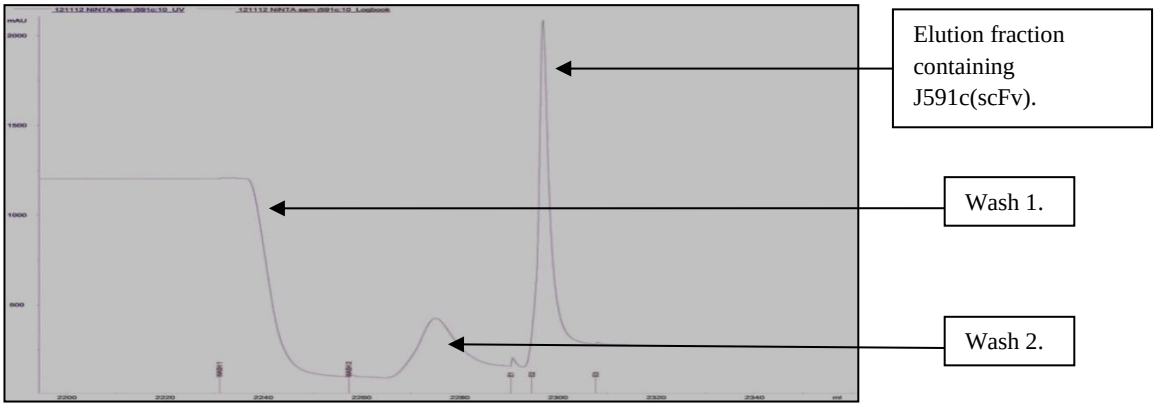

Figure-3.3: Chromatogram showing different fractions of J591c(scFv) eluted from Ni-NTA column using FPLC. Wash 1 (10 mM imidiazole), Wash 2 (20 mM imidiazole) and elution fractions (250 mM imidiazole).

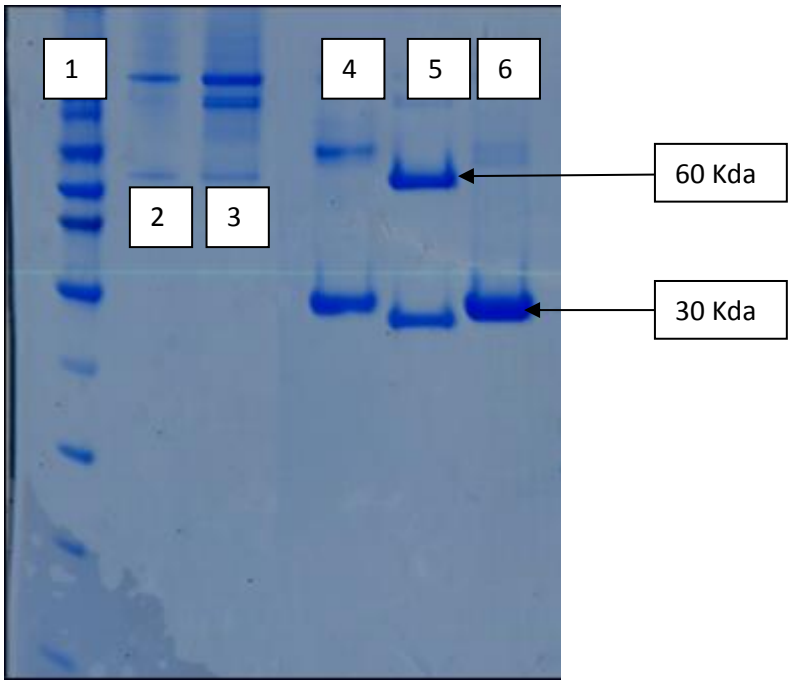

Figure-3.4: SDS-PAGE gel of J591c(scFv) after Ni-NTA step. 1: Marker. 2: Wash 1. 3: Wash 2. 4: Elution fraction 2. 5: Elution fraction 2. 6: Reduced Elution fraction 2.

3.5.3-Size-exclusion step

After the Ni-NTA step the J591(scFv) and J591c(scFv) were in elution buffer (250 mM imidazole), so the buffer was adjusted to PBS (pH 7) in the gel filtration step. In the case of J591(scFv) the protein was eluted in fractions 8-12 in a volume of 1 ml each

(Fig-3.5). However, in the case of J591c(scFv) in the size exclusion step two peaks can be seen, one representing the monomer and the other representing the dimer because of covalent or non-covalent interactions and they are quite fused together as observed from the chromatogram (Fig-3.7), so elution fractions contain a mixture of monomer and dimers. It was further confirmed by SDS-PAGE. According to SDS-PAGE in the case of J591(scFv) fractions 8 and 9 contained both monomers and dimers and fractions 10, 11 and 12 were monomers (Fig-3.6). Starting with 12 mg of protein, 8-10 mg was recovered after the size-exclusion step. On the other hand SDS-PAGE (Fig-3.8) for J591c(scFv) shows a mixture of monomer and dimer in all the fractions.

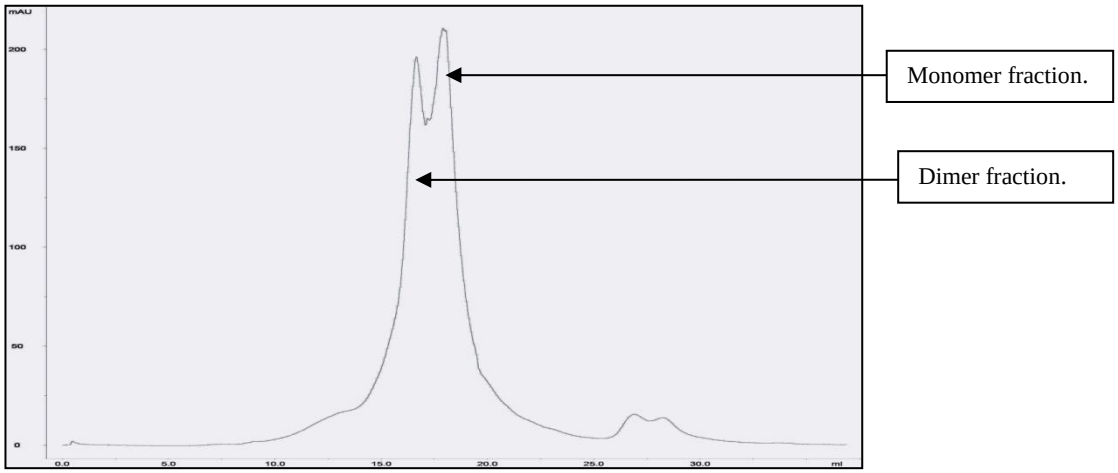

Figure-3.5: Chromatogram showing monomer and dimer fractions of J591(scFv) as eluted from size-exclusion column using FPLC.

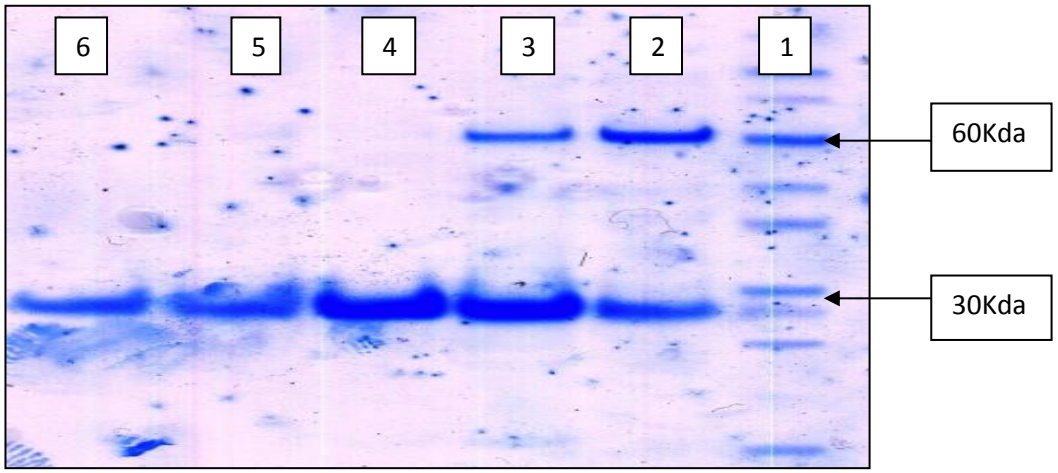

Figure-3.6: SDS-PAGE gel of J591(scFv) after buffer adjustment using Superdex 75 10/300GL column. 1: Marker. 2: Fraction 8 (monomer & dimer). 3: Fraction 9 (monomer & dimer). 4: Fraction 10 (monomer). 5: Fraction 11 (monomer). 6: Fraction 12 (monomer).

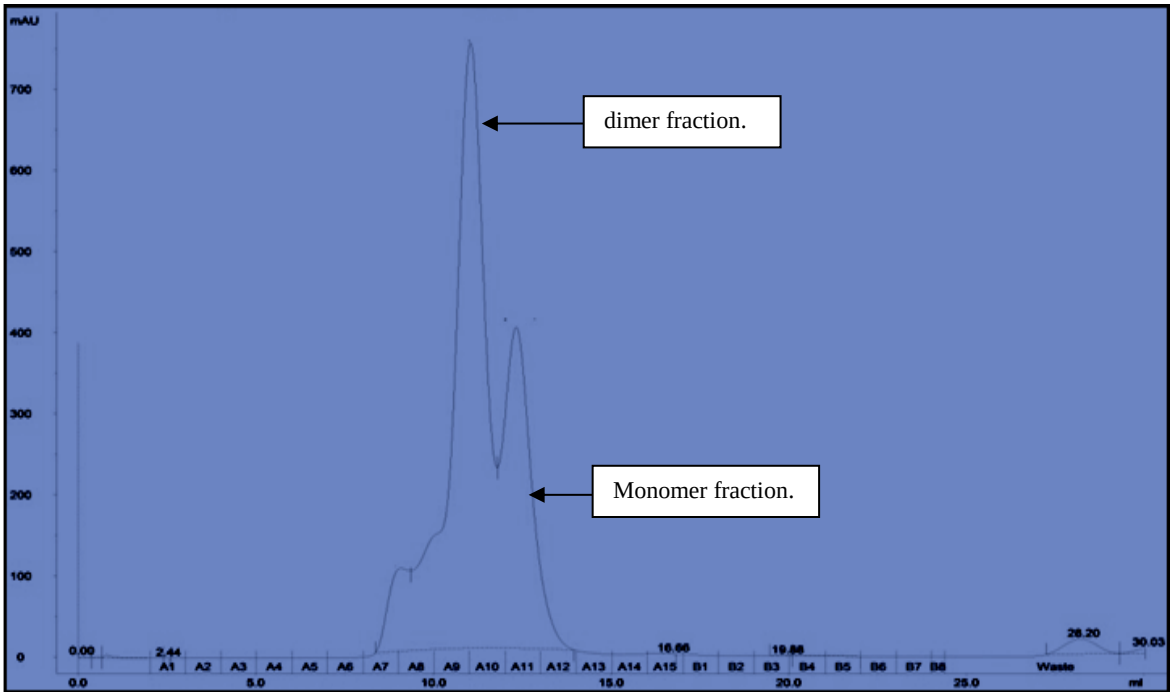

Figure-3.7: Chromatogram showing monomer and dimer fractions of J591c(scFv) as eluted from size-exclusion column using FPLC.

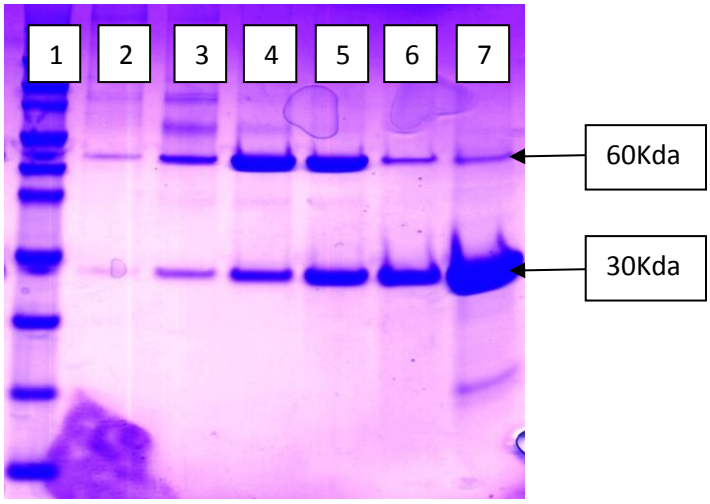

Figure-3.8: SDS-PAGE gel of J591c(scFv) after buffer adjustment using Superdex 75 10/300GL column. 1: Marker. 2: Fraction 8. 3: Fraction 9 (monomer & dimer). 4: Fraction 10 (monomer & dimer). 5: Fraction 11 (monomer & dimer). 6: Fraction 12 (monomer & dimer).

The fractions obtained after size-exclusion chromatography were further analysed by size-exclusion HPLC (SEC-2000, Phenomenex). PBS was used as a running buffer with

a flow rate of 1 ml/min. Dimers eluted at 8 min and monomer eluted at 9 min (Fig-3.9, 3.10). Formation of J591(scFv) and J591c(scFv) was also analysed by Western blotting and a strong band was observed at 30 kDa. For J591c(scFv) a dimer band was formed at 60 kDa (Fig-3.11).

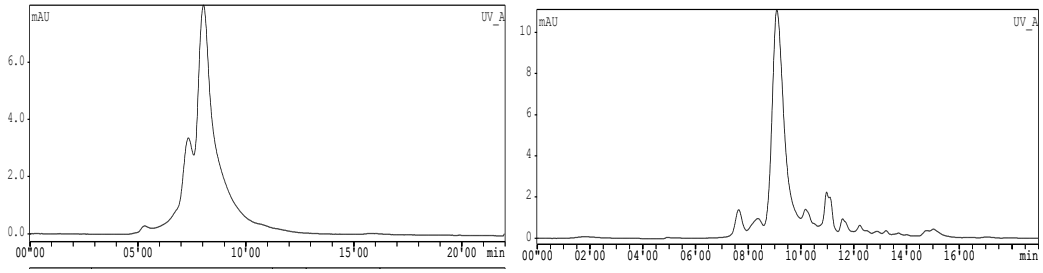

(A) **(B)**

Figure-3.9: HPLC of the fractions of J591(scFv) obtained after size-exclusion chromatography via FPLC. Mixture of monomer (9 min) and dimer (8 min) in SEC-2000 column (A) using PBS as running buffer. Monomer fraction of J591 at 9 min (B).

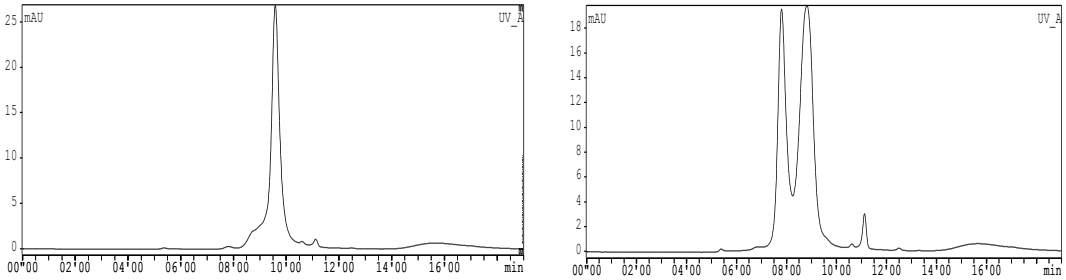

(A) **(B)**

Figure-3.10: HPLC of the fractions of J591c(scFv) obtained after size-exclusion chromatography via FPLC J591c predominantly monomer (9 min) and small amount of dimers (8 min) in SEC-2000 column using PBS as running buffer (A). Mixture of monomer (9 min) and dimers (8 min) (B).

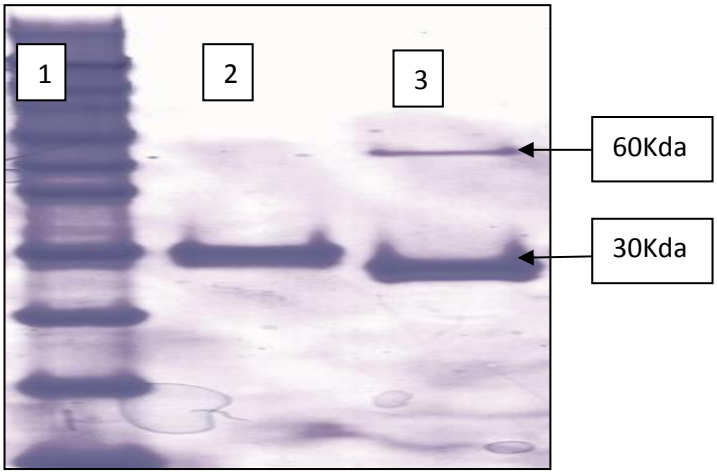

Figure-3.11: Western blot with anti His-tag antibody
1: Markers 2: J591(scFv). 3: J591c(scFv).

3.5.4-Effect of storage temperature and glycerol on dimer formation

The effect of dimerisation was measured by HPLC (SEC-2000, PBS as running buffer). It was observed that glycerol did not have any effect on the degree of dimerisation in both J591(scFv) and J591c(scFv). The extent of dimer formation was least at -80^{o}C, followed by 4^{o}C and then -20^{o}C. It increased with time over 3 weeks, but it was least at -80^{o}C (Fig-3.12).

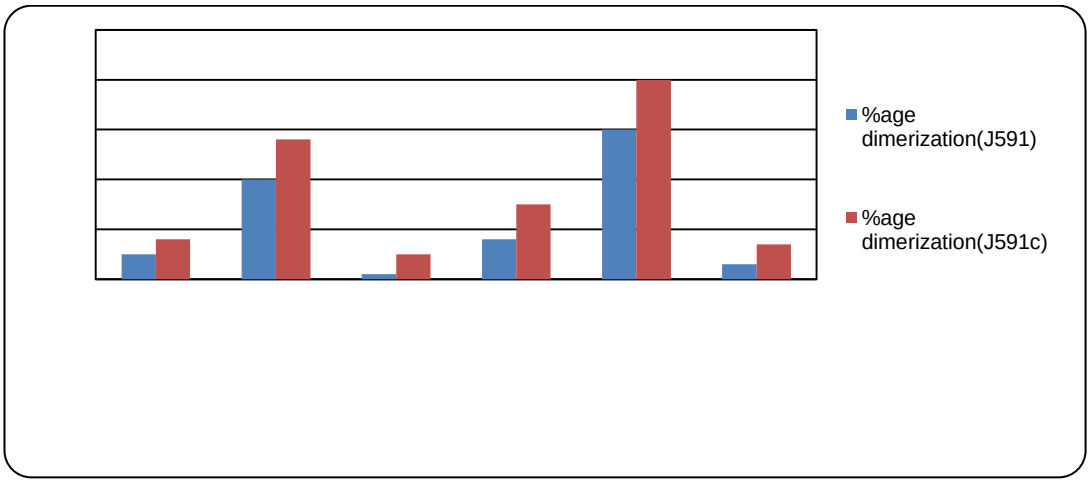

(A)

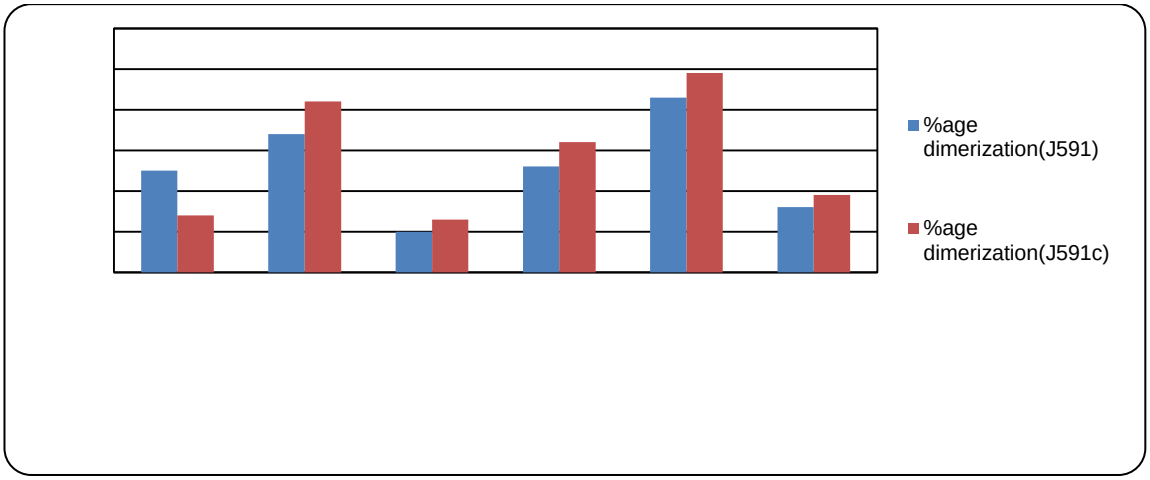

(B)

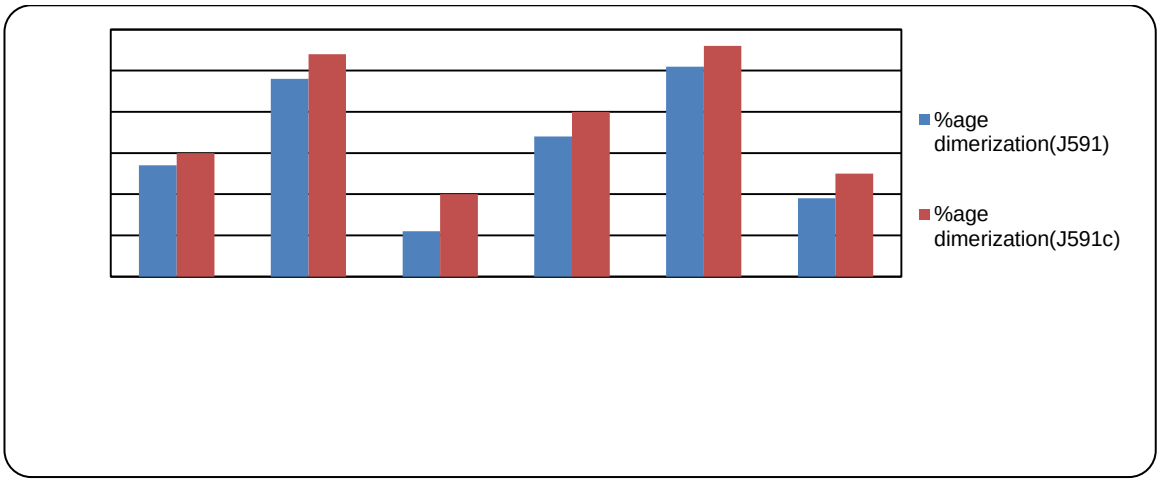

(C)

Figure-3.12: J591(scFv) and J591c(scFv) were analysed by size-exclusion chromatography using Sec-2000 column and PBS as a running buffer. Least dimers are formed at -80^{o}C over the time period of 3 weeks. (A) 1st week; (B) 2nd week; (C) 3rd week.

It was observed that both J591(scFv) and J591c(scFv) are capable of forming dimers under certain conditions, and the extent of dimerisation appears to depend on linker length, antibody sequence, and external factors such a temperature, pH, concentration etc. We have analysed only one parameter in the above mentioned experiment i.e temperature and we have observed that keeping them at low temperature will help reduce dimerisation.

3.6: Discussion

Initially the proteins were produced through bacterial BL21 cells growing in LB media. Lac Z promoter controls the expression of the scFv gene, which is induced by IPTG [122] and these cells secrete the scFv into the periplasm and supernatant. However, it was observed that yields of J591(scFv) and J591c(scFv) were not very high using bacterial BL21 cells (6 mg/L for J591(scFv) and 2 mg/L for J591c(scFv)). Therefore, we switched to another method in which mammalian HEK293T cells (10-12 mg/L for J591(scFv) and 4-6 mg/L for J591c(scFv)) were used to produce the scFv in the supernatant, which is then collected over the period of a few weeks and then purified by Ni-NTA chromatography using FPLC (Fig-3.1, 3.3, 3.13).

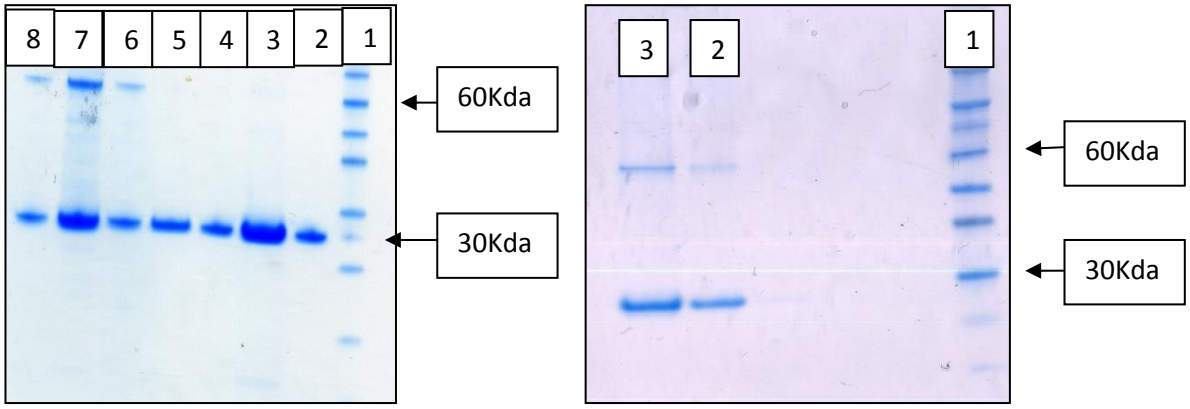

(A) **(B)**

Figure-3.13: In panel (A) protein is obtained through 293T cells by collecting supernatant 1:Marker.2-5: different fractions of J591(scFv).6-8:different fractions of J591c(scFv). In panel (B) protein is obtained from peri-plasmic extract using bacterial BL21 cells. 1: Marker. 2: J591(scFv). 3: J591c(scFv).

The chelators commonly used as ligands for IMAC (immobilised metal affinity chromatography) are nitrilotriacetic acid (NTA) and iminodiacetic acid (IDA). Once IDA-agarose or NTA-agarose resin is prepared, it can be "loaded" with the desired divalent metal (e.g. Ni, Co, Cu, Fe). NTA has four chelation sites for nickel ions, and binds nickel more tightly than IDA that only have three sites available for interaction with metal ions. The extra chelation site prevents nickel-ion leaching and results in a greater binding capacity and protein preparations with higher purity. Nickel is the most widely available metal ion for purifying histidine-tagged proteins. The Ni-NTA column shows high affinity and selectivity for 6xHis-tagged recombinant proteins and purity

was confirmed by SDS-PAGE analysis (Fig-3.2, 3.4). In Ni-NTA chromatography scFv was eluted in the form of a single peak. In Western blotting, both monomers and dimers were observed. Normally, during metal affinity chromatography, proteins bind to beads when they have an opposite charge than the bead, therefore elution buffers must alter this charge in order to release the protein efficiently. This can be done either by decreasing the pH or by increasing the NaCl concentration [123]. After Ni-NTA purification the buffer was adjusted to PBS of pH 7 by using the size-exclusion column (Superdex 75 10/300 GL) and FPLC. Both monomer and dimer can be seen in the chromatogram as two separate peaks, which are quite close together. The dimer elutes first followed by monomer because of higher molecular weight (Fig-3.5, 3.7). Two types of dimers are observed in this case: covalent and non-covalent because the two scFv molecules that form dimers which are not linked covalently can be readily dissociated when changes in environmental conditions such as pH or temperature occur, or during freeze/thawing [124]. The environment in which a protein is synthesised and allowed to fold is a significant determinant of its final shape. J591(scFv) has only non-covalent dimers and J591c(scFv) has both covalent and non-covalent dimers. Covalent dimers are formed because of cysteines, which are used for conjugation with maleimide of YM103. They are reduced by adding reducing agent like TCEP prior to the conjugation with YM103. In size-exclusion chromatography, such aggregated proteins pass through at a faster rate as compared to the monomer because of higher molecular weight than expected [125]. The presence of monomers and dimers was further established using Western blotting (Fig-3.11), SDS-PAGE (Fig-3.6, 3.8) and HPLC using size-exclusion column (SEC-2000) (Fig-3.10) in which monomer eluted around 9 min and dimer around 8 min. Further strong bands at 30 kDa for monomer and 60 kDa for dimer were observed both in Western blotting and in SDS-PAGE gel.

The effect of temperature and glycerol on the formation of aggregates during storage was also studied at three different temperatures ($4^{o}C$, $-20^{o}C$, $-80^{o}C$) on both J591(scFv) and J591c(scFv) with and without glycerol and it was observed that dimerisation was reduced considerably by keeping the protein samples at the temperature of $-80^{o}C$ (Fig-3.12). It was also observed that glycerol has little effect on the extent of dimerisation. The monomeric form is favoured in a dilute solution; however in a concentrated form dimerisation is favoured. Dimer to monomer ratio is an equilibrium reaction and it depends on several factors like temperature, pH and ionic strength [79].

3.7- Summary

We were able to produce 12 mg/L J591(scFv) and 4-6 mg/L J591c(scFv) using HEK293-T cells. Each was purified by using Ni-NTA column and buffer was adjusted to PBS using size-exclusion chromatography. HPLC chromatograms showed that it was pure with some extent of dimerisation, which we have tried to overcome by storing the protein at low temperature (-80^0C) after purification and separation of monomeric and dimeric form by size-exclusion chromatography.

Chapter 4: Radiolabelling of J591(scFv) with Technetium-99m Tricarbonyl

4.0-Introduction

Inorganic chemistry is challenged to find easy ways to introduce physiologically stable ^{99m}Tc cores into biomolecules without altering their bioactivity. Proteins seem to be an interesting target for direct labelling with low-valent organometallics. On one hand, a protein offers various sites for attaching an organometallic moiety but monodentate coordination only is probably not sufficient to block cross-linking to other proteins and formation of larger aggregates. The histidine-tagged recombinant scFv proteins are an exception to this expected behaviour as coordination is not monodentate in His-Tag. They carry a chain of 3–6 histidines at the N-terminus which are vital for purification but not for receptor binding. This histidine tag can be treated as a multidentate ligand since two or more imidazoles from histidine can coordinate at the same time. In comparison to the direct unspecific labelling, improved stability against cross-linking is expected along with site-specificity and *in vivo* stability. Histidine-tagged scFv has been labelled at 37°C to a high degree and labelling occurred specifically at the His-tag [82,83]. It was observed that recombinant scFv antibodies which bear a histidine tag can conveniently be labelled just by mixing the protein with $[^{99m}Tc(OH_2)_3(CO)_3]^+$ [82, 83]. Labelling of the same protein without His-tag gave very low yields. These histidine derivatives are easily introduced into biomolecules. The complex $[^{99m}Tc(His)(CO)_3]$ is hydrophilic and can be combined with hydrophilic peptides. HPLC typically shows that retention times of the native and labelled peptide do not differ much. Histidine is a very competent ligand and quantitative labelling occurs, in general, at the micromolar level. The radiolabelling procedures involving scFv with His-tag are quite simple and straightforward. The complex $[^{99m}Tc(H_2O)_3(CO)_3]^+$ is prepared in one single step directly from $[^{99m}TcO_4]^-$ followed by the one-step labelling procedure with scFv with His-tag.

The main aim of the work described in this chapter was to prepare the $[^{99m}Tc(H_2O)_3(CO)_3]^+$ using ^{99m}Tc pertechnetate and a tricarbonyl kit with high purity and then use this ^{99m}Tc tricarbonyl to radiolabel the J591(scFv). To achieve this aim it was necessary:

1. To optimize the labelling conditions to get maximum radiolabelling yield.
2. To analyze the serum stability of the radiolabelled compound.
3. To perform cell binding studies using PSMA positive and PSMA negative cell lines to show that radiolabelling did not damage the ability of J591(scFv) to bind specifically with PSMA.

4.1-Method

4.1.1-Preparation of tricarbonyl kit

Two methods have been used for the preparation of tricarbonyl kits (Isolink, Covidien Healthcare). One involved splitting of the kit contents into three equal parts and then radiolabelling an individual part with pertechnetate. This is an in house modification. The other involved the use of the full kit. Which method is adopted depended upon the number of users of the tricarbonyl kit on a particular day.

4.1.2-Splitting of tricarbonyl kit and radiolabelling

The contents of an Isolink kit were dissolved in 1 ml of distilled water. After mixing the contents of the kit by gently shaking, the kit contents were removed with the same syringe and divided into three equal parts (0.33 ml) each stored in a microcentrifuge tube with a screw top (Wheaton vial, Pierce). These tubes were immediately frozen in liquid nitrogen followed by lyophilisation (freeze drying) for 24 h at -4^{o}C [116].

For radiolabelling of this split kit 500-600 MBq (90 µl) of pertechnetate (^{99m}Tc generator eluate) was used. After adding the pertechnetate to the tricarbonyl split kit, the tube was heated at 100^{o}C for 25 min. The kit contents were then neutralised by adding 1 M HCl (~40 µl) and checking the pH with pH paper. For quality control purposes to check the formation of ^{99m}Tc-tricarbonyl, silica gel TLC plates (Sigma Aldrich) were developed with 1% HCl in methanol. Any colloid will stay at the baseline, free pertechnetate moves toward the solvent front (Rf = 0.7), and tricarbonyl will be at Rf= 0.4. ^{99m}Tc-tricarbonyl was then used to radiolabel the protein, J591(scFv).

4.1.3-Radiolabelling of full kit

For preparation of tricarbonyl from a full kit, up to 1000 MBq (500-700 µl) of ^{99m}Tc pertechnetate was used. After adding the activity, the contents of the kit were dissolved by gentle shaking. The kit was then heated at 100^{o}C for 25 min. The contents of the kit

were transferred to a microcentrifuge tube (1 ml) after cooling as it is easy to handle. The pH of the kit contents was adjusted to 7 by adding 1 M HCl (~120 µl) and checking its pH with pH paper. For quality control purposes, the formation of ^{99m}Tc-tricarbonyl was checked as described above.

4.2-General method of radiolabelling of J591(scFv) and effect of time on radiolabelling yield

For radiolabelling of J591(scFv), the appropriate amount of tricarbonyl (230 MBq, ~90 µl) was added to 100 µl of J591(scFv) (1 µg/µl) in PBS and heated at 37^{o}C for 60 min. Samples were taken out at 30 and 60 min for analysis on iTLC-SA strips (Agilent) developed in 0.1 M citrate buffer (sodium tribasic citrate) of pH 6. ^{99m}Tc tricarbonyl moves with the solvent front and radiolabelled J591(scFv) stays at the origin.

4.2.1-MiniTrap purification step

The Sephadex G-25 MiniTrap column (GE Healthcare Life Sciences) was used for purification. This is efficient in separation of high molecular weight substances from low molecular weight substances. Furthermore, it was also used for desalting, buffer exchange and sample clean up. Small molecules like salt, free labels and other impurities were efficiently separated from the high molecular weight substances of interest. The chromatography technique was gel filtration and molecules were separated on the basis of differences in size. The column was pre-washed with 60 ml of PBS. The crude ^{99m}Tc-J591(scFv) reaction mixture was applied to the MiniTrap column in order to remove any free pertechnetate and ^{99m}Tc tricarbonyl. Thirty fractions of 100 µl were collected. The activity in each fraction was measured in a dose calibrator. The fractions with highest activity were 8, 9 and 10. These fractions were analysed by iTLC-SA. If radiochemical purity was satisfactory the three fractions 8, 9 and 10 were mixed (~300 µl).

4.3-Radiolabelling of different concentrations of J591(scFv)

Different concentrations of J591(scFv) (from 72 µM to 4 µM) were prepared by diluting the stock solution of J591(scFv) with PBS. These different concentrations were then radiolabelled with the same amount of ^{99m}Tc tricarbonyl (30 MBq in 10 µl), and after incubating for 60 min at 37^{o}C the radiochemical purity was analysed by iTLC-SA.

4.4-Difference between 140 mM and 500 mM salt concentration

J591(scFv) was in PBS, which contains roughly 140 mM NaCl, along with 2.7 mM KCl, 10 mM Na_2HPO_4 and 2 mM KH_2PO_4. For a comparative study of J591(scFv) in 140 mM salt solution with high salt concentration, 5 M NaCl solution was added to the original 140 mM solution to increase its molarity to 500 mM. The same amount of PBS was added to the samples containing 140 mM NaCl so that concentration of protein remained the same in all the samples. In total there were four samples of two different salt and protein concentrations.

i) 140 mM NaCl, 0.5 mg/ml J591(scFv).

ii) 140 mM NaCl, 1 mg/ml J591(scFv).

iii) 500 mM NaCl, 0.5 mg/ml J591(scFv).

iv) 500 mM NaCl, 1 mg/ml J591(scFv).

^{99m}Tc-tricarbonyl was used to radiolabel all the samples (225 MBq in 125 µl each). Samples were taken in triplicate at four different time points, i.e. 30, 60, 90 and 120 min, and analysed by iTLC-SA.

4.5-Serum stability

After addition of 90 µl of ^{99m}Tc tricarbonyl (260 MBq) to 50 µl of J591(scFv) (3.78 µg/µl, 500 mM salt), the tube was incubated on a heating block at 37^{o}C. Samples were taken at 30 min and 60 min and analysed by iTLC-SA. After purification by MiniTrap column, the 3 combined fractions (~300 µl) were added to human serum (300 µl of serum plus 150 µl of 0.9% saline). The first sample was taken at 0 min. The tube was incubated at 37^{o}C and samples collected 30, 60, 120, 180, 240 min and 24 h (5 µl in each case) and stored at -80^{o}C until the last sample was taken. A human serum standard was also prepared by adding 10 µl of ^{99m}Tc-tricarbonyl to 50 µl of serum. An aliquot of 5 µl was taken out after incubation of 120 min and stored at -80^{o}C as a reference. A sample of ^{99m}Tc-J591(scFv) (5 µl) was also stored at -80^{o}C as a reference so that we know exactly where the radiolabelled protein migrates on SDS-PAGE gel. All these samples were analysed by radioelectrophoresis via SDS-PAGE. All the samples were stored at -80^{o}C to stop the further reaction as they were analysed after collecting last sample at 24 h.

Fresh samples were also analysed by iTLC-SA. However, iTLC was not of great help in this assay because human serum protein radiolabelled with ^{99m}Tc tricarbonyl stays at the origin and radiolabelled J591(scFv) also stays at the origin, while free pertechnetate and ^{99m}Tc tricarbonyl move with the solvent front. Thus, with this method we cannot detect any dissociation between the J591(scFv) and association of radioactivity with human serum, as both them stay at the origin but it can detect any release of free pertechnetate or ^{99m}Tc tricarbonyl as they move with the solvent front.

For analysis by SDS-PAGE, the samples (5 µl) were mixed with 10 µl of LDS buffer (lithium dodecyl sulfate, pH 8.4) and applied on the gel (10 µl). The gel was developed in MES buffer (2-ethanesulfonic acid) for 40 min at the voltage of 200 V and variable current of 120-130 A. Afterwards the gel was removed, activity markers were placed for analysis by phosphorimager and the gel was finally stained with Coomassie blue.

4.6-FACS analysis

Flow cytometry simultaneously measures and analyses multiple physical characteristics of cells as they flow in a fluid stream through a beam of light. It depends on the use of a fluorescent marker, e.g. fluorescein isothiocyanate (FITC), which is conjugated to a mAb that specifically binds to the primary antibody bound to the target of interest. Flow cytometry can measure the relative size of the cells, their relative granularity or internal complexity, and their relative fluorescence intensity. The results can be represented graphically [126]. FACS analysis was performed to measure PSMA expression on cell lines. For FACS analysis, the medium was removed from the 75 cm^3 flasks in which the PSMA negative and PSMA positive cells (PC3LN3 and PC3LN3-PSMA, respectively) were growing and replaced with 10 ml of PBS. After a few minutes the PBS was removed. A 1 ml aliquot of 0.25% w/v trypsin-0.53 mM EDTA was added and incubated for 60 s at 37^{o}C. Addition of 10 ml of fresh media (RPMI) stopped the trypsinisation reaction. The cells were scraped and homogenised by pipetting. A volume of 8 ml was transferred to a 15 ml polypropylene tube and centrifuged for 4 min at 1000 rpm to obtain the cell pellet. After removal of the supernatant, the pellet was resuspended in PBS and the cells were counted in a Cell Countess (Invitrogen). There were three samples each for PSMA positive (PC3LN3-PSMA) and negative (PC3LN3) cell lines. J591(scFv) was used in a quantity of 1 µg/µl. The three samples were:

1. Cells alone (PSMA positive and negative cell lines).
2. Penta–His mAb conjugated to Alexa fluor fluorescent dye (Penta-His-Alexa Fluor 488 conjugate, Qiagen). The penta-His mAb recognises an epitope comprising five consective histidines and cells (PSMA positive and negative cell lines).
3. J591(scFv) and Penta–His-Alexa Fluor 488 conjugate and cells (PSMA positive and negative cell lines).

For FACS analysis 950 µl aliquots of cells were placed in FACS tubes and centrifuged at 1000 rpm for 4 min. The supernatant was discarded and the pellet was resuspended in 500 µl of PBS by vortexing. An aliquot of 1 µl of J591(scFv) (primary antibody) was added, mixed and incubated on ice for 20 min. The tubes were then centrifuged for 4 min. The supernatant was removed and 2 ml of PBS was added to resuspend the pellet. This process was repeated twice. An aliquot of 1 µl of detection antibody (secondary antibody, Penta-His-Alexa Fluor 488 conjugate) was added, mixed and placed on ice for 20 min in the dark. The tubes were then centrifuged and the supernatant was removed. The pellet was resuspended in 2 ml of PBS, again centrifuged for 4 min at 1000 rpm, the supernatant removed and this process was repeated thrice. Finally, the pellet was resuspended in 300 µl of PBS and the samples were analysed by FACS.

4.7-Cell-binding experiments with labelled antibodies

The cell binding experiments were done in triplicate using 24-well plates both for PC3LN3 and PC3LN3-PSMA cell lines. The 24-well plates were prepared 24 h before the experiment. For preparation of the plates RPMI-1640 media was removed from the T-75 cm^3 flasks in which the cells were growing and the flasks were washed with 5 ml of PBS to remove any dead cells. Then 1 ml of trypsin-EDTA was added to loosen the cells from flask surface. The bottle was kept at 37^oC for 60 s in an incubator. Then 10 ml of fresh RPMI-1640 was added and the cells were scraped and mixed using a pipette to obtain a homogeneous suspension of cells. In order to measure the number of cells, an aliquot of 10 µl of the cell suspension was transferred to a microcentrifuge tube and mixed with 10 µl of Trypan blue for few seconds and an aliquot of 10 µl was placed on the slide to measure the number of cells using Cell Countess. The bulk cell suspension was then diluted with RPMI-1640 so that each well in 24-well plate received equal number of cells ($4x10^5$) in a volume of 500 µl. The 24-well plate was incubated at 37^oC for 24 h.

^{99m}Tc-tricarbonyl was prepared according to the above mentioned method. The protein J591(scFv) (117 µg in 100 µl) was labelled with ^{99m}Tc tricarbonyl (139 MBq in 100 µl) at 37^{o}C for 60 min. After 60 min the formation of radiolabelled complex was checked by iTLC-SA using 0.1 M citrate buffer. A 1:3 dilution of the radiolabelled protein was prepared in triplicate for both PC3LN3 and PC3LN3-PSMA cell lines. Starting with 90 µg in 450 µl, for 1:3 dilution a volume of 150 µl was removed from this radiolabelled mixture and added to 300 µl PBS to make the volume up to 450 µl. This was continued for 10 dilutions. Thus each set in the triplicates started with 15 µg in 75 µl, from which was taken out 25 µl (5 µg) and made up the rest of the volume by adding PBS for 1:3 dilution to produce 10 dilutions [7220 nM (15 µg in 75 µl), 2410 nM (5 µg in 75 µl), 770 nM (1.6 µg in 75 µl), 240 nM (0.5 µg in 75 µl), 89.05 nM (0.185 µg in 75 µl), 28.88 nM (0.06 µg in 75 µl), 9.63 nM (0.02 µg in 75 µl), 4.81 nM (0.01 µg in 75 µl), 1.44 nM (0.003 µg in 75 µl), and 0.4 nM (0.001 µg in 75 µl)].

The 24-well plates were removed from the incubator and the supernatant was aspirated carefully without disturbing the cells. A volume of 450 µl of Hanks solution was added to each of the wells along with 50 µl of the prepared dilution of radioactive complex. The incubation of the cells with the labelled antibody was carried out at 4^{o}C for 60 min. The reduced temperature will result in less internalisation and thus result in better detection of the antibody bound to the cell surface. After incubating the cells for 60 min, the cells were washed three times carefully with 500 µl HBSS to remove any unbound protein. The cells were then lysed with 0.5 M NaOH (200 µl) and the lysate was collected in FACS tubes to count the activity in the lysate using a gamma counter.

4.8-Mass spectrometry

The spectrometer used to analyse the samples was Agilent 6500 Series Q-TOF LC/MS. It is a liquid chromatograph Q-TOF mass-spectrometer that supports atmospheric pressure ionization (API) and performs MS/MS using a quadrupole, consisting of four cylindrical rods, set parallel to each other. The quadrupole is the component responsible for filtering sample ions, based on their mass-to-charge ratio (*m/z*). For mass spectrometry direct injection of J591(scFv) was used. The amount of J591(scFv) used was 20 µl, which contained ~30 µg protein.

4.9- Results

4.9.1-Preparation of ^{99m}Tc tricarbonyl

Preparation of ^{99m}Tc tricarbonyl was performed by two methods. One involved splitting of the kit and the other used a full kit. The choice of method depended on the amount of tricarbonyl required for the particular experiment and the results of the two methods were same; i.e. the radiochemical yield of ^{99m}Tc tricarbonyl obtained in both the methods was the same. Typically, we obtained 90-95% ^{99m}Tc tricarbonyl and 5-10% free pertechnetate. Figure 4.1 shows a typical chromatogram for analysis of ^{99m}Tc tricarbonyl formation. In this case we achieved 90% total radiolabelling yield for ^{99m}Tc tricarbonyl and ~10% free pertechnetate. In the mobile phase of 1% HCl in methanol with glass backed TLC(SG), any colloid will stay at the origin with Rf value of 0, free pertechnetate will move towards the solvent front with Rf value of 0.7 and tricarbonyl will stay in the centre with Rf value of 0.4.

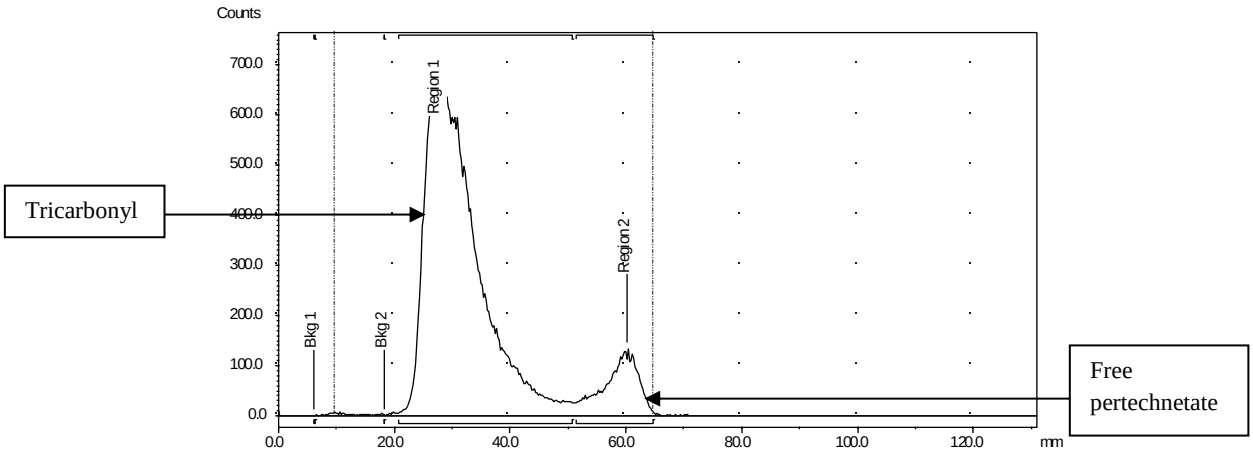

Figure-4.1: QC for tricarbonyl: mobile phase is 1% HCl in methanol with glass backed TLC(SG). Any colloids would stay at base line with Rf value of 0, tricarbonyl moves to the centre of strip with Rf value of 0.4 and free pertechnetate with Rf value of 0.7.

4.9.2-Time course of radiolabelling of J591(scFv)

For radiolabelling of J591(scFv) the 250 MBq (100 µl) of ^{99m}Tc tricarbonyl was added to 50 µl of J591(scFv) (1 µg/1 µl) and heated for 60 min at 37^{o}C. To follow the time course of radiolabelling, samples were taken at different time points from 0 min to 180 min as shown in Figure 4.2. With time the radiolabelling yield increased, with almost 70% radiolabelling yield at 60 min. It increased to 80% in 120 min and 90% in 180 min.

We have to keep in mind that there is some unreacted pertechnetate also present in the reaction mixture and that remaining 10% might account for that free pertechnetate.

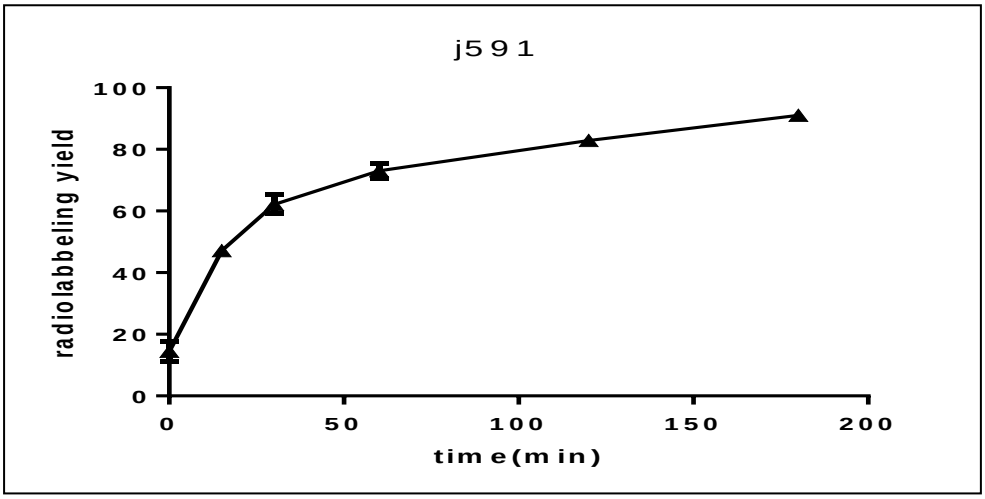

Figure-4.2: Radiolabelling yield (%) against time. Figure shows increase in radiolabelling yield of J591(scFv) with time.

4.9.3-MiniTrap purification step

The MiniTrap step was introduced to remove any unreacted ^{99m}Tc tricarbonyl or free pertechnetate from the reaction mixture on the basis of size. Thirty fractions of 100 µl each were eluted from the MiniTrap column using PBS. The protein was eluted in the fractions 8, 9 and 10 as shown in Figure 4.3. Unreacted ^{99m}Tc tricarbonyl eluted in fractions 17 and 18 and free pertechnetate eluted around 29 and 30. Different fractions obtained after the MiniTrap step were also analysed by iTLC-SA and HPLC. On iTLC-SA developed with 0.1 M citrate buffer, both ^{99m}Tc tricarbonyl and free pertechnetate moved with the solvent front, while any colloid and J591(scFv) stayed at the origin (Fig-4.5). In the case of HPLC a size-exclusion column (SEC-2000) was used to analyse the different fractions. The monomer fraction eluted at 9 min, dimer at 8 min, ^{99m}Tc tricarbonyl at 12 min and free pertechnetate at 14 min. Samples before the MiniTrap showed some unreacted tricarbonyl, which was efficiently removed by the MiniTrap step (Fig-4.4, 4.5).

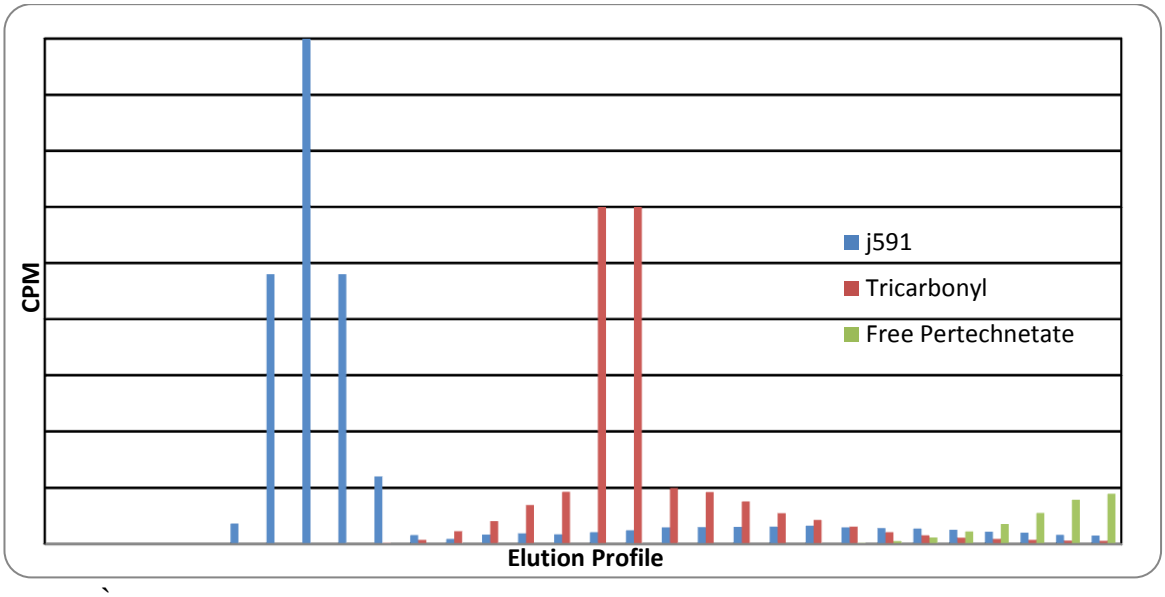

Figure-4.3: Elution profiles of J591(scFv), tricarbonyl and free pertechnetate from MiniTrap column based on their sizes.

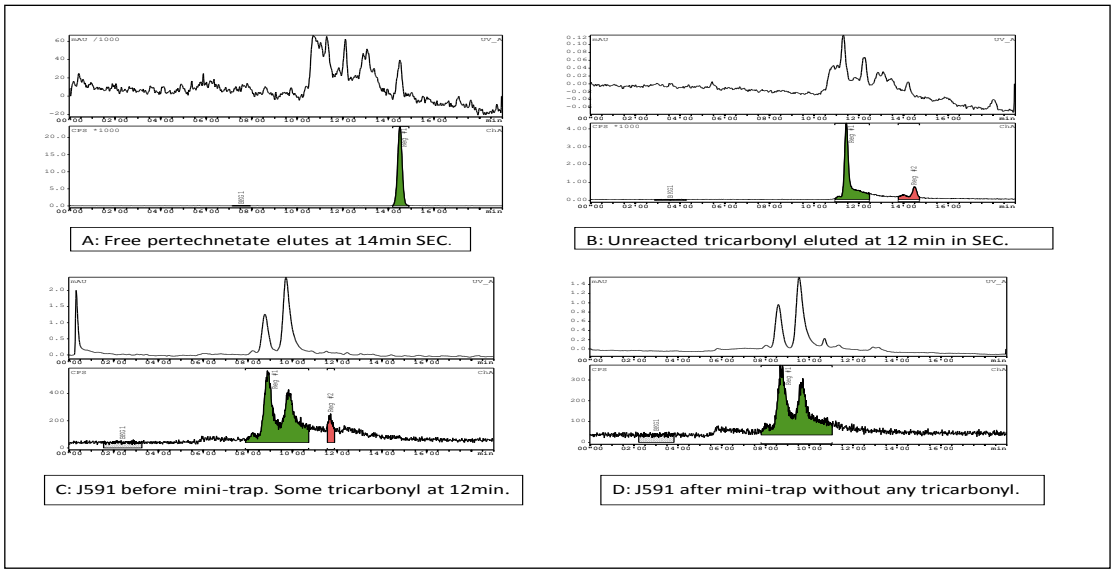

Figure-4.4: HPLC of free pertechnetate (A), ^{99m}Tc tricarbonyl (B), radiolabelled J591(scFv) before MiniTrap (C) and after MiniTrap (D). In each panel the upper tracing is UV absorbance at 280 nm and the lower panel is the radioactivity detector. The column used is a size-exclusion SEC-2000 and flow rate is 1 ml/min.

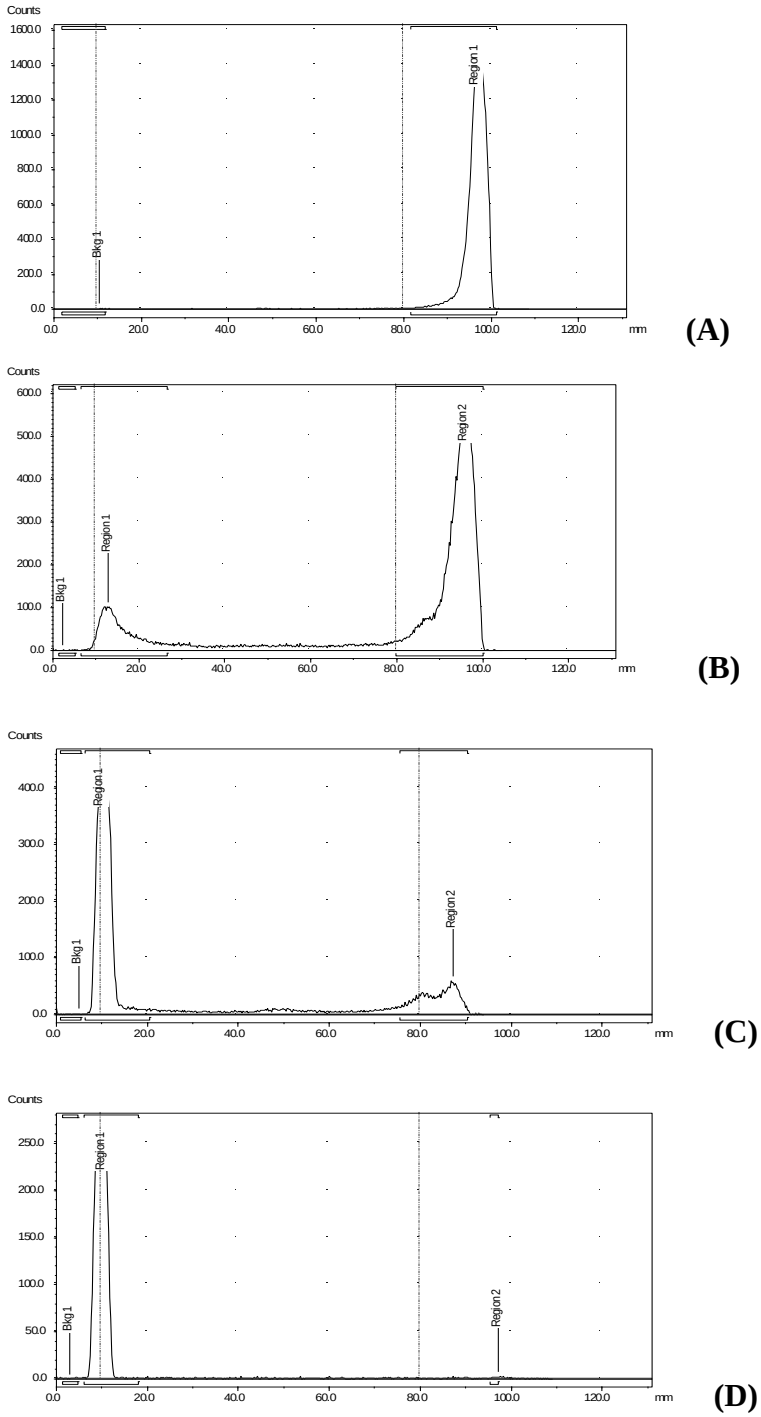

Figure-4.5: iTLC-SA was used as a stationary phase and 0.1 M citrate buffer as a running buffer. iTLC of free pertechnetate (A), ^{99m}Tc tricarbonyl (B), radiolabelled J591(scFv) before MiniTrap (C), radiolabelled J591(scFv) after MiniTrap (D).

It was also observed that the ITLC method in this case further strengthens the HPLC results. After the MiniTrap step no free pertechnetate or ^{99m}Tc tricarbonyl was observed in the ITLC method as in the HPLC chromatogram, which demonstrated its purity if we

just consider the solvent front in Figure 4.5-C and -D. The peak at the solvent front in Figure 4.5-C disappeared in Figure 4.5-D. However, there was a small peak at origin with ^{99m}Tc tricarbonyl on its own, which might represent colloid. The MiniTrap column is an effective way for buffer exchange and clean up of biological samples if required. The different components were separated on the basis of their size. The recovery of protein was between 90-98% depending upon the concentration of the protein applied to the column: the higher the concentration the more is the recovery. A small amount of radioactivity remained stuck on the column but 90-95% was always recovered from column. The activity which stuck on the column could be free pertechnetate, ^{99m}Tc tricarbonyl or radiolabelled protein.

4.9.4-Radiolabelling of different concentrations of J591(scFv)

Different concentrations of J591(scFv) were taken, ranging from 72.2 µM to 3.61 µM, and radiolabelled with tricarbonyl (30 MBq, ~10 µl). Samples were taken out at 30 and 60 min and analysed by iTLC-SA. As can be seen in Figure 4.6, even a low concentration such as 3.61 µM gave ~70% radiolabelling yield within 60 min. To further verify the results HPLC analysis was performed and Figures 4.7-4.11 show HPLC radiochromatograms for the different concentrations of J591(scFv) when radiolabelled with ^{99m}Tc-tricarbonyl. It was observed in each case that by decreasing the amount of single chain, the UV signal is gradually decreased. The HPLC column used was size-exclusion (SEC-2000) and it separates the protein on the basis of size, so the monomer fraction of the J591(scFv) elutes around 9 min and dimer around 8 min. PBS was used as running buffer. ^{99m}Tc tricarbonyl and free pertechnetate eluted around 10.5-12 min and 14 min respectively. The ITLC method in this case is in agreement with the HPLC results, as the amount of radiolabelled protein decreased in the sample with the Rf value of 0, the amount of unreacted ^{99m}Tc tricarbonyl increased with the Rf value of 1. As shown in Figure 4.6, the radiolabelling yield decreased with the decrease in the concentration of the protein.

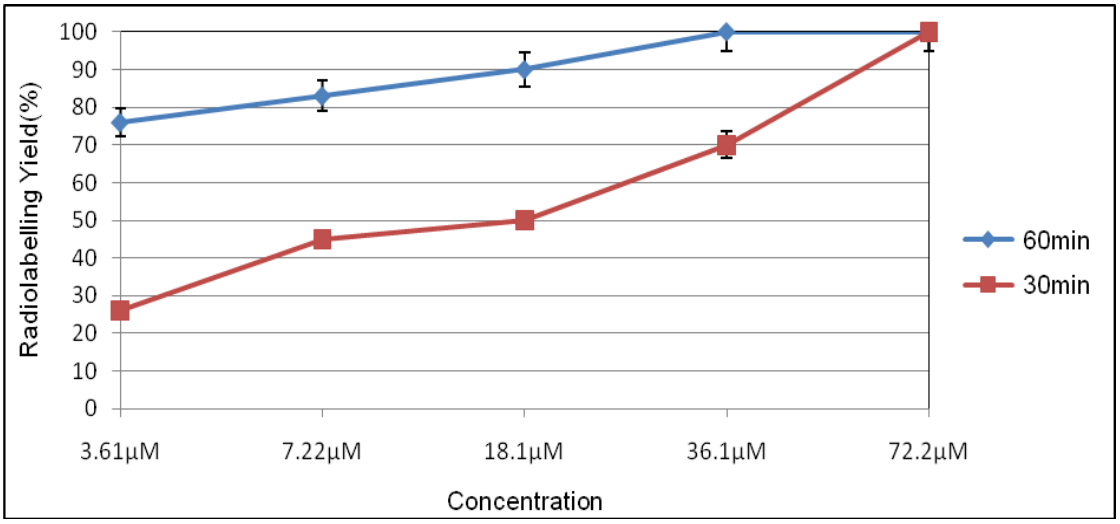

Figure-4.6: Different concentrations of protein are radiolabelled J591(scFv)at 30 min and 60 min and analysed by ITLC.

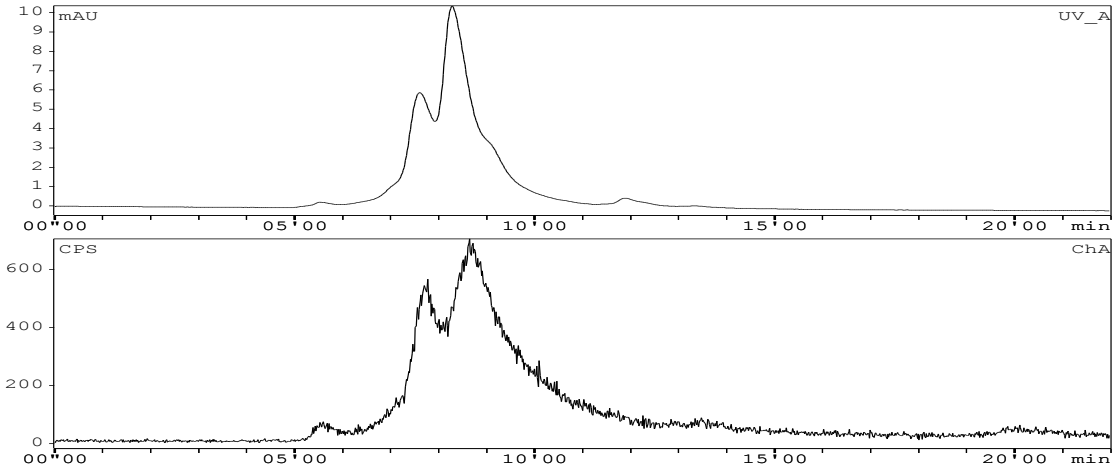

Figure-4.7: 72.2 µM protein radiolabelled with tricarbonyl. Radiolabelled J591(scFv) eluted around 9 min in SEC-2000 column in HPLC.

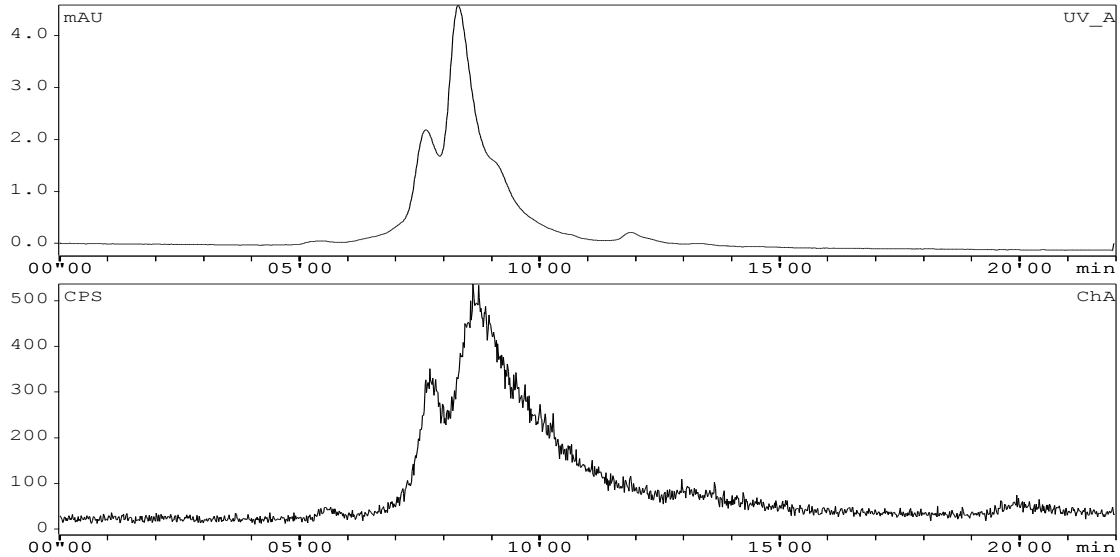

Figure-4.8: 36.1 µM protein radiolabelled with tricarbonyl. Radiolabelled J591(scFv) eluted around 9 min in SEC-2000 column in HPLC.

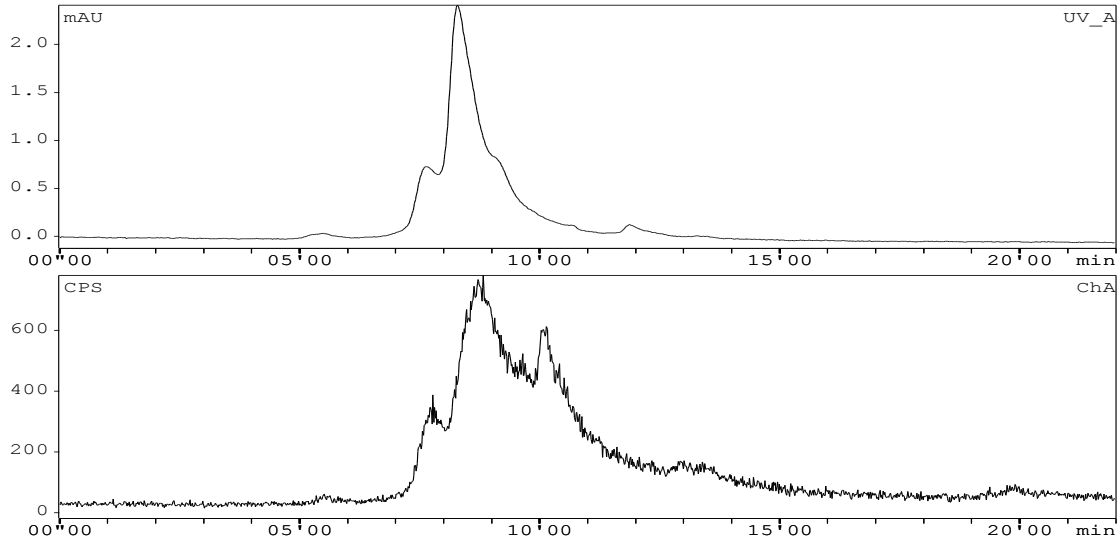

Figure-4.9: 18.2 µM protein radiolabelled with tricarbonyl. Radiolabelled J591(scFv) eluted around 9 min in SEC-2000 column in HPLC.

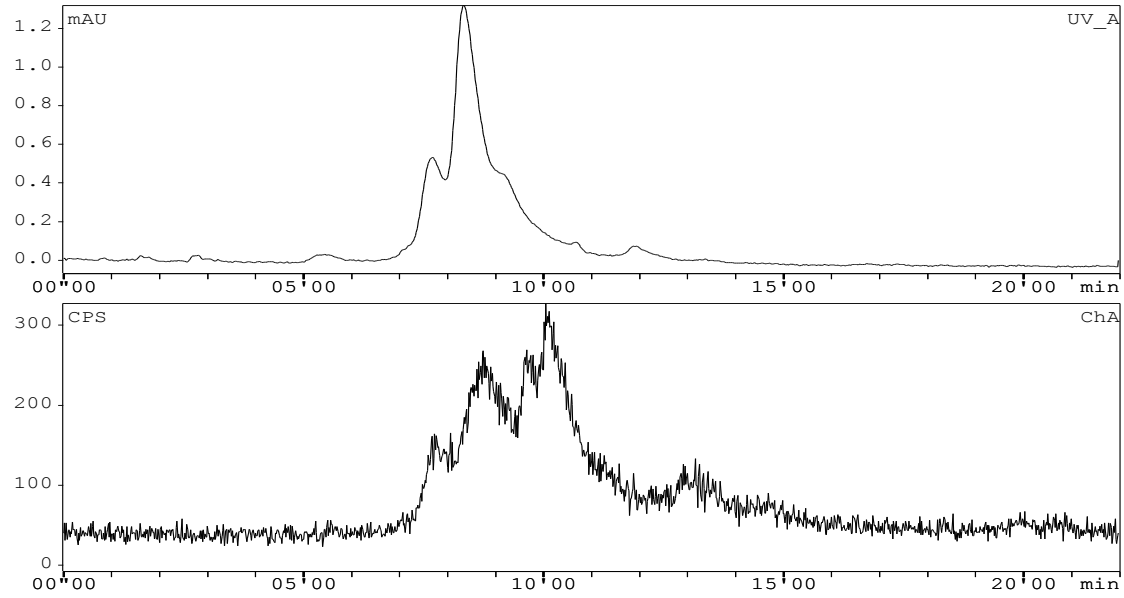

Figure-4.10: 7.22 µM protein radiolabelled with tricarbonyl. Radiolabelled J591(scFv) eluted around 9 min in SEC-2000 column in HPLC.

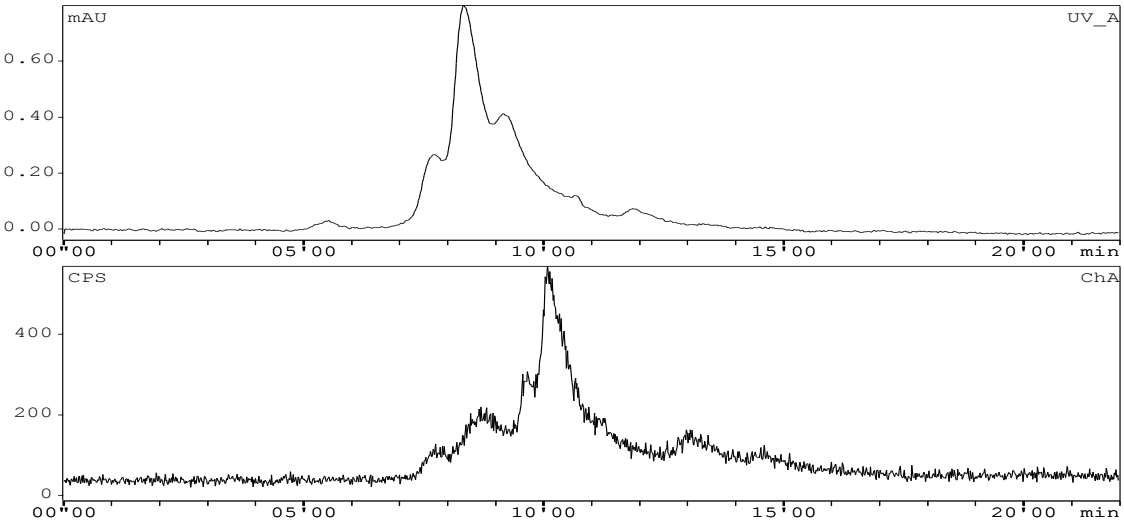

Figure-4.11: 3.61 µM protein radiolabelled with tricarbonyl. Radiolabelled J591(scFv) eluted around 9 min in SEC-2000 column in HPLC.

At higher protein concentrations there was no unreacted ^{99m}Tc tricarbonyl detected in the chromatograms (Fig-4.8, 4.7) but as the concentration of the protein decreased the unreacted ^{99m}Tc tricarbonyl peak became prominent around 10.5 minutes in the radiochromatogram (Fig-4.10, 4.11). A small amount of free pertechnetate was also observed in the radiochromatograms. There was no clear peak around 14 minutes but still we can see some activity in the form of streak. We cannot find this peak in the

ITLC method for higher protein concentration but for low protein concentration there was a peak at the solvent front, which most probably represents the unreacted ^{99m}Tc tricarbonyl instead of free pertechnetate.

4.9.5-Difference between 140 mM and 500 mM salt concentration

Two different concentrations of J591(scFv), 1 mg/ml and 0.5 mg/ml, each at two different salt concentrations, 140 mM and 500 mM, were radiolabelled with ^{99m}Tc tricarbonyl to check the effect of salt concentration on radiolabelling yield [141]. It was observed that high salt concentration resulted in modestly higher radiolabelling yield at both protein concentrations. In the case of 1 mg/ml protein, with higher salt concentration the radiolabelling yield was 95% and at lower salt concentration 88% after 120 min (Fig-4.12).

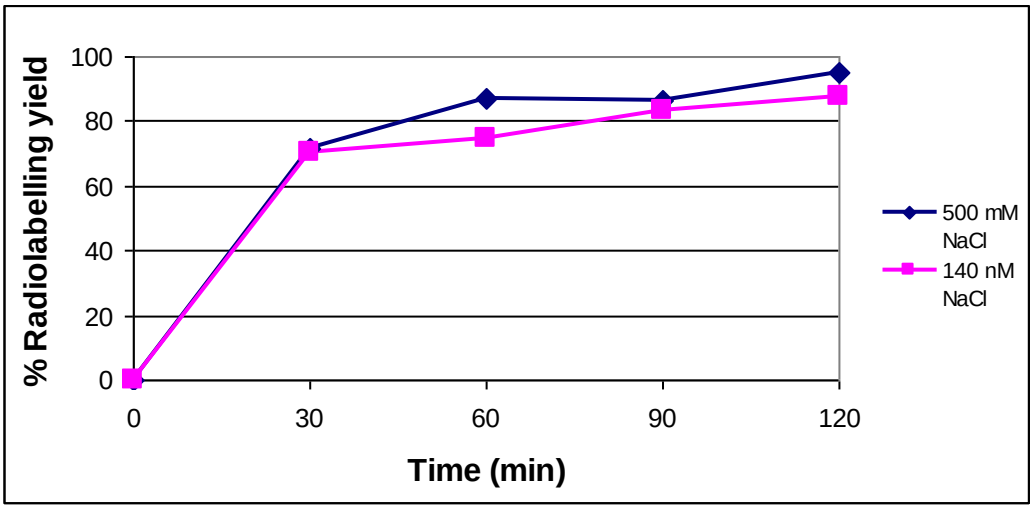

Figure-4.12: J591(scFv) 1 mg/ml radiolabelling yield with 500 mM salt conc is better than at 140 mM.

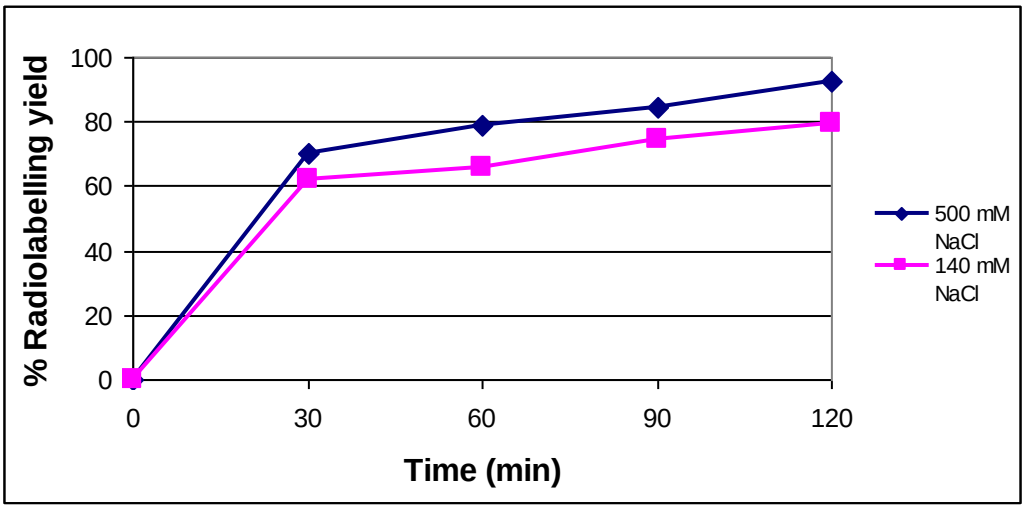

Figure-4.13: J591(scFv) 0.5 mg/ml radiolabelling yield with 500 mM salt conc is better than at 140 mM.

Slightly larger differences in the radiolabelling yield were observed with the lower J591(scFv) concentration (Fig-4.13). Radiolabelling yield was 92% at 120 min with the higher salt concentration but only 80% with the lower salt concentration at the same time point. However, statistical analysis could not be applied as the experiments were single replicates.

4.9.6-Serum stability

Serum stability measurement was performed over the time period of 24 h. Samples were taken out at each time point for analysis by iTLC-SA (Fig-4.15) and stored at -80^{o}C for 24 h until the last sample was collected. These samples were then analysed by SDS-PAGE and a cyclone phosphorimager. It was observed that radiolabelled J591(scFv) was quite stable. Even after 24 h there was no evidence by SDS-PAGE of dissociation of the label by iTLC-SA nor degradation of the labelled protein or transfer of ^{99m}Tc tricarbonyl to other proteins (Fig-4.14).

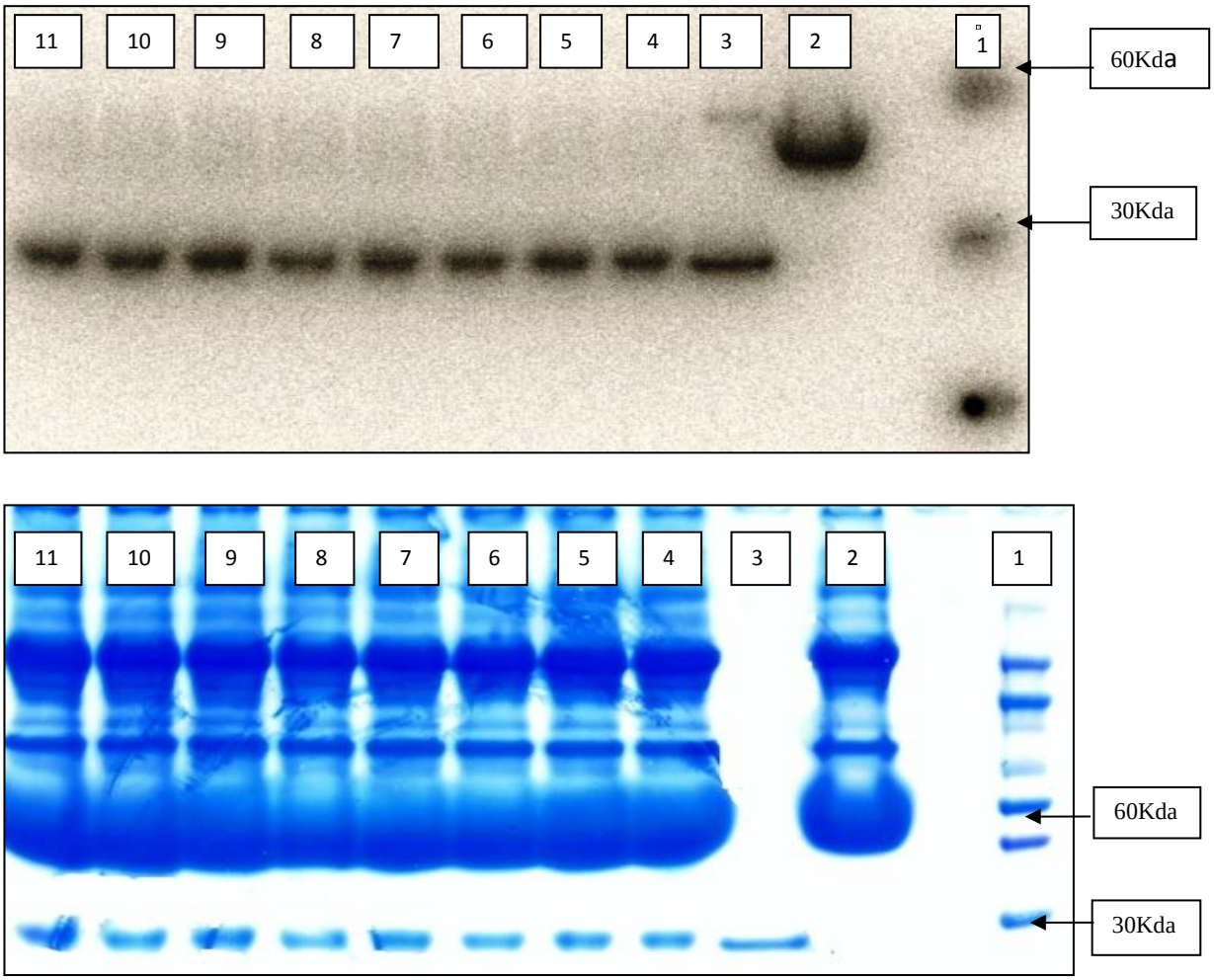

Figure-4.14: SDS-PAGE gel for serum stability. Radiolabelled J591(scFv) is quite stable in serum even after 24 h. No dissociation between J591 and tricarbonyl was observed. 1: Marker. 2: Human serum protein + tricarbonyl. 3: J591+tricarbonyl. 4: J591(scFv)+serum+tricarbonyl (0 min). 5: J591(scFv)+serum+tricarbonyl (30 min). 6: J591(scFv)+serum+tricarbonyl (60 min). 7: J591(scFv)+serum+tricarbonyl (120 min). 8: J591(scFv)+serum+tricarbonyl (180 min). 9: J591(scFv)+serum+tricarbonyl (240 min).10: J591(scFv)+serum+tricarbonyl (340 min). 11: J591(scFv)+serum+tricarbonyl (24 h).

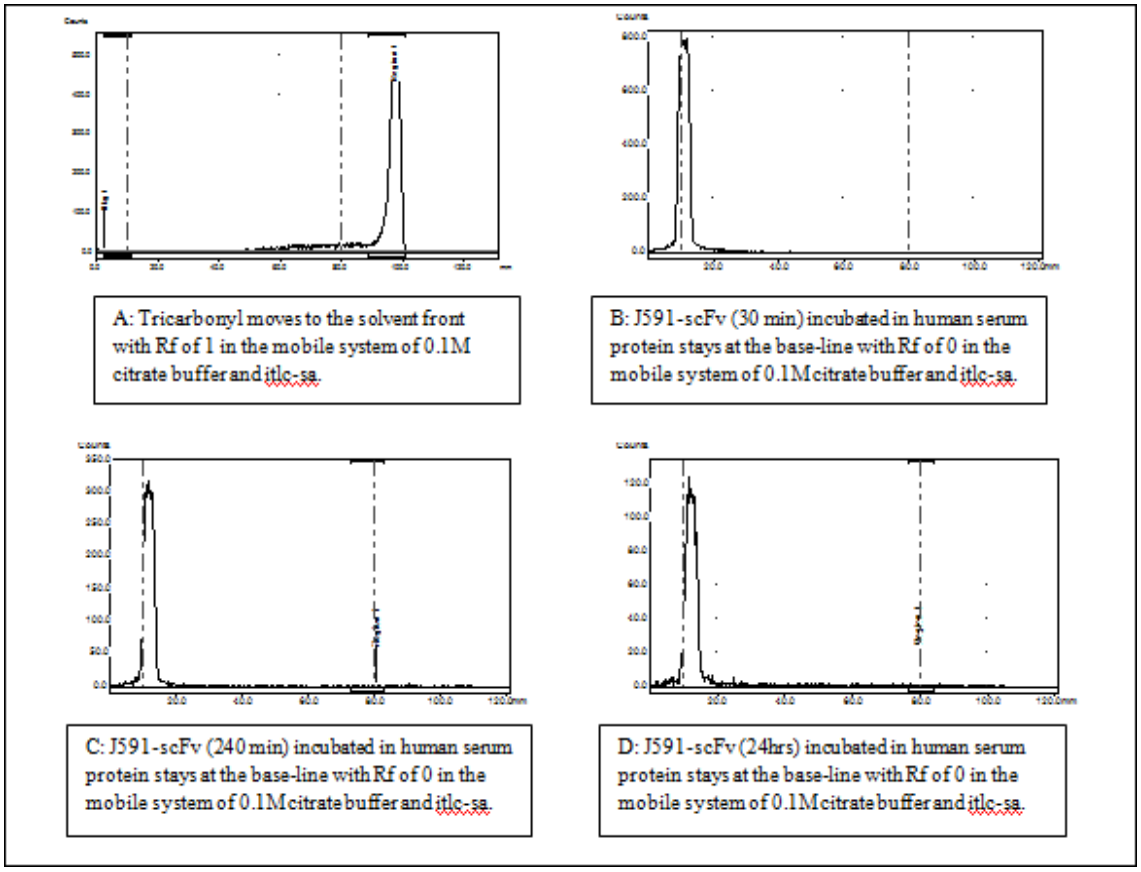

Figure-4.15: Radiochromatograms showing the result of strong binding of J591(scFv) with ^{99m}Tc tricarbonyl in the presence of human serum at different time points.

It was observed that labelled J591(scFv) was kinetically stable and did not lose radioactivity in the form of ^{99m}Tc tricarbonyl or pertechnetate.

4.9.7-FACS

FACS analysis was performed for both PSMA positive and negative cell lines before the cell binding experiment with radiolabelled J591(scFv) to confirm that cells were still showing specific binding to J591(scFv). In FACS analysis three samples were used for each cell line. One was just cells alone, the second was cells with Penta-His-Alexa Fluor 488 conjugate and the last sample contained cells with Penta-His-Alexa Fluor 488 conjugate and J591(scFv). In flow cytometers separate fluorescence (FL-) channels are used to detect light emitted. In this case it was FL1 (488 nm). These detectors are usually photomultiplier tubes (PMTs) and are sensitive to scatter and fluorescence. In a graph (Fig-4.16-D and -C), the left quadrant represents the negative events and right shows positive events. PC3LN3-PSMA showed a positive shift in a graph towards the

right in FL1 as compared to the PC3LN3 cells, which are PSMA negative. Histogram A in Figure 4.16 illustrates the entire population of cells present in a sample. This graph plots the side scatter (SSC), which is a measure of the cells' granularity and general shape, against forward scatter (FSC), a measure of cell size. Being able to view the entire population enables the gating and separation of sub-populations that one wishes to analyse. Apoptosing cells and cell debris are indicated at the bottom left and can be excluded from analysis by the gating system. Histogram B shows the gated population of cells. Histogram C illustrates the level of fluorescence due to cell-associated Penta-His-Alexa Fluor 488 conjugate (FL1). The sample with cells alone and Penta-His-Alexa Fluor 488 conjugates was used to measure the background. Histogram D, which contains cells, Penta-His-Alexa Fluor 488 conjugate and J591(scFv) shows the shift towards right with increasing fluorescence, indicating positive cells for the target of interest. Negative cells do not possess the fluorescent marker and thus remain on the left-hand side (Fig-4.17).

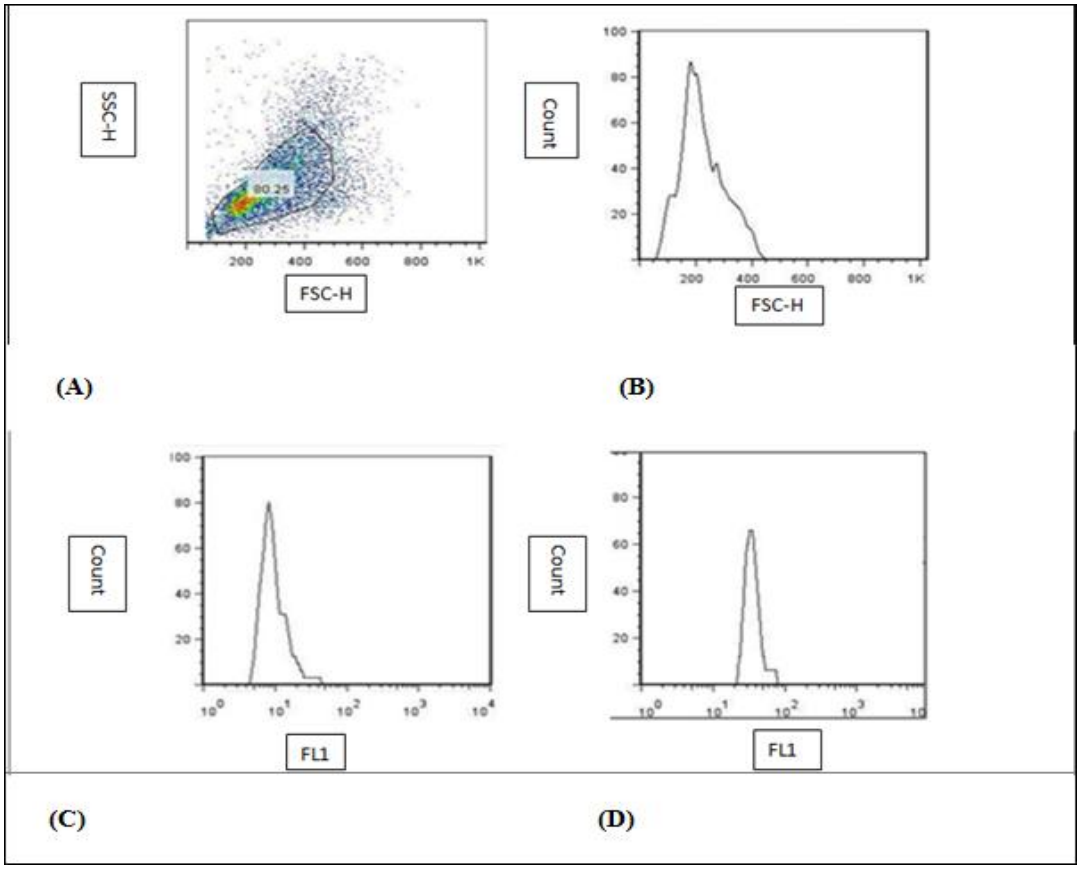

Figure-4.16: FACS analysis of PC3LN3-PSMA using J591(scFv) and penta-His alexa 488 conjugate

A: Just cells. FSC-H vs.SSC-H.

B: FSC-H of gated cells.

C: His-tag (FL1).

D: His-tag and J591(scFv) (FL1) Cells showing positive shift towards right.

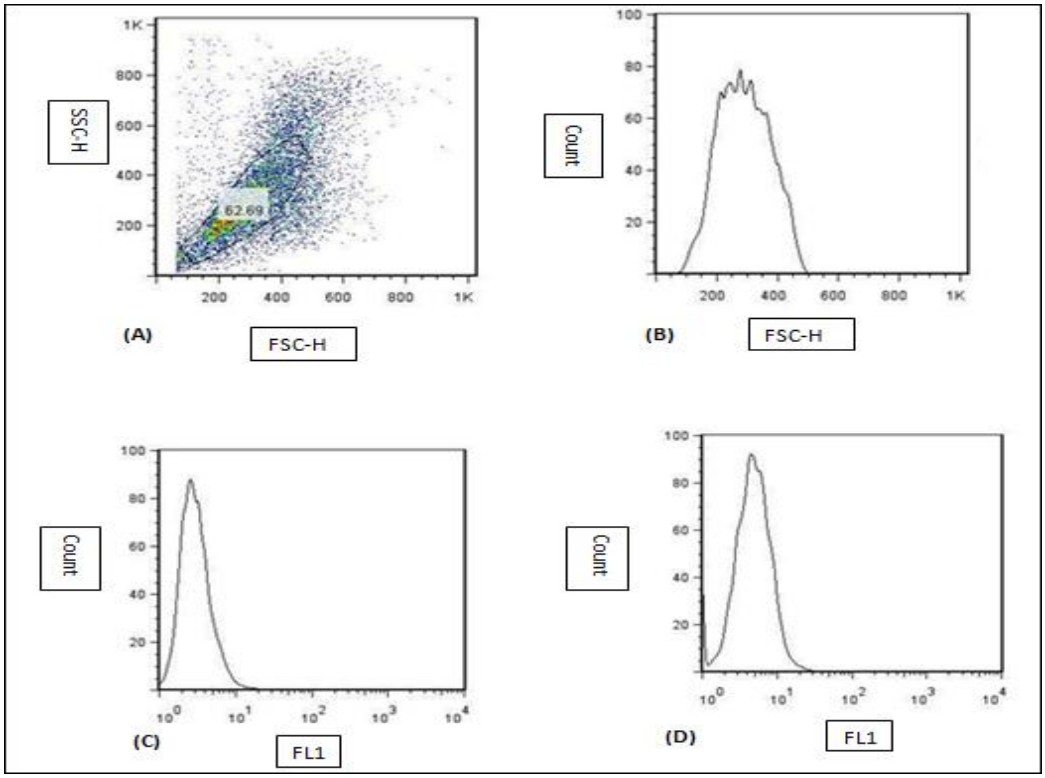

Figure-4.17: FACS analysis of PC3LN3 using J591(scFv) and Penta His alexa 488 conjugate

A: Just cells. FSC-H vs.SSC-H.

B: FSC-H of gated cells.

C: His-tag (FL1).

D: His-tag and J591(scFv) (FL1) Cells showing no shift towards

4.9.8-Cell-binding of ^{99m}Tc-labelled J591(scFv)

Once the J591(scFv) was radiolabelled with ^{99m}Tc tricarbonyl, 10 serial dilutions were prepared in triplicate in order to determine whether it has retained its receptor-binding affinity, and it had not been compromised in any way. This affinity was measured in a radioligand binding assay.

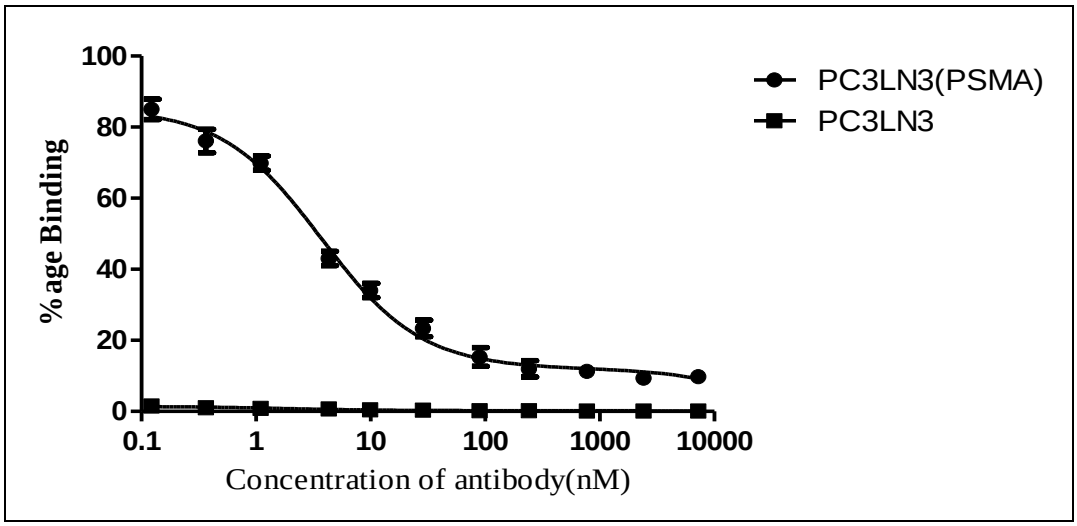

Figure-4.18: Non-specific binding with negative cell lines (PC3LN3) vs total binding with PSMA positive cell lines (PC3LN3-PSMA). Increase in cell labelling in positive cell lines with the decrease in concentration of J591. Kd value is 3.72 nM in case of PC3LN3-PSMA.

Serial dilutions of the radiolabelled J591(scFv) were incubated with the cells at 4°C (to minimise internalisation) for 60 min in order for binding equilibrium to be reached. As well as specific binding to the receptors, non-specific binding can also occur due to hydrophobic and ionic interactions with other sites on the cell surface, and it is important to identify the proportions that are specific and non-specific from the total binding observed. Non-specific binding was measured using a negative cell line. The 24-well plate was prepared at least 24 h before to obtain a uniform layer of cells which adhere to the surface. Different concentrations of the radiolabelled protein were added to the both positive and negative cell lines to measure total and nonspecific binding respectively. Specific binding with the receptors increased with the decrease in the concentration of the J591(scFv) in PSMA positive cell lines (PC3LN3-PSMA) and in comparison no such increased binding was observed in negative cell line (PC3LN3) (Fig-4.18). The results were analysed by plotting % binding against concentration of radiolabelled antibody in PRISM software, using non-linear regression fit (one-site total) and a Kd value was calculated, which was 3.72 nM in the case of PC3LN3-PSMA.

4.9.9-Electrospray Mass-Spectroscopy:

The mass spectral data from the direct injection of the J591(scFv) shows the strong peak at 27700, which corresponds with the molecular weight of the J591(scFv), 27.7 kDa (Fig-4.19). A dimer fraction was also observed at 55401.45, which corresponds with the molecular weight of the dimer.

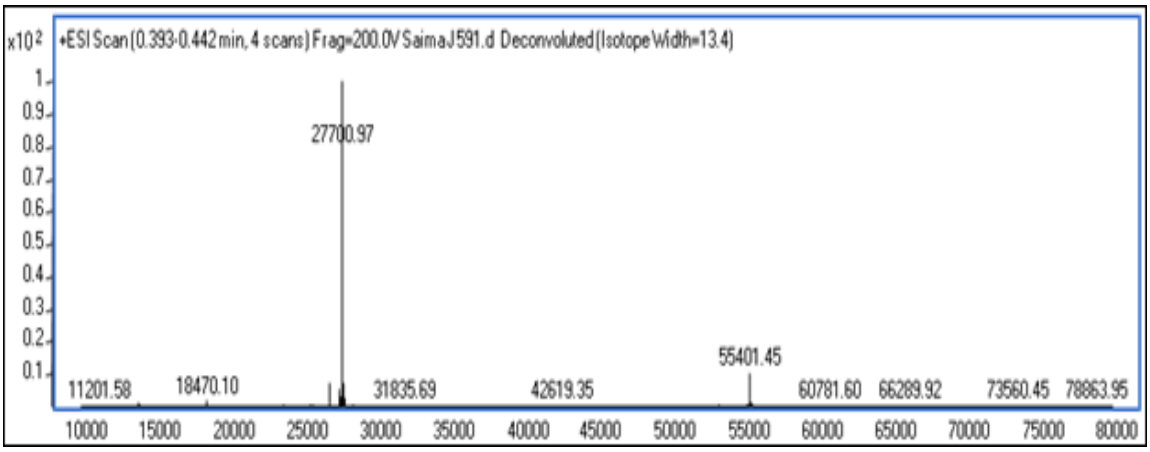

Figure-4.19: Mass-spectrum of J591(scFv). A strong peak at 27700, which corresponds with the molecular weight of the monomer J591(scFv). A small peak at 55401.45 showed the prescence of dimer.

4.10-Discussion

For radiolabelling of the protein with ^{99m}Tc, J591(scFv) incorporating a His-tag was radiolabelled using an Isolink ^{99m}Tc tricarbonyl kit from Covidien. QC was performed by using TLC to determine the radiolabelling yield (Fig-4.1). ^{99m}Tc tricarbonyl gives an Rf value of 0.4, while any free pertechnetate moves with the solvent front because of its hydrophilic nature. J591(scFv) was radiolabelled with ^{99m}Tc tricarbonyl at 37^{o}C and samples were taken out at different time points to check the radiolabelling yield. It was observed that radiolabelling yield increased from 50% at 30 min to almost 70% at 60 min and 90% at 180 min (Fig-4.2) when labelling was performed at the normal 140 mM salt concentration. In later experiments, 500 mM salt concentration was used and a comparative study of 140 mM and 500 mM salt concentration and its effect on the radiolabelling yield was studied. It was observed that increasing the salt concentration from 140 mM to 500 mM resulted in an increase in yield. At 60 min 0.5 mg/ml with

500 mM salt concentration the radiolabelling yield was 80% and for same amount of protein in the case of 140 mM salt concentration it was 59% (Fig-4.12, 4.13). By increasing the salt concentration the radiolabelling yield was increased, which further reduced the need to purify the protein through a MiniTrap column. In this regard salt concentration in a protein sample is important factor, as demonstrated recently in our department [141]. It was also observed that different concentrations of the protein react at different rates when incubated with ^{99m}Tc tricarbonyl. A higher concentration of the protein produced greater radiolabelling yields in less time. The main reason for this is the simple statistics of the law of mass-action. The rate of reaction is higher at high concentration of the protein, the chances of the interaction between the ^{99m}Tc tricarbonyl and protein is greater at high protein concentration and there is greater probability of forming the radiolabelled complex. At 72.2 µM the radiolabelling yield was 100% at 30 min; on the other hand it was 25% with 3.61 µM protein. By increasing the time to 60 min the radiolabelling yield at higher concentration was still 100% and lower concentration increased to almost 80% (Fig-4.6). In order to remove any unreacted ^{99m}Tc tricarbonyl or free pertechnetate a MiniTrap column was used through a gravity protocol (Fig-4.3, 4.4, 4.5). Although this step may result in a loss of protein, it is important to remove any unreacted ^{99m}Tc tricarbonyl or free pertechnetate, especially for experiments such as serum stability, as it binds with the serum protein and produces a strong band at 60 KDa on the SDS-PAGE gel and it would be difficult to interpret the results. In the long term the main point of removing the tricarbonyl is to avoid injecting it into the patient. A PD-10 MiniTrap column contains G-25 medium Sephadex and it separates the small molecules like salt, free labels and other impurities from high molecular weight compounds. Two protocols are available to use this column: spin and gravity. In the spin protocol the sample is not diluted but recovery is 90%. In the gravity protocol although the sample is diluted the recovery is 98%. Recovery of the protein is 95-98% in a volume of 300 µl. It was also observed on ITLC and HPLC analysis that protein samples were without any free pertechnetate and ^{99m}Tc tricarbonyl as shown in Figure 4.4 and 4.5.

Serum stability was analysed by SDS-PAGE (Fig-4.14). Since any unreacted tricarbonyl and free pertechnetate had been removed through the MiniTrap step, if there was any binding between serum protein and ^{99m}Tc tricarbonyl then it was because of dissociation between protein and ^{99m}Tc tricarbonyl. The radiolabelled complex was

quite stable over time (Fig-4.14, 4.15). In SDS-PAGE gel it was observed that there was strong band at 30 KDa (corresponding to the molecular weight of the monomer fraction of protein) and nothing at 60 KDa (serum protein and dimers) as there was no binding of these with ^{99m}Tc tricarbonyl. The main conclusion from serum stability is that it is stable in serum even after 24 h and this test makes it a strong candidate to proceed towards an *in vivo* study. It also means the chelator (His tag sequence) is behaving well under challenging conditions.

For the cell binding study, PC3LN3 (PSMA negative cell line) and PC3LN3-PSMA (PSMA positive cell line) were used, which were kindly provided by Dr John Maher (King's College London). Radiolabelled proteins must retain their receptor-binding capacity if they are to function as effective radiopharmaceuticals. The radioligand binding assay was performed on both negative and positive cell lines to get the binding affinity (Kd) which was found to be 3.72 nM by non-linear regression, by analysis of non-specific binding and total binding. Non-specific binding, importantly, occurs in many types of binding assay. In addition to specific binding to target receptors, radioligands may also bind non-specifically to other sites, notably the cell membrane. The details of the molecular interactions remain unclear, but charge and hydrophobicity of the ligand are involved, more so than sequence-specific binding. Non-specific interactions may also occur to other receptors and transporters expressed on the surface of the cell membrane, and is usually directly proportional to the concentration of the radioligand (the addition of twice the concentration of radioligand doubles the amount non-specifically bound) [127]. This experiment did demonstrate that there was effective cell binding with PSMA positive cell line as compared to the negative cell lines (Figure 4.18).

Mass-spectroscopy was also performed on J591(sdFv). A non-radiolabelled sample of protein on direct injection gave a strong peak at 27700 (molecular weight of the protein) for monomer fraction of the protein and there was also small peak for dimer around 55401.45 (Fig-4.19), which further confirms the SDS-PAGE and HPLC results.

4.11-Summary

J591(scFv) was radiolabelled with ^{99m}Tc tricarbonyl. The radiolabelled complex was purified uing a MiniTrap column, and ~98% of the radiolabelled complex was recovered with high purity (without any unreacted ^{99m}Tc tricarbonyl and free pertechnetate). This radiolabelled complex was highly stable in human serum even after 24 h as analysed by SDS-PAGE and showed specific binding to a PSMA positive cell line (PC3LN3-PSMA) but not to the PSMA negative cell line (PC3LN3). This provides justification for evaluation of the potential new radiopharmaceutical *in vivo* in a tumour model.

Chapter 5: Radiolabelling and *in vivo* biodistribution of J591c(scFv) with Gallium-68

5.0-Introduction

PET (positron emission tomography) is rapidly becoming a most important imaging modality. The most commonly used PET radioisotope is ^{18}F, which is accelerator produced. However, recently many alternative PET radioisotopes have been explored. Gallium-68 is one of them. It is a generator produced PET radioisotope with a half-life of 68 minutes. It is used to radiolabel biomolecules using bifunctional chelators. In this project instead of a whole antibody, J591, a single chain fragment, J591c(scFv), is used. The half-life of ^{68}Ga matches perfectly with the expected pharmacokinetic properties of the scFv. The scFv contains a His-tag and one cysteine is present near the His tag. This cysteine can be used to conjugate it with the maleamide group of bifunctional version (YM103) of the in-house produced chelator (CP256) for radiolabelling with ^{68}Ga. The main aim of the work described in this chapter involved the conjugation of the scFv and bifunctional chelator, followed by radiolabelling with ^{68}Ga. Its serum stability was analysed by SDS-PAGE and *in vitro* work using PSMA positive and negative cell lines followed by *in vivo* work using male SCID mice having PSMA positive and negative tumours.

5.1-Methods

5.1.1- Reduction of J591c(scFv) with TCEP

The sulfhydryl in J591c(scFv) can form a disulfide bond (-S-S-) with another J591(scFv) to form a dimer. In order to reduce these disulfide bonds so that the sulphydryl (-SH) groups are available for conjugation with maleimide, TCEP was used as a reducing agent. In order to optimise the concentration of TCEP which is required to reduce these disulfide bonds, different amounts of TCEP were used, ranging from 0.5 fold molar excess over protein to 30 fold molar excess. After incubating these different molar amounts of TCEP with the same amount (5 µg) of J591c(scFv) for 90 min at room temperature, aliquots were loaded onto a 12% Neupage gel and run for 45 min with a constant voltage of 200 V and a current of 100-125 mA in MES buffer. The gel was developed in simple blue safe stain.

5.1.2- Conjugation of J591c(scFv) with Fluorescein-5-maleimide (F-5-M) and YM103

After reduction with TCEP (1.7 µl), sulfhydryl (-SH) groups were free for conjugation with the maleimide group of YM103 (1 mg) dissolved in 10 µl of DMSO. However, before performing the conjugation with YM103, J591c(scFv) (819 µg/600 µl, ~887 nmol) was conjugated with the F-5-M (1 mg) dissolved in 10 µl of DMSO, to optimise the conditions for conjugations, as F-5-M also contains a maleimide group. A 35-fold molar excess of F-5-M and YM103 was used for conjugation with respect to the molar amount of J591c(scFv) [5]. In the case of F-5-M incubation was done in the dark because of light sensitivity. The incubation time with F-5-M and YM103 was 4 h at room temperature. After incubation, the excess of YM103 and F-5-M was removed using a size-exclusion column (Superdex 75 10/300 GL from GE, flow rate 0.5 ml/min and max pressure 1.8 MPa). The column was equilibrated with water followed by PBS. J591c(scFv) (500 µl) was injected and 1 ml fractions were collected automatically. Afterward the column was washed with water and stored in ethanol. The fractions of conjugated J591c(scFv) ready for radiolabelling were stored at -80^{o}C.

5.2-^{68}Ga generator elution protocol and radiolabelling of J591c(scFv)-YM103 with ^{68}Ga

The IGG100 ^{68}Ge/^{68}Ga wet column generator was used for elution of ^{68}Ga. It was eluted with 5 ml of 0.1 N HCl of high purity (hydrochloric acid, 0.1 N, BioChemica, 84428-500ML, Sigma-Aldrich-Fluka) without using a metal needle over the time period of 2 min. ^{68}Ga was further concentrated using a SCX cartridge (Varian, BondElut-SCX, 100 mg, 1 ml). The cartridge was preconditioned with 1 ml of 5.5 M HCl and then further with 10 ml of distilled water. The generator eluate was applied to the column using a 5 ml syringe and a Chromabond adapter (Macherey-Nagel). The entire radioactivity bound to the column. The radioactivity trapped on column was then eluted with a mixture of 12.5 µl of 5.5 M HCl and 500 µl of 5 M NaCl [102]. ^{68}Ga eluted from the SCX column was acidic with pH ~3. The pH was then adjusted to 7 using ammonium acetate buffer (1 M). A volume of 200 µl of ^{68}Ga required 300 µl of ammonium acetate to neutralise it. For radiolabelling J591c(scFv)-YM103 (10 µg/20 µl) was incubated with ^{68}Ga (12 MBq/50 µl) for 10-15 min at room temperature (25^{o}C). However, at lower concentrations more time may be required to achieve maximum radiolabelling

yield. Conjugated J591c(scFv) radiolabelled with ^{68}Ga was then analysed using a size-exclusion column (SEC-2000) by injecting 20 µl into the HPLC. PBS was used as a running buffer at a flow rate of 1 ml/min, with UV detection at 280 nm and gamma detection through an HPLC gamma detector. Further, the radiolabelled complex was also analysed using TLC. ITLC-SA was used as a stationary phase and 0.1 M sodium citrate as running buffer. ^{68}Ga acetate moved with the solvent front with the Rf value of 1 and radiolabelled conjugated protein stayed at the origin with Rf value of 0.

5.3-Effect of time and temperature on radiolabelling of different concentrations of J591c(scFv)-YM103 with ^{68}Ga

Different concentrations of J591c(scFv)-YM103 ranging from 1 µg/µl to 0.1 µg/µl were incubated with 7 MBq of ^{68}Ga for 60 min. Samples were taken at different time points (0, 5, 10, 20, 30, 40 and 60 min) and analysed for the formation of radioactive complex (J591c(scFv)-YM103-^{68}Ga) with the help ITLC-SG developed with 0.1 M sodium citrate buffer (pH 6). To check the effect of temperature on radiolabelling, 25 µg/50 µl of J591c(scFv)-YM103 was incubated with 90 MBq ^{68}Ga in volume of 150 µl at two different temperatures (room temperature i.e. 25^{o}C and 37^{o}C) and samples were taken at different time points (0, 5, 10, 20, 30, 40 and 60 min). CP256 (25 µg/50 µl) and unconjugated J591c(scFv) (25 µg/50 µl) were also incubated with same amount of ^{68}Ga as controls.

5.4- Mass spectroscopy

20 µl (30 µg) of J591c(scFv)-YM103 was assessed by mass-spectroscopy using direct injection. Two samples of unconjugated J591c(scFv) were also analysed by direct injection, one of which had been incubated with a 30-fold molar excess of TCEP reducing agent for 60 min to reduce the covalent dimers.

5.5- Serum stability

A volume of 300 µl of ^{68}Ga acetate (60 MBq) prepared as described above was added to 200 µl of J591c(scFv)-YM103 (0.4 µg/µl) and kept for 15-20 min at room temperature. Samples were taken at 20 min and analysed by ITLC-SA in 0.1 M citrate buffer and HPLC using a size-exclusion column (SEC-2000), PBS as running buffer, flow rate of 1 ml/min and UV detection at 280 nm and gamma detection with gamma detector of HPLC. The radiolabelled conjugated J591c (100 µl) was mixed with serum (200 µl of

serum and 100 µl of 0.9% saline). The mixture was incubated at 37^{o}C and samples were collected at 30, 60, 120, 180, 240 and 300 min (5 µl in each case) and stored at -80^{o}C until all the time points were collected.

The behaviour of unchelated Ga-68 in serum was determined by adding 10 µl of ^{68}Ga-acetate to 50 µl of serum protein, incubating for 60 min at 37^{o}C and taking out 5 µl and storing at -80^{o}C until all the time points were collected for gel analysis. J591c(scFv)-YM103 (2 µg/5 µl) was radiolabelled with ^{68}Ga acetate (2 MBq/~10 µl) and a 5 µl sample was taken out after incubation of 20 min at room temperature and stored at -80^{o}C as a reference. For analysis by SDS-PAGE, the samples (5 µl) were mixed with 10 µl of LDS buffer (lithium dodecyl sulfate, pH 8.4) and applied on the gel (10 µl). The gel was developed in MES buffer (2-ethanesulfonic acid) for 40 min at 200 V and 120-130 A. Afterwards the gel was removed, activity markers were placed and it was analysed by phosphorimager and then stained with Coomassie blue.

5.6- FACS analysis

FACS analysis was performed to measure the PSMA expression on the cell lines. For FACS analysis, the medium was removed from 75-cm^{3} flasks containing Du145 (PSMA negative) and Du145-PSMA (PSMA positive) cell lines, and replaced with 10 ml of PBS. After a few minutes the PBS was discarded. A 1 ml aliquot of 0.25% w/v trypsin-0.53mM EDTA was added and incubated for 60 s at 37^{o}C. Addition of 10 ml of fresh media (RPMI) terminated the reaction. The cells were scraped and homogenised with pipetting to resuspend them. A volume of 8 ml of cell suspension was removed from the flask and added to a 15 ml polypropylene tube. The tube was centrifuged for 4 min at 1000 rpm to obtain a pellet. The supernatant was discarded and the pellet was resuspended in PBS and the cells were counted in a Cell Countess. There were three samples each for PSMA positive (Du145-PSMA) and PSMA negative (Du145) cell lines: cells alone and anti-PSMA antibody (Phycoerythrin, Abcam) in two different concentrations.

For FACS analysis, 950 µl of cells were placed in FACS tubes and centrifuged at 1000 rpm for 4 min. The supernatant was discarded and the pellet was resuspended in 500 µl of PBS by vortexing and 1 µl of monoclonal anti-PSMA antibody was added in two different quantities, 500 ng and 100 ng. After mixing tubes were incubated on ice for 20 min. The tubes were then centrifuged for 4 min, the supernatant discarded, and the

pellet resuspended in 2 ml of PBS. This process was repeated twice. Finally, the pellet was resuspended in 300 µl of PBS and analysed by FACS.

5.7- Cell binding of ^{68}Ga-J591c(scFv)-YM103

For cell binding experiment, a 96-well plate was prepared 24 h before the experiment, seeded with $5x10^4$ cells per well. For preparation of the plates RPMI-1640 media was removed from the T-75 cm^3 flasks in which the cells were growing and the bottles were washed with 5 ml of PBS to remove any dead cells. Then 1 ml of trypsin-EDTA was added to loosen the cells from the bottle surface. The flask was kept at 37^{o}C for 60 s in an incubator. Then 10 ml of fresh RPMI-1640 was added and the cells were scraped and mixed using a pipette to obtain a homogeneous suspension of cells. In order to measure the number of cells, an aliquot of 10 µl of the cell suspension was transferred to a microcentrifuge tube and mixed with 10 µl of Trypan blue for few seconds and an aliquot of 10 µl was placed on the slide to measure the number of cells using Cell Countess. The bulk cell suspension was then diluted with RPMI-1640 so that each well in the 96-well plate received an equal number of cells ($5x10^4$) in a volume of 100 µl. The 24-well plate was incubated at 37^{o}C for 24 h. After 24 h it was removed from the incubator and the supernatant was removed carefully without disturbing the cells. A serial dilution of cold antibody was prepared in a volume of 75 µl in triplicate [7220 nM (15 µg in 75 µl), 2410 nM (5 µg in 75 µl), 770 nM (1.6 µg in 75 µl), 240 nM (0.5 µg in 75 µl), 89.05 nM (0.185 µg in 75 µl), 28.88 nM (0.06 µg in 75 µl), 9.63 nM (0.02 µg in 75 µl), 4.81 nM (0.01 µg in 75 µl), 1.44 nM (0.003 µg in 75 µl), and 0.4 nM (0.001 µg in 75 µl)].

The cells were washed with 100 µl of HBSS. In cell binding experiments ^{68}Ga-J591c(scFv)-YM103 was prepared as described above. After 20 min the formation of radiolabelled complex was checked by ITLC-SA using 0.1 M citrate buffer as running buffer. The stock solution of radiolabelled antibody was composed of 5 µg/900 µl. The radiolabelled antibody was added at a constant 2 nM (0.33 MBq/~1 µl) concentration into the serial dilution of cold antibody and incubated with the cells at 4^{o}C for 40 min. The reduced temperature will result in less internalisation and reflects the binding of the antibody to the cell surface better. After incubating for 40 min, the cells were washed three times carefully with 100 µl HBSS to remove any unbound radioactivity. The cells

were then lysed with 0.5 M NaOH (200 µl) and lysate was collected in tubes and counted in a gamma counter.

5.8- *In vivo* experiment

All *in vivo* experiments were performed according to the animal ethics under a home office licence in accordance with the Animals (Scientific Procedures) Act 1986. For *in vivo* analysis, 4 male SCID mice (age 8 weeks, ~20 g) were injected subcutaneously on the left flank with $3.5x10^6$ (90 µl) of Du145-PSMA (PSMA positive) cells. One of them was used for imaging and four were used for biodistribution studies. For imaging of Du145 tumours (PSMA negative) one male SCID (age 8 weeks, ~20 g) mouse was injected with Du145 cells on both right and left flank with $3.5x10^6$ (90 µl) of Du145 (PSMA negative) cells. For biodistribution studies 4 male mice (age 8 weeks) were injected on the left flank with $3.5x10^6$ (90 µl) of Du145 (PSMA negative) cells. For injection cells were grown over the period of 2 weeks in 175 cm^3 flasks, splitting the cells after every 3rd day and replacing the media with fresh RPMI-1640. Eight flasks were prepared for both PSMA positive and negative cell lines. For injection the cells were first washed with PBS, trypsinised and resuspended in 10 ml of fresh RPMI medium, pelleted by centrifugation for 5 min at 1100 rpm, resuspended in 5 ml of PBS and counted by combining 10 µl of cell suspension with 10 µl of trypan blue and then counting cells in a Cell Countess. Again, the cells were centrifuged and resuspended in PBS to get the desired concentration in required volume ($3.5x10^6$ in 90 µl). Slowly, 90 µl of cell suspension was withdrawn into the insulin syringe which was the kept on ice. Before injecting the cells, animals (n = 4 for PSMA+ and n = 5 for PSMA-) were anaesthesised using isoflurane. Cells were injected into the flank (by pinching the the skin of the animal between index finger and thumb and pulling the skin away from the body of the mouse) slowly and evenly into the pouch created by fingers, creating a single bubble of cells beneath the skin and avoiding too much spread of the cells. The mice were regularly monitored over the period of 4 weeks until the tumours were ~5 mm in size. The size of tumours was monitored through visual inspection and a vernier calliper. J591c(scFv)-YM103 was radiolabelled with ^{68}Ga as described earlier and quality control was performed with HPLC and ITLC before administration to the mice by tail vein injection. The amount of radioactivity injected into each mouse was 7 MBq in a volume of 90 µl and containing 10 µg of protein. Imaging (n = 1 each group) was performed with a Bioscan Mediso NanoPET/CT scanner over the time period of 4 h

from the time of injection using PET dynamic scan, 3 weeks and 4 days after tumour inoculation. Biodistribution studies with the group of mice bearing PSMA positive tumours (n = 4) and with the group bearing negative tumours (n = 4) were performed after 4 weeks of growth with sacrifice at 90 min post injection of 7 MBq of the labelled antibody. Mice were culled by dislocation of the neck and organs and tissues were excised and collected in pre-weighed scintillation tubes to be measured in the gamma counter. At the same time, 90 µl of the injectate was taken in another syringe and ten 1:3 serial dilutions were prepared from it. They were measured at the same time in the gamma counter along with organs. The counts obtained in the standards were then used to calculate the percent uptake of injected radioactivity per g of tissue (% ID/g). ^{68}Ga acetate and ^{68}Ga-CP256 imaging and biodistribution were also performed in normal mice as an additional control. For ^{68}Ga acetate one male balb/c mouse (8 weeks, ~20 g) was used for the imaging and then biodistribution of the same mouse was done at the end of the 4 h scan. For the preparation of the ^{68}Ga acetate, the generator was eluted according to the procedure mentioned above, and concentrated using a BondElut column. A volume of 100 µl (60 MBq) of this concentrated generator eluate was taken and neutralised by adding 500 µl of acetate buffer (pH 6). A volume of 70 µl of this neutralised ^{68}Ga-acetate (7 MBq) was injected into the mouse. The mouse was culled and biodistribution studies were performed as mentioned above at the end of the 4 h scan. For ^{68}Ga-CP256 two normal balb/c mice were used (age 8 weeks, ~20 g). They were injected simultaneously with ^{68}Ga-CP256. One of them was used for imaging purposes and other was kept in the cage for 4 h. At the end of the scan (after 4 h) both mice were culled and biodistribution studies were performed as mentioned above. For the preparation of ^{68}Ga-CP256, radiolabelling was done according to the method in Chapter 3 and the radiolabelled complex (4 µg, 7 MBq) was injected into the tail vein.

5.9-Results:

5.9.1- Reduction of J591c with TCEP

J591c(scFv) forms both covalent and non-covalent dimers. In order to reduce these dimers TCEP was used as a reducing agent. The reaction of the TCEP with disulfides involved initial cleavage of disulfide bond (–S-S) accompanied by the oxidation of phosphine. The phosphine oxide bond formed is quite stable. Different amounts of TCEP were used to see the extent of reduction of these dimers, so as to find out the

appropriate amount of TCEP to reduce the protein. As seen in Figure 5.1, in lower concentrations of TCEP there was not much reduction of dimers observed but as the amount of TCEP was increased there was gradual decrease in the extent of dimerisation of the protein. The dimer band at 60 kDa was quite weak at 5 and 10-fold molar excess of TCEP with respect to J591c(scFv) as compared to the lower molar concentrations of TCEP. The dimer band was negligible in 15, 20 and 30 fold molar excess of TCEP.

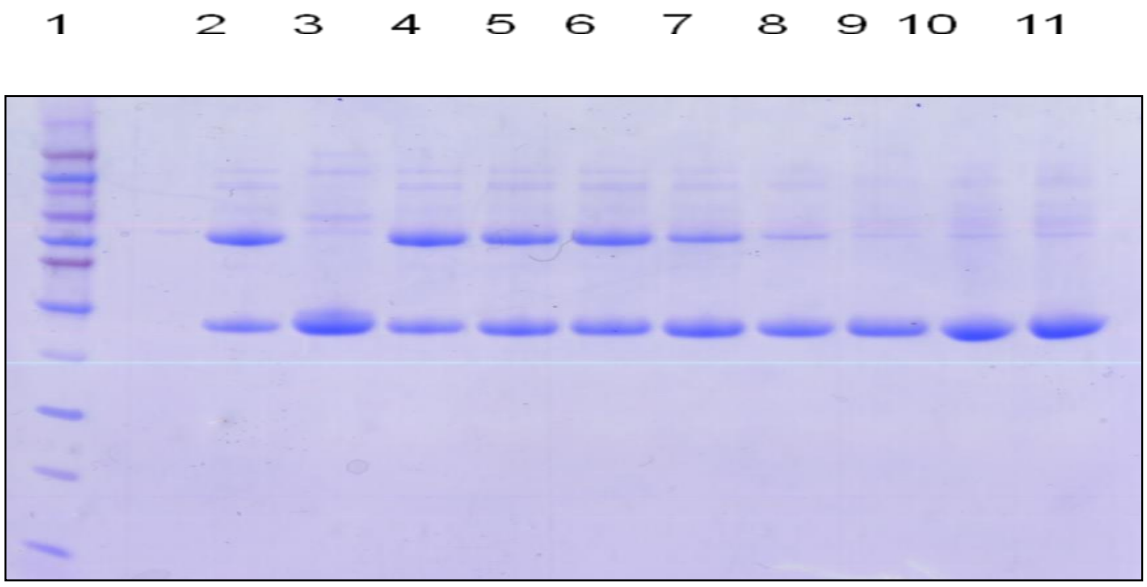

Figure-5.1: Showing the effect of different molar concentrations of TCEP on dimerisation in J591c (scFv).
1: Marker. 2: Protein (not reduced). 3: Reduced protein (Neupage reducing agent). 4: 0.5 fold molar excess of TCEP. 5: 1 fold molar excess of TCEP. 6: 2 fold molar excess of TCEP. 7: 5 fold molar excess of TCEP. 8: 10 fold molar excess of TCEP. 9: 15 fold molar excess of TCEP. 10: 20 fold molar excess of TCEP. 11: 30 fold molar excess of TCEP.

However, for subsequent experiments we have used 30-fold molar excess in respect to concentration of protein to reduce the dimerisation for maleimide conjugation. One of the benefits of using the TCEP as a reducing agent is that it did not require removal prior to the conjugation reaction with the maleimide (YM103) because there is no –SH compound added or formed as in the case of DTT (dithiothreitol), which interfere in the maleimide conjugation and must be removed before conjugation reaction resulting in possible loss of protein, so conjugation of these sulfhydryl group with the maleimide group of YM103 can be done without any need for the removal of TCEP. However, one research group in a recent study observed the formation of byproduct somatostatin-maleimide-TCEP conjugates by MS analysis in the case of halomaleimides [128].

5.9.2- Conjugation of J591c(scFv) with F-5-M and YM103

After reduction with 30-fold molar excess of TCEP, sulfhydryl (-SH) groups in J591c(scFv) are free to conjugate with maleimide. J591c(scFv) was first conjugated with fluorescein-5-maleimide (F-5-M) to check the binding and then later on with YM103. A 35-fold molar excess of F-5-M or YM103 was incubated for 4 h with J591c(scFv) for conjugation. The excess of F-5-M or YM103 was removed using FPLC and a Superdex 75 10/300 GL size-exclusion column. The conjugated protein eluted in the form of a single peak from 9-11 ml as it is heavier in molecular weight as compared to the free YM103 and F-5-M which eluted from 15-20 ml (Fig-5.2). Conjugation of YM103 was further verified using radiolabelling with ^{68}Ga and HPLC using a SEC-2000 column and by SDS-PAGE. Both the UV and radioactive peaks eluted at 9 min (Fig-5.5) and on SDS-PAGE there was a strong band at 30 kDa. Conjugation with F-5-M was analysed using SDS-PAGE and G-box (Syngene). It showed a strong band of fluorescent protein at 30 kDa (Fig-5.3). After conjugation the protein concentration was measured using Nano-drop and stored in appropriate aliquots (100 µg/200 µl) at -80^{o}C.

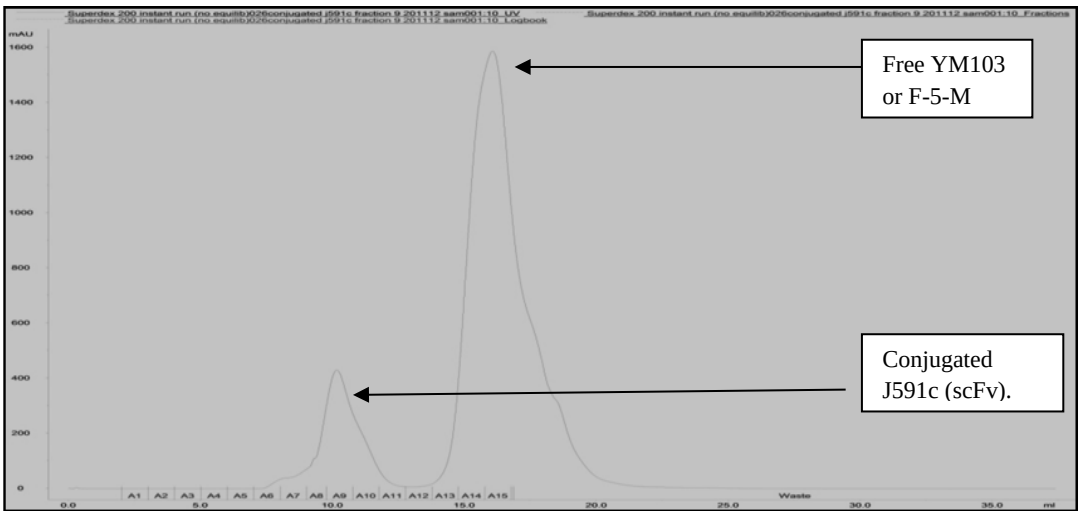

Figure-5.2: After reduction with TCEP and conjugation with maleimide the excess of unreacted maleimide was removed using Sephadex GL column via FPLC. Conjugated protein elutes first followed by the unreacted maleimide.

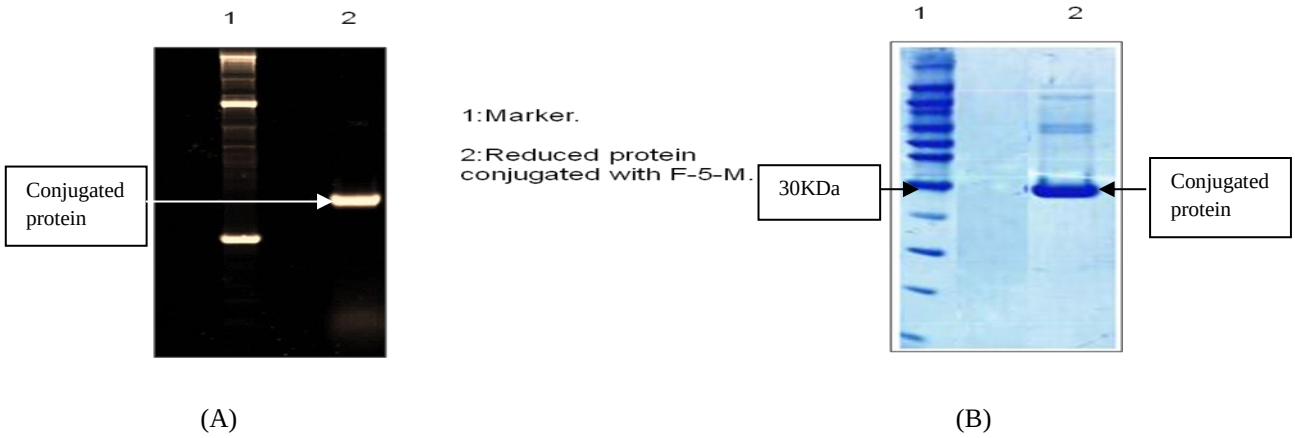

(A) (B)

Figure-5.3: J591c(ScFv) conjugated with fluorecein-5-maleimide (F-5-M). Strong band at 30 KDa.
1: Marker. 2: Reduced protein conjugated with F-5-M. J591c-scFv conjugated with F-5-M in G-box (A). Same gel developed in safe blue stain (B).

5.9.3- ^{68}Ga generator elution protocol and radiolabelling of J591c(scFv)-YM103 with ^{68}Ga

Following the elution and preconcentration protocol described in the method section, 95-99% of the eluted ^{68}Ga activity was recovered from the Bond Elut column [102]. The eluate was neutralised with acetate buffer to pH 7 and then used for radiolabelling of protein. Neutralisation required 300 µl buffer to 200 µl of column eluate giving a final concentration of 0.24 MBq/µl. The conjugation of YM103 with J591c(scFv) was determined by radiolabelling with ^{68}Ga. For that purpose, ^{68}Ga acetate (12 MBq, ~50 µl) was incubated with J591c(scFv)-YM103 (20 µl, ~5 µg) for 15-20 min and then analysed by HPLC using a size-exclusion column (SEC-2000, flow rate 1 ml/min, UV detection at 280 nm). ^{68}Ga acetate eluted at 12 min (Fig-5.4) and both the radiolabelled and UV peaks of ^{68}Ga-J591c(scFv)-YM103 eluted at 9 min (Fig-5.5). The small UV and radioactive peaks at 8 and 9 min in Figure 5.4 are most probably residual ^{68}Ga-J591(scFv) from a previous injection, as we have analysed ^{68}Ga acetate after ^{68}Ga-J591(scFv), so most probably some protein remained stuck on the column and eluted with the ^{68}Ga acetate HPLC run. The broad radioactive peak from 11-12 min is ^{68}Ga acetate.

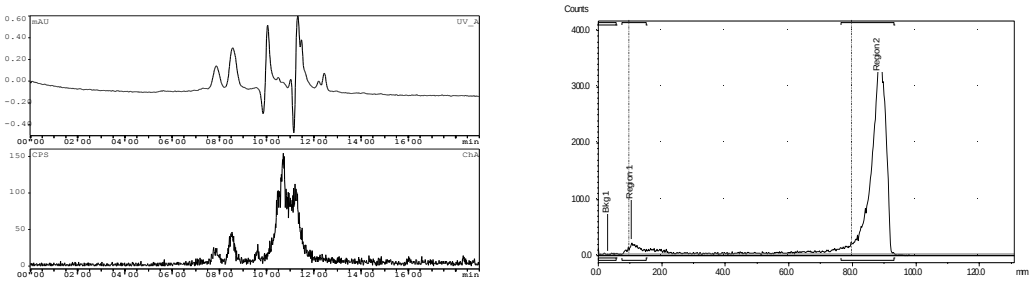

(A) (B)

Figure-5.4:^{68}Ga acetate elutes at 11.5 min in size-exclusion column (A) in HPLC. ^{68}Ga acetate moves to the solvent front with Rf value of 1 in ITLC-SA and 0.1 M citrate buffer (B).

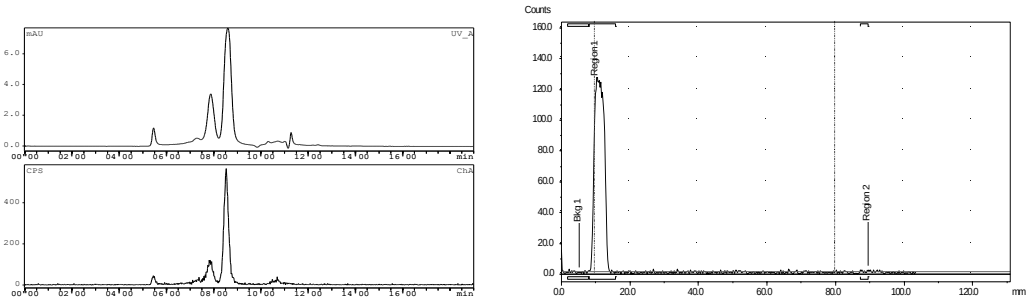

(A) (B)

Figure-5.5: ^{68}Ga J591c(scFv) elutes at 9 min in size-exclusion column (A) in HPLC. ^{68}Ga J591c-scFv stays at the origin with Rf value of 0 in ITLC-SA and 0.1 M citrate buffer (B).

The radiolabelling reaction between the ^{68}Ga and J591c(scFv)-YM103 is quite quick, it was complete in 5 min at room temperature (25^{o}C), compared to the other available chelators for ^{68}Ga such as DOTA can require heating for up to 30 min at 100^{o}C. Radiochemical yield was close to 100% and a high purity radiochemical complex was obtained as seen in the HPLC chromatogram. Although there is dimer peak in the UV, radiolabelling of the dimer was minimal, with most of the ^{68}Ga binding the monomer fraction of the scFv.

5.9.4- Effect of time and temperature on radiolabelling of different concentrations of J591c(scFv)-YM103 with ^{68}Ga

J591c(scFv)-YM103 (25 µg/100 µl) was incubated with ^{68}Ga acetate (70 MBq, ~120 µl) at two different temperatures: room temperature (25^{o}C) and 37^{o}C and samples were taken out at different time points (<1, 5, 10, 15, 20, 30 and 40 min). The samples were

analysed by ITLC-SG and 0.1 M citrate buffer. However, it was observed that temperature had no effect on the radiolabelling yield with time. Radiolabelling yield was ~100% at both the temperatures. In fact, within a few seconds 100% radiolabelling yield was obtained at room temperature (Fig-5.6-B). Free CP256 (0.2 µg/µl) and unconjugated J591c(scFv) (0.2 µg/µl) were also radiolabelled with ^{68}Ga as controls. J591c(scFv) showed no binding with ^{68}Ga as there was no YM103 (bifunctional chelator) attached to it. CP256 (free chelator) showed binding with ^{68}Ga in a similar way as the conjugate; YM103 is a bifunctional version of CP256 (Fig-5.6-A; Fig-5.8).

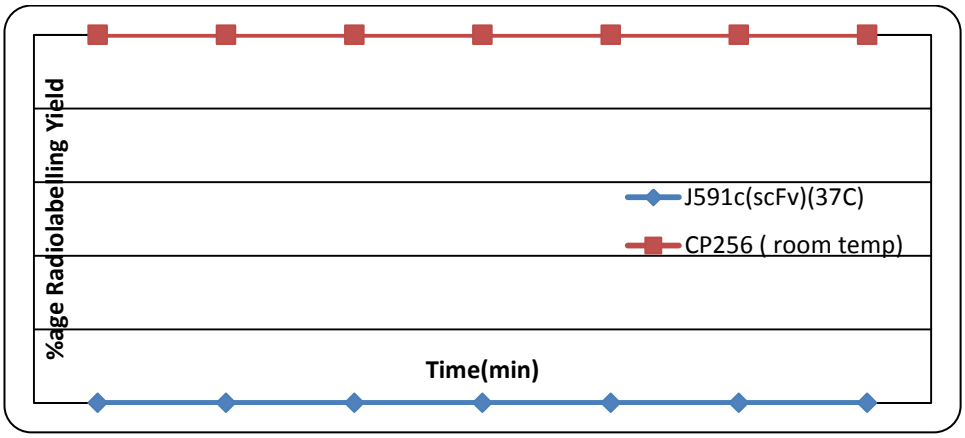

(A)

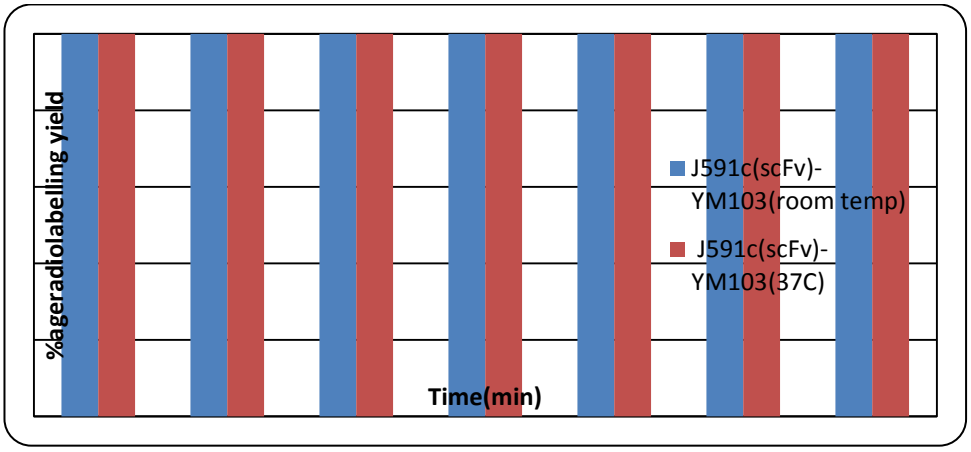

(B)

Figure-5.6: (A) shows two controls, CP256 which showed radiolabelling with ^{68}Ga and J591c(scFv) without YM103, which showed no binding with ^{68}Ga. (B) shows that there was no effect of temperature on the radiolabelling yield of conjugated J591c(scFv)-YM103 with time using iTLC-SG and mobile phase of 0.1 M citrate buffer.

The above experiment indicates that efficient radiolabelling of conjugated J591(scFv) with ^{68}Ga can be obtained at room temperature with 100% radiolabelling yield at a protein concentration of 0.2 µg/µl, pH 7 and a change in temperature did not affect the radiolabelling yield.

In another experiment to understand the effect of change in concentration of conjugated protein on radiolabelling yield, different concentrations of J591c(scFv)-YM103 ranging from 1 µg/µl to 0.125 µg/µl were radiolabelled with ^{68}Ga acetate (0.5 MBq) at room temperature. Quantitative radiolabelling was obtained at higher concentrations of protein (1 µg/µl to 0.25 µg/µl) at all the time points measured (<1, 5, 10, 20, 30, 40, 50 and 60 min). However, at a lower concentration (0.125 µg/µl), the radiolabelling yield increased with time from 70% at 5 min to almost 90% at 40 min (Fig-5.7). From this experiment we have concluded that at concentrations higher than 0.25 µg/µl, there was 100% radiolabelling with in a few seconds, however at 0.125 µg/µl, we had to wait for 30 min to get a 90% radiolabelling yield.

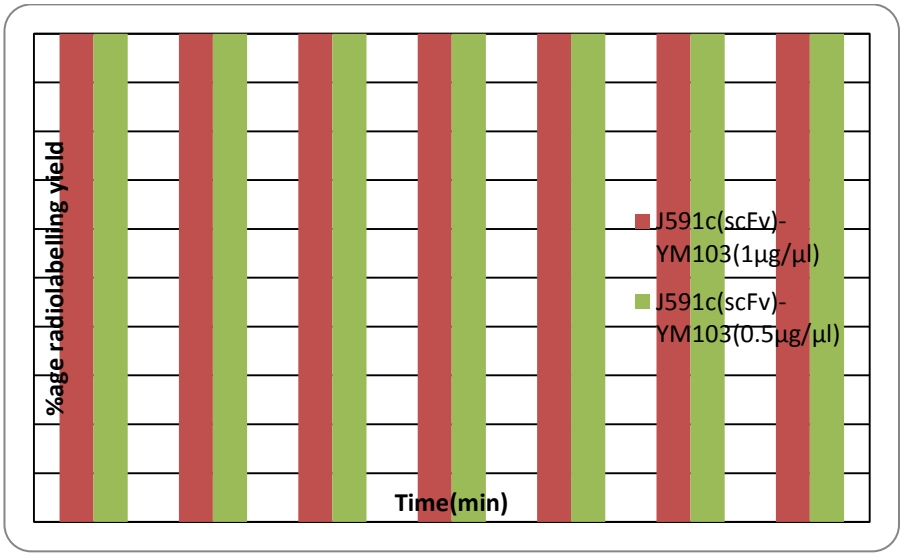

(A)

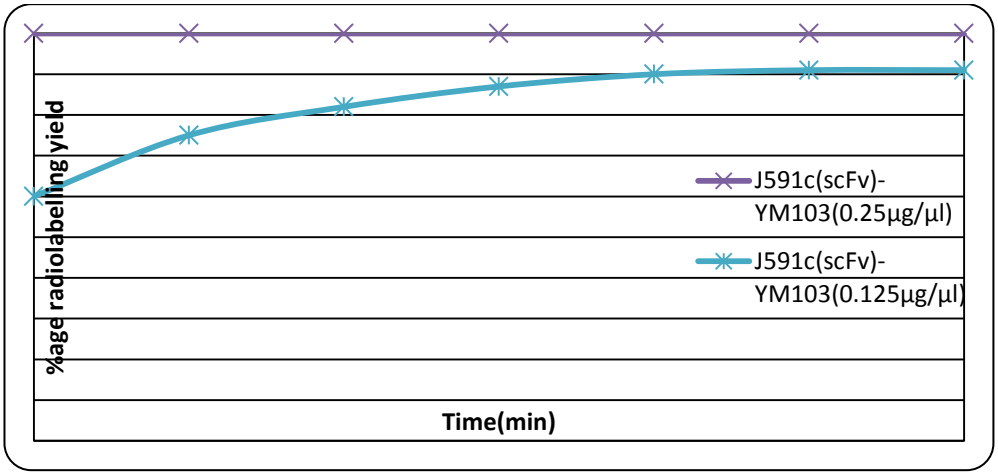

(B)

Figure -5.7: (A) shows no change in radiolabelling yield with time at higher concentrations of J591(scFv)-YM103. At lower concentration it increases from 70% at 5 min to 90% at 40 min (B).

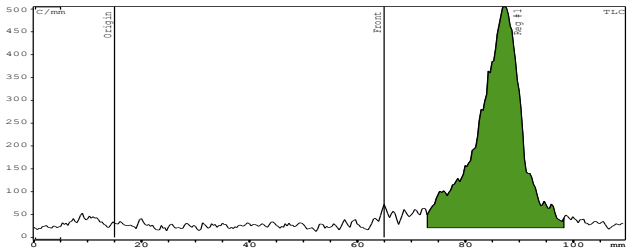

A: ^{68}Ga-acetate. control to show specifity of Ga-binding to the chelator (5 min)

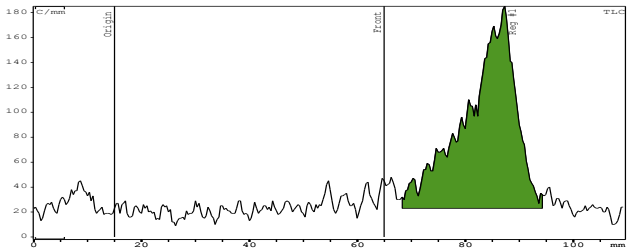

B: ^{68}Ga+J591c(scFv). control to show specifity of Ga binding to the chelator (5 min)

Figure-5.8: Two controls to show the specificity of ^{68}Ga-binding to the chelator. iTLC-SG with mobile phase of 0.1 M citrate buffer. A**: shows ^{68}Ga acetate moves with the solvent front with Rf value of 1.** B: **Unconjugated J591c(scFv) does not bind with ^{68}Ga and ^{68}Ga acetate moves with the solvent front with Rf value of 1.**

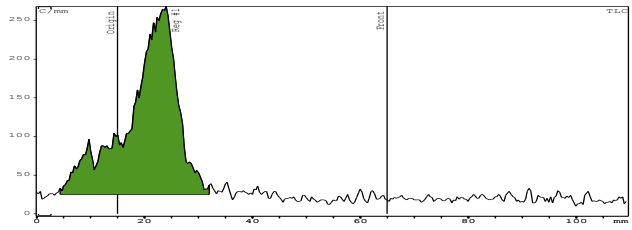

A: 0.2 µg/µl of ^{68}Ga-CP256 (5 min)

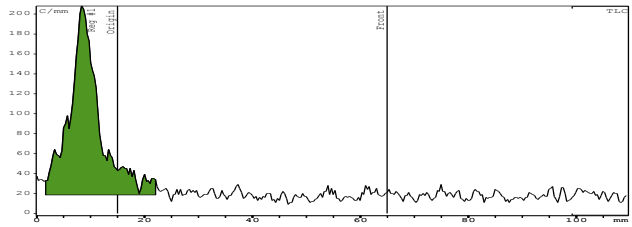

B: 0.2 µg/µl of ^{68}Ga-conjugated J591c(scFv) (5 min)

Figure-5.9: A: **^{68}Ga-CP256 stays at origin with Rf value of 0.** B: **Conjugated J591c(scFv) radiolabelled with ^{68}Ga stays at origin with Rf value of 0.**

5.9.5- Mass spectroscopy

Unconjugated J591c(scFv) gives a peak at 27803, which represents the molecular mass of unconjugated J591c(scFv). However, J591c(scFv) can bind to other thiols, including other J591(scFv) molecules and cysteine in the media, by forming disulfide bonds, as they are grown in the media containing human serum. The disulfide bonds can be reduced by adding TCEP, which make cysteine of J591c(scFv) available for conjugation with the maleimide in YM103 instead of holding other cysteines in the system via disulfide bond and generates the MS peak corresponding to the correct mass of the J591c(scFv) as shown in Fig-5.10A and 5.10C.

Fig-5.10B (top panel) shows the mass spectrum of the chelator YM103 with molecular mass of 920.414. The second panel in Fig-5.10B shows the spectrum of unconjugated J591c(scFv) before reduction with TCEP with increased molecular mass of 27923.20 and the presence of corresponding dimer at 55845.62. The increase in molecular weight corresponds to the formation of a disulfide bond between the cysteine residue of the protein and another cysteine. This indicates that TCEP should be added into this sample to reduce the disulfide bond and make sure that cysteine in J591c(scFv) is available for conjugation with the YM103 (Fig-5.10C, second panel). A small amount of dimers can

be observed at 55606.50 (molecular weight of dimer). Fig-5.10C, first panel, shows reduced J591(scFv) conjugated to YM103. Again a small amount of dimer is observed at 55607 even with reduced and conjugated protein.

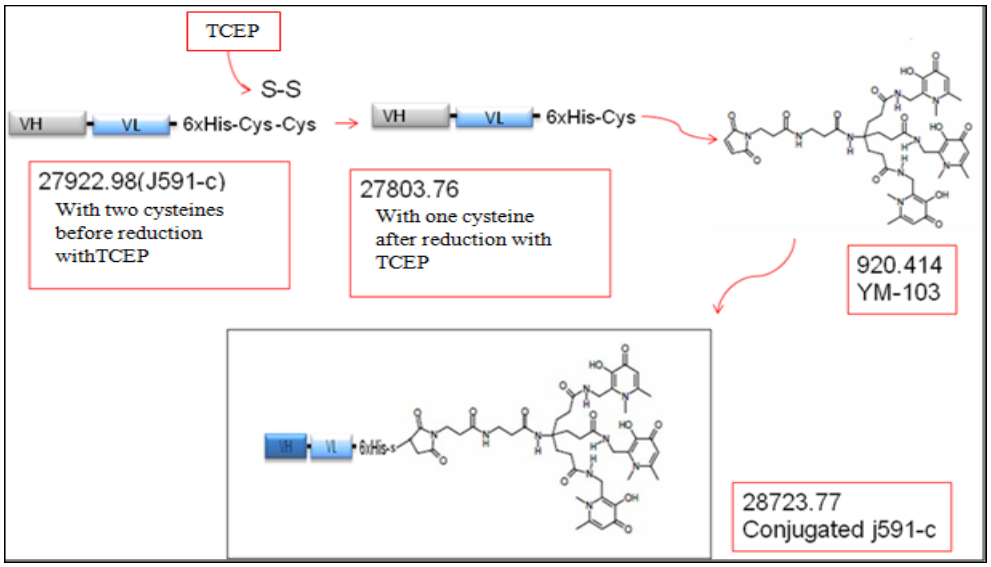

(A)

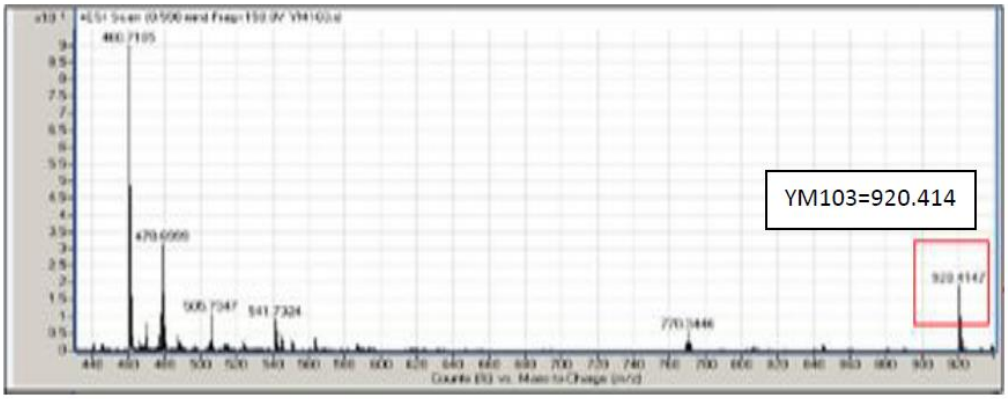

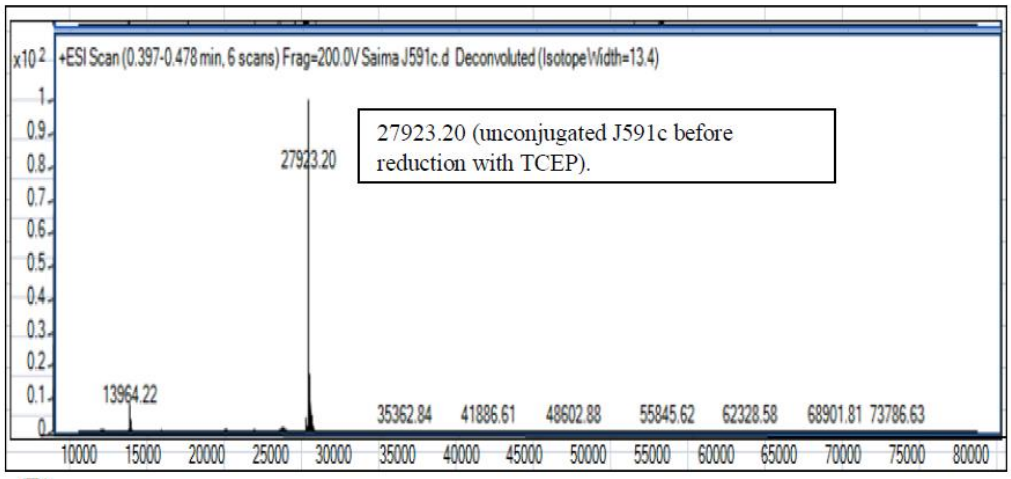

(B)

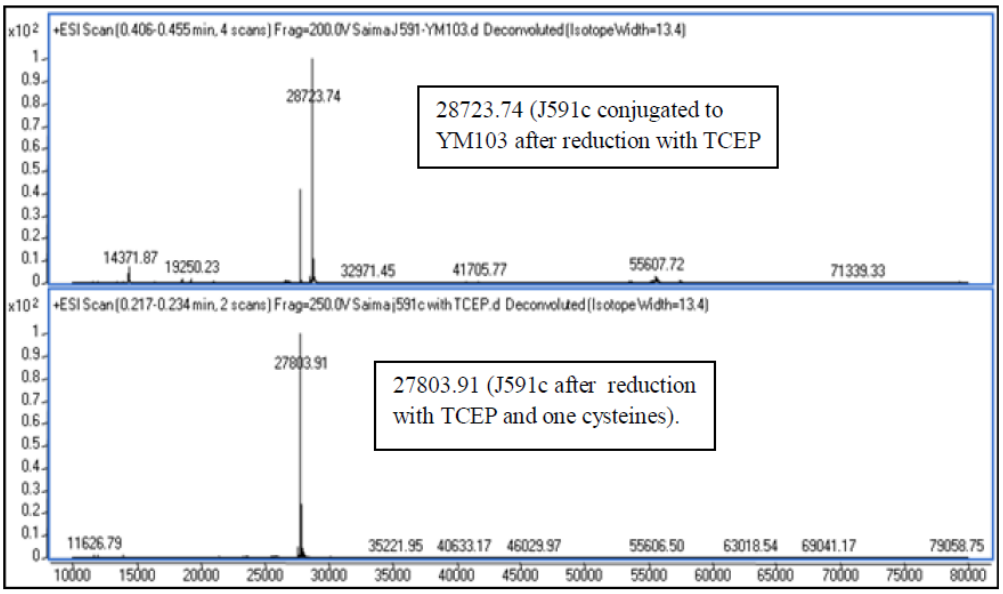

(C)

Figure-5.10: Mass-spectra of conjugated and unconjugated J591c(scFv). A: **Diagrammatic representation of the J591c(scFv) with two cysteines and conjugation with YM103 (bifunctional chelator).** B: **Mass-spectrum of YM103, unconjugated J591c(scFv) before reduction with TCEP.** C: **J591c(scFv) conjugated to J591c after reduction with TCEP and unconjugated J591c(scFv) after reduction with TCEP .**

The above experiments indicated that J591c(scFv) was vulnerable to form disulfides with other thiols and could also form dimers with itself, which would lead to blocking of the conjugation with the maleimide of YM-103. However, this could be removed by using reducing agent TCEP, which reduced these disulfide bonds ensure that the cysteine in J591c(scFv) was available to bind covalently with one YM-103 molecule.

5.9.6- Serum stability

Gel electrophoresis (Fig-5.11) showed that J591c(scFv)-YM103 when radiolabelled with ^{68}Ga and incubated in human serum protein was quite stable even after 6 h. There was no dissociation between ^{68}Ga and J591c(scFv)-YM103 or transfer of ^{68}Ga to human serum protein. Lane 1 is a MW marker. Lane 2 showed radiolabelled human serum protein, with a strong band at 60 KDa. Lane 3 indicates radiolabelled conjugated J591c(scFv) with a strong band at 30 KDa. Lanes 4-10 are samples taken from the serum incubation at different time points. It is observed that there is strong band at 30 KDa, which matches with the lane 3 of the gel, and there is nothing at the 60 KDa, which indicates that there is no association between the ^{68}Ga and human serum proteins.

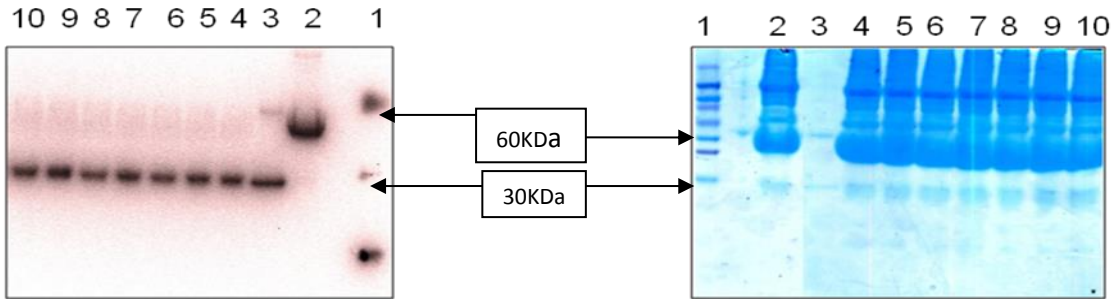

(A) **(B)**

Figure-5.11: SDS-PAGE for serum stability of ^{68}Ga-J591c(scFv)-YM103. A: Radioactive gel analysed with Cyclone phosphorimager. B: SDS-PAGE gel is stained with Coomassie blue. 1: Marker. 2: Human serum radiolabelled with ^{68}Ga. 3: Conjugated radiolabelled J591c(scFv). 4-10: Radiolabelled conjugated J591c(scFv) incubated in human serum protein at different time-points, 30 min, 60 min, 120 min, 180 min, 240 min and 360 min respectively.

5.9.7- FACS analysis

FACS analysis was performed before the cell binding and *in vivo* experiment to check the PSMA expression on cell lines. For this purpose monoclonal anti-PSMA antibody conjugated to Phycoerythrin (Abcam) (PE, FL2) was used. Phycoerythrin is a member of a family of proteins called phycobiliproteins, which are derived from cyanobacteria and eukaryotic algae and exhibit extremely bright fluorescence. In flow cytometers separate fluorescence (FL-) channels are used to detect light emitted. In this case it is FL2 (560-590 nm). Both Du145 and Du145(PSMA) cell lines were incubated with monoclonal antibody in two different concentrations. It was observed that the Du145 cell line (PSMA negative) did not show any positive shift in FL2 in contrast to the Du145(PSMA) cell line (PSMA positive). Figure 5.12 shows the comparison of the geometric mean of the shifts of PSMA positive and negative cell lines at two different concentrations of monoclonal anti-PSMA antibody. Figure 5.12 clearly shows that anti-PSMA monoclonal antibody conjugated to Phycoerythrin bound with the cell surface recptors on the PSMA positive cell lines (Du145-PSMA) and it was detected in the flow cytometry by positive shift in FL2 in contrast to the PSMA negative cell line (Du145), which did not show any binding with the same antibody. Enhancement in the binding was also observed in PSMA positive cell lines by increasing the amount of anti-PSMA monoclonal antibody conjugated to Phycoerythrin from 100 ng to 500 ng,

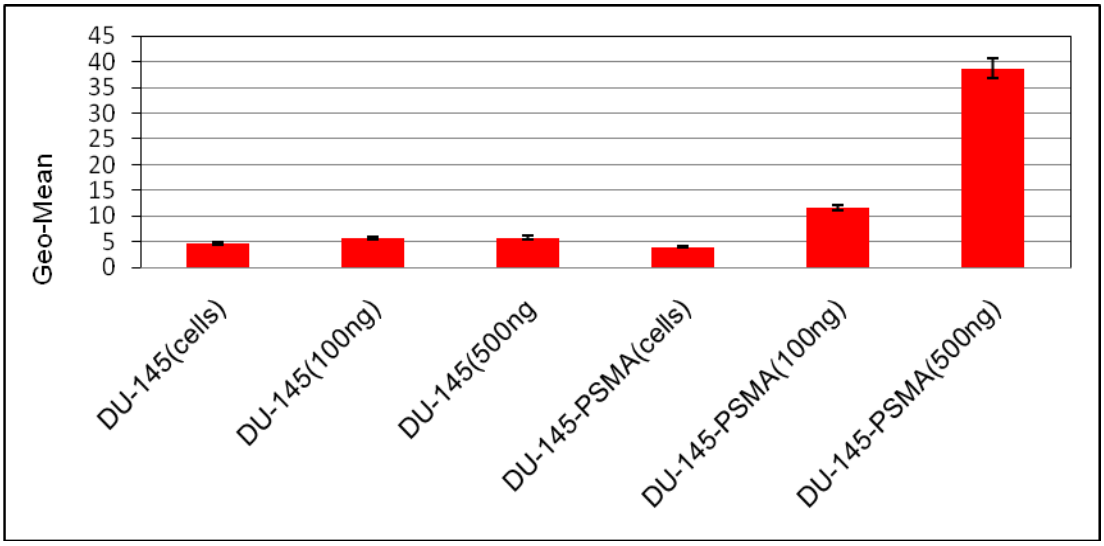

Figure-5.12: Comparative study of PSMA positive and negative cell lines, when they were incubated with anti-PSMA monoclonal antibody. These results show the specificity of the PSMA positive cell lines for anti-PSMA antibody. The higher the value of monoclonal antibody the greater is the shift shown by PSMA positive cell lines in FL2 (PE). Each value is mean ± SD for three measurements.

5.9.8-Cell binding

Serial dilutions of different concentrations of cold antibody were mixed with a constant amount of ^{68}Ga-J591c(scFv)-YM103 (2 nmol). Cells were incubated with this mixture of radiolabelled and cold antibody at 4^{o}C for 45 min. It was incubated at 4^{o}C to minimise internalisation of scFv. The result demonstrated the competition between cold and radiolabelled antibody (Fig-5.13). Non-specific binding was measured using the Du145 (PSMA negative) cell line and total binding was measured using the Du145-PSMA (PSMA positive) cell line. As there was competition between the cold and radiolabelled antibody, the total binding of radiolabelled antibody increased as the amount cold antibody decreased in the mixture. Kd (31.52 nM) value was calculated using Prism software for the PSMA positive cell line using non-linear regression fit (one-site total). This result indicated that radiolabelled J591c(scFv)-YM103 showed specific binding and high affinty to the PSMA positive cell line (Du145-PSMA) but not to the PSMA negative cell line (Du145). Furthermore, the conjugation reaction between the YM103 and J591c(scFv) and radiolabelling between the ^{68}Ga and J591c(scFv)-YM103 did not interfere with the binding ability with the PSMA positive cell lines (Du145-PSMA).

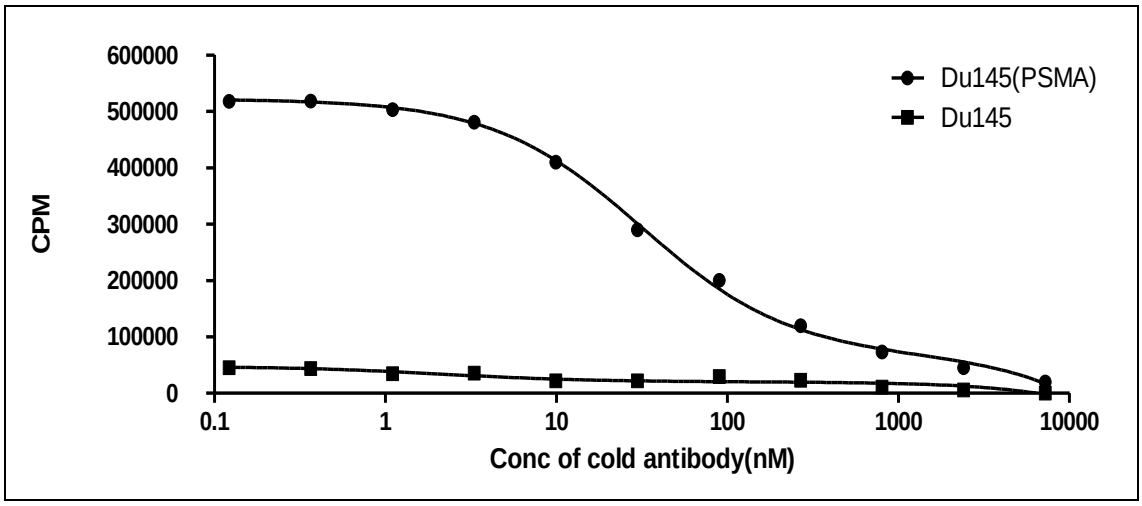

Figure-5.13: Graph shows the competitive binding of conjugated J591c with PSMA positive cell line. Du-145 (PSMA negative) shows non-specific cell binding.

5.9.9- *In vivo* experiments

For *in vivo* experiments mice were injected with 7 MBq and 10 µg of ^{68}Ga-J591c(scFv)-YM103 in a volume of 90 µl. For the imaging of ^{68}Ga acetate and ^{68}Ga CP256, 7 MBq was injected intravenously in normal mice. For ^{68}Ga CP256, the amount of CP256 injected was 4 µg. Imaging (dynamic scans) was done over the time period of 4 h with PET/CT scanner. At the end of 4 h mice were culled and organs were weighed and measured in a gamma counter in pre-weighed scintillation tubes along with standards. The imaging data of ^{68}Ga acetate after 4 h (Fig-5.14A) showed the accumulation of radioactivity in all the soft tissues, bone, bladder and lungs. A large amount of activity also accumulated in urinary bladder. Biodistribution data corresponded with the imaging data with the highest amount of activity located in bladder followed by trachea, thyroid and bones (Fig-5.15).

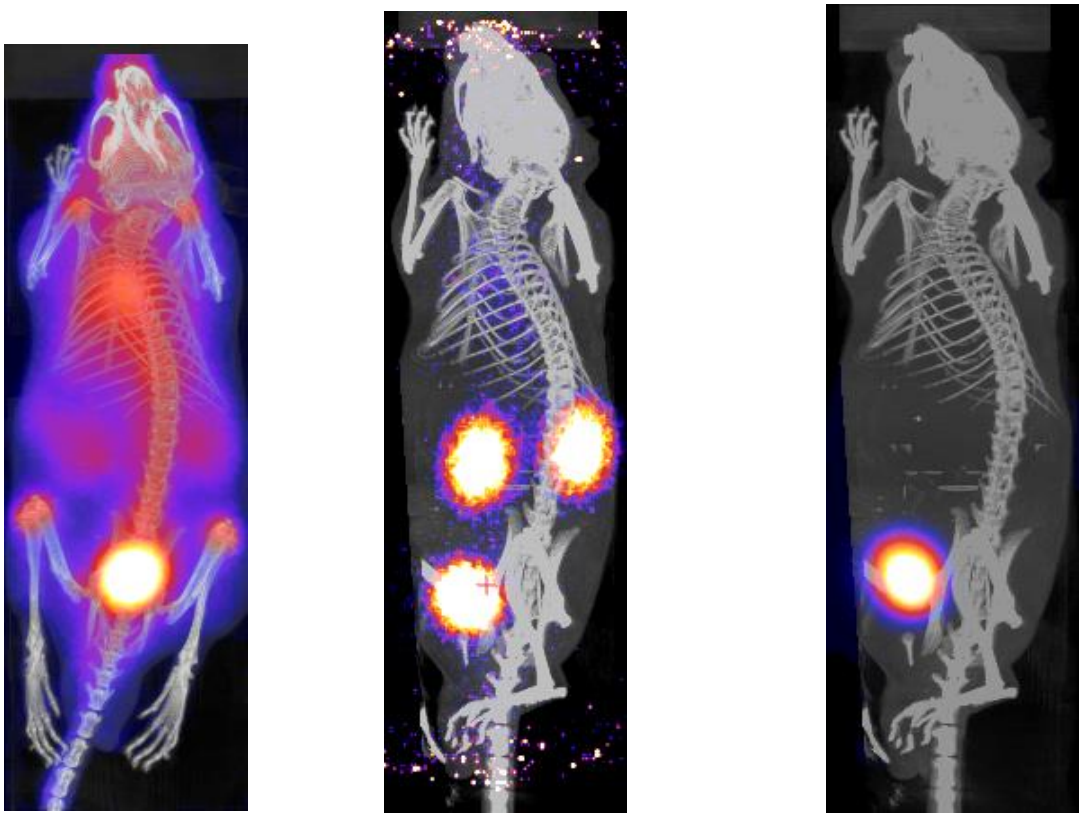

A: ^{68}Ga acetate B: ^{68}Ga CP256 (60sec) C: ^{68}Ga CP256 (4 hr)

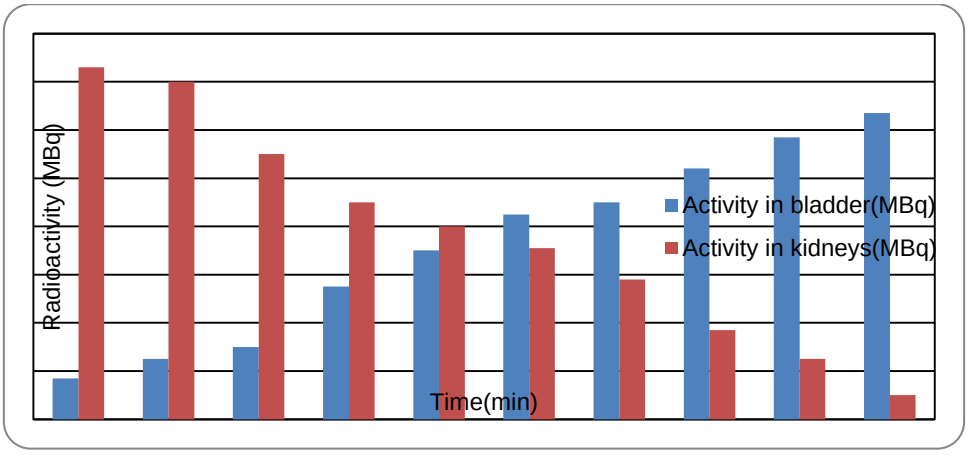

D: Changes in radioactivity in kidneys and bladder over the time-period of 10 min in mouse injected with ^{68}Ga-CP256.

Figure-5.14: PET/CT Imaging data for ^{68}Ga acetate and ^{68}Ga CP256. A: **^{68}Ga-acetate, most of the activity is dispersed in the soft tissues, trachea, thyroid and bones.** B**: Reconstruction of ^{68}Ga-CP256 images at 60 sec showing activity in the kidneys and bladder, which represents fast clearance from the system. C: ^{68}Ga CP256 after 4 h post injection, all the activity is in bladder. D: Time course of activity in bladder and kidneys with ^{68}Ga CP256.**

In the case of ^{68}Ga-CP256 (Fig-5.14B, 5.14C), it was observed that all the activity rapidly cleared from the system and accumulated in the urinary bladder. Although images showed activity only in the bladder and biodistribution data corresponded with the imaging data with the highest amount of activity in the bladder (Fig- 5.16), at the 4 h time of sacrifice this activity was only 3% of the injected dose due to excretion of urine over the intervening period. The time course of activity in bladder and kidneys was plotted for the first 10 min in the case of ^{68}Ga-CP256 and it was observed that ^{68}Ga-CP256 accumulated in the kidneys in the first 60 s (Fig-5.14B, D).

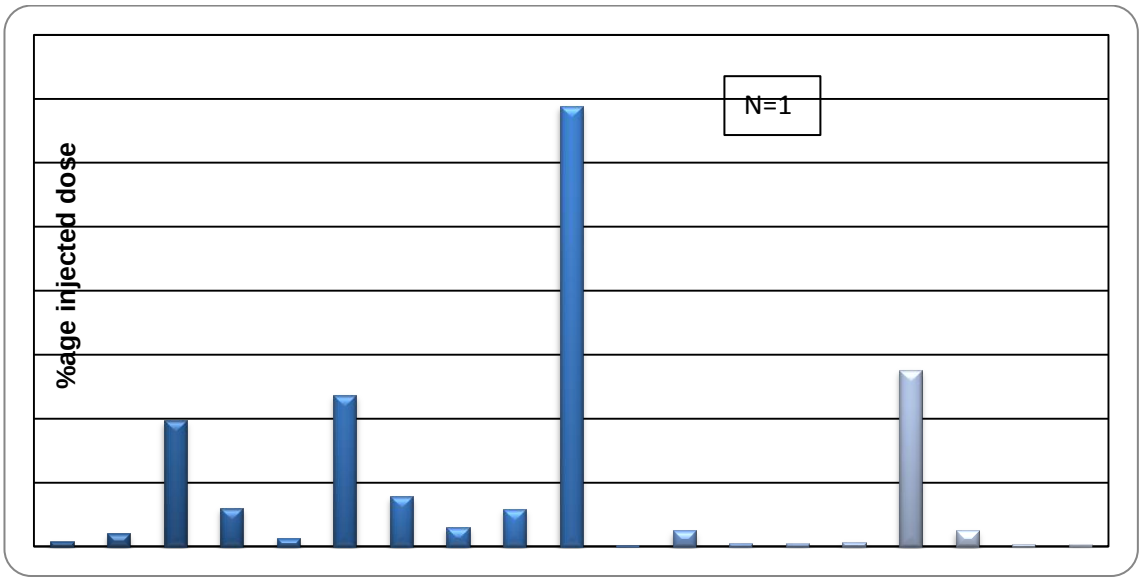

(A)

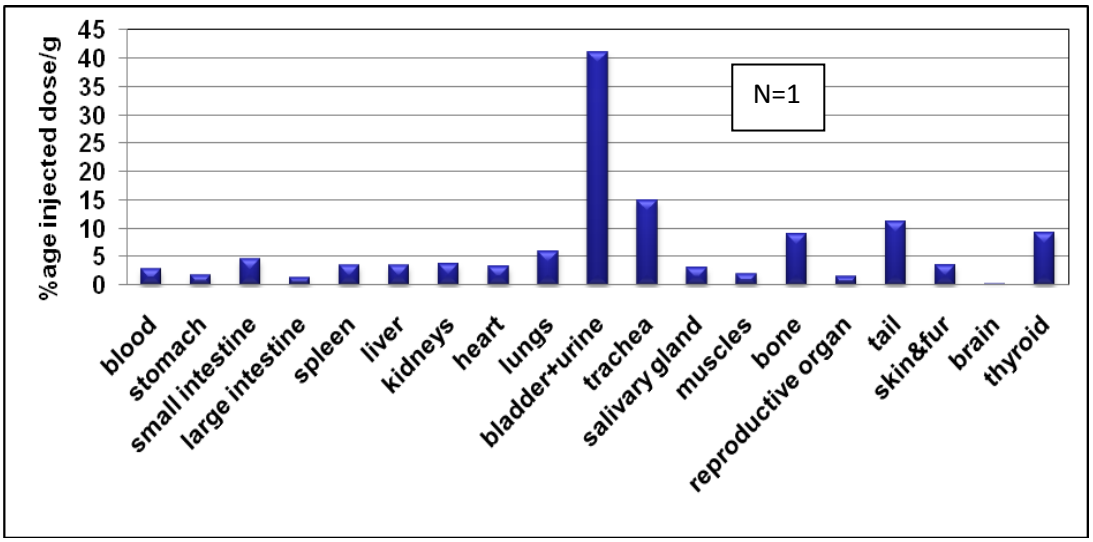

(B)

Figure- 5.15: Biodistribution data for ^{68}Ga-acetate after 4 h. Most of activity is in bladder followed by trachea, thyroid, bone and soft tissue. A:% injected dose. B:% injected dose/g.

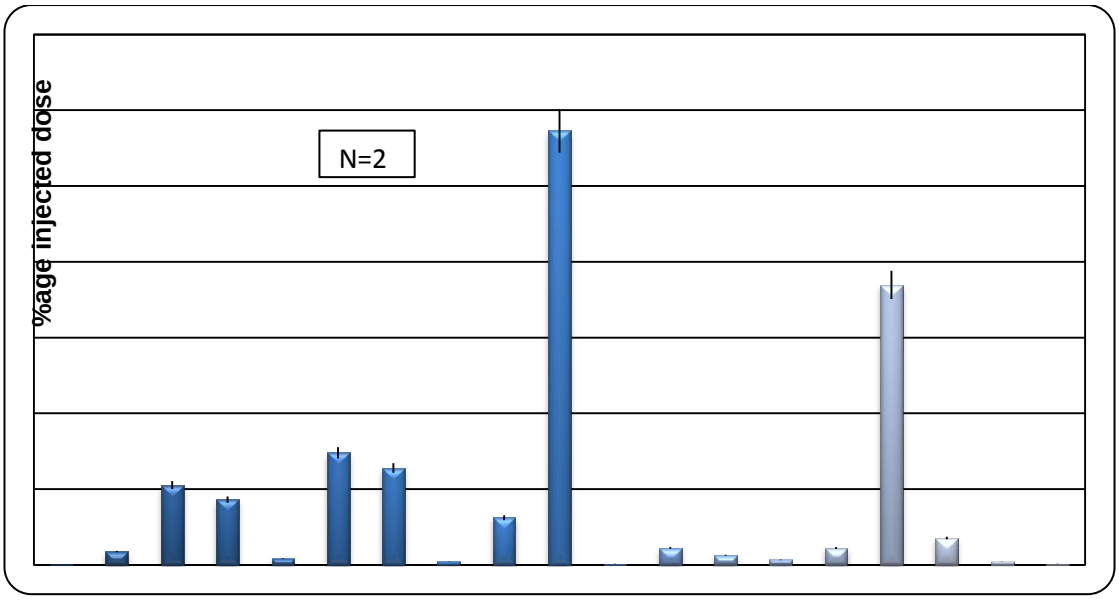

(A)

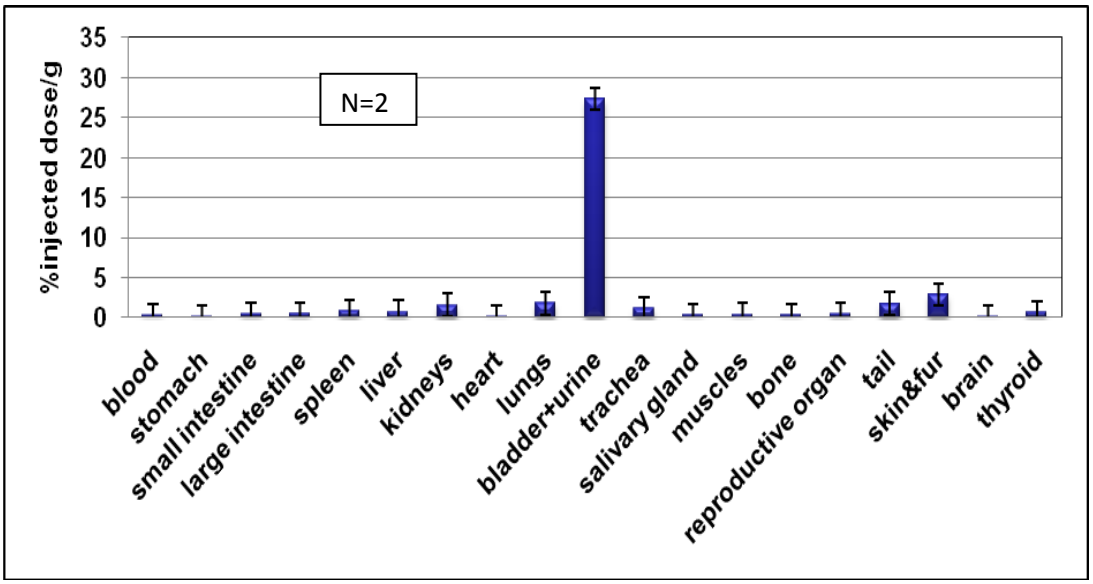

(B)

Figure- 5.16: Biodistribution data of ^{68}Ga-CP256 after 4 h. All the activity is accumulated in the bladder after 4 h. A: %age injected dose. B: %age injected dose/g.

In Du145 (PSMA negative), imaging was carried out with one mouse over the time period of 4 h (Fig-5.17, 5.18, 5.19) and on the basis of that imaging data it was observed that maximum uptake in tumour occurred at 60-90 min. Thus, for biodistribution studies

four mice were injected with 7 MBq of activity on 10 µg of protein and culled at 90 min post-injection.

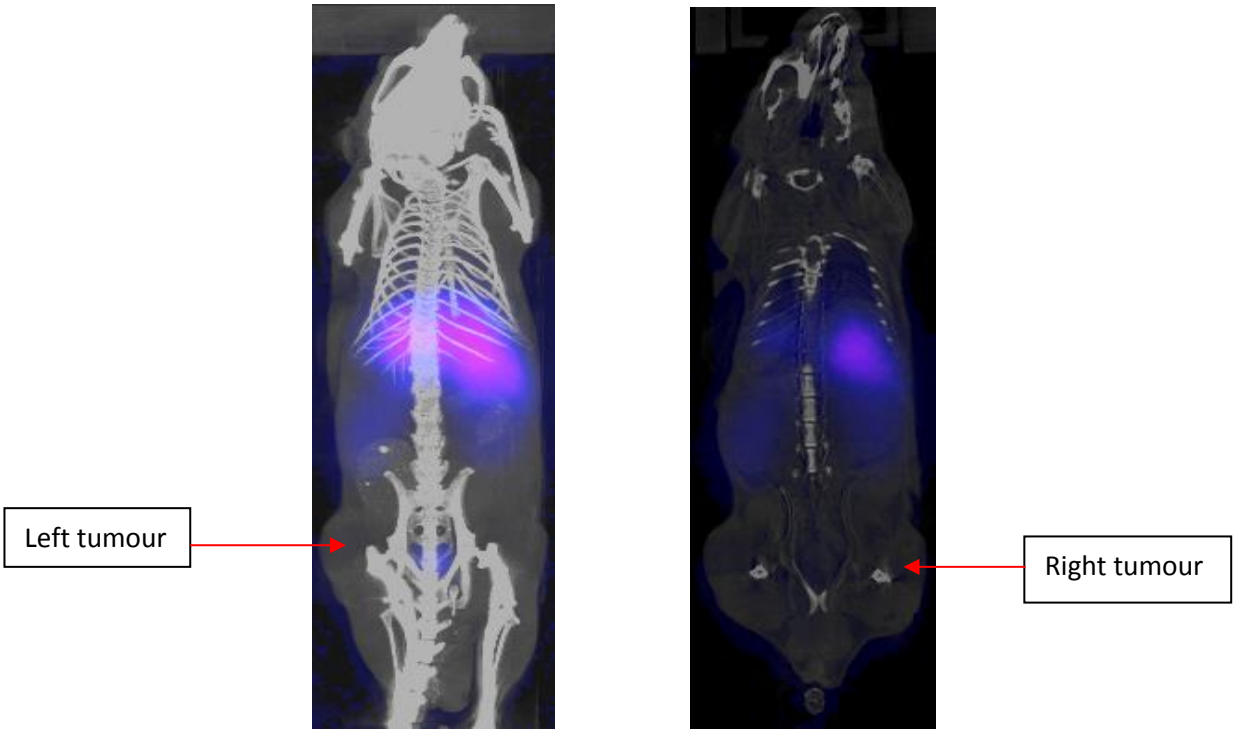

A: MIP view B: Coronal view.

Figure-5. 17: PET/CT image of the mouse containing tumours on right and left flank produced from Du145 (PSMA negative) cells at 90 min. There was no accumulation in the tumours as compared to the PSMA positive tumour. Conjugated J591c is cleared through the kidneys.

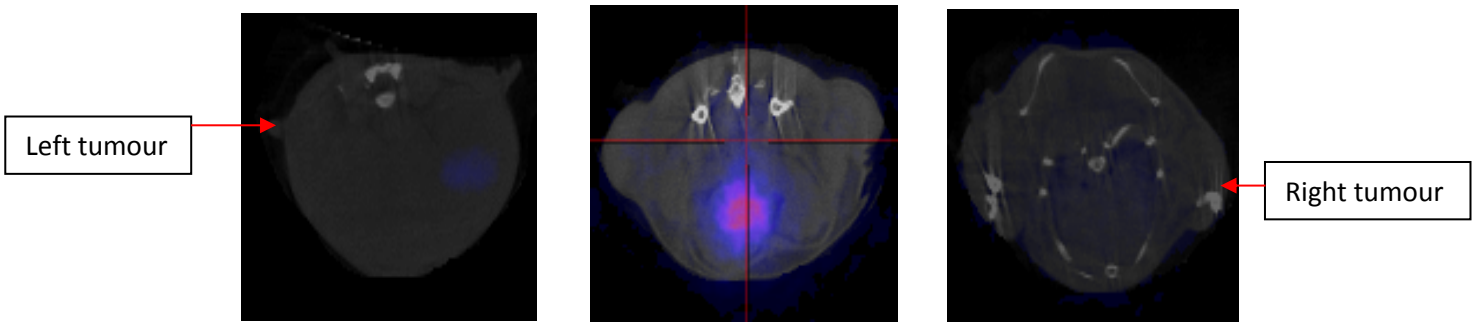

(A) (B) (C)

Figure-5.18: Transverse view of PSMA negative tumour. ^{68}Ga-J591c-YM103 was injected followed by scanning for 3.5 h. No accumulation of activity at different time points was observed in both right and left tumour. A: **0-30 min,** B: **60-90 min,** C: **180-210 min.**

Uptake in the PSMA negative tumour increased with time and then decreased, although it is quite negligible as compared to the PSMA positive tumour (Fig-5.17, 5.18, 5.19, 5.20). Biodistribution data showed that activity cleared through kidneys (Fig-5.19). Tumour/muscle ratio was 2.74 and tumour/blood ratio was 0.34 (Fig-5.25).

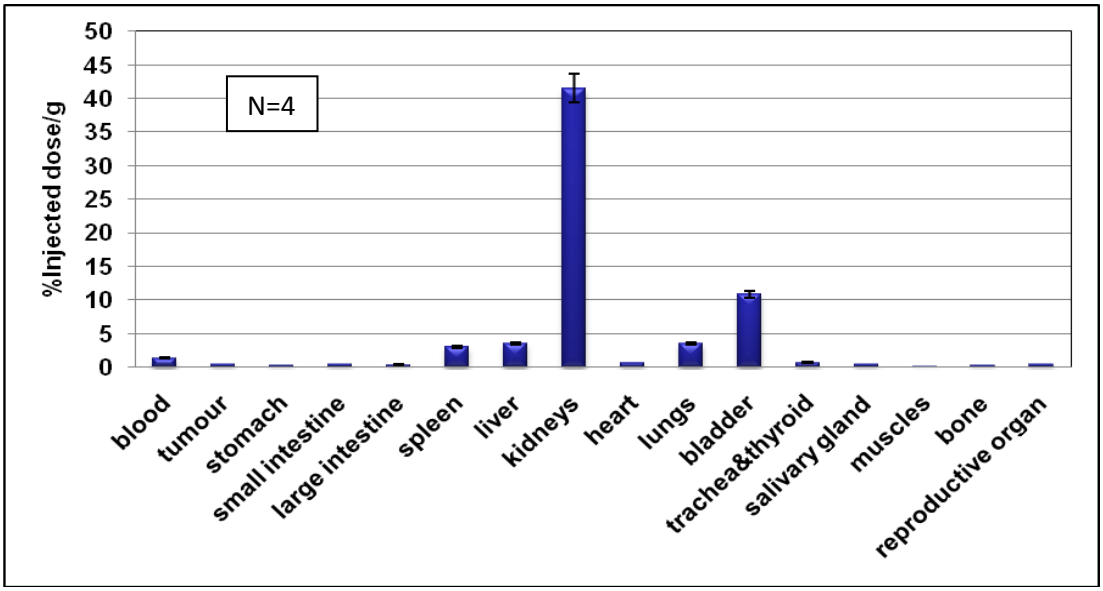

Figure-5.19: Graph shows the biodistribution data based on four mice bearing PSMA negative tumours on left and right flanks, they were injected with ^{68}Ga-J591c-YM103 and then culled at 90 min. Highest concentration of activity was in kidneys, as ScFv clears through kidneys. Uptake in PSMA negative tumours was very low.

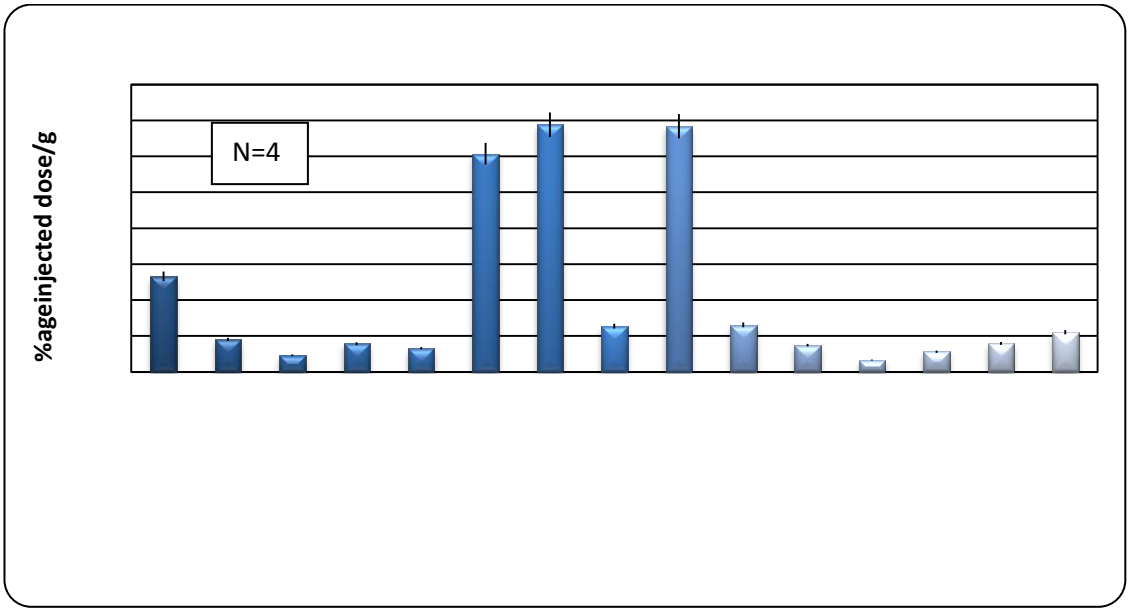

Figure- 5.20: Four mice with PSMA negative tumour was injected with ^{68}Ga-J591c-YM103 and culled at 90 min. Uptake in the bladder and kidneys were removed from the above graph to show the uptake in rest of the organs and tumour. It was clear from the above graph that there was not much uptake in the negative tumour, besides liver and lung also showed uptake. This finding also corresponds with the imaging data (Fig-5.17 and 5.18).

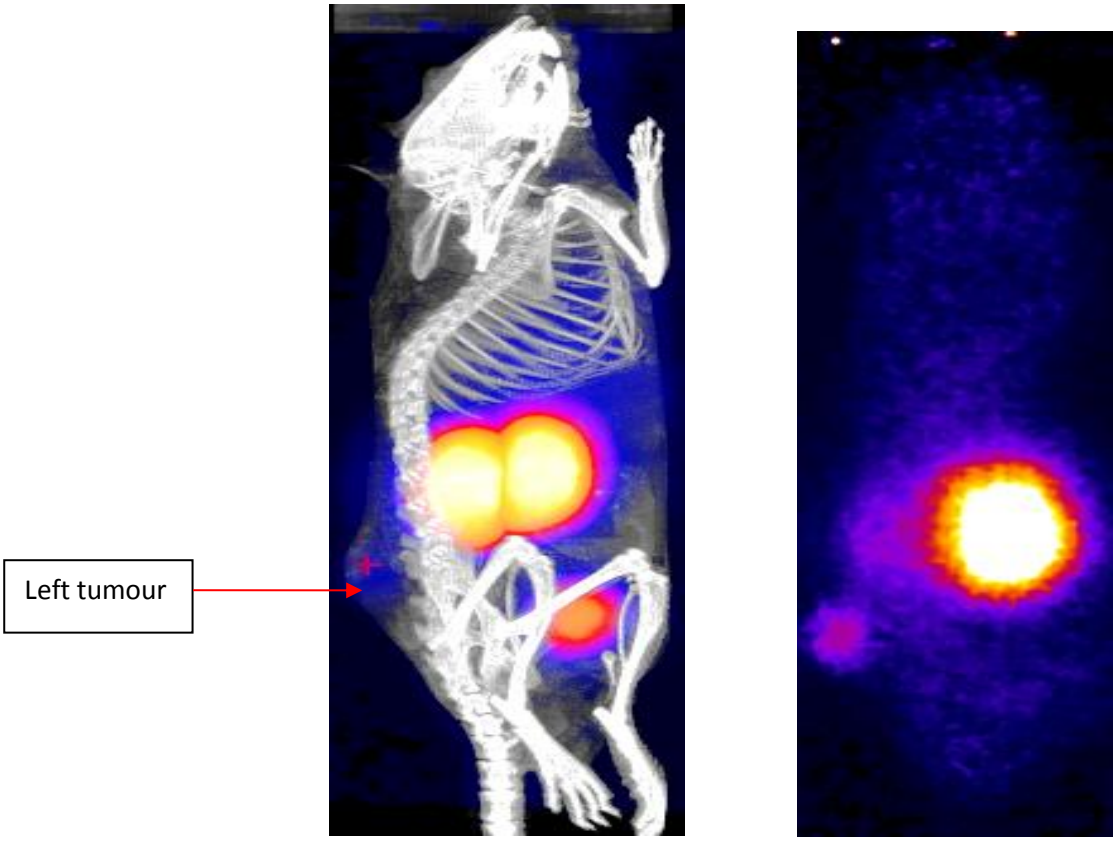

(A) MIP view (B) without CT Coronal view

Figure-5.21: Mouse with PSMA positive tumour (left flank) injected with ^{68}Ga-J591c-YM103 and scanned for 4 h. MIP view (A) shows uptake in kidneys and bladder and tumour at 90 min. Coronal view (B) without CT showed uptake in left PSMA positive tumour after 90 min.

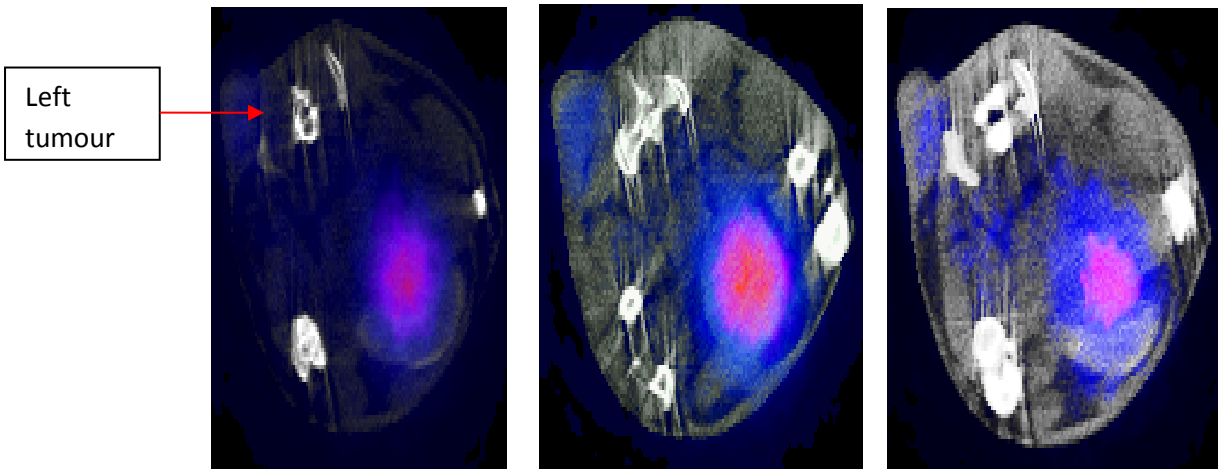

(A) (B) (C)

Figure-5.22: Tranverse view of mouse with PSMA positive tumour (left flank) injected with ^{68}Ga-J591c-YM103 and scanned for 4 h. Transverse view of PSMA positive tumour. Shows accumulation of activity in PSMA positive tumour at different time points. A: **0-30 min,** B: **60-90 min,** C: **180-210 min.**

In contrast to the results with the PSMA negative tumour, accumulation of ^{68}Ga-J591c(scFv)-YM103 in the PSMA positive Du145(PSMA) xenografts was much higher (Fig-5.21, 5.22). The complex showed rapid clearance from all organs except kidneys. It is quite clear from the imaging and biodistribution data that uptake in the PSMA positive tumour was higher than the PSMA negative tumour and it showed selective localisation in the PSMA expressing prostate tumour xenograft with high tumour/blood (5.00) and tumour/muscle (9.25) ratios (Fig-5.23, 5.24, 5.25, 5.26). In contrast, for the PSMA negative tumour these values were tumour/blood (0.34) and tumour/muscle (2.74). The kinetics of the complex are suitable for the 68-min half life of ^{68}Ga. Uptake gradually increased with time and was maximum at 90 min, after which it started declining as seen in the imaging data (Fig-5.26). The ratio of specific/nonspecific uptake was also quite high at 9.1 (Fig-5.25). Specific-uptake was calculated on the basis of the uptake in PSMA positive tumour and non-specific on the basis of uptake in the PSMA negative tumour.

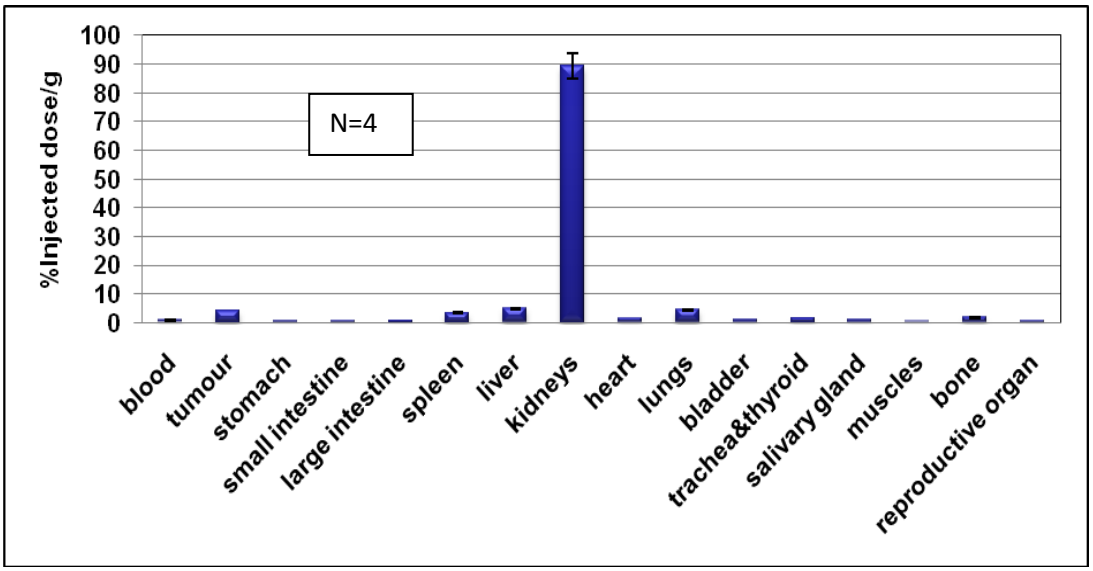

Figure-5.23: Four mice with PSMA positive tumour (left flank) injected with ^{68}Ga-J591c-YM103 and then culled at 90 min for biodistribution studies. Most of the activity was in kidneys, as ScFv clears through kidneys. It showed uptake in PSMA positive tumours.

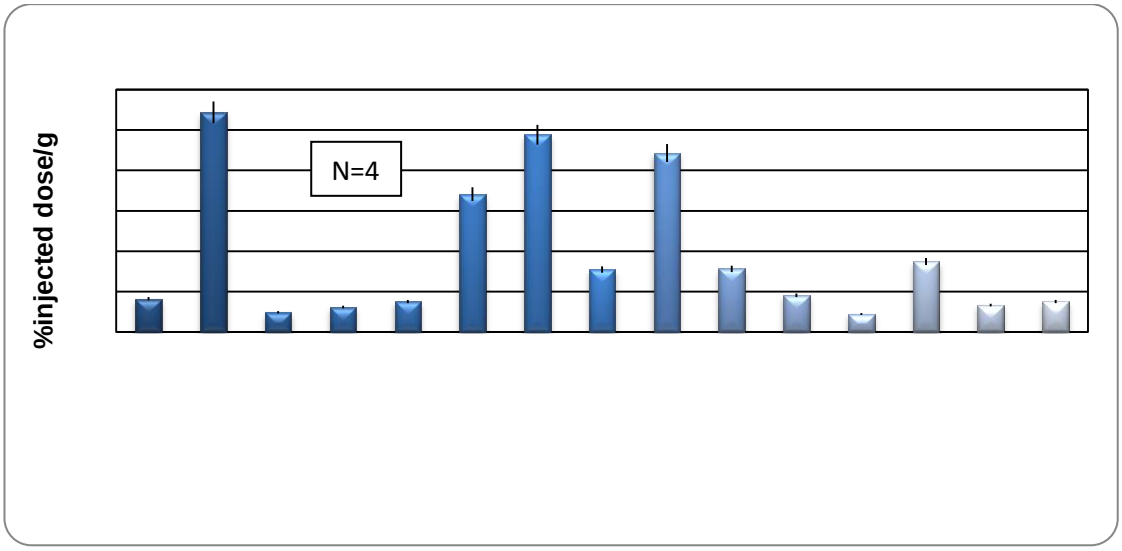

Figure- 5.24: Four mice with PSMA positive tumour injected with ^{68}Ga-J591c-YM103 and culled at 90 min. Uptake in the bladder and kidneys were removed from the above graph to show the uptake in rest of the organs and tumour. It was clear from the above graph that after kidneys PSMA positive tumour show highest uptake in mice, besides liver and lung also showed uptake.

In Fig-5.20 and 5.24, data for kidneys and bladder were removed from the biodistribution data of PSMA positive and negative mice. It is observed that in PSMA negative biodistribution data, after the kidneys the lungs, liver and spleen showed highest uptake and there was not much uptake in the negative tumour. On the other hand, the PSMA positive tumour showed highest uptake after kidneys, followed by liver, lungs and spleen. The high uptake in the kidneys is normal and was expected as scFv antibodies typically clear through the kidneys with a high level of kidney retention.

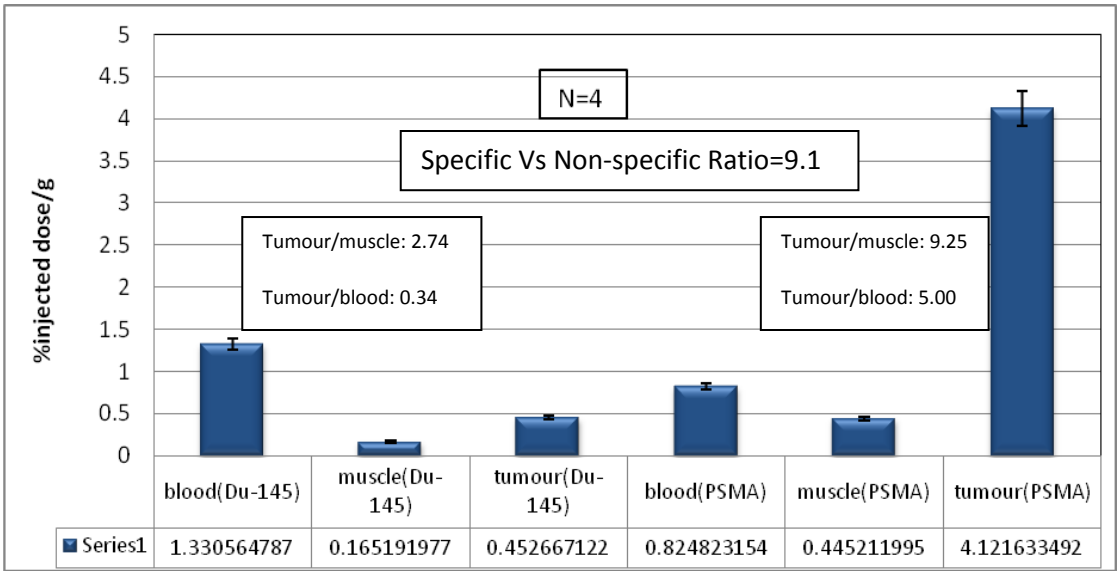

Figure-5.25: This graph shows specific vs non-specific uptake in PSMA positive and PSMA negative tumours. This data are based on 4 mice in each group and the ratio of specific to non-specific is 9.1. It also depicts the tumour/blood and tumour/muscle ratio of both PSMA positive and negative tumours.

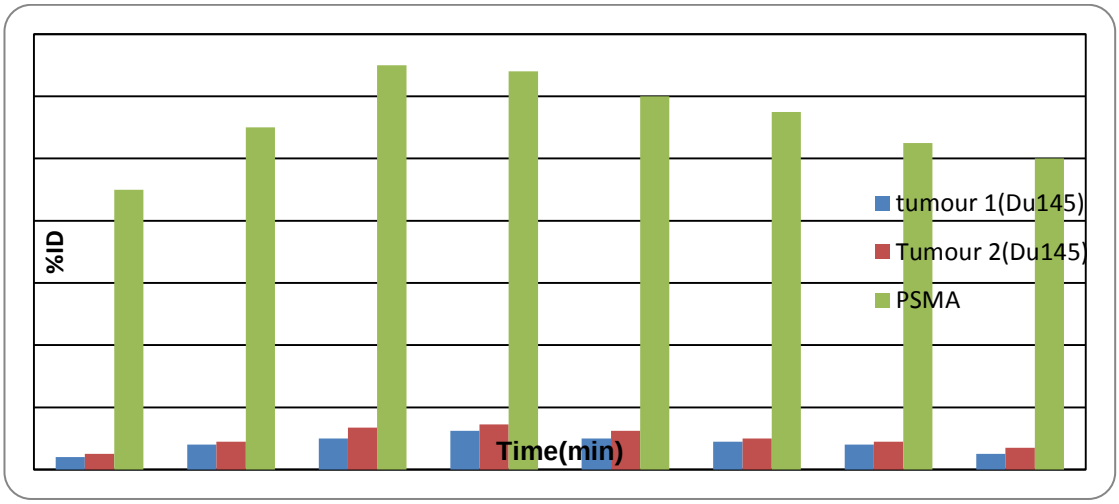

Figure -5.26: Comparison of uptake in PSMA positive and negative tumour based on imaging data (one mouse each for PSMA positive and negative tumour) over the period of 4 h. The PSMA positive tumour showed higher uptake as opposed to the PSMA negative tumour. Mice were injected with ^{68}Ga-J591c-YM103 and scanned for 4 h. Both PSMA positive and negative tumours showed uptake which then gradually started clearing from the tumour after 90 min.

The imaging and biodistribution data indicates that there was specific uptake in the PSMA positive tumour but not in the PSMA negative tumour.

5.10-Discussion

For J591c(scFv) radiolabelling was done with ^{68}Ga. Cysteine was introduced along with a His-Tag and used to conjugate the protein with an in-house produced bifunctional ^{68}Ga chelator (YM103) containing a maleimide group. J591c(scFv) can form dimers which are both covalent and non-covalent in nature. Covalent dimers can be reduced by incubating with a reducing agent such as TCEP (Fig-5.1). Different concentrations of TCEP were evaluated to reduce the dimers. Out of those concentrations 15-fold reduced the dimers considerably but we have adopted 30-fold molar concentration to completely remove the dimers. However, non-covalent dimers were not affected by the reducing agent; to some extent their formation depended upon the handling of the protein and temperature. If the protein was frozen down to -80^{o}C immediately after purification then it was observed from our experience that there will be less chance of the formation of dimers or aggregation in the protein sample.

As was observed in the mass-spec of the J591c(scFv), the mass of conjugated protein was 28723.74. The unconjugated protein with an extra cysteine linked by a disulfide bond gave the molecular weight of 27923.20 and if reducing agent was added to the same sample then it gave the exact molecular weight of the protein with no disulfide bond (27803.91) (Fig-5.10). There was also no evidence for trace metal binding to the conjugate (e.g. scavenging iron). In the case of J591c(scFv) small amount of dimers were also observed around 55606.

The radioisotope used here was ^{68}Ga which is a generator produced radionuclide. The generator is eluted with 0.1 M HCl followed by pre-concentration of the eluate [102]. This new method of concentrating the generator eluate involved a combination of cationic trapping and intermediate transformation of the absorbed $^{68}Ga^{+3}$ into $[^{68}GaCl_4]^-$ by elution with 5 M NaCl solution followed by retransformation to $^{68}Ga^{+3}$ by adding acetate buffer [102]. Another important finding was that ^{68}Ge breakthrough from the generator did not absorb on the SCX cartridge which trapped ^{68}Ga. Therefore, ^{68}Ge was found in the SCX wash through waste, and even if a small amount of ^{68}Ge was retained on the column it was not eluted with NaCl/HCl solution [102].

As in the case of radiolabelling of J591(scFv) with ^{99m}Tc tricarbonyl, different concentrations of the conjugated protein were radiolabelled with the same amount of ^{68}Ga and a similar result was observed. At higher concentrations of protein, time was not an important factor and 100% radiolabelling yield was obtained within a few minutes. However, at a lower concentration of 0.125 µg/µl time was a vital factor in increasing the radiolabelling yield. As we increased the time from 5 min to 20 min, radiolabelling yield increased from 70% to 80% (Fig-5.7). For serum stability SDS-PAGE was used to analyse the results (Fig-5.11). The results showed that radiolabelled conjugated protein was quite stable even in human serum protein. It was also observed that no radioactivity was released as small molecules or complexes, nor was it transferred to other proteins in human serum.

Cell binding assays were performed using both PSMA positive (Du145-PSMA) and negative cell lines (Du145) at 4^{o}C. The main reason for keeping the samples at low temperature was less internalisation of the protein at low temperature. In this experiment a sigmoid curve was obtained and it was possible to calculate the Kd (31.2 nM) value using PRISM software (Fig-5.13). This result indicated the specific binding of radiolabelled complex with the PSMA positive cell lines (Du145-PSMA) as opposite to the PSMA negative cell lines (Du145), which did not show any such binding.

5.10.1-*In vivo* work

For *in vivo* experiments two groups of 4 mice were used, one with PSMA positive and other with negative tumours. The animals were injected with the positive cells on left flank and both flanks in the case of PSMA-negative cells. The tumours were allowed to grow over the time period of 4 weeks. During this time animals were kept under supervision and their tumour growth was regularly monitored using vernier calliper and visual inspection until they were 5 mm in diameter. The pharmacokinetics of radiopharmaceutical uptake by tumours is particularly dependent on vascularity and tumour size. It is generally observed that smaller tumours show proportionately greater uptake of radiolabelled protein than larger ones, possibly due to their greater proportion of proliferating cells and better vascularisation. With an increase in tumour size, regions of necrosis become common, and poor vascularisation has been seen within them [129]. Along with imaging and biodistribution of radiolabelled conjugated protein in mice with PSMA positive and negative tumour, imaging and biodistribution of ^{68}Ga-acetate was

also done in one mouse without tumour and ^{68}Ga-CP256 with two mice without tumour. These served as controls for the free label and untargeted chelator respectively. In the case of animals with tumours, imaging was done on one animal and for biodistribution 4 animals were used.

In the case of ^{68}Ga-acetate, the activity was distributed in the whole animal (Fig-5.14A), showing uptake in the soft tissues, bones and a large amount was visible in the bladder, with biodistribution data corresponding to the imaging data and it is typical for gallium (Fig-5.15). In the case of imaging data for ^{68}Ga-CP256, we were expecting some accumulation in the brain, as the CP256 complex is uncharged and quite hydrophobic so we were assuming that it would cross the blood brain barrier. Instead of this, it washed out very quickly from the animal system and within 60 s we could see activity in the kidneys and bladder (Fig-5.14C). After 4 h all the activity was in the bladder (Fig-5.14B) and biodistribution data corresponded with the imaging data (Fig-5.16). This behaviour was highly unexpected. In the future it could be evaluated as an imaging agent for kidney function.

In the case of the animals with PSMA positive (Fig-5.21, 5.22) and negative tumours (Fig-5.17, 5.18) imaging was done over the time period of 4 h and images were reconstructed for every 30 min. It is observed that the PSMA positive tumour showed higher uptake than the PSMA negative tumour and the imaging data was further supported by the biodistribution data (Fig-5.25, 5.26, 5.23, 5.24). It was also observed that accumulation of activity in the tumours increased with time, reaching a maximum around 90 min and then started decreasing (Fig-5.19, 5.20). The ratio of specific to non-specific binding was 9.1 (Fig-5.25), which reflected specific binding to the PSMA positive tumour as opposed to the PSMA negative tumour.

Labelling of J591c(YM103) with ^{68}Ga was quite simple and straightforward. It did not require any heating because of the novel chelator (YM103), in contrast to DOTA, or any purification step after the labelling. J591c(scFv)-YM103 required a few minutes depending upon the concentration to radiolabel at room temperature (25^{o}C).

5.11-Summary

^{68}GaJ591c(scFv)-YM103 is a new radiopharmaceutical for imaging prostate cancer. J591c(scFv) can easily be prepared in the supernatant of mammalian cell culture,

yielding almost 6 mg/L. The radiolabelling procedure is quite simple and straight-forward and it is carried out at room temperature (25^{o}C). Almost 100% radiolabelling yield is obtained within a few minutes of incubation. The radiolabelled complex is highly stable in serum even after 6 h of incubation. ^{68}Ga prefers to bind with the conjugated J591c(scFv) instead of serum protein. In *in vivo* studies J591c(scFv)-YM103 radiolabelled with ^{68}Ga showed specific binding to PSMA positive tumours as compared to PSMA negative tumours and biodistribution data also showed that there is clear uptake in the PSMA positive tumour as opposed to the PSMA negative tumour.

Chapter 6: Discussion

6.1-Aims of the project

The main aims of this project were: firstly, to evaluate the full potential of the new ^{68}Ga chelator (CP256) and its bifunctional derivative (YM103) suitable for linkage to a cysteine residue in a protein or peptide; secondly, to produce an anti-PSMA scFv with a modification for site specific incorporation of radiolabel; finally, to evaluate the targeting ability of these ^{99m}Tc and ^{68}Ga labelled bioconjugates in cultured cell lines relevant to prostate cancer, and select the tracers that show promise *in vitro* and evaluate them in animal xenograft models of PCa using PET imaging and biodistribution studies. Based on the *in vivo* data a decision could be made on the potential for these tracers to be evaluated in the clinic.

6.2-Thesis Discussion

Various techniques are employed for the early diagnosis and treatment of PCa. The PET radionuclide mainly employed in this project is ^{68}Ga with a half-life of 68 minutes, matching the kinetics of scFv, which clears quite quickly from the system. ^{68}Ga is a generator produced radioisotope and currently in the market there are various generators available for ^{68}Ga but the one which is used in this project is IGG-100 from Eckert and Ziegler via Imaging Equipment Ltd. However, ^{68}Ga was not the only radioisotope used in this project. ^{99m}Tc, which is a SPECT radioisotope, was also used to radiolabel the J591(scFv) via His-tag without the requirement for a bifunctional chelator. In contrast, ^{68}Ga does require a bifunctional chelator to introduce it into a biomolecule. The chelator used in this project was YM103, which is a bifunctional derivative of a new in-house produced ^{68}Ga chelator CP256. YM103 was first conjugated with J591c(scFv) and then subsequently radiolabelled with ^{68}Ga.

There are various chelators available for ^{68}Ga in market or presented in the literature, such as DOTA, NOTA, HBED and most recently, TRAP [11,96,111,112]. A comparative study of CP256 with the traditional ^{68}Ga chelators showed that CP256 was a unique chelator and its behaviour created advantages over the traditional chelators. DOTA requires heating for 30 min at 100^{o}C, NOTA and HBED showed radiolabelling with ^{68}Ga at room temperature but they require 7 and 10 min respectively and the % radiolabelling yield was also lower than CP256. TRAP, which is a recent ^{68}Ga chelator,

requires low pH. On the other hand CP256 can radiolabel with ^{68}Ga at room temperature (25^{o}C), neutral pH within 5 min or even less depending upon the concentration of the chelator and can give 100% radiolabelling yield. It can also be radiolabelled with the ^{68}Ga in small quantitities. At 1 µM CP256 still showed radiolabelling yield of more than 80% after 5 min where HBED gave radiolabelling yield of 70% after 10 min. NOTA at pH 7 gave ~40% after 7 min. For both DOTA after 30 min and NOTA (pH 4.5) after 7 min there was almost no binding at this concentration (Table 5). The characteristics of CP256 are especially suitable for ^{68}Ga, as this radionuclide has a short half life (68 min) so it requires a chelator with which it can bind rapidly. Radiolabelling at room temperature and neutral pH is especially suitable for a biological compound for which heating at high temperature may lead to denaturation. It was also observed that the ^{68}Ga complexes of CP256, HBED and NOTA were stable in human serum when analysed at two different time-points i.e. 5 min and 60 min (Fig-2.2, 2.3, 2.4, 2.5). In addition to this, CP256 can also be radiolabelled with some other imaging and therapeutic radionuclides such as ^{111}In, ^{99m}Tc, ^{90}Y and ^{89}Zr, although it has not been fully evaluated for these metals and its utility for them is likely to be less than for ^{68}Ga. CP256 showed binding with all these radionuclides and the radiolabelled complex was stable in human serum with ^{111}In and ^{89}Zr. Stability with ^{99m}Tc was not analysed and with ^{90}Y it was not very stable in human serum. The stability of these radionuclides will need to be evaluated over longer time periods as these isotopes have longer half-lives.

However, the unique characteristics of CP256 make it very unusual chelator leading to its evaluation in a novel "pretargeting" mode, because the chelation of ^{68}Ga can occur in serum even when ^{68}Ga has already been bound by serum protein. In the putative pretargeting approach, an antibody derivatised with YM103 (bifunctional version of CP256) would be administered to the patient, allowed to distribute for several days, then a simple ^{68}Ga chelate such as citrate or acetate would be given. In theory the ^{68}Ga would rapidly distribute, find the derivatised antibody in the tumour, and bind to the chelator allowing imaging within the half life of ^{68}Ga. Although pretargeting is well-established (e.g. with the avidin-biotin interaction) it has never been done before using the binding between a metal and its chelator. In one study, it was observed that the half-life for dissociation of an antibody-ligand complex is more than an order of magnitude lower than the half-life times for decay of medically useful radiometal ions [130]. A metal

chelate-based ligand will not be bound to its receptor long enough for all of the bound radiometal to decay. One approach to solve this problem is to add mildly reactive group on the metal chelate adjacent to a complementary reactive group on the antibody when the complex is formed. The partners are chosen to be sufficiently unreactive so that they coexist with other molecules in living systems without undergoing reaction. When the antibody-chelate complex is formed the effective local concentrations of the two groups can be non-physically large, so that a permanent link is formed in the complex even though no reaction occurs when the partners are free in solution [130]. In one review a pretargetting technique was used for the noninvasive measurement of human islet cell mass in pancreas or following islet transplantation [131]. In this pretargeting strategy anti-human islet cell antibody HPi1 was conjugated to a phosphorodiamidate morpholino oligomer (MORF) that binds specifically to a ^{99m}Tc labelled complementary MORF (cMORF). Sensitivity and specificity of pretargeting were first validated in culture using a human beta cell line (betalox5) and a negative control human cell line (HEK293). Pretargeting was then used to target and visualize these two cell lines and human islets transplanted subcutaneously in NOD-*scid* mice. In culture, ^{99m}Tc accumulation on the betalox5 cells pretargeted by MORF-HPi1 was 100-fold higher than on untreated betalox5 cells or following treatment with native HPi1 and much higher than on the MORF-HPi1 pretargeted control HEK293 cells. Small animal imaging readily localized the transplanted betalox5 cells and human islets, but not the HEK293 cells. *Ex vivo* counting demonstrated 3-fold higher ^{99m}Tc accumulation in the transplanted betalox5 cells and human islets than in the control HEK293 cells [131]. The same group further extended the model to predict the effector behavior, in particular, its maximum percent tumour accumulation (MPTA) in mice pretargeted with three different MORF-conjugated antibodies (MN14, B72.3, and CC49). The MN14 and the CC49 target different antigens in the same tumour, whereas the CC49 and the B72.3 target the same antigen but with very different tumour accumulation. By comparing the pretargeting results of these three antibodies, the authors found that MPTA of the radiolabelled cMORF effector in the LS174T tumor was independent of the antibodies. In conclusion, the MPTA cannot be improved through the use of different pretargeting antibodies, although different antibodies may improve the maximum absolute tumour accumulation, the heterogeneity, and/or the tumour-to-normal tissue ratios of the effector [132].

In one of the most recent reviews on pretargetting by Goldenberg et al, they focused on a highly flexible anti-hapten bsMAb platform that has been used to target a variety of radionuclides to image (SPECT and PET) as well as treat tumours [133]. Radiometals are usually coupled to antibodies through an intermediate, a chelating agent. Chelating agents often have differing affinities for various metals, and thus the *in vivo* stability of one radiometal bound to a particular antibody-chelate conjugate might not be the same as another radiometal bound to the same conjugate. Radiometals that are brought into cells by an antibody are retained for long periods, because cells tend to retain metals, but metals held by chelates also are inhibited from being expelled. Thus, radiometal-labelled antibodies will have significantly higher uptake in the liver and kidneys for IgG or smaller fragments, respectively. For optimal targeting, systemically-administered, directly-radiolabelled antibodies might need to use two different forms, e.g., a fragment for imaging and an IgG for therapy. They explained pretargeting as a multi-step process, firstly an unlabeled bispecific antibody (bsMAb) localize within a tumor by virtue of its anti-tumor binding site(s) before administering a small, fast-clearing radiolabelled compound that then attaches to the other portion of the bsMAb. The compound's rapid clearance significantly reduces radiation exposure outside of the tumour and its small size permits speedy delivery to the tumour, creating excellent tumour/nontumour ratios in less than 1 h. Haptens that bind to an anti-hapten antibody, biotin that binds to streptavidin, or an oligonucleotide binding to a complementary oligonucleotide sequence have all been radiolabelled for use by pretargeting [133,138].

We have developed an *in vitro* model to check the binding and stability of the ^{68}Ga with CP256 in human blood serum, with analysis by a PD-10 column (Fig-2.21-E). In the first set of experiments, human serum was exposed to the chelator first and then ^{68}Ga was added (instead of the usual method of radiolabelling the chelator first and then adding it to human serum). It was observed that ^{68}Ga preferred to bind with the chelator even in the presence of the human serum. Even after 60 min and at chelator concentrations as low as 0.02 mg/ml ^{68}Ga preferred to bind with the chelator (Fig-2.22, 2.24). In the second set of experiments, human blood serum was exposed to free ^{68}Ga first (allowing the ^{68}Ga to bind to transferrin) and then the chelator was added and it was observed that not only the low molecular weight ^{68}Ga in the pre-sample bound with the chelator, almost all of the ^{68}Ga which bound with the human serum in the pre-sample (^{68}Ga+human serum) detached from it and preferred to bind with the chelator in

the post-sample (^{68}Ga+human serum+CP256) (Fig-2.25). The same pretargeting model was evaluated with HBED and NOTA, two other chelators which bind ^{68}Ga at room temperature. However, NOTA showed no promise for pretargeting using the same technique. However, the behaviour of the HBED was somewhat more complex. Some of the activity remained bound to serum and some preferred to bind with the HBED in pretargeting techniques and the results shown by HBED are not as clear as in the case of CP256 (Fig-2.29, 2.30).

Based on above mentioned work Prof Phil Blower's group have done some *in vivo* studies in which the macrophage binding antibody SER4 was coupled with YM103. Three groups of 2-3 wild type or sialoadhesin knockout mice were studied. Group 1 was a positive control and were injected with prelabelled $^{67/68}$Ga-YM103-SER4, Group 2 was a negative control injected with unmodified SER4 followed by $^{67/68}$Ga citrate, and Group 3 was a pretargeting group in which mice were injected with YM103-SER4 followed by $^{67/68}$Ga citrate. It was observed that CP256 rapidly and efficiently bound ^{68}Ga in the presence of serum, even if the ^{68}Ga had been incubated with serum and bound to transferrin prior to addition of CP256. Under the same conditions no labelling of NOTA was detectable. In the wild type mice, Group 1 showed targeting of macrophages in the spleen (36% ID/g) whereas Group 2 showed only 4% in the spleen. Group 3, with pretargeting, showed 10% in the spleen. In the sialoadhesin knockout mice there were no differences in splenic activity between groups, indicating the role of macrophage sialoadhesin in targeting. NanoPET/CT images showed spleen and liver activity in Group 3 but only blood pool and joints in Group 2. This would make antibody targeting feasible despite the short half life of ^{68}Ga [134].

The other aspect of this study was PSMA (prostate specific membrane antigen), which is an extensively studied antigen in PCa [29] and has attracted a lot of interest due to its potential for being both a diagnostic and therapeutic target [135]. J591 is a monoclonal antibody which recognises an external epitope of PSMA. In one recent study, results of flow cytometry analysis, competitive binding experimental assays, Western, and immunoblot analysis of the J591(scFv) confirmed its functionality and PSMA specificity [121]. J591(scFv) not only bound specifically to PSMA but also competed for the same extracellular epitope of PSMA as the J591 mAb [121]. We have used J591(scFv) with His-tag attached to it for binding with ^{99m}Tc tricarbonyl and J591c(scFv), in which an additional cysteine is attached to the His-tag for attachment of

a chelator for ^{68}Ga. The protein was produced using mammalian 293-T cells and purified through Ni-NTA and size exclusion columns. The final yield of the protein obtained was 12 mg/L J591(scFv) and 4-6mg/L J591c(scFv). It was analysed using SDS-PAGE as it appeared around 30KDa and with HPLC using size-exclusion column, in which it eluted around 9 min using PBS as a running a buffer. One of the problems which we have encountered is the formation of dimers in the protein sample. We have observed that if we immediately kept the protein at low temperature (-80^{o}C) in a diluted form then to some extent this problem can be resolved (Fig-3.12). J591(scFv) was radiolabelled with ^{99m}Tc tricarbonyl via the His-tag attached to the J591(scFv).

^{99m}Tc is commonly used by different groups to radiolabel the scFv because of their rapid tumour penetration and high tumour-to-tissue ratios at early time points. Free thiol groups necessary for labelling with ^{99m}Tc are not normally found on these molecules. Marlics et al have attached free cysteines to the C-terminus of MFE-23, an scFv directed against carcinoembryonic antigen (CEA). They demonstrated that the radiolabelled product was stable *in vivo* and *in vitro* and but showed high kidney uptake [136].

We have used quite simple and straightforward radiolabelling procedure; it is done by incubating the protein with ^{99m}Tc tricarbonyl at 37^{o}C for 60 min. After this the protein was purified using a MiniTrap column, which removed the excess of unreacted ^{99m}Tc tricarbonyl or free pertechnetate if present in the sample (Fig-4.4, 4.5). It was also observed that by increasing the salt concentration from 140 mM to 500 mM, the extent of radiolabelling yield was also increased (Fig-4.13, 4.12). The radiolabelled complex was quite stable when incubated with human serum even after 24 h. It was analysed by SDS-PAGE and ITLC method (Fig-4.14, 4.15). It was observed that ^{99m}Tc tricarbonyl remained bound to the J591(scFv) and that J591(scFv) showed specific binding to PSMA positive cell lines as opposed to PSMA negative cell lines, with a Kd value of 3.72 nM (Fig-4.16,4.17,4.18) when analysed by FACS and a cell binding experiment.

J591c(scFv) was conjugated with YM103. The conjugation reaction was quite simple and straightforward. It involved incubating the protein with reducing agent (TCEP) for 60 min to break the disulfide bonds, making free cysteine available to form a bond with the maleimide of the YM103 (3-4 h). Schumacher et al have proved that prolonged reaction times did not improve the isolated yield of product [128]. They analysed the

different reagents which can be suitable for disulphide cleavage bridging and at the same time reagents should be tolarent of the reducing agent TCEP. They observed that the halomaleimides showed a greater reactivity toward TCEP than the dithiomaleimides. They also observed the formation of side products, somatostatin-maleimide-TCEP conjugates by MS analysis in case of halomaleimides [128]. In recent years many groups have shown different methods of conjugation. Many of the methods which are available for the conjugation of chelator with antibody are not very effective. Kerry Chester's group overcame this problem by using 3,4-substituted maleimides to bridge and thus functionalize disulfide bonds to generate homogeneous antibody conjugates. They reported a one-step conjugation reaction, which was fast, site-specific, quantitative and gave products with full binding activity, good plasma stability and the desired functional properties. They also described that the rigid nature of this modification by disulfide bridging enables the successful detection of antigen with a spin labelled antibody fragment by continuous-wave electron paramagnetic resonance (cw-EPR) [137].

Radiolabelling of the conjugated J591c(scFv) is done with ^{68}Ga, simply by incubating the conjugated protein with ^{68}Ga at room temperature for 5-10 minutes at neutral pH. Quantitative radiolabelling was obtained, which means that no purification step was required. One of the benefits of using the ^{68}Ga as a radionuclide is that it is easily available from a generator, which is comparatively cheap and easily available as compared to the cyclotron produced radionuclides. Its half life is 68 min, which is comparable with the pharmacokinetic properties of the single chain. The radiolabelling reaction was simple, quick and straightforward as opposed to the other chelators available for the ^{68}Ga, like for DOTA required heating at 100^{o}C for up to 30 min, which is first not very compatable with the half-life of ^{68}Ga and besides also not good for biological molecules as high temperature may lead to their denaturation. Furthermore, the radiolabelled complex did not require any further purification (Fig-5.2, 5.5). This is a major advantage of the new chelator used. It was observed that at lower concentrations (0.125 µg/µl), the radiolabelling yield increased with time from 70% at 5 min to almost 90% at 40 min (Fig-5.8, 5.9). The serum stability gel (Fig-5.11) showed that J591c(scFv)-YM103 when radiolabelled with ^{68}Ga and incubated in human serum was quite stable even after 6 h. There was no dissociation between ^{68}Ga and J591c (scFv)-YM103 or transfer of ^{68}Ga to human serum. In addition, cell binding

experiments were performed with PSMA positive cell lines (Du145-PSMA) and PSMA negative cell lines (Du145) and it was observed that conjugated radiolabelled protein showed binding with the PSMA positive cell lines with a Kd value calculated to be 31.2 nM.

^{68}Ga-CP256 is quite hydrophobic, so we were expecting it might be able to cross the blood brain barrier when we injected mice with ^{68}Ga-CP256 but in fact it cleared from the body within 10 min and accumulated in bladder (Fig-5.14-B). In future this could be evaluated as a imaging agent for kidney function. In mice with PSMA negative tumours (Du145) no accumulation of radioactive complex was observed either in imaging or biodistribution data (Fig-5.17, 5.18, 5.19, 5.20). On the other hand, in mice with PSMA positive tumours high uptake and specific binding was observed. The imaging and biodistribution data showed no evidence of release of ^{68}Ga from the chelator but as required they probably reflect the distribution of the antibody. As expected, high uptake was observed in the kidneys, as this is known to be the route of excretion of scFv proteins (Fig-5.21, 5.22, 5.23, 5.24).

6.3- Summary

We have in fact been able to develop two new potential radiopharmaceuticals for imaging prostate cancer. Although clearly there is more work to be done, it is a big step forward. We have produced J591(scFv), which can be radiolabelled with ^{99m}Tc tricarbonyl and in the future there is a possibility of using it as a SPECT imaging agent for prostate cancer and J591c(scFv)-YM103 radiolabelled with ^{68}Ga and used as a PET imaging agent for prostate cancer. The radiolabelling method in both the cases is very simple and efficient, especially in the case of ^{68}Ga. Using YM103 it is possible to obtain high radiolabelling yield within 5 min at room temperature and neutral pH. The importance of this bifunctional chelator is further enhanced because of its peculiar behaviour in metal based pretargetting. The use of ^{68}Ga will likely grow in the next few years as the generator gains marketing authorization and there will be a need for truly kit-based formulations for radiolabelling biomolecules with ^{68}Ga. We have observed that this new tracer has the potential to be useful in imaging prostate cancer. In future it might be clinically helpful in staging, monitoring and treatment of prostate cancer in humans.

6.4-Future work

It would be good to do histochemical analysis of the tumours after the *in vivo* experiments as it would give an idea about the tumour vascularisation and necrosis. Maximum uptake can be observed in tumours without necrosis. It might give some useful information for planning of next *in vivo* experiment.

Another important thing to accomplish is the production of the protein which is fit to use in humans (cGMP). Also, scaling up the labelling procedure to produce sufficient activity for human studies and finally, to evaluate the imaging potential of this new radiopharmaceutical in clinical trials.

Furthermore, it would also be useful to do radiolabelling with other diagnostic and therapeutic radionuclides and explore the possibility of using this chelator and scFv complex for therapeutic purposes, although this might be limited because of the high uptake in kidneys. There are other ways which we can explore to reduce the kidney uptake, such as preparation of a diabody. Moreover, to further explore the full potential of the chelator and to determine the extent of the possibilities allowed by the ability of the chelator to bind ^{68}Ga in serum and ultimately *in vivo* - pretargeting by metal chelation.

Chapter 7: References

1: Zhou Y, Chakraborty S, Liu S. Radiolabeled cyclic RGD peptides as radiotracers for imaging tumors and thrombosis by SPECT. Theranostics. 2011; 1:58-82.

2: Kumar VL, Majumder PK. Prostate gland: structure, function and regulation. Int Urol Nephrol. 1995; 27:231-243.

3: Miki J, Rhim J. Prostate cell cultures as in vitro models for the study of normal stem cells and cancer stem cells. Prostate Cancer and Prostatic Diseases. 2008; 11:32–39.

4: Adam J. The case of scirrhous of the prostate gland nwith corresponding afflication of the lymphatic glands in the lumber region and in the pelvis. Lancet. 1853; 1:393.

5: Websites of CRUK and American Prostate Cancer Society.

6: http://vpo.orchid-cancer.org.uk/316/Facts-and-stats, Facts and stats on prostate cancer. 2009, Orchid - Fighting Male Cancer.

7: Russell PJ, Jackson P, Kingsley EA (ed). Prostate cancer methods and protocols. Totawa, NH: Humana Press. 2003.

8: Oh WK, Hurwitz M, D'Amico AV, Richie JP, Kantoff PW. Biology of prostate cancer. In: Kufe DW, Pollock RE, Weichselbaum RR, Bast RC, Gansler TS, Holland JF, Frei E (ed). Holland-Frei Cancer Medicine, 6th edition. Hamilton, ON: BC Decker. 2003.

9: Heinlein CA, Chang C. Androgen receptor in prostate cancer. Endocrine Rev. 2004; 25:276–308.

10: LaMonica V, Stewart L, Nancy L.Vitamin D and prostate cancer. Exp Biol Med. 2004; 229:277-284.

11: Hricak H, Choyke PL, Eberhardt SC, Leibel SA, Scardino PT. Imaging prostate cancer: A multidisciplinary perspective. Radiology. 2007; 243:28–53.

12: Rorvik J, Haukaas S. Magnetic resonance imaging of the prostate. Curr Opin Urol. 2001; 11:181–188.

13: Reubi JC, Maecke HR. Peptide-based probes for cancer imaging. J Nucl Med. 2008; 49:1735–1738.

14: Bouchelouche K, Oehr P. Positron emission tomography and positron emission tomography/computerized tomography of urological malignancies: An update review. J Urol. 2008; 179:34–45.

15: Gambhir SS. Molecular imaging of cancer with positron emission tomography. Nat Rev Cancer. 2002; 2:683–693.

16: Schroeder FH, Maas PV, Beemsterboer P, et al. Evaluation of the digital rectal examination as screening test for prostate cancer. J Natl Cancer Inst. 1998; 90:1817-23.

17: Bhatnagar V, Stewart ST, Bonney WW, Kaplan RM. Treatment options for localized prostate cancer: quality-adjusted life years and the effects of lead-time. Urology. 2004; 63:103-9.

18: Humphrey P. Gleason grading and prognostic factors in carcinoma of the prostate. Modern Pathology. 2004; 17:292-306.

19: Mathews D, Oz OK. Positron emission tomography in prostate and renal cell carcinoma. Curr Opin Urol. 2002; 12:381–385.

20: Effert PJ, Bares R, Handt S, Wolff JM, Bull U, Jakse G. Metabolic imaging of untreated prostate cancer by positronemission tomography with ^{18}F-labeled deoxyglucose. J Urol. 1996; 155:994–998.

21: Zaheer A, Cho SY, Pomper M. New agents and techniques for imaging prostate cancer. J Nucl Med. 2009; 50:1387-1390.

22: He Y, Yin DG, Perera MA, Kirkovsky L, Stourman N, Li W. Novel ligands with high binding affinity and potent functional activity for the androgen receptor. Eur J Med Chem. 2002; 37:619–634.

23: Dalton JT, Mukherjee A, Zhu Z, Kirkovsky L, Miller DD. Discovery of nonsteroidal androgens. Biochem Biophys Res Commun. 1998; 244:1–4.

24: Larson SM, Morris M, Gunther I, Beattie B, Humm JL, Akhurst TA, et al. Tumor localization of 16-beta-18-F-fluoro-5a-dihydrotestosterone versus ^{18}F-FDG in patients with progressive, metastatic prostate cancer. J Nucl Med. 2004; 45:366–373.

25: Beattie JB, Smith-Jones PM, Jhanwar YS, et al. Pharmacokinetic assessment of the uptake of 16β-^{18}F-fluoro-5a-dihydrotestosterone (FDHT) in prostate tumors as measured by PET. J Nucl Med. 2010; 51:183–192.

26: Bonasera TA, O'Neil JP, Xu M, Dobkin JA, et al. Preclinical evaluation of fluorine-^{18}F-labeled androgen receptor ligands in baboons. J Nucl Med. 1996; 37:1009 –1015.

27: Dehdashti F, Joel P, Michalski JM, Dence CS, Siegel BA, Katzenellenbogen JA. Positron tomographic assessment of androgen receptors in prostatic carcinoma. Eur J Nucl Med Mol Imaging. 2005; 32:344–350.

28: Jacobson O, Laky D, Carlson KE, Elgavish S, et al. Chiral dimethylamine flutamide derivatives--modeling, synthesis, androgen receptor affinities and carbon-11 labeling. Nucl Med Biol. 2006; 33:695–704.

29: Sweat SD, Pacelli A, Murphy GP, Bostwick DG. Prostate specific membrane antigen expression is greatest in prostate adenocarcinoma and lymph node metastases. Urology. 1998; 52:637–640.

30: Chang SS, Reuter VE, Heston WD, Bander NH, Grauer LS, Gaudin PB. Five different anti-prostate-specific membrane antigen (PSMA) antibodies confirm PSMA expression in tumor-associated neovasculature. Cancer Res. 1999; 59:3192-3198.

31: Chang SS, O'Keefe DS, Bacich DJ, Reuter VE, Heston WD, Gaudin PB. Prostate-specific membrane antigen is produced in tumor-associated neovasculature. Clin Cancer Res. 1999; 5:2674-2681.

32: Rajasekaran AK, Anilkumar G, Christiansen J. Is prostate-specific membrane antigen a multifunctional protein? Am J Physiol Cell Physiol. 2005; 288:975-981.

33: Bander NH, Nanus DM, Milowsky MI, Kostakoglu L, et al. Targeted systemic therapy of prostate cancer with a monoclonal antibody to prostate-specific membrane antigen. Oncol. 2003; 30:667–676.

34: Davis MI, Bennett MJ, Thomas LM, Bjorkman PJ. Crystal structure of prostate-specific membrane antigen, a tumor marker and peptidase. Proc Natl Acad Sci USA. 2005; 102:5981–5986.

35: Schülke N, Varlamova OA, Donovan GP, et al. The homodimer of prostate-specific membrane antigen is a functional target for cancer therapy. Proc Natl Acad Sci USA. 2003; 100:12590–12595.

36: Ananias HJ, de Jong IJ, Dierckx RA, van de Wiele C, et al. Nuclear imaging of prostate cancer with gastrin-releasing-peptide-receptor targeted radiopharmaceuticals. Curr Pharm. 2008; 14:3033–3047.

37: Yang YS, Zhang X, Xiong Z, Chen X. Comparative in vitro and in vivo evaluation of two ^{64}Cu-labeled bombesin analogs in a mouse model of human prostate adenocarcinoma. Nucl Med Biol. 2006; 33:371–380.

38: Parry JJ, Kelly TS, Andrews R, Rogers BE. In vitro and in vivo evaluation of ^{64}Cu-labeled DOTA-linker-bombesin (7–14) analogues containing different amino acid linker moieties. Bioconjug Chem. 2007; 18:1110–1117.

39: Prasanphanich AF, Nanda PK, Rold TL, et al. [^{64}Cu-NOTA-8-Aoc-BBN(7–14)NH_2] targeting vector for positron-emission tomography imaging of gastrin-releasing peptide receptor-expressing tissues. Proc Natl Acad Sci USA. 2007; 104:12462–12467.

40: Garrison JC, Rold TL, Sieckman GL, et al. In vivo evaluation and small animal PET/CT of a prostate cancer mouse model using ^{64}Cu bombesin analogs: side-by-side comparison of the CB-TE2A and DOTA chelation systems. J Nucl Med. 2007; 48:1327–1337.

41: Huang SS, Wang X, Zhang Y et al. Improving the biodistribution of PSMA-targeting tracers with a highly negatively charged linker. The Prostate. 2014; 74: 702–713.

42: Banerjee SR, Pullambhatla M, Fosset CA, et al. ^{64}Cu-labeled inhibitors of prostate-specific membrane antigen for PET imaging of prostate cancer. J Med Chem. 2014; 57: 2657–2669.

43: Hao G, Kumar A, Oz O, Hsieh JT, Sun X. A multivalent strategy to prepare PET probes for prostate specific membrane antigen (PSMA) detection. J Nucl Med. 2013; 54:1156-1158.

44: Biddlecombe GB, Rogers BE, de Visser M, Parry JJ, de Jong M, Erion JL, Lewis JS. Molecular imaging of gastrin releasing peptide receptor-positive tumors in mice using ^{64}Cu and^{86}Y-DOTA-(Pro1,Tyr4)-bombesin (1–14). Bioconjug Chem. 2007; 18:724–730.

45: Liu Z, Niu G, Wang F, Chen X. ^{68}Ga-labeled NOTA-RGDBBN peptide for dual integrin and GRPR-targeted tumor imaging. Eur J Nucl Med. 2009; 36:1483-1494.

46: Misra P, Humblet V, Pannier N, et al. Production of multimeric prostate specific membrane antigen small molecule radiotracers using a solid phase ^{99m}Tc preloading strategy. J Nucl Med. 2007; 48:1379-1389.

47: Nanni C, Schiavina R, Boschi S, et al. Comparison of ^{18}F-FACBC and ^{11}C-choline PET/CT in patients with radically treated prostate cancer and biochemical relapse: preliminary results. Eur J Nucl Med Mol Imaging. 2013; 40 (suppl 1):S11-S17.

48: Brogsitter C, Zöphel K, Kotzerke J. ^{18}F-Choline, ^{11}C-choline and ^{11}C-acetate PET/CT: comparative analysis for imaging prostate cancer patients. Eur J Nucl Med Mol Imaging. 2013; 40:18-27.

49: Foss CA, Mease RC, Fan H, Wang Y, et al. Radiolabeled small-molecule ligands for prostate-specific membrane antigen: in vivo imaging in experimental models of prostate cancer. Clin Cancer Res. 2005; 11:4022–4028.

50: Mease RC, Dusich CL, Foss CA, et al. N-[N-[(S)-1,3-Dicarboxypropyl] carbamoyl]-4-[^{18}F] fluorobenzyl-L-cysteine, [^{18}F] DCFBC: a new imaging probe for prostate cancer. Clin Cancer Res. 2008; 14:3036–3043.

51: Chondrogiannis S, Colletti PM, Ferretti A, et al. Role of ^{18}F-choline PET/CT in suspicion of relapse following definitive radiotherapy for prostate cancer. Eur J Nucl Med Mol Imaging. 2013; 40:1356-1364.

52: Banerjee RS, Pullambhatla M, Pomper MG, et al. ^{68}Ga-labeled inhibitors of prostate-specific membrane antigen (PSMA) for imaging prostate cancer. J Med Chem. 2010; 30:5333-5334.

53: Lapi SE, Wahnishe H, Pham D, et al. Assessment of an ^{18}F-labeled phosphoramidate peptidomimetic as a new prostate-specific membrane antigen-targeted imaging agent for prostate cancer. J Nucl Med. 2009; 50:2042-2048.

54: Afshar-Oromieh A, Haberkorn U, Eder M, Eisenhut M, Zechmann C. [^{68}Ga]Gallium-labelled PSMA ligand as superior PET tracer for the diagnosis of prostate cancer: comparison with ^{18}F-FECH. Eur J Nucl Med Mol Imaging. 2012; 39:1085–1086.

55: Afshar-Oromieh A, Malcher A, Eder M, Eisenhut M, Linhart HG, Hadaschik BA, et al. PET imaging with a [^{68}Ga]gallium-labelled PSMA ligand for the diagnosis of prostate cancer: biodistribution in humans and first evaluation of tumour lesions. Eur J Nucl Med Mol Imaging. 2013; 40:797-798.

56: Eder M, Schafer M, Bauder-Wust U, Hull WE, Wangler C, Mier W, et al. ^{68}Ga-complex lipophilicity and the targeting property of a urea-based PSMA inhibitor for PET imaging. Bioconjug Chem. 2012; 23:688–697.

57: Lesche R, Kettschau G, Gromov AV, et al. Preclinical evaluation of BAY 1075553, a novel ^{18}F-labelled inhibitor of prostate-specific membrane antigen for PET imaging of prostate cancer. Eur J Nucl Med Mol Imaging. 2014; 41:89-101.

58: Website of Progenics Ltd. (www.progenics.com)

59: Tjoa BA, Simmons SJ, Bowes VA, et al. Evaluation of phase I/II clinical trials in prostate cancer with dendritic cells and PSMA peptides. The Prostate. 1998; 36:39-44.

60: Website of Molecular Insight Ltd. (www.molecularinsight.com).

62: Zechmann CM, Oromieh AA, Armor T, et al. Radiation dosimetry and first therapy results with a ^{124}I/^{131}I-labeled small molecule (MIP-1095) targeting PSMA for prostate cancer therapy. Eur J Nucl Med Mol Imaging. 2014; 41:1280-1292.

63: Tesson M, Mairs R, Maresca K, et al. Enhancement of prostate-targeted radiotherapy using [^{131}I]MIP-1095 in combination with radiosensitizing chemotherapeutic drugs. J Nucl Med. 2013; 54:119-121.

64: Eder M, Eisenhut M, Babich J, Haberkorn U. PSMA as a target for radiolabelled small molecules. Eur J Nucl Med Mol Imaging. 2013; 40:819–823.

65: Hillier SM, Maresca K, Lu G. ^{99m}Tc-labeled small-molecule inhibitors of prostate-specific membrane antigen for molecular imaging of prostate cancer. J Nucl Med. 2013; 54:1369-1376.

66: Sodee DB, Nelson AD, Faulhaber PF, Maclennan GT, Resnick MI, Bakale G. Update on fused capromab pendetide imaging of prostate cancer. Clin Prostate Cancer. 2005; 3:230–238.

67: Seo Y, Aparici CM, Cooperberg MR, et al. In vivo tumor grading of prostate cancer using quantitative ^{111}In-capromab pendetide SPECT/CT. J Nucl Med. 2010; 51:31-36.

68: Liu H, Rajasekaran AK, Moy P, et al. Constitutive and antibody-induced internalization of prostate-specific membrane antigen. Cancer Res. 1998; 58:4055-4060.

69: Nargund V, Al Hashmi D, Kumar P, Gordon S, et al. Imaging with radiolabelled monoclonal antibody (MUJ591) to prostate-specific membrane antigen in staging of clinically localized prostatic carcinoma: comparison with clinical, surgical and histological staging. BJU Int. 2005; 95:1232–1236.

70: Farokhzad OC, Karp JM, Langer R. Nanoparticle-aptamer bioconjugates for cancer targeting. Expert Opin Drug Deliv. 2006; 3:311–324.

71: Frampas E, Rousseau C, Bodet-Milin C, Barbet J, Chatal JF, Kraeber-Bodéré F. Improvement of radioimmunotherapy using pretargeting. Front Oncol. 2013; 3:159.

72: Farokhzad OC, Cheng J, Teply BA, et al. Targeted nanoparticle aptamer bioconjugates for cancer chemotherapy in vivo. Proc Natl Acad Sci USA. 2006; 103:6315–6320.

73: Moffatt S, Papasakelariou C, Wiehle S, et al. Successful in vivo tumor targeting of prostate-specific membrane antigen with a highly efficient J591/PEI/DNA molecular conjugate. Gene Ther. 2006; 13:761–772.

74: Moffatt S, Cristiano RJ. Pegylated J591 mAb loaded in PLGA-PEGPLGA tri-block copolymer for targeted delivery: In vitro evaluation in human prostate cancer cells. Int J Pharmacol. 2006; 317:10–30.

75: Shi C, Zhu Y, Xie Z, Chung WK, et al. Visualizing human prostate cancer cells in mouse skeleton using bioconjugated near-infrared fluorescent quantum dots. Urology. 2009; 74:446–451.

76: Abdolahi M, Gahrouei DS, Laurent S, et al. Synthesis and *in vitro* evaluation of MR molecular imaging probes using J591 mAb-conjugated SPIONs for specific detection of prostate cancer. Contrast Media Mol Imaging. 2013; 8:175–184.

77: Nelson AL. Antibody fragments: hope and hype. MAbs. 2010; 2:77–83.

78: Kaur S, Venktaraman G, Jain M, Senapati S, et al. Recent trends in antibody based oncologic imaging. Cancer Lett. 2012; 315:97-111.

79: Maher J, Brentjens RJ, Gunset G, Riviere I, Sadelain M. Human T-lymphocyte cytotoxicity and proliferation directed by a single chimeric TCRzeta /CD28 receptor. Nat Biotechnol. 2002; 201:70-75.

80: Jennewein M, Lewis MA, Zhao D, Mason RP, Thorpe PE, et al. Vascular imaging of solid tumors in rats with a radioactive arsenic-labeled antibody that binds exposed phosphatidylserine. Clin Cancer Res. 2008; 14:1377–1385.

81: Olafsen T, Gu Z, Sherman MA, Leyton JV, Reiter RE, et al. Targeting, imaging, and therapy using a humanized antiprostate stem cell antigen (PSCA) antibody. J Immunother. 2007; 30:396–405.

82: Leyton JV, Olafsen T, Lepin EJ, et al. Humanized radioiodinated minibodies for imaging of prostate stem cell antigen-expressing tumors. Clin Cancer Res. 2008; 14:7488-7496.

83: Leyton JV, Olafsen T, Sherman MA, Bauer KB, Aghajanian P, Reiter RE, Wu AM. Engineered humanized diabodies for microPET imaging of prostate stem cell antigen-expressing tumors. Protein Eng Des Sel. 2009; 22:209–216.

84: Frigerio B, Fracasso G, Luison E, et al. A single-chain fragment against prostate specific membrane antigen as a tool to build theranostic reagents for prostate cancer. Eur J Cancer. 2013; 49:2223–2232.

85: He J, Wang Y, Feng J, Zhu X, Lan X, Iyer AK, Zhang N, Seo Y, Van Brocklin HF, Liu B. Targeting prostate cancer cells in vivo using a rapidly internalizing novel human single-chain antibody fragment. J Nucl Med. 2010; 51:427-432.

86: Alberto R, Ortner K, Wheatley N, Schibli R, Schubiger AP. Synthesis and properties of boranocarbonate: A convenient in situ CO source for aqueous preparation of $[^{99m}Tc(OH_2)_3(CO)_3]^+$. J Am Chem Soc. 2001; 123:3135-3136.

87: Waibel R, Alberto R, Plückthun A, Schubiger PA, et al. Stable one-step technetium-99m labeling of His-tagged recombinant proteins with a novel Tc(I)-carbonyl complex. Nature Biotechnol. 1999; 17:897-901.

88: Tsui P, Rubenstein M, Guinanet P. Correlation between PSMA and VEGF expression as markers for LNCaP tumor angiogenesis. J Biomed Biotechnol. 2005; 3:287-290.

89: Ruggiero A, Holland JP, Lewis J, Grimm J. Cerenkov luminescence imaging of medical isotopes. J Nucl Med. 2010; 51:1123-1130.

90: Beile EU, Reischl G, Wiehr S, et al. PET imaging of prostate cancer xenograft with a highly specific antibody against the prostate specific membrane antigen. J Nucl Med. 2009; 50:606-611.

91: Bander NH, Milowsky M, Nanus D, et al. Phase I Trial of ^{177}Lu-labeled J591, a monoclonal antibody to prostate-specific membrane antigen, in patients with androgen-independent prostate cancer. J Clin Oncol. 2005; 20:4591-4601.

92: Website of Dandreon. (www.dandreon.com).

93: Castaneda L, Maruani A, Schumacher FF, Chester K, et al. Acid-cleavable thiomaleamic acid linker for homogeneous antibody–drug conjugation. Chem Commun. 2013; 49:8187-8189.

94: Bandekar A, Zhu C, Jindal R, et al. Anti-prostate-specific membrane antigen liposomes loaded with ^{225}Ac for potential targeted antivascular alpha-particle therapy of cancer. J Nucl Med. 2014; 55:107–114.

95*:* Maecke HR, Andre JP. ^{68}Ga-PET radiopharmacy: a generator based alternative to ^{18}F-radiopharmacy. In: Schubiger PA, Lehmann L, Friebe M (ed). PET chemistry: the driving force in molecular imaging.: Springer. 2007: pp215-242.

96: Velikyan I, Beyer G, Långström B. Microwave-supported preparation of ^{68}Ga bioconjugates with high specific radioactivity. Bioconjugate Chem. 2004; 15:554-560.

97: Modular Lab, Eckert & Ziegler. www.eurotope.com.

98: Rösch F, Zhernosekov KP, Filosofov DV. Processing of ^{68}Ge/^{68}Ga generator elutes for labelling molecular targeting vectors. Nuklearmedizin. 2005; 44:A191.

99: Zhernosekov KP, Filosofov DV, Baum RP, Rosch F, et al. Processing of generator-produced ^{68}Ga for medical applications. J Nucl Med. 2007; 48:1741-1748.

100: Ocak M, Antretter M, Knopp R, Kunkel F, Petrik M, Bergisadi N, et al. Full automation of ^{68}Ga labelling of DOTA-peptide including cation exchange pre purification. Appl Radiat Isot. 2010; 68:297-302.

101: Celler A, Grimes J, Shcherbinin S, Piwowarska-Bilska H, Birkenfeld B. Personalized image-based radiation dosimetry for routine clinical use in peptide receptor radionuclide therapy: pretherapy experience. In: Baum RP, Rösch F (ed). Theranostics, gallium-68, and other radionuclides. Recent Results Cancer Res. 2012; 194:497-517.

102: Mueller D, Klette I, Baum RP, et al. A simplified NaCl based ^{68}Ga concentration and labeling procedure for rapid synthesis of ^{68}Ga radio-pharmaceuticals in high radiochemical purity. Bioconjug Chem. 2012; 23:1712-1717.

103: Breeman WAP, de Jong M, de Blois E, Bernard BF, Konijnenberg M, Krenning EP. Radiolabelling DOTA-peptides with ^{68}Ga. Eur J Nucl Med Mol Imaging. 2005; 32:478-485.

104: Andronov VG, Bruskin AB, Kodina GE, et al. Sorption conditioning of eluate of ^{68}Ge/^{68}Ga generator for medical purposes. Radiochemistry. 2008; 50:535-540.

105: Gebhardt P, Opfermann T, Saluz HP. Computer controlled ^{68}Ga milking and concentration system. Appl Radiat Isot. 2010; 68:1057-1059.

106: Weiner RE, Thakur ML. Chemistry of gallium and indium radiopharmaceuticals. In: Welch MJ, Redvanly CS (ed). Handbook of radiopharmaceuticals: radiochemistry and applications. Wiley. 2005: pp363-401.

107: Olakanmi O, Rasmussen TS, Lewis JB, et al. Multivalent metal induced iron acquisition from transferring and lactoferrin by myeloid cells. J Immunol. 2002; 169:2076-2084.

108: Berry DJ, Ma Y, Ballinger JR, Tavare R, Koers A, Sunassee K, Zhou T, Nawaz S, Mullen GE, Hider JR, Blower PJ. Efficient bifunctional gallium-68 chelators for positron emission tomography: tris(hydroxypyridinone) ligands. Chem Commun. 2011; 25:7068-7070.

109: Smith-Jones PM, Stolz B, Bruns C, et al. $^{67/68}$Ga[DFO]-Octreotide: A potential radiopharmaceutical for PET imaging of somatostatin receptor positive tumors. J Nucl Med. 1994; 35:317-325.

110: Govindaswamy N, Quarless DA, Koch SA. New amine trithiolate tripod ligand and its iron complexes. J Am Chem Soc. 1995; 117:8468-8469.

111: Marchi-Artzner V , Lorz B, Gosse C, et al. Adhesion of Arg-Gly-Asp (RGD) peptide vesicle onto an integrin surface: visualization of the segregation of RGD ligand into the adhesion plaque by fluorescence. Langmuir. 2003; 19:835-841.

112: Notni J, Pohle K, Wester HJ. Comparative gallium-68 labeling of TRAP-, NOTA-, and DOTA-peptides: practical consequences for the future of gallium-68-PET. EJNMMI Research. 2012; 2:28.

113: Zhou T, Neubert H, Liu DY, Ma YM, Hider RC, et al. Iron binding dendrimers: a novel approach for the treatment haemochromatosis. J Med Chem. 2006; 49:4171-4182.

114: Chang CH, Sharkey R, Rossi E, Karacay H, Goldenberg D. Molecular advances in pre-targeting radioimmunotherapy with bispecific antibodies. Mol Cancer Ther. 2002; 1:553-563.

115: Goldenberg D, Sharkey R, Paganelli G, et al. Antibody pretargeting advances cancer radioimmunodetection and radioimmunotherapy. J Clin Oncol. 2006; 24:823-834.

116: Tavare R, Torres Martin de Rosales R, Blower PJ, Mullen GE. Efficient site-specific radiolabeling of a modified C2A domain of synaptotagmin I with $[^{99m}Tc(CO)_3]^+$: a new radiopharmaceutical for imaging cell death. Bioconjug Chem. 2009; 20:2071–2081.

117: Thrall JH, Freitas J, Swanson D, et al. Clinical comparison of cardiac blood pool visualization with technetium-99m red blood cells labeled in-vivo and with technetium-99m human serum albumin. J Nucl Med. 1978; 19:796-803.

118: Velikyan I, Maecke H, Langstrom B. Convenient preparation of ^{68}Ga based radiopharmaceuticals at room temperature. Bioconjug Chem. 2008; 19:569-573.

119: Abou DS, Ku T, Smith-Jones PM. In vivo biodistribution and accumulation of ^{89}Zr in mice. Nucl Med Biol. 2011; 38:675-681.

120: Wadas TJ, Wong E, Weisman G, Anderson C. Coordinating radiometals of copper, gallium, indium, yttrium and zirconium for PET and SPECT imaging of disease. Chem Rev. 2010; 110:2858–2902.

121: Parker S, Diaz IC, Anderson K, Batt C. Design, production, and characterization of a single-chain variable fragment (ScFv) derived from the prostate specific membrane antigen (PSMA) monoclonal antibody J591. Prot Expr Purif. 2013; 89:136–145.

122: Hudson PJ, Kortt AA. High avidity scFv multimers: diabodies and triabodies. J Immunol Meth. 1999; 231:177-189.

123: Bonner PLR. Protein purification. New York: Taylor & Francis. 2007.

124: Creighton TE (ed). Protein function: a practical approach. 2nd ed. Oxford: Oxford University Press. 1997.

125: Gooding K, Regnier F (ed). HPLC of biological macromolecules. 2nd ed. New York: Marcel Dekker. 2002.

126: Givan, AL. Flow cytometry: first principles. New York: Wiley-Liss. 1992.

127: Motulsky H, Christopoulos A. Fitting models to biological data using linear and nonlinear regression: a practical guide to curve fitting. New York: Oxford University Press. 2004.

128: Schumacher FF, Nobles M, Ryan CP Smith ME, Tinker A, Caddick S, Baker JR. In situ maleimide bridging of disulfides and a new approach to protein PEGylation. Bioconjug Chem. 2011; 22:132-136.

129: Harrington K, Rowlinson-Busza G, Syrigos K, Abra R, et al. Influence of tumour size on uptake of [^{111}In]-DTPA-labelled pegylated liposomes in a human tumour xenograft model. Brit J Cancer. 2000; 83:684–688.

130: Corneillie TM, Whetstone PA, Meares CF. Irreversibly binding anti-metal chelate antibodies: artificial receptors for pretargeting. J Inorg Biochem. 2006; 100:882-890.

131: Liu G, Dou S, Cheng D, Greiner D, et al. Human islet cell MORF/cMORF pretargeting in a xenogeneic murine transplant model. Mol Pharmaceut. 2011; 8:767–773.

132: Liu G, Dou S, Rusckowski M, et al. An experimental and theoretical evaluation of the influence of pretargeting antibody on the tumor accumulation of effector. Mol Cancer Ther. 2008; 7:1025-1032.

133: Goldenberg DM, Chang CH, Rossi EA, McBride WJ, Sharkey RM. Pretargeted molecular imaging and radioimmunotherapy. Theranostics 2012; 2:523-540.

134: Blower PJ, Cooper MS, Nawaz S, O'Neill A, Koers A, Sunassee K, Berry DJ, Mullen G, Ballinger JR. Metal ion chelation as a basis for pretargeting. Eur J Nucl Med Mol Imaging. 2012; 39 (suppl 2): S262.

135: Elsässer-Beile U, Bühler P, Wolf P. Targeted therapies for prostate cancer against the prostate-specific membrane antigen. Curr Drug Targets. 2009; 8:118-125.

136: Verhaar MJ, Keep PA, Hawkins RE, Robson L, Casey JL, Pedley B, Boden JA, Begent RH, Chester KA. Technetium-99m radiolabeling using a phage-derived single-chain Fv with a C-terminal cysteine. J Nucl Med. 1996; 37:868-872.

137: Schumacher FF, Sanchania VA, Tolner B, Wright ZV, Ryan CP, Smith ME, Ward JM, Caddick S, Kay CW, Aeppli G, Chester KA, Baker JR. Homogeneous antibody fragment conjugation by disulfide bridging introduces 'spinostics'. Sci Rep. 2013; 3:1525.

138: Sharkey RM, Cardillo TM, Rossi EA, Chang CH, Goldenberg DM, et al. Signal amplification in molecular imaging by pretargeting a multivalent, bispecific antibody. Nat Med. 2005; 11:1250–1255.

139: Safarnejad MR, Jouzani G, Tabatabaie M, Schillberg RS. Antibody-mediated resistance against plant pathogens. Biotechnol Adv. 2011; 29:961-971.

140: Nawaz S. Evaluation of chelators for gallium-68: quality control and transferrin stability. MSc thesis, Kings College London, 2009.

141: Badar A, Williams J, de Rosales RT, Tavaré R, Kampmeier F, Blower PJ, Mullen GE. Optimising the radiolabelling properties of technetium tricarbonyl and His-tagged proteins. EJNMMI Res. 2014; 4(1):14.